

Thèse  
en vue d'obtenir le diplôme  
d'Habilitation à diriger des recherches  
de l'Université Paris 7, D. Diderot

**GPS: de la Tectonique à la Sismologie**

Par Christophe Vigny  
Chargé de recherches au laboratoire de Géologie de l'ENS

Résumé	3
--------	---

<b>Section 1: discours sur la méthode</b>	
Introduction	4
Quelques explications sur le GPS	5
Pourquoi faire du GPS permanent	5
Facteurs limitants la précision du GPS	8
Les domaines d'application	11
Conclusion	19
<b>Section 2: résumé des travaux effectués par chantiers géographiques</b>	
Alpes	20
Plaque Arabie - Afar – Iran - Inde	22
Asie du Sud Est: Bloc de la Sonde, Birmanie, Indonésie, le séisme de Sumatra	26
Chili	43
Antarctique: rebond post-glaciaire	48
Erosion: GPS cinématique sur une plage du Nord (Merlimont)	51
<b>Section 3: renseignements administratifs</b>	
C.V.	53
Enseignements et encadrements de recherches	54
Bibliographie	56
<b>Section 4: articles détaillant les travaux les plus importants</b>	
Le bloc de la sonde :	63-75
A decade of GPS measurements in SE Asia: (Re)Defining Sundaland motion and boundaries	
Simons, W., A. Socquet, <b>C. Vigny</b> , S. Matheussen, B. Ambrosius, C. Subarya, R. Mattindas, D. Sarsito, J. Kahar, S. Abu, H. Ali, C. Promthong, P. Swangnet, M. Iwakuni, T. Kato, P. Morgan, and W. Spakman	
<i>J. Geophys. Res, submitted, 2004.</i>	
Le mouvement Inde/Sonde :	77-100
GPS determination of the relative motion between India and Sunda, and its accommodation in Myanmar	
Socquet, A., <b>C. Vigny</b> , W. Simons, N. Chamot-Rooke, C. Rangin, B. Ambrosius	
<i>J. Geophys. Res, in press, 2006.</i>	
Le séisme de Banda Aceh du 26 décembre 2004	101-106
Insight into the 2004 Sumatra-Andaman earthquake from GPS measurements in southeast Asia	
<b>Vigny, C.</b> , W. Simons, S. Abu, R. Bamphenyu, C. Satirapod, N. Choosakul, C. Subarya, A. Socquet, K. Omar, H. Abidin and B.A.C. Ambrosius	
<i>Nature, vol 436, 14/07/05, pp201-206, doi:10.1038/nature03937, 2005</i>	
La déformation dans les Célèbes	107-123
Kinematic behaviour, crustal block rotations and plate coupling in the triple junction area in SE Asia from inversion of GPS and slip vector data (Sulawesi, Indonesia)	
Socquet, A., W. Simons, <b>C. Vigny</b> , R. McCaffrey, B. Ambrosius, W. Spakman, C. Subarya and D. Sarsito	
<i>J. Geophys. Res, accepted, 2006.</i>	
Le mouvement de la plaque Arabie	125-140
Confirmation of Arabia plate slow motion by new GPS data in Yemen.	
<b>Vigny, C.</b> , P. Huchon, J.C. Ruegg, K. Khanbari, and L. Asfaw,	
<i>J. Geophys Res., 111, B02402, doi:10.1029/2004JB003229, 2006.</i>	
La déformation du rift d'Asal, Djibouti	141-154
25 years of geodetic measurements along the Tadjoura-Asal rift system, Djibouti, East Africa	
<b>Vigny, C.</b> , J.B. DeChabalier, J.C. Ruegg, P. Huchon, K. Feigl, R. Cattin, L. Asfaw and K. Khanbari	
<i>J. Geophys. Res, accepted, 2005.</i>	

## Résumé

Depuis une quinzaine d'années, j'ai travaillé sur la mesure par géodésie spatiale (GPS) de la déformation sur différents chantiers et à différentes échelles, depuis la plaque tectonique jusqu'à la faille.. Collision continentale : Alpes, Népal, Iran ; Subduction : Chili , Indonésie; Extension : Afar ; Grands décrochements : Sumatra, Sulawesi, Birmanie ; Rebond post-glaciaire : Antarctique ; Erosion : Merlimont, Baie de Somme.

Les résultats les plus significatifs concernent:

1. Le **Sud-Est asiatique** : mise en évidence de l'existence du bloc de la Sonde et de son mouvement indépendant de l'Eurasie (1 cm/an vers l'Est). Détermination d'un nouveau mouvement de l'Inde (plus lent et plus oblique que Nuvel-1A) qui conduit à la quantification du mouvement relatif Inde-Sonde, évidemment assez différent du mouvement Australie-Eurasie. Au Nord, en Birmanie, ce mouvement est accommodé par la subduction sous l'Arakan Yoma et le décrochement sur la faille de Sagaing. Les mesures sur le réseau GPS que j'ai installé en Birmanie montrent que la faille n'accorde que les 2/3 du décrochement total (2 cm/an), impliquant un mouvement oblique sur la subduction. Celle-ci est probablement bloquée, c'est à dire qu'elle accumule de la déformation au rythme de 1 à 2 cm/an. Plus au Sud, en Indonésie, le mouvement est complètement partitionné entre la fosse de la Sonde et la grande faille de Sumatra. Nos mesures dans toute la région montrent une accumulation de déformation sur plusieurs centaines de km en arrière de la fosse générée par un plan à très faible pendage. C'est le point de départ du séisme de Banda Aceh du 26 Décembre 2004, étudié en détail grâce aux réseaux GPS continu à haute fréquence de la région. Nous avons montré en particulier comment il est possible d'utiliser ces instruments comme des sismographes très longue période, jamais saturés. Ainsi, on détermine une vitesse de propagation de la rupture différente sur les deux segments Sud et Nord, et l'on peut étayer le scénario de deux ruptures distinctes, la première déclenchant la seconde. J'ai également étudié la marge orientale du bloc de la Sonde, dans l'archipel des Célèbes, et en particulier les rotations rapides des micro-blocs qui accroissent une convergence importante avec les plaques pacifiques et philippines: un véritable mécanisme d'extrusion. Dans cette région, j'ai particulièrement étudié la faille de Palu et la subduction Minahassa en réalisant des campagnes annuelles depuis plus de dix ans et en installant un réseau GPS permanent de 7 stations.
2. Le **Chili** : mesure de l'accumulation de déformation élastique dans les lacunes sismiques de Concepcion-Constitucion (Sud Chili) et Coquimbo (Chili central). Détermination de la convergence Nazca-Amérique du Sud à 7 cm/an (8 cm/an dans Nuvel-1A) et orientée 10° plus Nord que l'azimut défini par Nuvel-1A. Caractérisation fine de l'accumulation de déformation sur près de 1000 km de subduction (entre 30°S et 38°S) qui montre en particulier une variation du couplage du Nord au Sud. Les premiers résultats semblent montrer une variation lente du couplage apparent (quelques % par an), signe de la préparation de l'interface à une grande rupture.
3. Les **Afars** : quantification de l'ouverture du rift d'Asal autour de 15 mm/an actuellement. Mise en évidence de mouvements non stationnaires dans le temps (pendant plus de 25 ans!) au voisinage du rift, et surtout détermination d'une vitesse de la plaque Arabe sensiblement plus lente que prédicta. L'ouverture par rapport à la plaque Somalie (en Afar) est à 11 mm/an seulement (soit inférieure à l'ouverture du rift), et la convergence avec la plaque Eurasie (en Iran) est de 20 à 25 mm/an seulement soit 30% plus lent que Nuvel-1A.

## Introduction

Au départ, ma problématique était d'ordre purement tectonique. Il s'agit de quantifier le déplacement de grandes unités (plaques ou blocs), de déterminer leur niveau de rigidité et de caractériser la vitesse sur leurs frontières: les failles. Pour quantifier convenablement le mouvement d'un bloc il suffit de répartir quelques points de mesure avec une bonne couverture géométrique. Le tout est d'être certain que les points de mesure sont représentatifs du mouvement du bloc rigide, c'est à dire qu'ils sont éloignés des zones en déformation: en général les bordures des plaques. Il est alors relativement facile de déterminer la vitesse angulaire de rotation des blocs échantillonnés, et d'en déduire le mouvement relatif sur la faille qui les sépare. Lorsque l'on procède ainsi, la vitesse mesurée est la vitesse instantanée des plaques, puisque mesurée à partir de la différence de position sur un intervalle de temps très court. Mais si l'on accepte l'hypothèse que la vitesse d'une plaque est constante sur une durée assez longue (au moins 100,000 ans), alors cette vitesse instantanée est aussi la vitesse à long terme des plaques, et donc de la faille qui les sépare. La vitesse des failles déterminée par GPS doit donc être comparable à la vitesse estimée sur des durées longues, que l'on qualifiera de "géologiques". Par contre, il n'y a aucune raison que celle-ci corresponde à la vitesse de la faille estimée sur des périodes plus courtes (de l'ordre ou inférieure à 10,000 ans) par les méthodes de datations de décalages de quelques dizaines de mètres (réseau hydrographique ou objets topographiques type volcans ou terrasses) ou encore par des tranchées destinées à mesurer le décalage cumulé de quelques séismes historiques ou archéologiques. En effet, absolument rien n'interdit qu'une faille accumule un déficit de glissement (trop peu de séismes, trop rares ou trop petits) *pendant un certain temps*, puis qu'elle rattrape ce retard lors d'une succession de séismes (plus gros ou plus fréquent) "anormaux". C'est seulement sur la moyenne d'un grand nombre de cycles sismiques que la vitesse de la faille devient comparable à la vitesse relative des blocs tectoniques. Une difficulté vient du fait que le nombre de cycles nécessaire à stabiliser la moyenne est inconnu, et peut être très élevé. Il est parfaitement envisageable que la vitesse d'une faille fluctue à très long terme avec des périodes plus lentes ou plus rapides que la moyenne et des périodes d'accélération ou de décélération de plusieurs milliers d'années, voire plus. C'est sans doute la rhéologie de la croûte terrestre qui contrôle ces paramètres, mais on peut sans risque évoquer l'absence ou la présence de fluides, l'existence et la taille d'une zone de gouge, et partant: l'âge lui même de la faille.

En tout état de cause, si l'on veut mesurer la vitesse actuelle d'une faille (afin d'estimer l'aléa sismique qu'elle présente aujourd'hui par exemple), il est donc nécessaire de la mesurer directement dans la zone de déformation. Cela ne suffira pas bien sur, puisqu'il faudra toujours savoir à quel moment de son cycle sismique on se trouve, mais c'est par là qu'il faut commencer. Je me suis donc trouvé amené à installer et mesurer des réseaux de plus en plus denses au voisinage des failles (souvent sous formes de profils) de manières à quantifier profondeur de blocage et vitesse à grande échelle. Pour cela, on fait le plus souvent l'hypothèse que la déformation répartie autour de la faille obéit à une loi géométrique simple (en général une forme d'arctangente qui provient des propriétés élastiques que l'on attribue à la croûte) et surtout *qu'elle est constante dans le temps*, du moins si l'on est assez éloigné d'un séisme passé ou futur. Cette hypothèse est en général vérifiée au premier ordre, mais de plus en plus souvent mise en défaut depuis que les mesures sont vraiment précises et réalisées sur des périodes de temps qui s'allongent. Là où une droite passait assez bien entre quelques points séparés par quelques années, il devient plus évident qu'une certaine courbure est parfois présente dans des séries dépassant la décennie et tenues par un grand nombre de mesures. A l'extrême, il se pourrait bien que la déformation en bordure de faille ne soit *jamais* constante dans le temps, mais toujours décroissante entre deux séismes. C'est une difficulté pour la modélisation élastique mais c'est peut être un futur outil pour la prévision sismique: Il suffirait alors de mesurer la déformation en continu avec une très grande précision pour savoir à quel moment du cycle sismique on se trouve. Ce raisonnement conduit à installer des réseaux GPS permanents plutôt qu'à réaliser des campagnes de mesures à intervalles réguliers. Ce faisant, on se rend compte que le

récepteur GPS devient un sismographe basse période et très large bande capable d'échantillonner la déformation depuis 10 Hz environ jusqu'à plusieurs décennies... Et c'est ainsi que l'on passe en quelques années de la tectonique à la sismologie.

## **Quelques explications sur le GPS**

Parce qu'il permet un positionnement précis à quelques millimètres près, le GPS est un merveilleux outil pour la mesure de la déformation de toute nature. En particulier les mesures en continu permettent d'établir des séries temporelles qui ont mis en évidence des phénomènes variable dans le temps à l'échelle de quelques jours à quelques années dans des contextes tectoniques où l'on parlait plutôt en termes de millions d'années auparavant. Dans les premiers temps du GPS on se satisfaisait de déterminer des vitesses de déformation à partir des déplacements constatés entre deux campagnes de mesures. Aujourd'hui que l'on dispose de mesures en continu sur bon nombre de structures actives, on constate de plus en plus :

1. que les modèles standard (ie. Okada) d'accumulation de déformation élastique n'expliquent pas toute la déformation constatée
2. que la déformation n'est pas constante dans le temps, et ce sur des durées assez courtes
3. que des déformations transitoires (parfois périodiques) se produisent régulièrement

Pour progresser sur l'aléa sismique, la compréhension de la physique de la friction sur les failles et la préparation des grandes ruptures il faut étudier les déformations transitoires sur les failles à toutes échelles de temps et d'espace. Cela se fait avec des outils différents : Géodésie pour la déformation de la surface, sismicité pour la déformation en profondeur, Tectonique/datation pour l'histoire récente des failles et l'étude du cycle sismique. En ce qui concerne la géodésie, il faut utiliser l'INSAR (grande résolution spatiale, précision modérée (cm au mieux), et faible résolution temporelle) **et** le GPS (résolution spatiale modérée, grande précision (mm), et résolution temporelle extrêmement fine (de la seconde à la décennie)). Pour l'INSAR, l'acquisition de données ne pose pas de problèmes : les agences spatiales s'en occupent, il ne faut qu'acheter les données. Pour le GPS il faut installer des stations sur le terrain.

## **Pourquoi faire du GPS permanent ?**

a) Pour améliorer la précision. En effet, les techniques de positionnement GPS permettent aujourd'hui d'atteindre des précisions de l'ordre de quelques millimètres sur les positions horizontales des points mesurés lors d'une campagne de quelques jours. En répétant de telles campagnes on arrive donc à définir des vitesses de déplacement horizontales pour ces points avec une précision de l'ordre de quelques mm/an en quelques années. A condition qu'aucune erreur n'ait été faite dans le centrage des instruments au dessus des marqueurs géodésiques, et *surtout que les déplacements des points soient linéaires dans le temps*. En effet, le déplacement d'une station (surtout vertical, mais pas uniquement) est souvent affecté par des phénomènes saisonniers (variation troposphériques, nappes phréatiques, etc...) qui n'ont rien à voir avec la tectonique et qui rendent difficilement interprétables des mouvements faiblement échantillonnés dans le temps (figure 1). Se rajoute à ces effets les erreurs de mesures de hauteur d'antenne ou encore la variabilité de la position du centre de phase des antennes différentes, fatallement utilisées à plusieurs années d'intervalle lors de campagnes répétées.

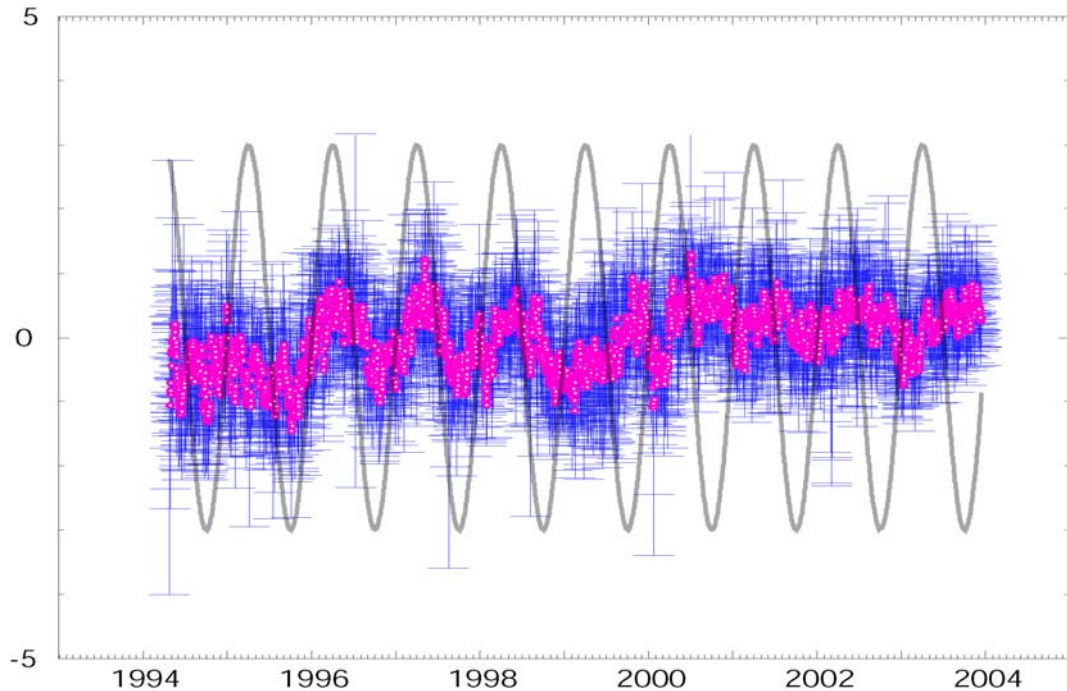


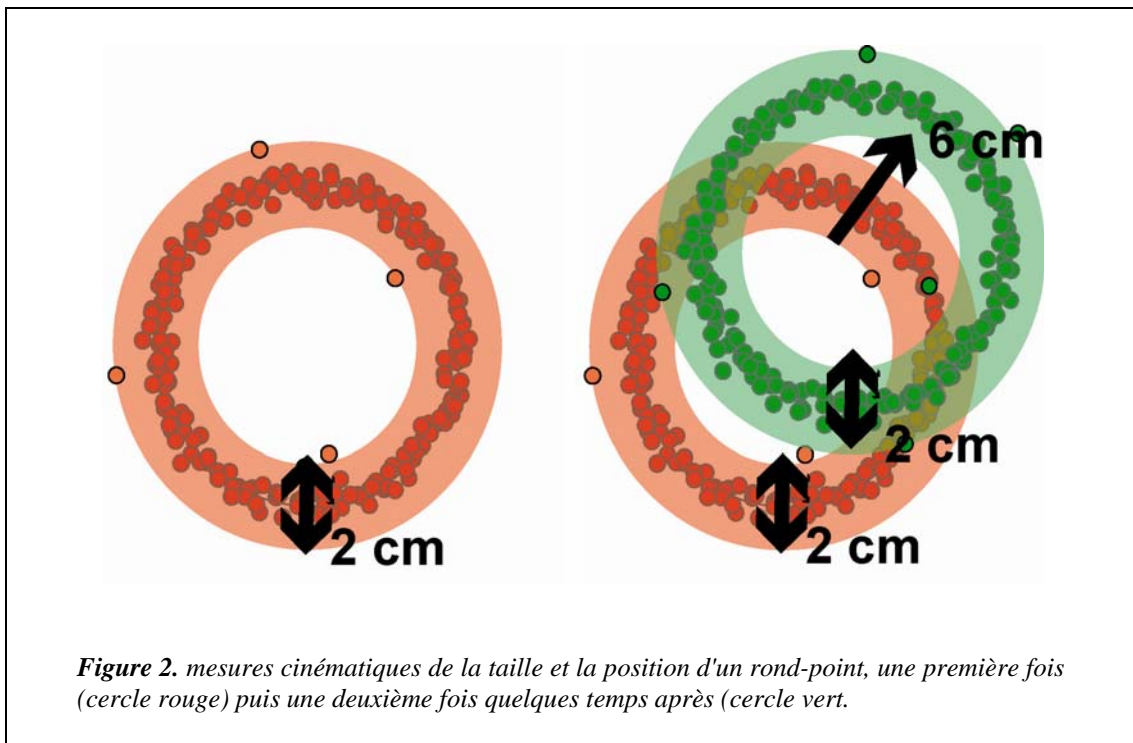
**Figure 1.** série temporelle de la station de Bruxelles. Mesures quotidiennes de la hauteur (en cm) avec incertitude en bleu, moyenne glissante sur 7 jours en violet, signal périodique annuel en gris

D'autre part, les mouvements transitoires dans les zones actives sont souvent de faible amplitude par rapport aux tendances à long terme : des variations temporaires de quelques millimètres se superposent à des déformations de quelques centimètres par an (sauf lorsque la station est très proche d'un séisme important évidemment). Il est donc nécessaire de réaliser des mesures très fines pour ne pas attribuer ces variations à du simple bruit de mesure mais bien à un signal, faible mais cohérent.

En conséquence, la seule méthode adaptée à la mesures de mouvements variables dans le temps (chargement élastique, mouvements pré- co- et post- sismiques) avec une forte composante verticale (failles normales) est celle du GPS permanent. L'antenne étant solidement fixée au repère géodésique, il est absolument certain que tout déplacement de cette antenne est attribuable à des mouvements du sol. Ensuite, le fait que les séries temporelles sont continues, permet de filtrer efficacement tout type de signal parasite qui se produirait avec une fréquence donnée (variation saisonnière du niveau des nappes phréatiques par exemple). Les différents exemples de réseau GPS permanent continu dans le monde (Canada, Californie, Japon, Alpes,...), montrent qu'il est possible de mesurer des vitesses très faibles (1 mm/an, voire moins) en quelques années, et surtout de voir des variations de très faible amplitude dans ces vitesses, soit instantanées (saut d'un jour à l'autre), soit plus étalées dans le temps (séismes lents, glissements a-sismiques, ...), le bruit résiduel étant de l'ordre de 1 à 3 mm au maximum.

b) Parce que précision et exactitude ne sont pas la même chose. Cela paraît évident mais nécessite souvent d'être rappelé. Le GPS ne prétend pas apporter une grande exactitude, il est simplement précis, dans des configurations d'utilisation bien particulières. Si l'on installe un GPS cinématique (à 1 Hz par exemple) sur une bicyclette avec laquelle on fait plusieurs dizaines de fois le tour d'un rond-point en 1 heure, on obtient un nuage de points de forme torique. La précision avec laquelle on connaît la circonference du rond-point se rapporte à dispersion des points dans le nuage, c'est à dire

au diamètre de l'enveloppe du nuage (figure 2a). On peut vérifier que la précision de la mesure est connue et constante en la répétant quelques temps après (une heure après, un autre jour, dans d'autres conditions météo, avec un autre mobile plus lent ou plus rapide, etc...). On obtient alors un autre nuage de point, dont la dispersion est sensiblement la même. Par contre, le barycentre du nuage peut être différent, d'une quantité largement supérieure à cette dispersion (figure 2b). C'est parce que la mesure de la position de chaque point est affectée par un biais systématique, constant sur la durée d'une série de mesure (les quelques tours en 1 heure) mais différent à chaque réalisation. De tels biais existent toujours et sont particulièrement difficiles à estimer. On peut penser les connaître tous et corriger la mesure de leurs effets mais c'est rarement le cas. Les mesures seront donc précises, mais éventuellement inexactes. Ce n'est pas forcément un problème, cela dépend de la question à laquelle on veut répondre en effectuant cette mesure. Dans l'exemple précédent, si l'on veut savoir quelle est la taille du rond-point (pour commander la quantité adéquate de peinture pour le peindre par exemple) c'est la précision qui compte. Si l'on veut savoir sa position (pour l'intégrer dans un SIG par exemple) c'est l'exactitude qui compte. Confondre précision et exactitude c'est croire que l'on connaît la position du rond-point avec la même "précision" que sa taille, et c'est courir le risque d'énoncer une théorie erronée (la tectonique des ronds-points...).



Dans le cas des mesures GPS sur les failles, il est clair que l'on a le plus grand mal à établir précisément l'exactitude et même l'incertitude de nos mesures. Les incertitudes formelles, à priori, basée sur des modèles de bruits de mesures intrinsèques sous estiment notoirement les incertitudes réelles. C'est bien la preuve qu'il y a des biais plus ou moins connus dans les mesures. La meilleure manière, à la fois d'éviter des biais dans les mesures et de détecter ceux qui restent, c'est de faire des mesures en continu, toujours avec le même appareil. Cela ne garantira pas que l'on aura éliminé tous les biais. Par exemple si la constante de gravitation universelle diminue au cours du temps, il est probable que l'éloignement progressif des satellites GPS se traduise par une dérive du système de référence et partant en une inflation apparente de la planète. Malgré tout, on aura éliminé les biais les plus flagrants, comme le décentrage du centre de phase des antennes de type différent par exemple.

## Facteurs limitants la précision du GPS

Aujourd'hui, réaliser des mesures GPS précises à quelques millimètres près sur un réseau à petite échelle (< 100 km) est relativement facile. Le traitement de données de bonne qualité est suffisamment standardisé et automatisé pour que le résultat soit garanti pour peu que l'on ait respecté et appliqué une méthodologie correcte sur le terrain :

- Chaque borne géodésique doit être mesurée en 3 ou 4 sessions indépendantes au moins. La statistique qui permet de quantifier la précision des mesures est basée sur la dispersion de celles ci autour de leur valeur moyenne. Il faut donc 2 mesures au moins pour calculer une valeur moyenne, 3 mesures au moins pour analyser les erreurs possibles, et réaliser 4 mesures au moins pour être certain d'en avoir 3 exploitables.
- Une session de mesure peut ne durer que quelques heures, mais plus elle est longue, meilleure sera la précision. La première raison est tout simplement liée au nombre de mesures acquises (1 point acquis toutes les 30s sur 8 satellites en moyenne donne 960 mesures par heure): plus la session de mesure est longue plus la moyenne des mesures est précise. La seconde raison est liée aux paramètres variables sur la durée d'une journée. Les satellites se déplacent lentement dans le ciel: leur configuration géométrique qui conditionne la précision du positionnement évolue donc au cours de la journée. Pour une bonne couverture du ciel, un temps au moins équivalent à une orbite complète (12h) est donc nécessaire. Enfin les conditions météorologiques et ionosphériques sont notamment différentes entre le jour et la nuit. Pour toutes ces raisons, il est acquis que des sessions de 24h sont requises pour obtenir la meilleure précision.
- Des antennes identiques doivent être utilisées, et celles ci doivent être orientées parallèlement les unes aux autres. En effet, bien que les constructeurs aient réalisé des progrès spectaculaires, les centres de phase des antennes (le point où le signal GPS se matérialise en courant électrique, et qui définit donc la position de l'antenne) ne sont pas toujours exactement au centre géométrique de l'antenne. Ceci ne peut d'ailleurs être réalisé qu'en moyenne: chaque mesure sera affectée par un petit décalage du à l'incidence du signal par rapport à l'axe de l'antenne. Lors du traitement des données, chaque mesure est corrigée par l'intermédiaire d'une table... toujours sujette à caution. Seul le fait d'utiliser des antennes identiques et alignées garanti que le biais éventuel sera éliminé lors d'un calcul différentiel. Il est malgré tout intéressant de noter que ceci ne fonctionne que sur un réseau suffisamment petit: en effet des antennes situées à 90° de longitude l'une de l'autre et rigoureusement alignées vers le Nord géographique... sont en fait à 90° l'une de l'autre si elles sont près des pôles !
- Le GPS étant essentiellement une mesure différentielle, la distance entre deux stations mesurées simultanément sera toujours plus précise que la distance déduite par l'intermédiaire de positions mesurées à des moments différents. Il est donc recommandé de disposer d'autant de récepteurs que de stations à mesurer, afin de les mesurer toutes simultanément. En pratique ce n'est que rarement le cas, et on est conduit à organiser une rotation des récepteurs sur les sites à mesurer. Cette rotation doit être organisée avec soin: Il faut en effet assurer une redondance suffisante (nombre de session minimum sur chaque ligne de base), une "accroche" suffisante entre les sous réseaux mesurés successivement, conserver la même échelle tout au long de la campagne de mesure, etc etc etc....

Aujourd'hui, observer ces différentes "règles" garantit l'obtention d'une précision de quelques millimètres à l'intérieur du réseau mesuré si celui ci est de faible extension. La précision se dégrade ensuite lentement en fonction de la longueur des lignes de base, passant de 2 mm en moyenne pour des lignes courtes à 5-6 mm pour des lignes de 10,000 km de long (figure 3).

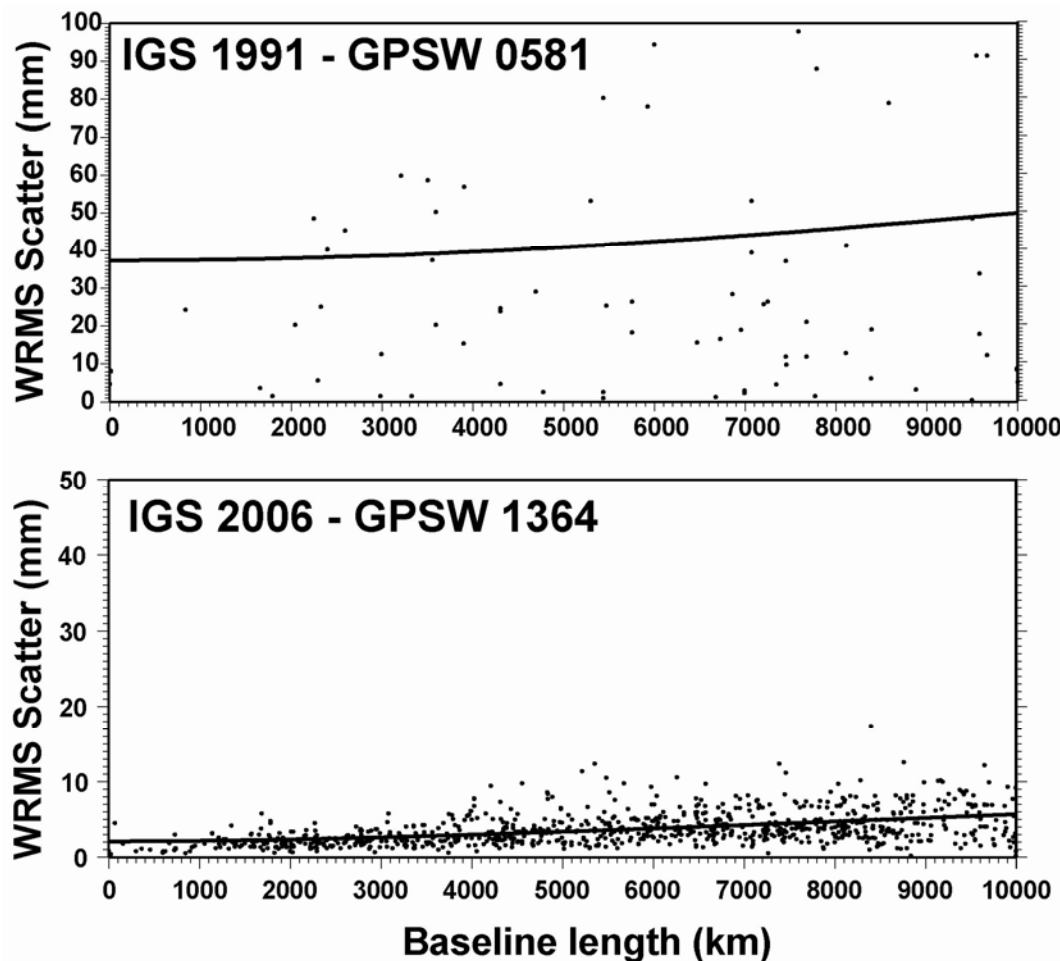
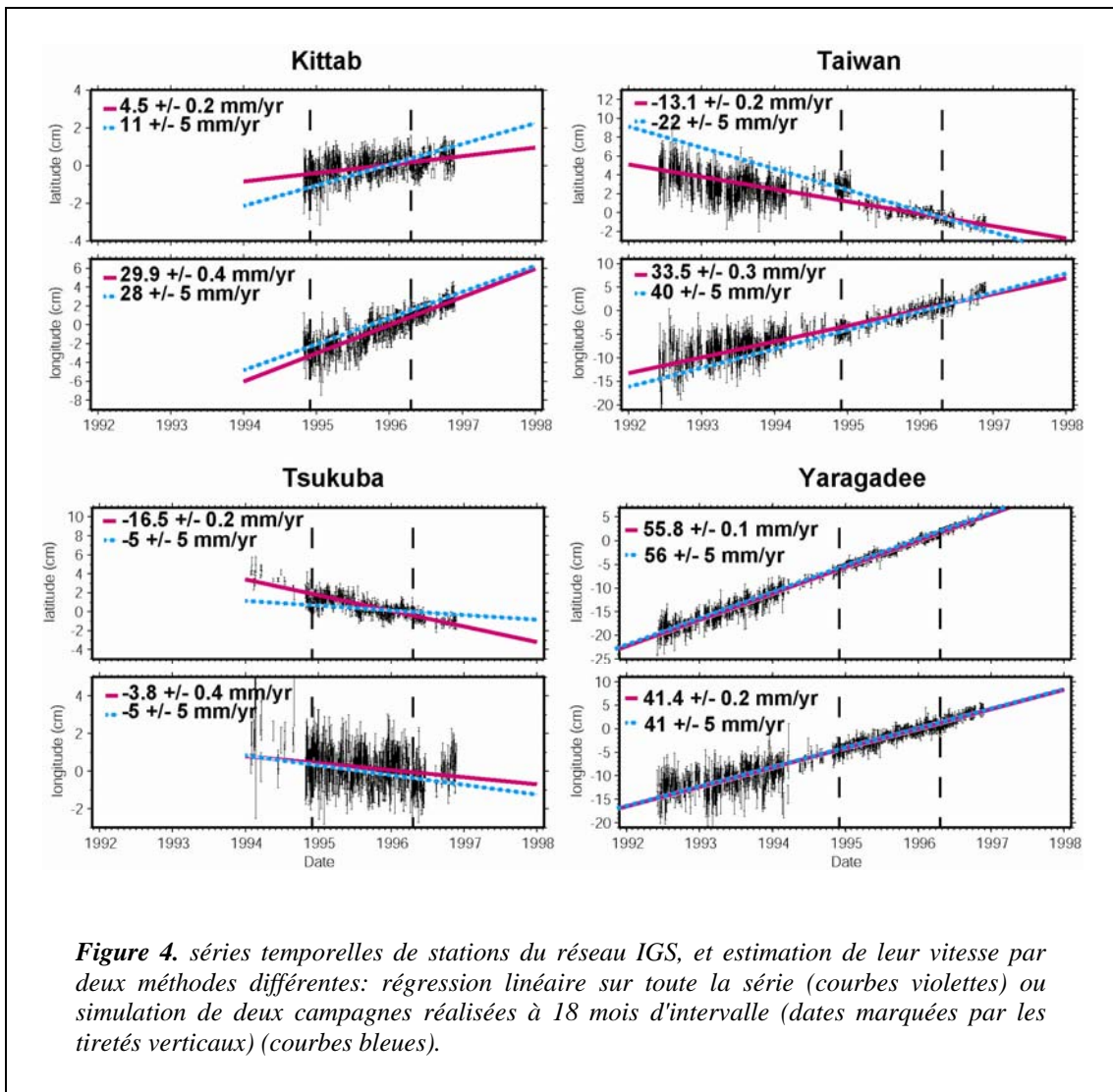


**Figure 3.** répétabilités (c'est à dire dispersion des mesures de la longueur d'une ligne de base donnée autour de sa valeur moyenne) du réseau mondial IGS, en fonction de la longueur des lignes de base. La courbe en trait plein montre la valeur moyenne du nuage de point. Le test est réalisé sur une semaine GPS ancienne (581 en mars 1991) en haut, et une semaine GPS récente (1364 en mars 2006) en bas, telle que traitée au centre de calcul du SIO (Scripps Institute of Oceanography). L'amélioration est flagrante: on gagne 1 ordre de grandeur(de quelques cm à quelques mm) en 15 ans !

La véritable difficulté réside ailleurs: dans la mise en référence des positions/vitesses ainsi obtenues. Lorsque l'on souhaite insérer ces vitesses dans un contexte régional, on intègre dans son traitement les données des stations permanentes du réseau international (IGS) qui se trouvent dans la région. On obtient alors dans un premier temps des vitesses relatives entre les stations intégrées dans le traitement; ce que l'on nomme une solution "libre" ou "non contrainte". A ce stade, il faut réaliser que les vitesses relatives par rapport aux stations régionales seront déterminées moins précisément que les vitesses relatives à l'intérieur du réseau local, parce que les distances entre stations sont plus grandes (figure 3). Dans un second temps on veut déterminer ces vitesses dans un référentiel donné: par rapport à une plaque par exemple. Pour ce faire il est nécessaire de connaître les vitesses des stations du réseau régional dans le référentiel en question, puis *d'imposer* que les vitesses déterminées soient exactement celles là. Dans un monde idéal et sans erreur, cela revient à appliquer une simple translation aux vitesses non contraintes (une rotation à la surface de la terre). Pour déterminer cette translation/rotation, il suffit de contraindre les vitesses non contraintes à prendre ces valeurs à-priori. En pratique, cette condition est extrêmement délicate à appliquer,

parce qu'il n'y a aucune raison pour qu'une vitesse déterminée par un certain nombre de points de mesure (campagnes) soit strictement égale à la vitesse déterminée sur une autre durée et avec un nombre différent de points de mesure.

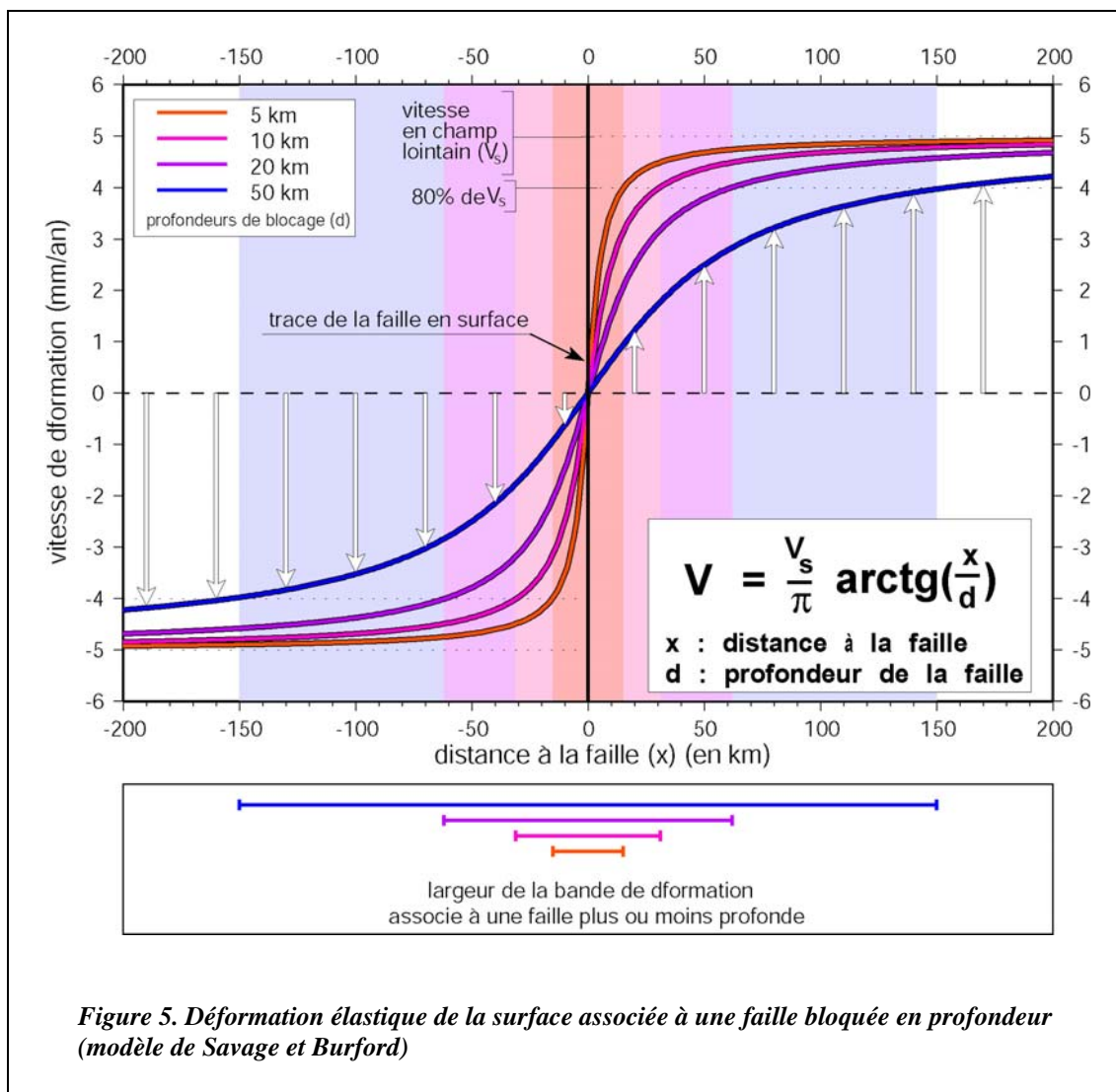


Cet effet est illustré par les séries temporelles de 4 stations du réseau IGS en Asie: Kittab (Ouzbekistan), Taïpe (Taïwan), Tsukuba (Japon) et Yaragadee (Australie) (figure 4). Les séries temporelles constituées d'un point par jour sont suffisamment "peu stables" pour que la vitesse déterminée par la différence de position aux dates de deux campagnes (octobre 1994 et Avril 1996) soit très significativement différente de la vitesse "long terme" de la station déterminée sur la totalité de sa série temporelle. La différence peut atteindre 100% à Taiwan, Kittab ou Tsukuba; seule Yaragadee est épargnée grâce à un déplacement très linéaire. Que cela soit du à une cause réelle (véritable mouvement du sol à un moment donné) ou à un artefact de la mesure (erreur troposphérique) importe peu: Forcer une vitesse à être égale à l'autre c'est déformer le réseau mesuré, les stations ne sont tout simplement pas là où elles devraient être. La mise en référence ne peut donc être réalisée en contrignant les vitesses des stations de référence mais en ajustant au mieux une rotation sur un sous ensemble de stations aux vitesses stables et bien définies (à supposer qu'elles existent). Le choix de ces stations est donc susceptible d'affecter la mise en référence. Le résidu après transformation donne une indication de la qualité de cette mise en référence.

## Les domaines d'application

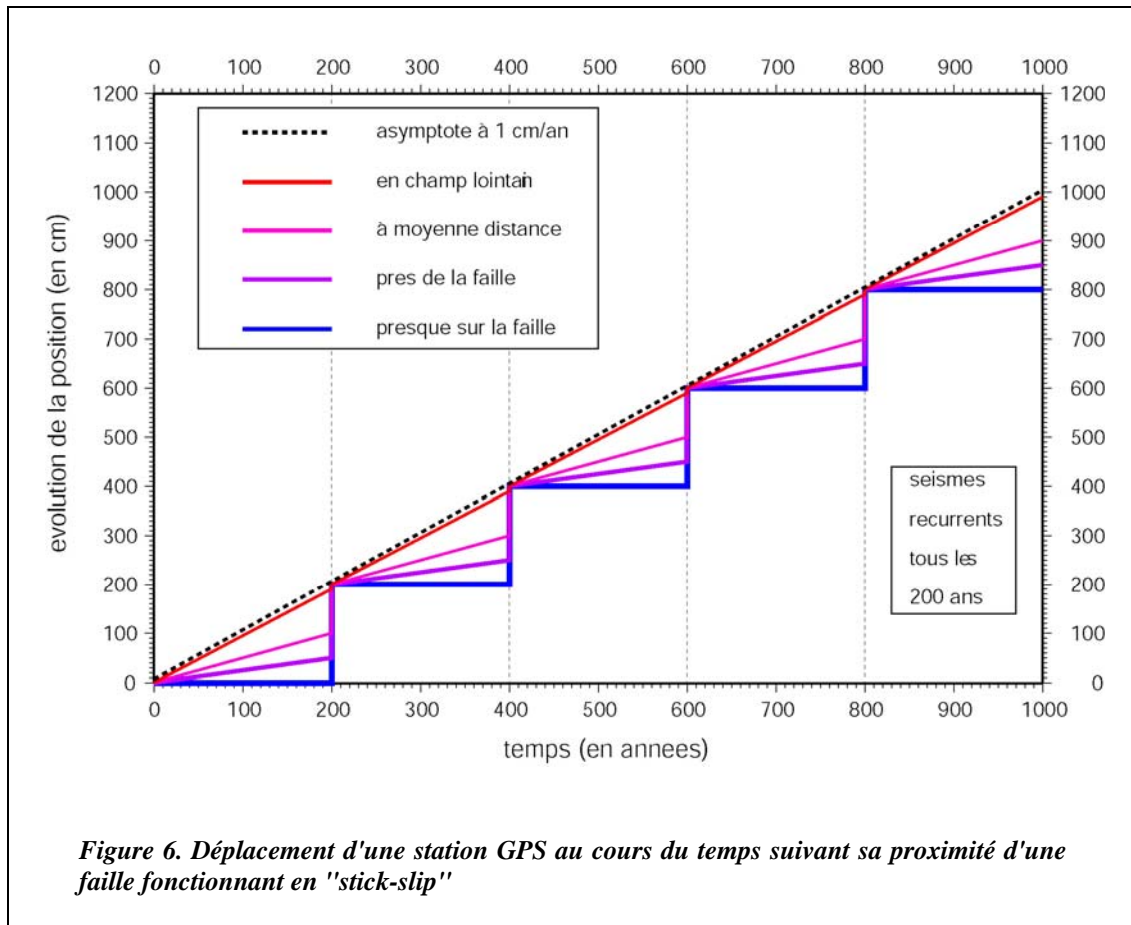
a) considérations sur le cycle sismique d'une faille en "stick-slip" et l'aléa sismique induit

Le modèle le plus simple de déformation est celui décrite par Savage et Burford. On considère qu'une couche élastique d'une certaine épaisseur (la croûte) est posée sur une couche visqueuse (le manteau). C'est le flux mantellique qui va déformer la couche élastique, localisant ainsi la déformation à l'aplomb du gradient des vitesses visqueuses.. Il est assez aisés de montrer que dans le cas simple d'une faille décrochante verticale la déformation obéit à une loi en arctangente. La déformation est concentrée dans une bande de part et d'autre de la faille. Plus la couche élastique est épaisse, plus la déformation est étalée en surface (figure 5).



Pour une faille plus générale, ce sont les équations élastiques d'Okada qui s'appliquent, mais le principe reste similaire. La variation des vitesses mesurées par GPS au long de profils de points géodésiques perpendiculaires à la faille permet donc de remonter à deux paramètres importants: la vitesse de la faille en champ lointain (et ce même si les points de mesure n'atteignent pas ce champ lointain), et la profondeur de blocage (c'est à dire l'épaisseur de la couche élastique qui accumule la déformation). Ces paramètres sont nécessaires (mais pas suffisant) pour déterminer le moment sismique des tremblements de Terre qui peuvent se produire sur cette faille.

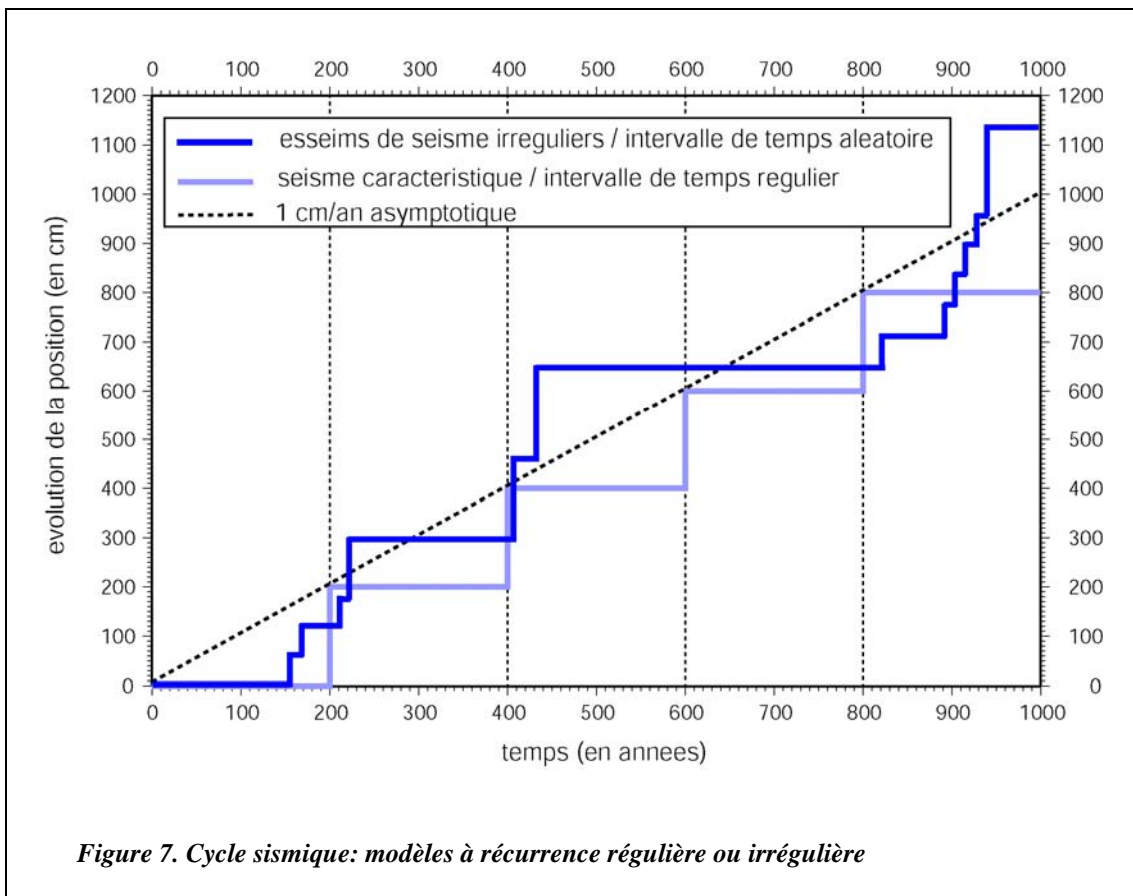
Ainsi, pendant l'intervalle de temps durant lequel la faille est bloquée, une station GPS enregistrera un déplacement quelconque entre zero et la vitesse long terme des plaques tectoniques suivant sa distance à la faille. Ensuite, la faille glissera par intermittence lors de séismes, et la station GPS rattrapera la déformation accumulée pendant l'intervalle de temps inter-sismique (figure 6).



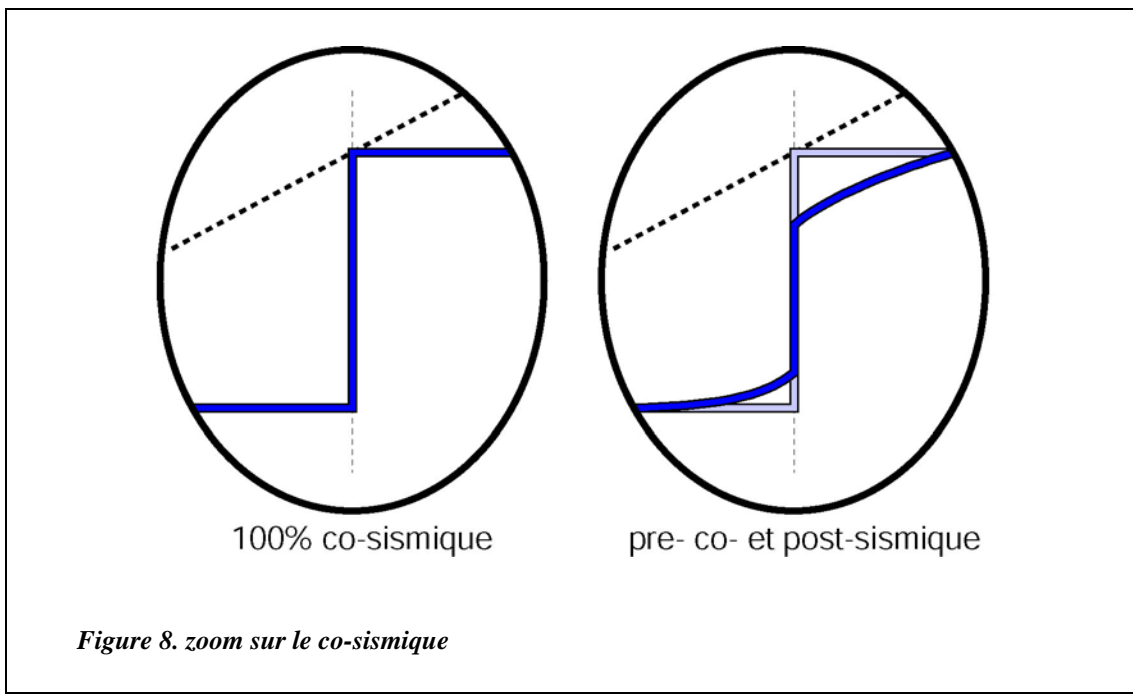
Dans le cas simple où l'on considère que les séismes vont se produirent à intervalle de temps réguliers et qu'ils vont relâcher toute la déformation élastique accumulée depuis le dernier séisme, il est relativement facile de calculer la date et la taille du futur séisme si l'on connaît la date du précédent bien sur. La vitesse de la faille donne la quantité de déformation accumulée et donc le glissement lors du prochain séisme. La profondeur de blocage permet d'estimer la surface du plan qui va rompre. Le produit des deux quantités est relié au moment sismique par un facteur "ad hoc" la rigidité ou coefficient de friction de la faille.

Dans la nature, les choses sont probablement plus complexes. Rien n'impose à priori qu'un séisme relâche toute la déformation disponible. On peut également supposer qu'une faille puisse accumuler de la déformation pendant un temps très long avant de rompre, puis de rompre plus fréquemment ensuite car "fragilisée" par ce premier séisme. Les séismes se produiraient alors en cascades (ou essaims) pendant un certain temps, jusqu'à "épuiser" le potentiel sismique de la faille, avant que le cycle ne recommence (figure 7). Il n'y aurait alors ni intervalle de temps régulier entre deux séismes (la récurrence) ni taille de séisme caractéristique des séismes produit par une faille donnée. C'est seulement sur un temps très long (la moyenne d'un grand nombre de cycles sismiques) que la somme des déplacements sismiques sur la faille doit être égal à la vitesse relatives des plaques. Il y a donc inévitablement des périodes durant lesquelles la faille va moins vite que la tectonique, et d'autres où elle va plus vite. On peut même imaginer des grands cycles plus ou moins réguliers au

cours desquels la faille va moins vite, puis accélère, puis va plus vite, puis ralentit, puis va de nouveau moins vite que la tectonique des plaques.



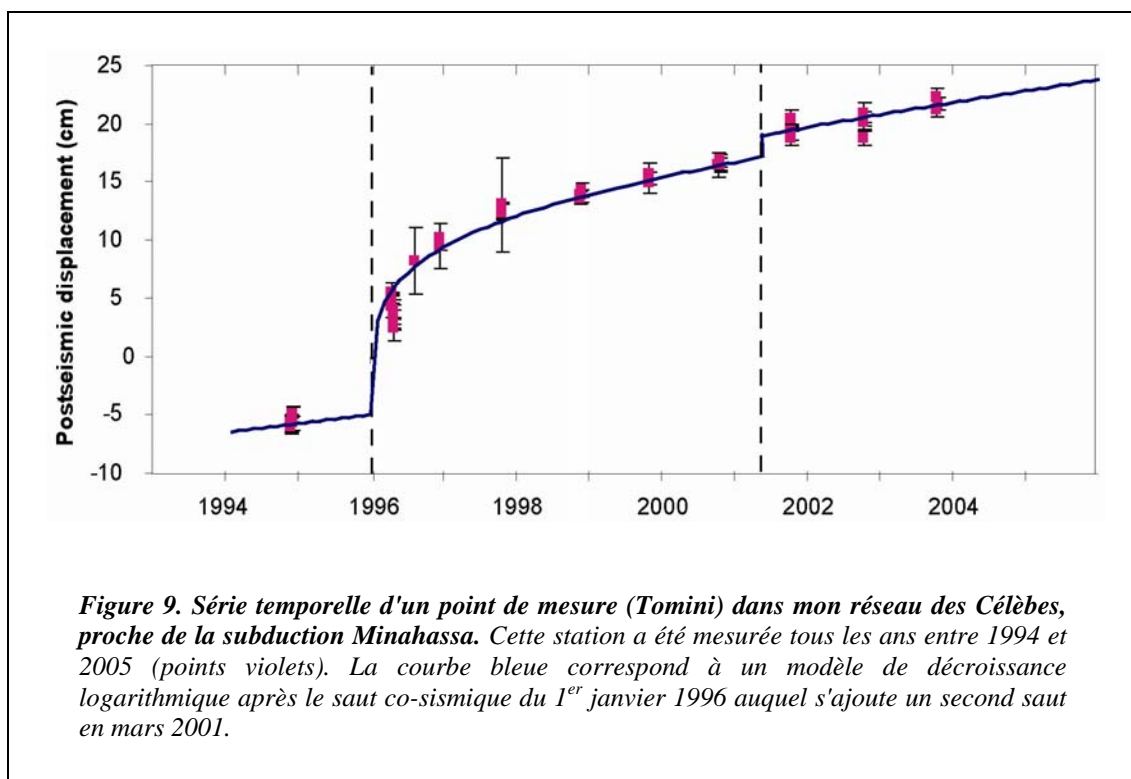
Dans cette optique, la détermination de la vitesse de la faille et de sa profondeur de blocage ne donne guère d'indication sur la date et la taille du prochain séisme.



Le seul espoir de "prédiction" réside dans l'analyse fine de la déformation pendant les périodes inter- et pré-sismique. En effet dans les modèles précédents, on considère que la faille est complètement bloquée (déplacement nul) pendant une très longue période d'accumulation, puis que la déformation accumulée est relâchée presque instantanément pendant le séisme. La encore, la nature est plus complexe que ce modèle simple. Les mesures GPS ont clairement montré (depuis Heki en 1997) que le co-sismique ne représente qu'une partie du relâchement de la déformation. Il existe des déformations post-sismiques qui peuvent s'étaler sur des temps très longs et qui au total relâchent autant de déformation que le séisme (figure 8). Si le post-sismique peut durer très longtemps, alors l'inter-sismique stable existe-t-il vraiment ? Y a t'il aussi des mouvements pré-sismiques précurseurs de la rupture ? Les mesures GPS extrêmement précises que l'on peut faire aujourd'hui peuvent contribuer à répondre à ces questions.

### b) Déformation post-sismique

On l'a vu, dans la zone de déformation d'une faille, la déformation n'est pas constante dans le temps. La courbe du déplacement au cours du temps d'une station située dans le zone de déformation (Tomini) de mon réseau des Célèbes, sur la subduction Minahassa (4 cm/an environ).le montre clairement (figure 9). Il est clair que la station n'a pas de vitesse stable parce qu'elle est affectée par des sauts co-sismiques intermittents (1996 et 2001) et des effets transitoires (post-sismiques du séisme de magnitude 8 de janvier 1996)



Trois constatations :

- si l'on ne corrige pas de ces effets, le taux moyen de déformation dépend de la période de temps sur laquelle on mesure.
- Le post-sismique sur 2 ans est d'amplitude au moins égale à celle du co-sismique. Ce résultat est tout a fait comparable à ceux obtenus sur la zone de subduction Japonaise lors de la séquence de Sanriku-haruka-Oki en 1994 (Heki et al, 1997).

- Y a-t-il un régime permanent ? on peut en douter au vu de cette figure. Rien ne dit que le dernier segment de mesures (2001-2002-2003) ait vraiment atteint une asymptote linéaire. Du coup, il serait tout simplement impossible de mesurer le taux long terme "tectonique" avec des campagnes intermittentes. Seul un modèle (la loi de puissance en bleu), construit sur des mesures continues (ou souvent répétées) permet d'estimer le taux à long terme une fois évalué les sauts co-sismiques et les relaxations post-sismiques. Le modèle serait évidemment mieux contraint par des mesures continues qui seules permettent de séparer exactement le co-sismique du post-sismique

### c) Déclenchement de séisme

Sur la faille de Palu, le même phénomène est également visible sur les 2 composantes horizontales de la ligne de base entre deux stations de part et d'autre de la faille (figure 10). Après le séisme du 1<sup>er</sup> janvier 1996, de la déformation supplémentaire se superpose à celle établie en régime permanent: 2 cm en co-sismique, puis encore 2 cm en post-sismique pendant environ deux ans. Ensuite, le mouvement redevient normal. Ce qui est plus étonnant c'est le comportement de la faille pendant cette durée de 2 ans : alors que normalement la faille est en compression (la distance entre les stations diminue au cours du temps), le mouvement s'inverse pendant deux ans !

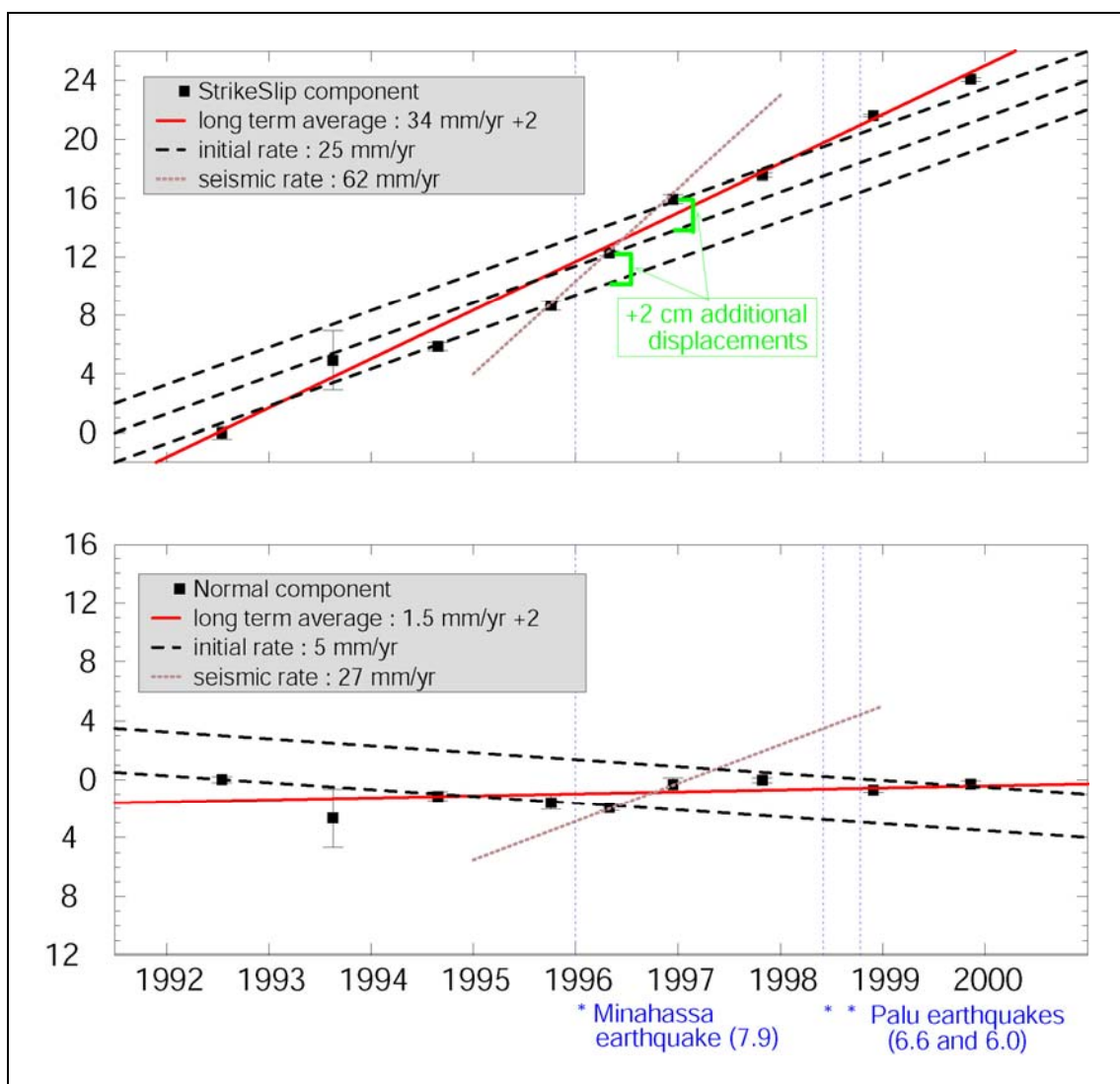


**Figure 10. Série temporelle de la ligne de base au travers de la faille de Palu (faille des Célèbes principalement décrochante à environ 4 cm/an)** Cette ligne a été mesurée tous les ans entre 1992 et 2000. Le panneau supérieur montre la composante parallèle à la faille, le panneau du bas la composante perpendiculaire.

La modélisation de la contrainte de Coulomb, montre qu'en effet, le séisme du 1<sup>er</sup> Janvier induit une augmentation de la contrainte cisaillante sur la faille et une diminution de la contrainte normale à la faille : c'est le phénomène d' "unclamping ", qui peut être la source du déclenchement de deux plus petits séismes, qui se produisent sur la faille à la fin de cette période anormale d'ouverture. Il est clair qu'il n'est pas très facile de quantifier les phénomènes de déformation post-sismique, transfert de déformation, ou encore déclenchement de séisme, à partir de mesures de campagnes annuelles. C'est pourquoi j'ai développé en collaboration avec le DUT de Delft un réseau de stations permanentes pour mesurer la déformation en continu (un point par jour), au cas où un autre événement de ce type se produirait. Le grand nombre de séismes sur la subduction Minahassa permet d'espérer un tel enchaînement dans un futur proche. Grâce à des mesures continues simultanées sur la subduction et la faille, il sera alors possible de suivre le transfert de la déformation d'une structure à l'autre.

#### d) Déformation a-sismique, séismes lents

En 2001, Dragert et al, découvrent que des « bulles de déformation » traversent leur réseau GPS permanent dans l'Ouest Canadien (sur la subduction des cascades). Ces « bulles » se manifestent comme des petits sauts (quelques mm) dans les séries temporelles des stations. Dans un premier temps, ces sauts sont attribués à des erreurs de mesures. Puis l'évidence s'impose, en particulier grâce à la cohérence spatio-temporelles de ces sauts : il s'agit d'une zone de déformation qui voyage au travers du réseau. Ces « pulses » se reproduisent à intervalles plus ou moins réguliers. Leur origine est discutée, mais l'hypothèse selon laquelle il s'agirait de glissements a-sismiques dans la zone de transition ductile-fragile le long de l'interface de la subduction semble solide. Pour l'instant, aucun séisme majeur ne s'est produit sur la partie fragile de la subduction mais à l'évidence la question est de savoir si une telle rupture pourrait être déclenchée par l'un de ces épisodes de glissement en profondeur.

De tels événements étaient inconnus il y a à peine 3 ans. Ils n'ont pu être mis en évidence que grâce à un réseau de stations GPS permanentes dense et précisément calculé. Le réseau des cascades était le premier à permettre cela. Des résultats encore plus récents (Larson et al, pers. Com.) semblent montrer que de tels événements se produisent également le long de la subduction mexicaine. La station permanente que j'ai installé en Indonésie montre également un glissement lent anormal sur une période de quelques mois. Or ces différentes subductions ne fonctionnent qu'à 2 ou 3 cm/an. Mon objectif est de développer un réseau permanent sur la subduction dans une région du Chili (7 cm/an !) pour laquelle l'amplitude de ces phénomènes (s'ils se produisent bien partout) devrait être au moins double. Le fait de positionner le réseau dans une lacune actuelle devrait permettre de confirmer ou infirmer le lien de causalité possible entre glissements a-sismiques dans la zone de transition et rupture dans la zone fragile.

#### e) Co-sismique

En cas de séisme important, la déformation co-sismique quasi instantanée atteint en surface des ordres de grandeur qui la rende aisément détectable et mesurable par GPS. Quantifier la déformation co-sismique est un objectif réalisable au moyen de réseaux de repères, mesurés de

temps en temps (pour refaire régulièrement un "état zéro") et remesurés immédiatement après le séisme. On obtient ainsi quantité d'informations sur la rupture en profondeur (longueur, profondeur, répartition du glissement, etc...). L'interférométrie RADAR est également très bien adaptée à cet objectif, avec quelques réserves importantes malgré tout :

- qu'un satellite passe suffisamment peu de temps après la rupture pour que la mesure soit purement co-sismique. Avec un temps de retour typique de l'ordre de 15 jours, on ne peut plus distinguer entre co-sismique, after-slip, et post-sismique. le cas du séisme d'Izmit est typique de cette difficulté
- que le séisme ne soit pas trop gros. On ne peut obtenir des franges de déformation cohérentes que si la déformation est inférieure à un certain gradient. Avec une longueur d'onde RADAR de quelques cm et une taille de pixel de quelques centaines de m, la limite est très vite dépassée en champ proche pour des séismes importants ( $Mw > 8$ )
- que le couvert végétal ne soit pas trop dense

C'est pourquoi les deux techniques sont très complémentaires.

Malgré tout, avec le GPS il est possible d'aller bien au delà de la simple mesure du déplacement co-sismique total. Il faut pour cela disposer de stations permanentes fonctionnant en continu. Il est alors possible de mesurer leur position à chaque instant de l'acquisition sur les satellites (30s usuellement, mais facilement portable à 1s), c'est à dire *pendant* le séisme. La précision que l'on obtient alors sur la position est évidemment légèrement moins bonne que celle obtenue par le cumul de 24h de données, mais les méthodes de "Precise Point Positioning (PPP)" qui s'affranchissent de la formation explicite des doubles différences permettent d'atteindre le cm, et ce quelle que soit la distance entre les stations. Une station GPS devient alors une sorte de sismographe très basse fréquence, qui mesure directement le déplacement (ni l'accélération, ni la vitesse) et qui a l'avantage de ne jamais saturer. Le cas du séisme de Sumatra est un exemple spectaculaire de ce qu'il est possible de faire (figure 11).

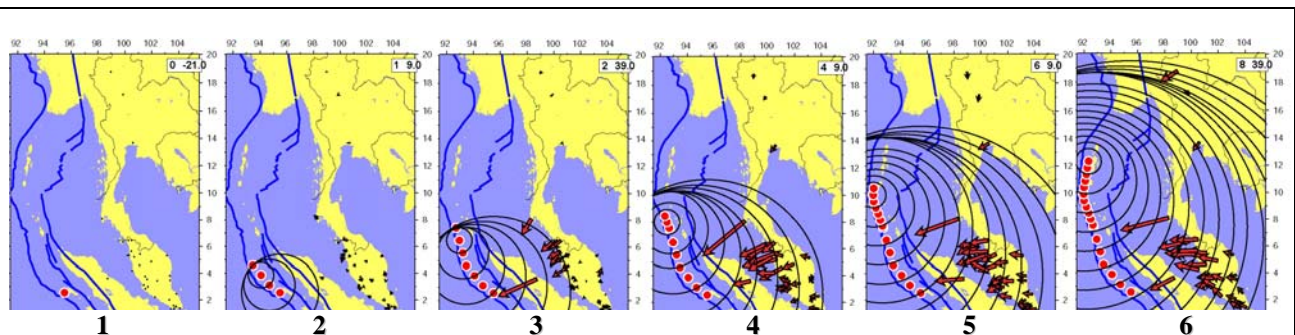


**Figure 11.** Traitement cinématique des données (extraits de la séquence à une image toutes les 30s) qui montre la propagation de la rupture contrainte par les déplacements mesurés aux stations GPS:

1. avant l'initiation de la rupture
2. la rupture se propage, mais les ondes de surface ne sont pas arrivées aux stations
3. les stations Malaises et Thaï bougent quand les ondes arrivent. Le déplacement initial de Phuket est vers le SSW, dans la direction de la zone où la rupture a commencé
4. Le vecteur déplacement de Phuket tourne en sens horaire au fur et à mesure que la rupture monte vers le Nord.
5. les ondes de surface arrivent seulement maintenant à Bangkok et sur le continent: la rupture a ralenti
6. les stations ont atteint leur position finale

Ces données uniques au monde, montrent quantité de choses:

- les stations bougent quand les ondes de surfaces (et non pas les ondes de volume) arrivent. L'incidence des ondes P et S à une distance supérieure à quelques centaines de km est sub-verticale. De ce fait le passage de l'onde P correspond à un mouvement vertical. Il n'est pas surprenant de ne pas en trouver trace dans les composantes horizontales du GPS (les seules

suffisamment précises pour être utilisées). Pour l'onde S, la raison de l'absence de sa détection est certainement plus complexe et probablement liée au très fort sous-échantillonnage du signal (1 point toutes les 30s pour un signal à 50 Hz)

- Phuket bouge d'abord vers le Sud (la direction de l'épicentre) puis tourne vers l'Ouest au fur et à mesure que la rupture monte vers le Nord. C'est entre autres la vitesse de rotation de ce vecteur qui permet de quantifier la propagation de la rupture à 3.7 km/s
- L'instant où les stations du Nord de la Thaïlande (Chiang Mai par exemple) bougent impose que la rupture s'arrête temporairement (environ 30s mais avec une grande incertitude) vers 7°N puis repart plus lentement sur le segment Nord à environ 2 km/s. L'inversion des données statiques montre que vers cette latitude on trouve également une zone de l'ordre de la centaine de km de long où le glissement est très faible, sinon nul. Enfin, cette zone correspond à l'intersection de la ride à 90°E (la frontière entre les plaques Inde et Australie) avec la fosse de subduction. Il s'agit donc du point triple entre les trois plaques en présence. Le scenario du franchissement de la frontière de plaque par déclenchement plutôt que par propagation de la rupture est construit sur cette triple constatation.
- 10 minutes après le début de la rupture, plus rien ne bouge, ce qui exclue l'hypothèse du séisme lent

## Conclusion

Pour tous les objectifs décrits plus haut, j'ai donc commencé à développer des réseaux GPS continus sur trois chantiers :

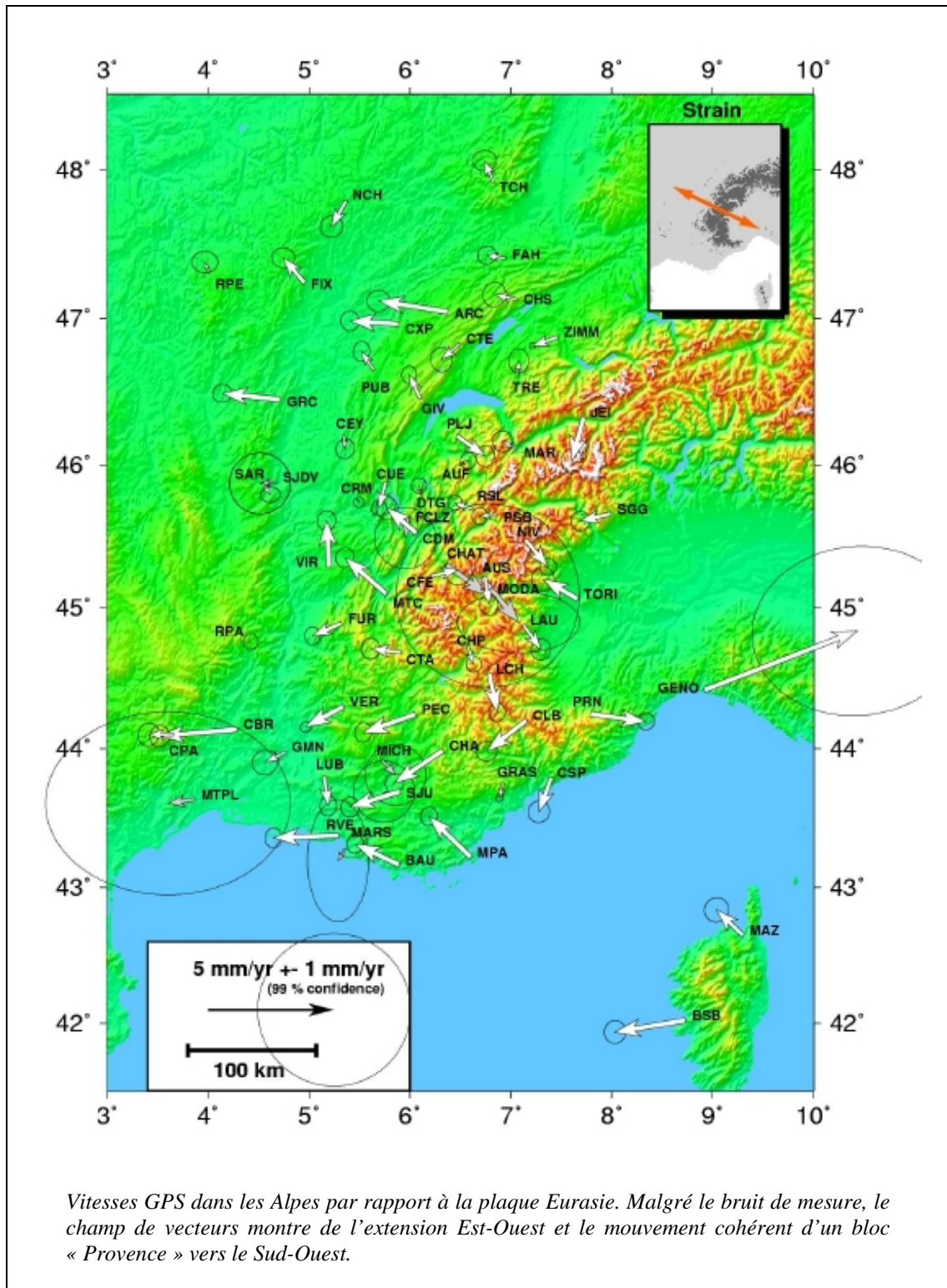
- En **Indonésie** sur la **faille de Palu** : **7 stations** depuis fin 1999
- En **Afar** (en collaboration avec l'IPGP) : **4 stations** installées de part et d'autre du **rift** en mars 2003.
- Au **Chili** (en collaboration avec l'IPGP et le DGF), sur la lacune sismique de **Concepcion-Constitucion** : 3 stations selon un profil perpendiculaire à la côte, et sur la lacune de **Coquimbo** : 4 stations. L'objectif (couvert par un projet ANR) est d'arriver à plusieurs dizaines de stations couvrant près de 1000 km de la subduction.

L'intérêt de travailler sur ces 3 chantiers en parallèle provient du fait qu'ils correspondent à des contextes tectoniques très différents. Une grande faille décrochante (Palu en Indonésie), une zone en extension (le rift d'Asal à Djibouti) qui est presque au stade de la dorsale aujourd'hui, et une grande subduction (au Chili). L'avantage de la subduction provient de sa géométrie oblique : elle produit un signal en 3 dimensions avec un mouvement vertical qui permet de contraindre la déformation. L'inconvénient est double : la moitié du problème est sous la mer, et l'on ne peut jamais s'approcher à moins d'une dizaine de kilomètres de la faille. Cet inconvénient n'existe pas dans le cas d'une faille décrochante pour laquelle on peut placer des stations jusqu'à exactement sur la trace de la faille en surface. Dans le passé récent, certains ont pu argumenter qu'il n'y a pas de mouvements transitoires sur ces failles continentales compte tenu de la faible profondeur sismogénique. La découverte récente de trémor sur la faille de San Andreas m'incite à continuer à penser le contraire et à persévéérer. Enfin, l'extension d'une dorsale naissante comme en Afar est très différentes des deux cas précédents car on se trouve en présence de lithosphère océanique pratiquement sans croûte continentale élastique et fragile. Malgré tout, là aussi, on trouve des épisodes de déformation transitoire dus à l'injection intermittente de magma depuis les profondeurs.

Il est donc essentiel de développer les réseaux GPS permanents de manière à apporter des éléments essentiels à la compréhension des mécanismes de déformation sur les failles et de sismo-génèse. Je pense réellement que nous sommes sur le point d'être capable de "voir les séismes arriver" à défaut de les prédire longtemps à l'avance.

## Les Alpes

Contexte : Le projet GPS-Alpes a été initialisé par Jean Chéry et moi-même en 1992 en collaboration avec un grand nombre d'équipes françaises ainsi qu'italiennes (ING Roma) et Suisses (ETH Zurich). Avec JC Ruegg et P. Briole de l'IPGP et T. Duquesnoy de l'IGN, nous avons défini le réseau, monumenté la soixantaine de sites. Nous avons ensuite organisé et réalisé les campagnes de mesures (en 1993 sur financement INSU, en 1998 sur financement Geofrance-3D, en 2004 sur financement du GDR G<sup>2</sup> et de DYETI).



Les vitesses calculées sur la période 1993-1998 montrent à l'évidence que la collision n'est plus le moteur de la déformation dans les Alpes puisque l'on mesure une faible (quelques mm/an) extension Est-Ouest à défaut de tout autre type de mouvement. Ce type de déformation correspond probablement à un « effondrement » gravitaire post-orogénique et est assez compatible avec la sismicité récente (Sue et al.), notamment autour de l'arc Briançonnais. Le seul endroit qui montre du raccourcissement est situé dans le Massif des Maures, alors qu'un bloc provençal semble s'échapper vers l'Ouest. Il est difficile d'estimer des vitesses sur des failles en raison de leur vitesse extrêmement faible (< 1 mm/an) largement inférieure au niveau de précision atteint pour l'instant. Par contre le grand nombre de points mesurés permet de calculer un tenseur de déformation moyen qui présente une certaine cohérence : on obtient une extension perpendiculaire à l'axe de la chaîne de  $3.5 \cdot 10^{-9}$  /an. Comment interpréter de l'extension dans une chaîne comme les Alpes ? Plusieurs hypothèses sont possibles :

- En premier lieu il faut constater que la collision Afrique-Asie, donnée à 6 mm/an en méditerranée occidentale par Nuvel-1a est un peu réduite: les mesures GPS actuelles dans la région donnent plutôt 4 mm/an.
- En second lieu, on peut conclure que l'absence de raccourcissement N-S dans les Alpes, et jusqu'au bloc Corso-sarde, implique que ce mouvement Afrique-Eurasie est accommodé à l'heure actuelle en Afrique du Nord, dans les maghrébides par exemple. Les séismes d'El Asnam et plus récemment de Boumerdes en Algérie étayent cette hypothèse.
- Une fois l'absence de compression N-S expliquée, il reste l'extension E-W, qui peut être due à un mécanisme d'étalement gravitaire ou au poids de la lithosphère Européenne qui agirait comme une force de type "slab pull" et induirait des forces extensives en surface.

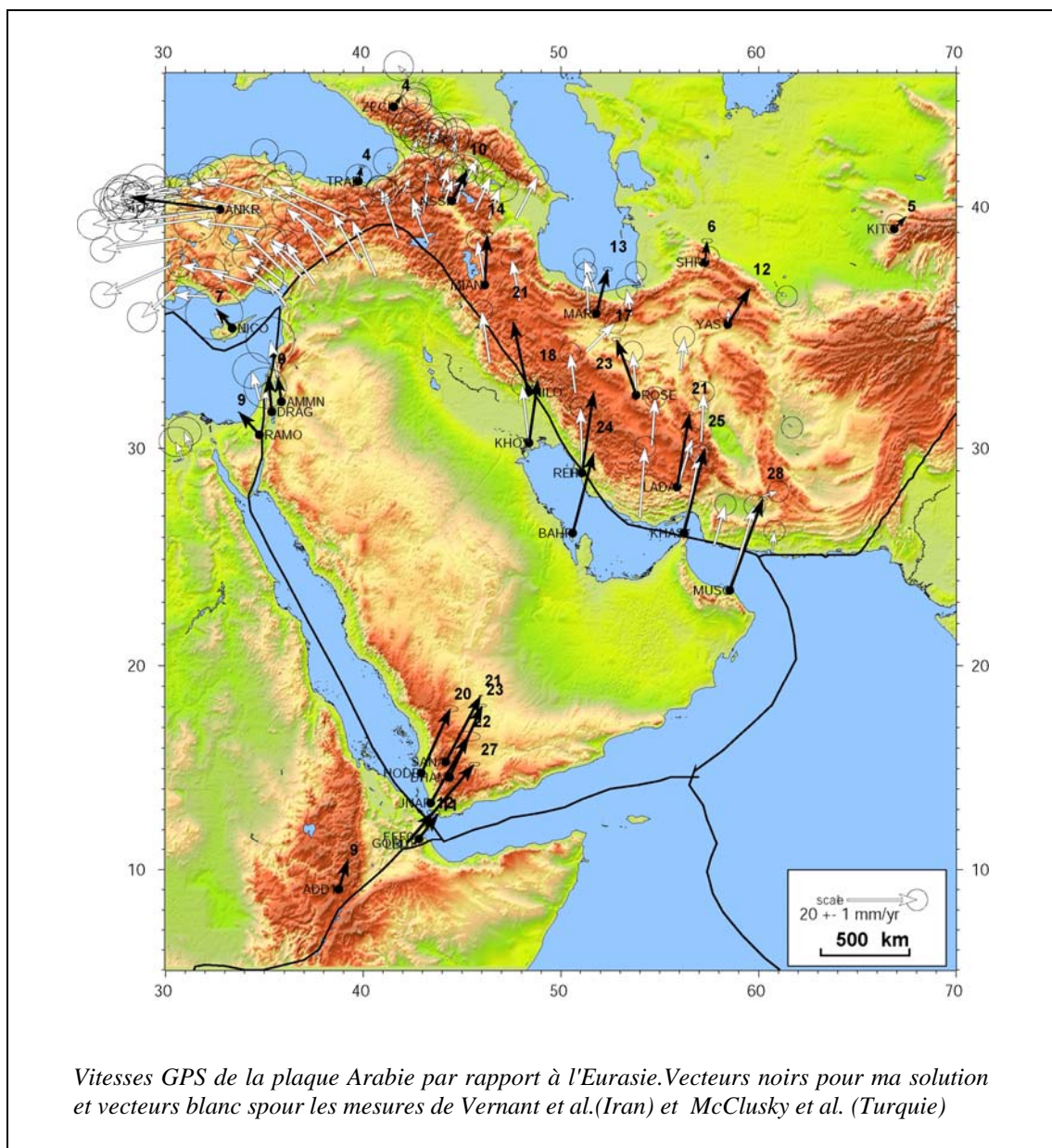
En tout état de cause, il convient d'être prudent sur les mécanismes: la mesure d'un étalement, peut être gravitaire, en surface n'est pas forcément en contradiction avec de la convergence en profondeur !

Nous avons procédé en juillet 2004 à une deuxième remesure du réseau, 11 ans après la première campagne de 1993 et 6 ans après celle de 1998. Ceci afin de quantifier les erreurs à long terme et de mieux déterminer les vitesses de déformation : la pente d'une droite est toujours mieux déterminée par 3 points que par 2 seulement, et c'est encore plus évident pour son incertitude. Les premiers résultats sont plutôt décevants: dès qu'un point semble avoir une vitesse supérieure à 1 mm/an, une analyse attentive des données montrent qu'il s'agit d'une erreur due à une antenne défectueuse. Ce problème c'était déjà posé en 1993 et est réapparu en 2003. Une mesure de calibration de l'antenne incriminée permet de déterminer précisément son décalage.... et annule le déplacement constaté. Peut être touche-t-on là aux limites des campagnes pour la mesure des déformations extrêmement faibles, et qu'il faudra attendre plusieurs dizaines d'années avec des remesures régulières avant de pouvoir exploiter les résultats en termes de mouvement sur des failles identifiées et d'aléa sismique.

## **Plaque Arabie – Afar – Iran - Inde**

Contexte : le projet GPS-Afar a été initialisé par JC Ruegg de l'IPGP. J'ai participé à toutes les campagnes de mesures depuis 1991, et j'ai également réalisé le traitement des données GPS dès qu'elles dépassent l'échelle du rift. Depuis le départ à la retraite de JC. Ruegg, je coordonne la suite du projet, avec notamment un financement IT pour la réalisation d'un programme de mesures GPS-nivellement-gravi-marégraphe, et un financement CNES (avec JB de Chabalier) pour la réalisation d'un réseau GPS continu de 4 stations. Je coordonne également les mesures en dehors du Djibouti, c'est à dire essentiellement au Yémen.

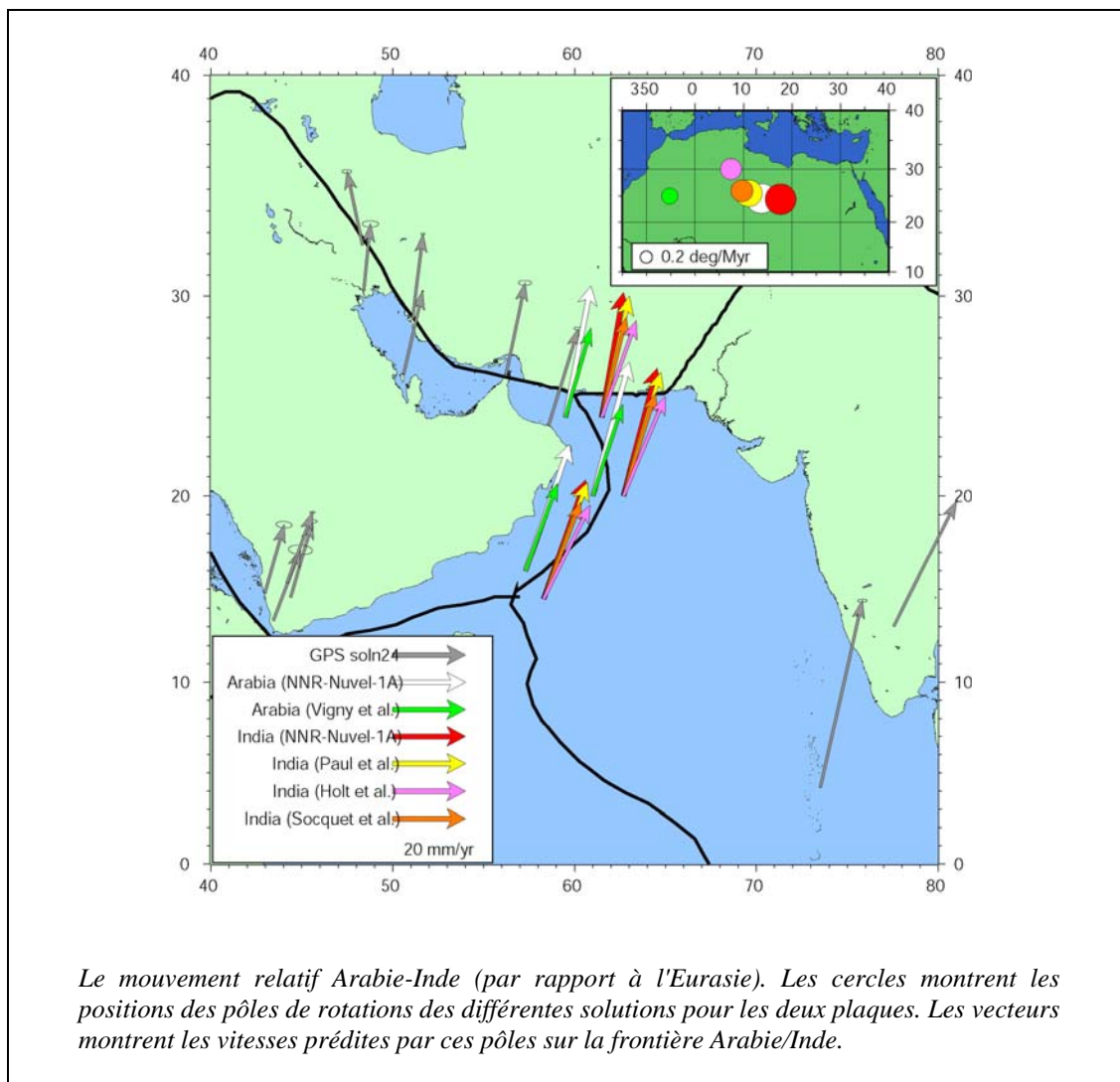
Dans le cadre d'un second projet (IT IRAN) mené par D. Hatzfeld du LGIT Grenoble , j'ai participé à la première mesure d'un réseau géodésique en Iran (fin 1999) et à sa remesure fin 2001. Le but de ces mesures est de quantifier la déformation dans différentes régions de l'Iran : Alborz, Zagros, Makran, dans un contexte de vitesses géologiques de plusieurs cm/an. De ce fait, le projet intègre des stations sur la plaque Arabie, en Oman. Des données Iraniennes provenant du programme APRGP sont également disponibles sur la région depuis 1997. Elles consistent en une semaine de mesures tous les ans sur 6 à 8 sites répartis en Iran, dont certains sont situés pratiquement sur la plaque Arabie.



A cause des progrès des mesures en Afar, il m'est apparu très intéressant de combiner ces trois jeux de données afin de confirmer la rotation plus lente qu'attendu de la plaque Arabie. Cette vitesse relativement faible explique à la fois les taux faibles sur la faille du levant (5 mm/an Avouac et al.) et le déficit de déformation co-sismique dans le Makran Iranien.

Enfin, dans le cadre d'un troisième projet au Népal (IDYLHIM), initialisé par P. Le Fort et J.L. Munier du LGTS de Grenoble, j'ai participé à la première campagne de mesures GPS française dans la région et réalisé le traitement des données acquises avec celles, plus anciennes, du groupe de Boulder (Bilham et Larson) sur un sous ensemble de nos points. Ce projet avait pour but d'établir le taux de raccourcissement aux pieds de la chaîne Himalayenne. On obtient une convergence de l'ordre de 11 mm/an au pieds de l'Himalaya (seulement), avec une composante très légèrement divergente des deux cotés. De manière très intéressante, et contrairement aux attentes, les stations situées au pied de la chaîne ne semblent pas vraiment être dans une zone de déformation mais au contraire montrent une vitesse très similaire à celle des stations au centre de l'Inde (Bangalore ou Hyderabad). Du fait de ces propriétés, nous avons pu utiliser ces données pour déterminer un nouveau pôle de rotation pour la plaque Indienne.

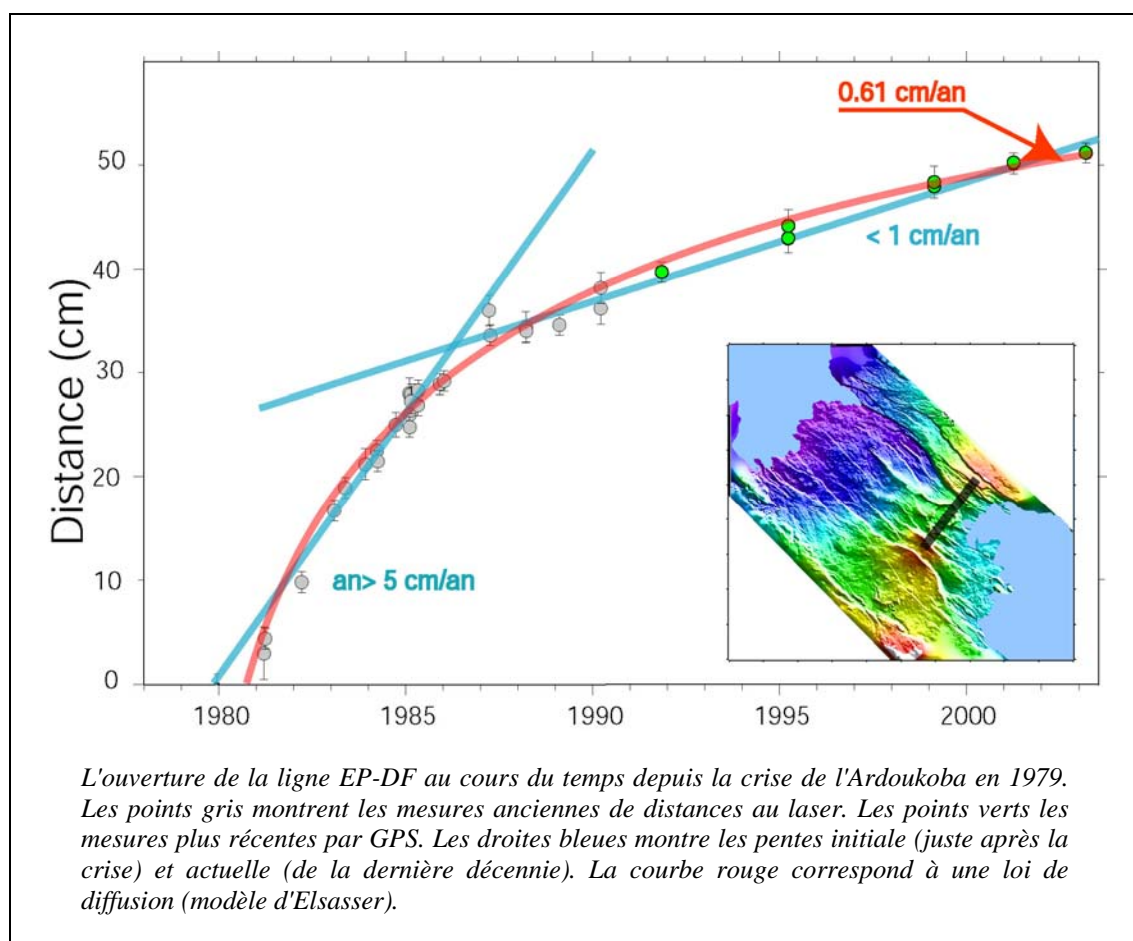
Dans les deux cas (l'Inde et l'Arabie) le GPS obtient un mouvement de convergence vers le Nord par rapport à l'Eurasie nettement et significativement plus faible que les prédictions de Nuvel-1a. Le point intéressant est que le ralentissement *simultané* de ces deux plaques permet de maintenir leur mouvement relatif qui correspond à un très faible cisaillement dans la "Owen fracture Zone", la frontière particulièrement peu active entre les deux plaques.



Depuis la première campagne en Afar (1991), et les mesures réalisées à trois reprises en 1993, nous avons acquis de nouvelles données en Mars 1995, Février 1997, Février 1999, Juin 2000, Mars 2001, et enfin Mars 2003. Ces données permettent de compléter la série temporelle des mouvements à l'intérieur du triangle Arta-Sana-Addis Abbeba. Nous avons mis en évidence un mouvement relatif de la station d'Arta par rapport au reste du bloc stable de Djibouti, plus ou moins en accord avec les modèles récents de la tectonique locale. Surtout, nous disposons maintenant d'un jeu de donné important (mesures dans le rift, mesures tout autour du golfe de Tadjoura, mesures au Yémen) qui permettent de :

- quantifier l'ouverture actuelle (c'est à dire en moyenne sur la dernière décennie) dans le rift:  $16 \pm 1$  mm/an orientés  $45^\circ\text{N} \pm 8^\circ$
- mettre en évidence des mouvements non stationnaires dans le temps à petite échelle (dans le rift) et grande échelle (autour du golfe de Tadjoura). Depuis la crise de l'Ardoukoba en 1979 durant laquelle le plancher du rift c'est ouvert de près de 2m, l'ouverture locale ne cesse de ralentir, passant de 6 cm/an en 1980 à moins de 1 cm/an aujourd'hui (voir figure).
- déterminer une vitesse de rotation de la plaque Arabie qui est sensiblement plus lente que ce qui est attendu : 13 mm/an au lieu de 17 mm/an prévu par Nuvel-1A au niveau de la dépression Afar.

Ces deux derniers points montrent que les vitesses varient dans le temps et dans l'espace. En effet l'ouverture actuelle du rift est toujours supérieure à l'éloignement des plaques tectoniques (Somalie/Arabie), et cela dure depuis 25 ans. Cette ouverture actuelle résulte de la conjonction de deux facteurs : extension à grande échelle à 11-13 mm/an et injection de magma par crises épisodiques dont la dernière est celle de l'Ardoukoba en 1979. Mais cette ouverture va diminuant comme le montre la mesure régulière d'une ligne (EP-DF) au travers du rift



Il est probable que l'on va bientôt atteindre un stade d'ouverture quasi nulle du rift, qui va alors recommencer à accumuler de la déformation élastique, susceptible de déclencher une nouvelle crise sismo-volcanique similaire à celle de 1979. Au rythme de l'éloignement entre les deux plaques (13 mm/an), on peut calculer qu'il faudra environ 200 ans avant d'avoir accumulé à nouveau 2m.

## **Asie du Sud Est: bloc de la Sonde, Birmanie, Indonésie, le séisme de Sumatra**

Contexte : Entre 93 et 98 j'ai été très fortement impliqué dans un projet d'acquisition de données GPS qui couvre toute l'Asie du sud-est (GEODYSSSEA). Ce projet (sous la direction de P. Wilson, GFZ Potsdam et de X. Le Pichon, ENS Paris) était une collaboration européenne et asiatique financée par l'UE. Nous avons installé un réseau d'une cinquantaine de points couvrant 7 pays de l'ASEAN (Indonésie, Malaisie, Thaïlande, Philippines, Vietnam, Brunei et Singapour) en 1993. Les premières mesures ont été effectuées en décembre 1994, puis une deuxième mesure en Avril 1996. Nous avons ensuite poursuivi nos efforts en réalisant une 3<sup>ème</sup> mesure du réseau (fin 98) en collaboration avec les instituts allemands partenaires (IFAG et GFZ). Puis une dernière mesure partielle en 2000 avec nos partenaires hollandais (DUT). Par ailleurs, nous avons développé un réseau dense sur l'archipel des Célèbes (Sulawesi) en Indonésie pour étudier en détail le point triple de la convergence Eurasie, Pacifique, Australie. Depuis 1997 j'ai installé une quarantaine de sites GPS dans cette région, sites qui sont mesurés régulièrement tous les ans avec nos partenaires Hollandais (DUT) et Indonésiens (ITB, BAKOSURTANAL). Dans ce cadre, nous avons développé un réseau de stations GPS permanentes (7 stations aujourd'hui, dont 3 de l'ENS) sur la faille de Palu, la grande faille décrochante des Célèbes qui accorde une partie de la convergence Pacifique-Eurasie à 4 cm/an.. Enfin, en coopération avec C. Rangin, j'ai développé le réseau SE-Asiatique au-delà des pays initiaux : en Birmanie.

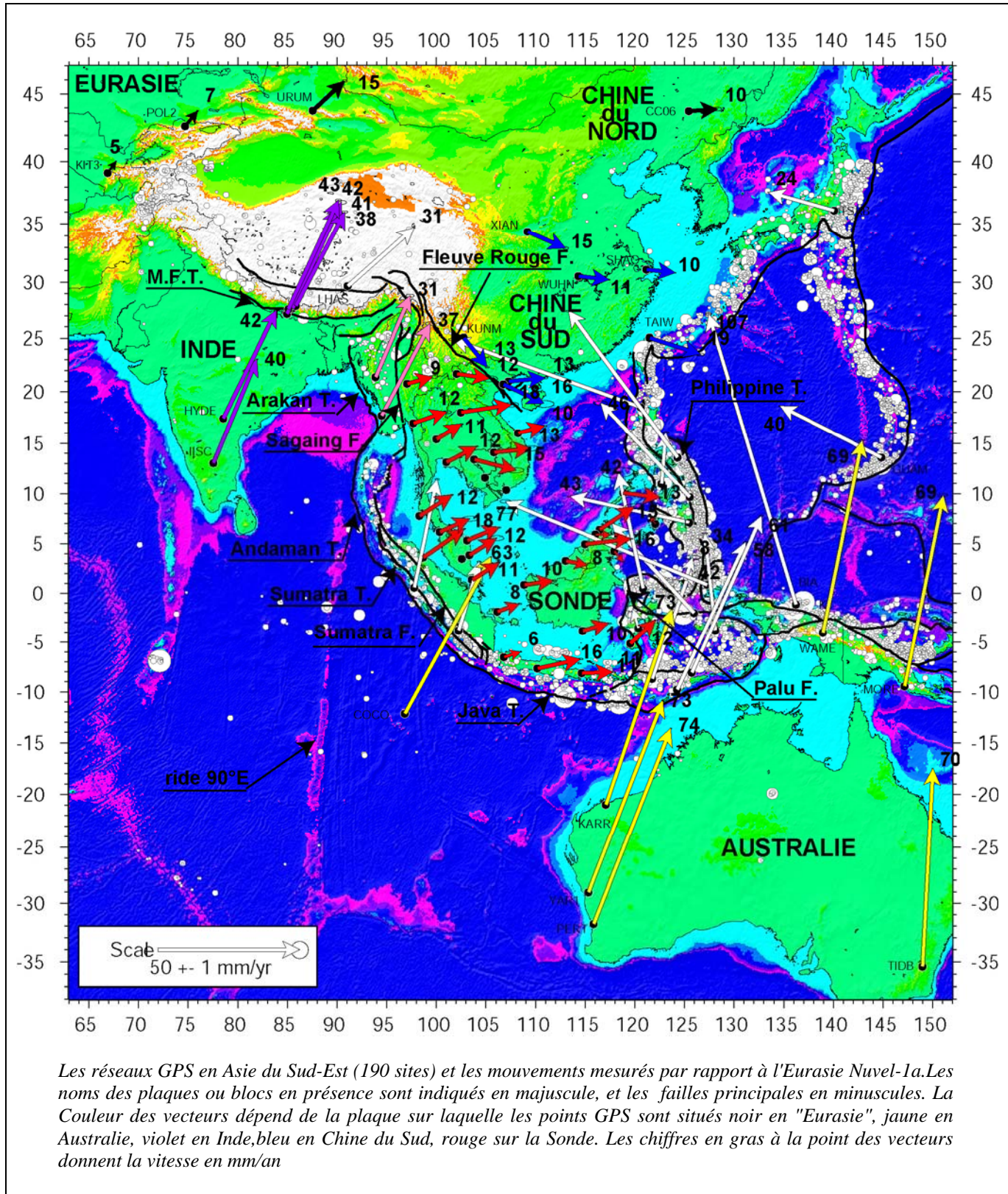
Depuis 2004 Nous avons développé avec nos partenaires Hollandais, Thaïlandais, Malais et Indonésiens un programme Européen de type "réseau et capital humain", le programme SEAMERGES. Il s'agit de faire de la formation et du transfert de savoir faire sur l'installation des réseaux GPS permanents, des campagnes et du traitement des données. C'est dans le cadre de cette coopération que nous avons continué nos travaux sur le bloc de la sonde et que nous sommes intervenus sur le séisme de Sumatra du 26 décembre 2004. Nous avons rassemblé et traité les données acquises par les agences nationales, complété par des campagnes de mesures ponctuelles là où c'était nécessaire (Thaïlande par exemple) et analysé la rupture avec un détail jamais atteint auparavant à l'aide du GPS dit cinématique.

### **Le bloc de la Sonde**

Depuis les mesures GEODYSSSEA, nous avons intégré les mesures APRGP (Asia-Pacific GPS Project) disponibles (au Vietnam, au Laos et au Cambodge en particulier) en sus des données des réseaux GPS permanents Malais "Department of Survey and Mapping Malaysia" (DSMM), Thaï "Royal Thai Survey Department" (RTSD), et Indonésien. Nous avons également incorporé les données disponibles en Inde, en particulier les campagnes de mesures que j'avais effectuée dans le cadre du projet IDYLHIM au Népal. Ce travail considérable (plusieurs centaines de stations mesurées sur une décennie entière) permet de montrer en détail la rigidité différente des deux blocs en contact (Inde très rigide et Sonde aux bordures plus déformées) et le mouvement relatif entre les deux blocs, à Sumatra et en Birmanie. En particulier, le mouvement de l'Inde est recalculé de manière plus précise grâce aux stations du Sud-Népal et à la station d'Hyderabad. Comme pour Sumatra, nous parvenons à mettre en évidence un effet de déformation élastique du à un blocage de la subduction sous l'Arakan, en Birmanie (prolongation vers le Nord des fosses de Sumatra et d'Adamant). Il y a donc là aussi un risque important de gros séisme de subduction, et potentiellement de Tsunamis destructeur.

Les mesures à grande échelle ont donc permis, entre autre, de mettre en évidence un mouvement autonome du "bloc de la Sonde" (en gros l'Indochine, bordée au nord par les failles de Sagaing en Birmanie, et du Fleuve Rouge au Vietnam et au Sud par les fosses de Java et Sumatra) par rapport à l'Eurasie d'environ 10 mm/an vers l'Est, mais aussi de montrer que le mouvement de l'Inde n'était que d'environ 35 mm/an vers le Nord par rapport à l'Eurasie. Une des raisons pour laquelle Il a fallu

attendre longtemps pour que ce mouvement soit considéré comme certain est que toute la région en fait est en déformation par rapport à l'Eurasie, y compris les stations au Nord du Tibet (comme Kittab en Ouzbékistan, ou POL2 au Kazakhstan par exemple). Le mouvement relatif de la Sonde par rapport à ces régions ou par rapport à la Chine du Sud est donc nettement plus faible que par rapport au cœur de l'Eurasie rigide, qu'il faut aller chercher sur le craton sibérien en fait.



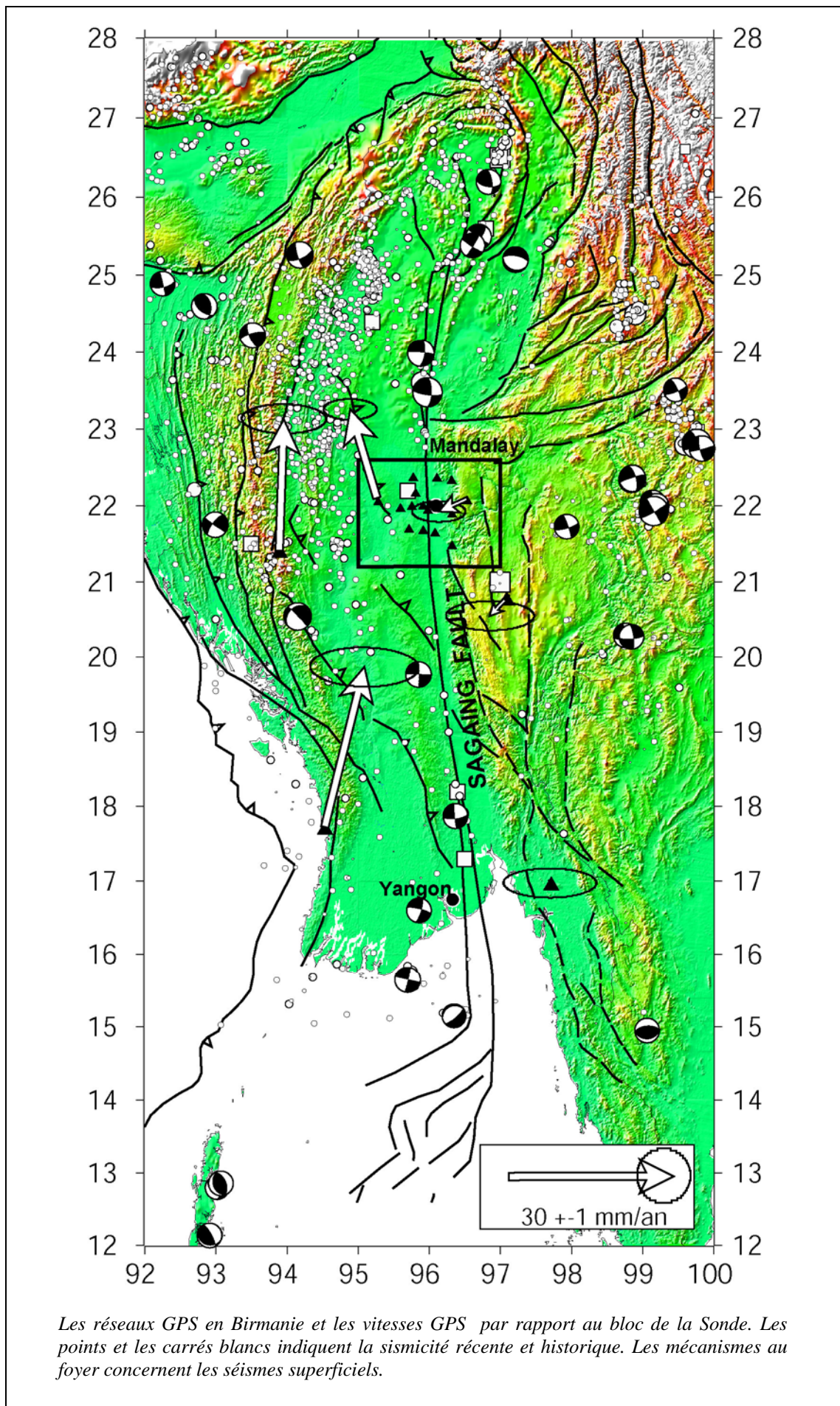
Tous ces réajustements ont un certain nombre de conséquences très importantes :

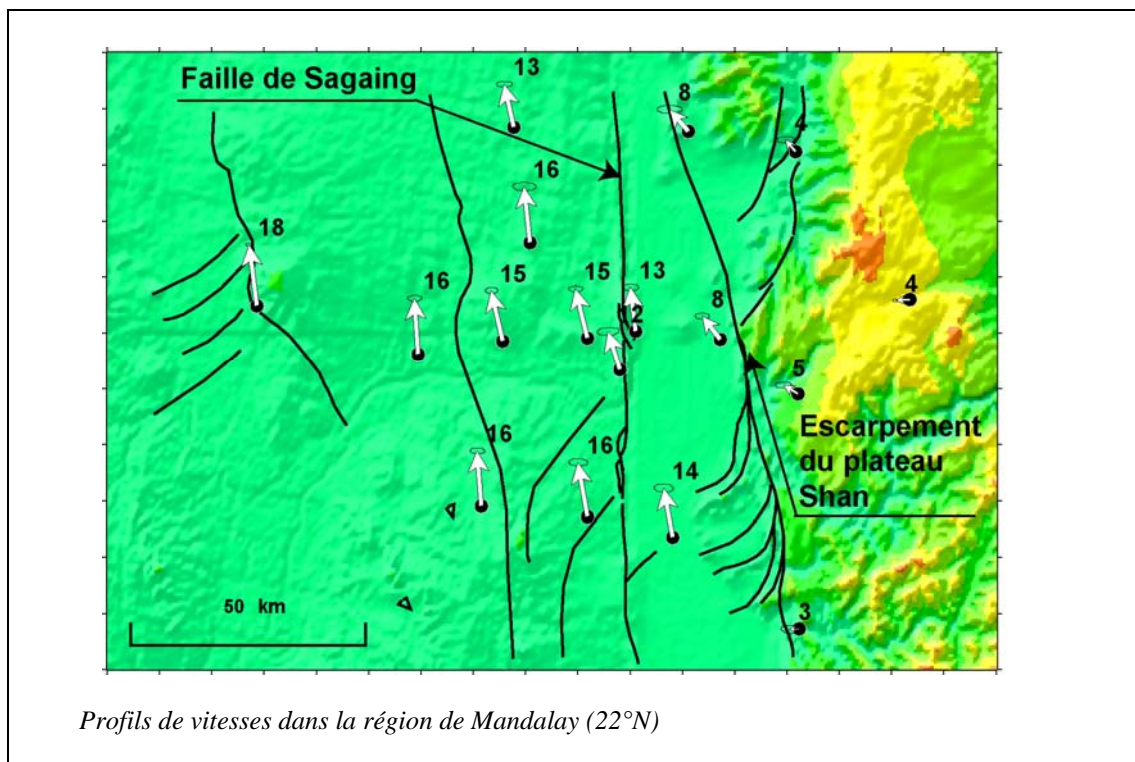
- les vecteurs glissements des séismes de la subduction Australie/Indonésie redeviennent alignés avec la direction de la convergence si l'on tient compte du mouvement du bloc de la Sonde
- Le mouvement relatif Inde/Sonde est revu à la baisse par rapport aux estimations initiales pour deux raisons principales : a) l'Inde est plus lente que prévue par Nuvel-1A, b) la Sonde n'est pas l'Eurasie fixe. De ce fait, le mouvement Inde/Sonde est très significativement du mouvement Australie/Sonde, avec un différentiel de vitesse de l'ordre de 2 cm/an au passage de la frontière Australie-Inde: la ride à 90° Est. Le mouvement Inde-Sonde est accommodé par un partitionnement complexe:
  - Au Sud, partitionnement total entre le décrochement sur la grande faille de Sumatra et la convergence sur la fosse de Sumatra.
  - Au nord, partitionnement partiel entre le décrochement sur la faille de Sagaing (à 2cm/an seulement) et la convergence oblique sur la fosse de l'Arakan
  - Entre les deux, le décrochement est accommodé par l'extension du rift en mer d'Andaman, sans que l'on sache très bien à quelle latitude exactement la convergence sur la fosse devient oblique.

Le mouvement Chine du Sud / bloc de la Sonde est lui aussi considérablement réduit et devient compressif (8 mm/an) avec une légère composante dextre de quelques mm/an au Nord de la faille du fleuve Rouge. On peut débattre longuement pour savoir si le mouvement mesuré à l'actuel sur la faille du fleuve rouge est significatif ou non. Ce qui est certain, c'est que les deux blocs (Chine du Sud et Sonde) bougent tous les deux vers l'Est par rapport à l'Eurasie avec une vitesse proche et de l'ordre du cm/an.

## **La Birmanie et la faille de Sagaing**

De manière à étudier complètement la déformation Inde-Sonde à plus petite échelle, j'ai également travaillé à l'extension du réseau SE-Asiatique en Birmanie. J'ai installé un réseau de points géodésiques en février 1997 autour de la faille de Sagaing, à la latitude de Mandalay, la deuxième ville du pays. J'ai ensuite organisé et réalisé les mesures de ce réseau en Octobre 1998 et Décembre 2000. Les résultats montrent que les points le plus à l'Est sont bien sur la partie stable du bloc de la Sonde et les points les plus à l'Ouest sont quasiment Indiens. De même, elles confirment que la faille est purement décrochante dextre, mais elle n'absorbe que 2 cm/an. Le reste de la déformation (3,5 cm/an entre l'Inde et la Sonde) est distribué sur d'autres structures, en particulier la subduction hyper-oblique sous l'Arakan. Nos modèles de rotations de blocs rigides séparés par des failles bloquées expliquent bien la déformation mesurée par GPS dans la région. Ils imposent un glissement oblique sur la fosse de l'Arakan, sans partitionnement (comme au Chili). Dans la région de Mandalay, la faille « oscille » entre le bord des bassins et l'escarpement du plateau Shan. Cette faille pose également un problème d'aléa sismique, puisqu'elle a produit de forts séismes dans le passé dans la région de Mandalay, et plus récemment (en septembre 2003) un séisme de magnitude 6.6 dans la région de Miktila (à mi chemin entre Yangon et Mandalay).

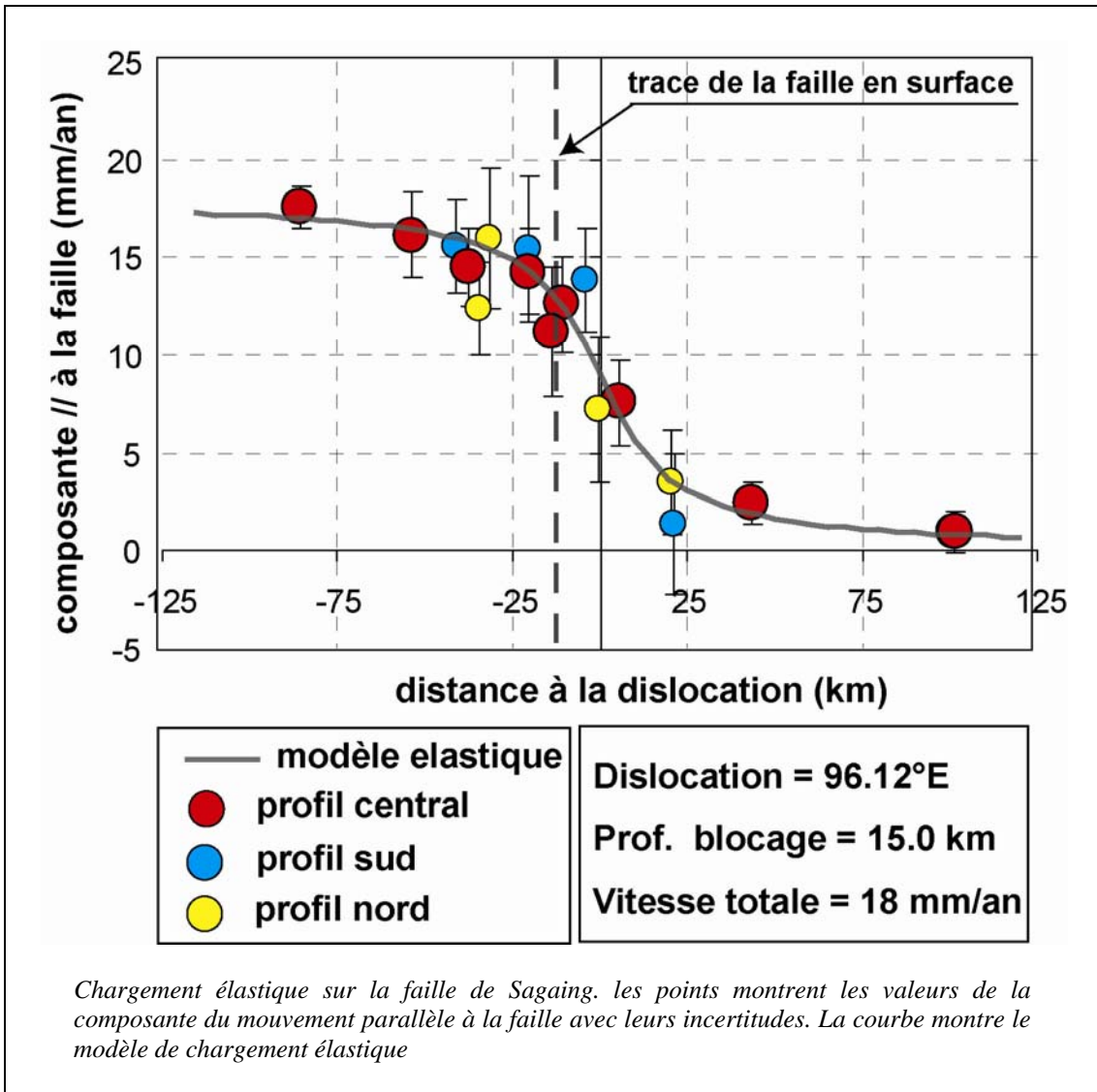




Notre étude sur la faille de Sagaing montre assez bien ce qu'il est possible d'obtenir quand on travaille dans les règles de l'Art, même si ce sont sur des durées assez courtes:

- tous les points sont des points à centrage forcé, grâce auxquels les antennes sont directement vissées sur le sol avec une précision sub-millimétrique.
- Quand les affleurements font défaut (ce qui est souvent le cas dans les bassins à l'Ouest de la faille) des bornes géodésiques ont été construites. Ce sont des pyramides de béton de  $1m^2$  de surface à la base et près de 2m de haut. Ces monuments sont très stables, au point que l'on ne peut discerner à-priori les mesures réalisées sur ces bornes de celles réalisées sur des affleurements rocheux.
- La disposition géographique des points est soigneusement réfléchie, en fonction de la déformation que l'on s'attend à mesurer. Ainsi un profil principal de 12 points est réalisé, avec un espacement faible entre les points en champ proche de la faille (quelques km), là où le gradient de déformation est important. Des stations lointaines (près de 100km) ont aussi été réalisées de manière à attendre le "plateau" de déformation à grande distance. Enfin deux profils supplémentaires de quelques points ont été réalisés à quelques dizaines du profil principal de manière à valider les mesures du profil principal en champ proche, et surtout pour permettre de calculer des tenseurs de déformation en deux dimensions.
- Les deux fois, le réseau a été mesuré longuement, avec une grande redondance, et le nombre de point fixes nécessaires pour assurer la conservation de l'échelle du réseau. Enfin, ce réseau "local" est intégré dans le réseau régional "bloc de la Sonde" par des mesures simultanées sur ces points lointains. Il est donc possible d'inverser les données à la fois pour la rotation des grands blocs rigides et le couplage élastique sur les failles.

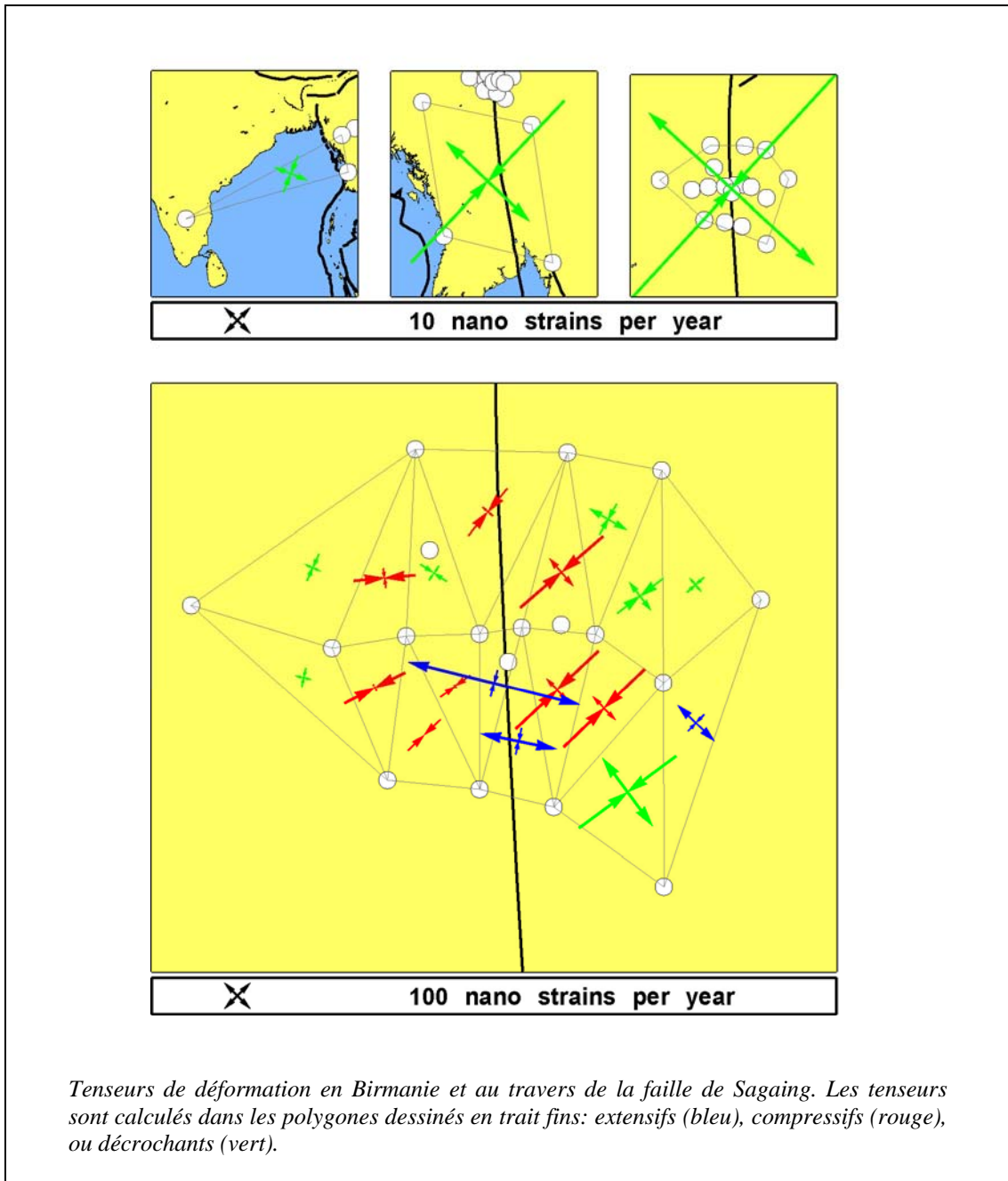
Tous ces éléments sont essentiels à la réalisation de mesures de bonne qualité. On les retrouvera dans mes autres réseaux, en particulier au Chili. Grâce à cela nous avons été en mesure d'obtenir des résultats fiables (un modèle de vitesse de la faille robuste, précis et crédible) alors que nous n'avons pu mesurer notre réseau qu'à deux reprises et à seulement deux ans d'écart. Ces résultats étaient suffisamment précis pour que la mesure 5 ans après des deux sites les plus au Sud permette de quantifier le déplacement co-sismique de quelques centimètres infligé par le séisme de Sumatra dans la région.



Le résidu entre le meilleur modèle de chargement élastique et les données est très faible : < à 1mm/an en moyenne sur les points du profil principal (points rouges). Lorsque l'on ajoute les points des deux profils supplémentaires (points bleus au Sud, points jaunes au Nord) on confirme la tendance au premier ordre et l'on devine un effet longitudinal: le profil Sud semble montrer un gradient plus fort que le profil Nord. Cela pourrait être du à une profondeur de blocage variable au long de la faille, mais il est clair que l'on touche là aux limites de l'incertitude de nos mesures. En moyenne, on obtient trois paramètres essentiels pour la faille et la tectonique de la région:

- une profondeur de blocage "standard", correspondant en gros à la profondeur sismogénique de la croûte: 15 km
- une vitesse à long terme en champ lointain de  $18 \pm 2$  mm/an, très significativement inférieur à la vitesse de la montée de l'Inde par rapport au bloc de la Sonde (environ 30 mm/an). Ce chiffre impose qu'une partie significative du décrochement, 1/3 environ soit accommodé *ailleurs* que sur la faille de Sagaing. Un mouvement oblique sur la fosse de l'Arakan est plausible et compatible avec nos mesures plus à l'Ouest. Une autre possibilité envisageable est un mouvement sur la faille de Kabaw, qui coure parallèlement à la faille de Sagaing le long de l'Arakan Yoma, de l'autre côté du bassin central
- le modèle élastique n'est pas centré sur la trace géologique de la faille en surface, mais bien 15 km à l'Est, entre la faille et l'escarpement du plateau Shan. En théorie, le modèle élastique est

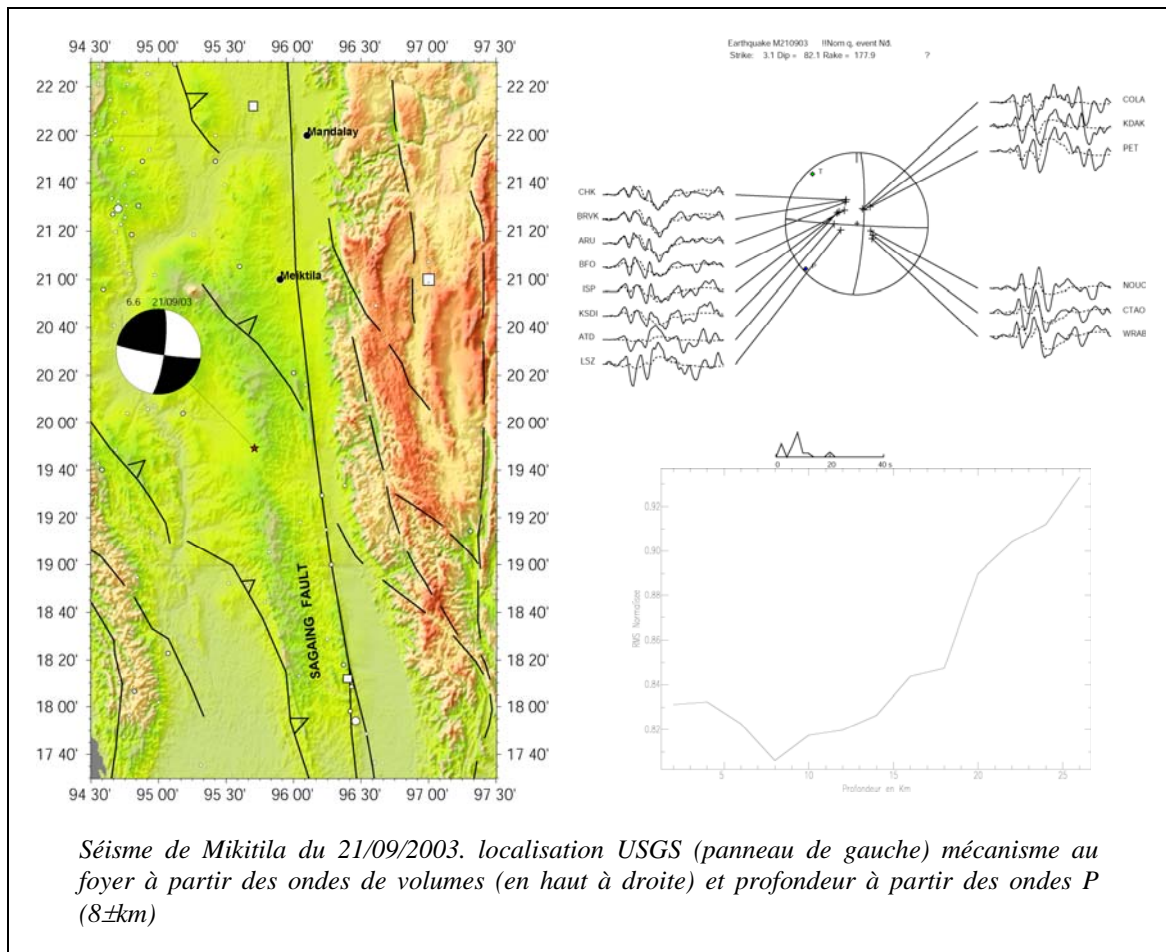
centré non pas sur la faille en surface mais bien sur le gradient de flux visqueux en profondeur. Les deux sont superposées pour une faille verticale, et décalés pour une faille avec un pendage non nul. Ici, un décalage de 15km pour une profondeur de 15km également, indiquerait un pendage de  $45^\circ$ , valeur surprenante pour une faille purement décrochante.



En effet, l'expression morphologique de la faille ne montre pas de composante perpendiculaire (inverse ou normale) prononcée. Il n'y a pas de marche topographique associé à cette faille (contrairement à l'escarpement du plateau Shan très marqué), et elle n'est visible (dans les environs de Mandalay où se trouve notre réseau) que grâce à des petites rides transpressives alignées tout au long de la faille. De manière tout à fait concordante, les tenseurs de déformation calculés grâce aux mesures GPS montre principalement du décrochement. Les valeurs ponctuelles associées à chaque triangle sont naturellement assez bruitées: la forme des triangles retenus affecte énormément le gradient de vitesses calculé. Par contre le tenseur moyen calculé à l'intérieur de l'ensemble du réseau, soit à petite échelle autour de Mandalay (20 points, cadre en haut à droite de la figure), soit

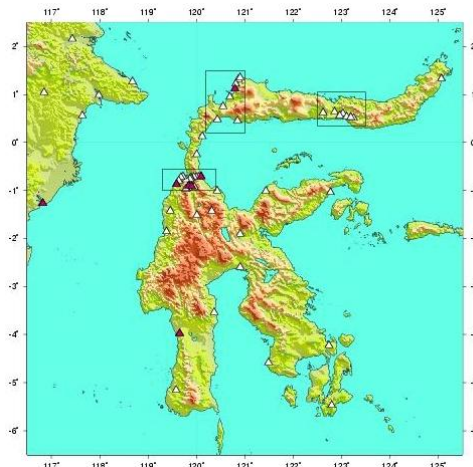
à l'échelle de toute la Birmanie (4 points, cadre en haut au centre de la figure) montrent bien un décrochement quasi pur, dont l'axe est Nord-Sud (celui de la faille de Sagaing). Un fort pendage de la faille est donc très probablement à exclure. La seule hypothèse plausible pour le décalage constaté est la disymétrie marquée entre les deux coté de la faille: croûte continentale épaisse à l'Est (le plateau Shan) et croûte amincie (les bassins centraux) à l'Ouest. Il est probable que cela se traduise par des propriétés rhéologiques différentes, et en particuliers les constantes élastiques des milieux considérés.

Aujourd'hui, et après le séisme de Sumatra, il serait particulièrement intéressant de compléter ces profils, en particuliers en les prolongeant vers l'Ouest et la fosse de subduction sous l'Arakan, afin de quantifier complètement et précisément le partitionnement du mouvement Inde-Sonde dans la région. De ce partitionnement dépend le risque sismique dans la région, et en particulier le potentiel pour un séisme sur la subduction, de nouveau générateur de Tsunami. La faille de Sagaing, elle a déjà prouvé son potentiel sismique par l'occurrence du séisme de Mikitila (septembre 2003, MW 6.6)



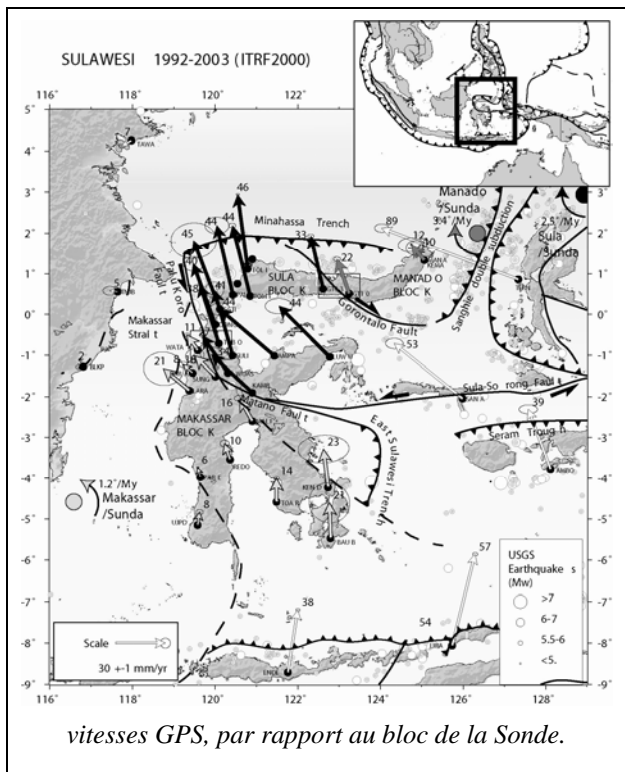
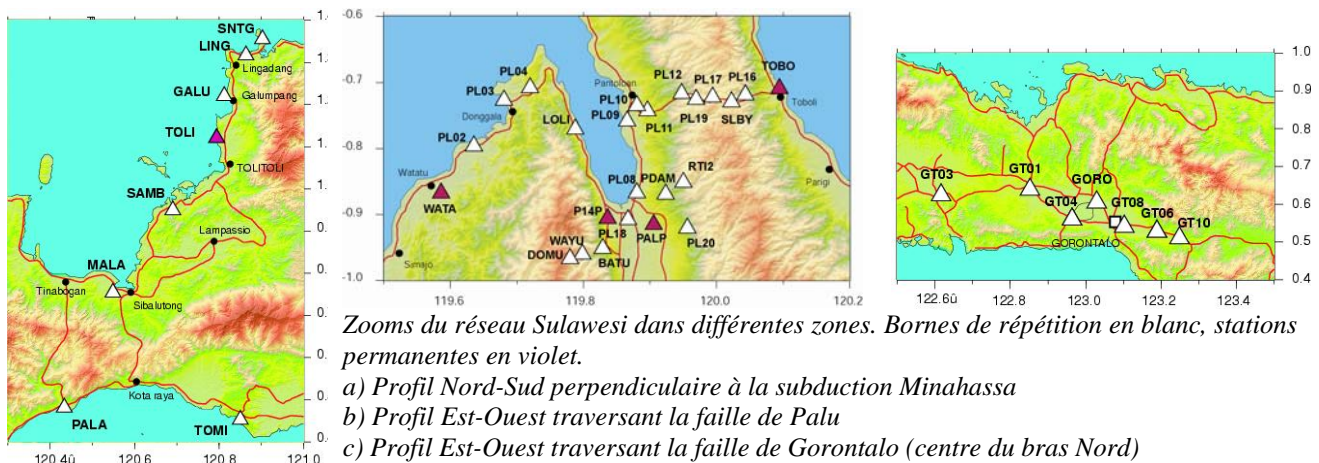
Compte tenu de l'imprécision relative des localisations par le réseau mondial dans cette région du monde, on peut considérer que le séisme c'est bien produit sur la faille de Sagaing. Son mécanisme au foyer recalculé à partir des ondes de volume (P et SH) correspond à un décrochement dextre pur, sur un plan vertical. Sa profondeur est très superficiel et correspond bien au milieu du plan bloqué estimé à partir du GPS. La rupture à du atteindre environ 30 km de long, et pourrait être visible dans un interférogramme SAR, bien que la géométrie (faille sans composante verticale, mouvement Nord-Sud) soit peu favorable. Un interférogramme synthétique suggère que 2 à 3 franges pourraient être visibles.

## Sulawesi, Faille de Palu



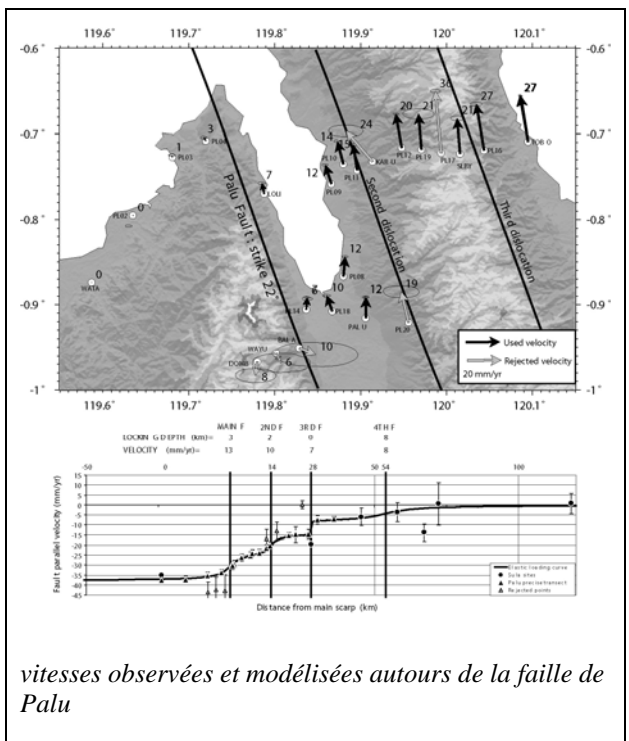
Depuis 1995, j'ai fourni un gros effort pour la densification du réseau dans la région du point triple Indonésien (Célèbes). Au fil des ans, j'ai installé une cinquantaine de points supplémentaires (5 points fin 2002, 11 nouveaux en juin et octobre 2003, 2 en octobre 2004, et encore 2 en juin 2005) dans cette région où la déformation est extrêmement complexe. En plus d'un réseau « large maille » qui couvre l'île entière, 3 réseaux très denses permettent d'étudier en détail les failles de Palu et Gorontalo ainsi que l'accumulation de déformation élastique en arrière de la subduction Minahassa.

Les points du réseau sont remesurés chaque année, tous les ans depuis 1997.



C'est la rotation rapide de petits blocs dans l'archipel qui permet d'accorder la convergence Pacifique/Sonde

- Le bloc de Sula (Nord des Célèbes) (*vecteurs noirs*) tourne rapidement sur lui-même à  $4^\circ/\text{Ma}$  pour « ouvrir » la porte à la collision Philippine/Pacifique
- le bloc de Makassar (Sud des Célèbes) (*vecteurs blancs*) tourne en sens inverse (anti horaire) à  $1^\circ/\text{Ma}$
- alors que le bloc Makassar est très peu déformé, le bloc de Sula, coincé entre la faille et la subduction montre une accumulation de déformation élastique très importante
- la faille de Palu entre ces deux blocs absorbe près 4 cm/an de décrochement sénestre. Elle se connecte à la subduction Minahassa qui fonctionne aussi à 4 cm/an environ.
- La faille de Gorontalo, peu active, accommode environ 1 cm/an en décrochement dextre.



Les mesures les plus récentes apportent un supplément d'information avec une grande précision sur le profil autour de la faille dans la région de la ville de Palu.

Là où, au premier ordre, on observe une faille à 40 mm/an environ, bloquée sur 5 à 10 km de profondeur, on voit maintenant que l'on a affaire à une structure plus complexe.

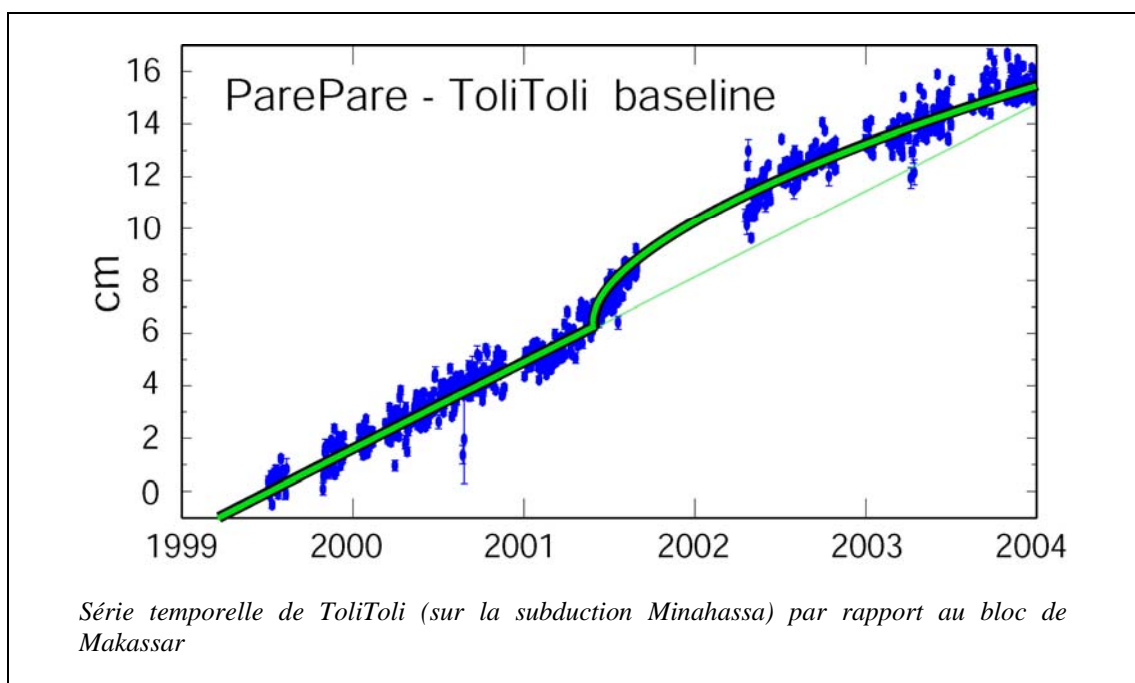
La densité des points de mesure permet de faire apparaître plusieurs dislocations successives et parallèles.

L'une d'entre elle au moins (la 3<sup>ème</sup>) semble en glissement continu puisqu'elle apparaît comme une discontinuité dans le champ de déformation. Cette répartition de la déformation est probablement la réponse au déficit apparent de séismicité historique de la faille, puisque les tranchées n'ont été effectuées que sur la trace principale de la faille (la plus à l'Ouest), et ne verrait donc que 1/3 de la sismicité environ.

Les événements les plus récents dans la région

semblent confirmer cette hypothèse de répartition de la déformation. Deux séismes (Janvier 2005 et Juillet 2005) de magnitude >6 se sont produits quelques dizaines de km au sud de Palu, très certainement sur la faille qui borde le versant Est de la vallée (2<sup>me</sup> dislocation de notre modèle). Les localisations et mécanismes CMT sont sujets à cautions (grande incertitude) mais les traces de rupture en surface que j'ai étudié sont sans équivoque.

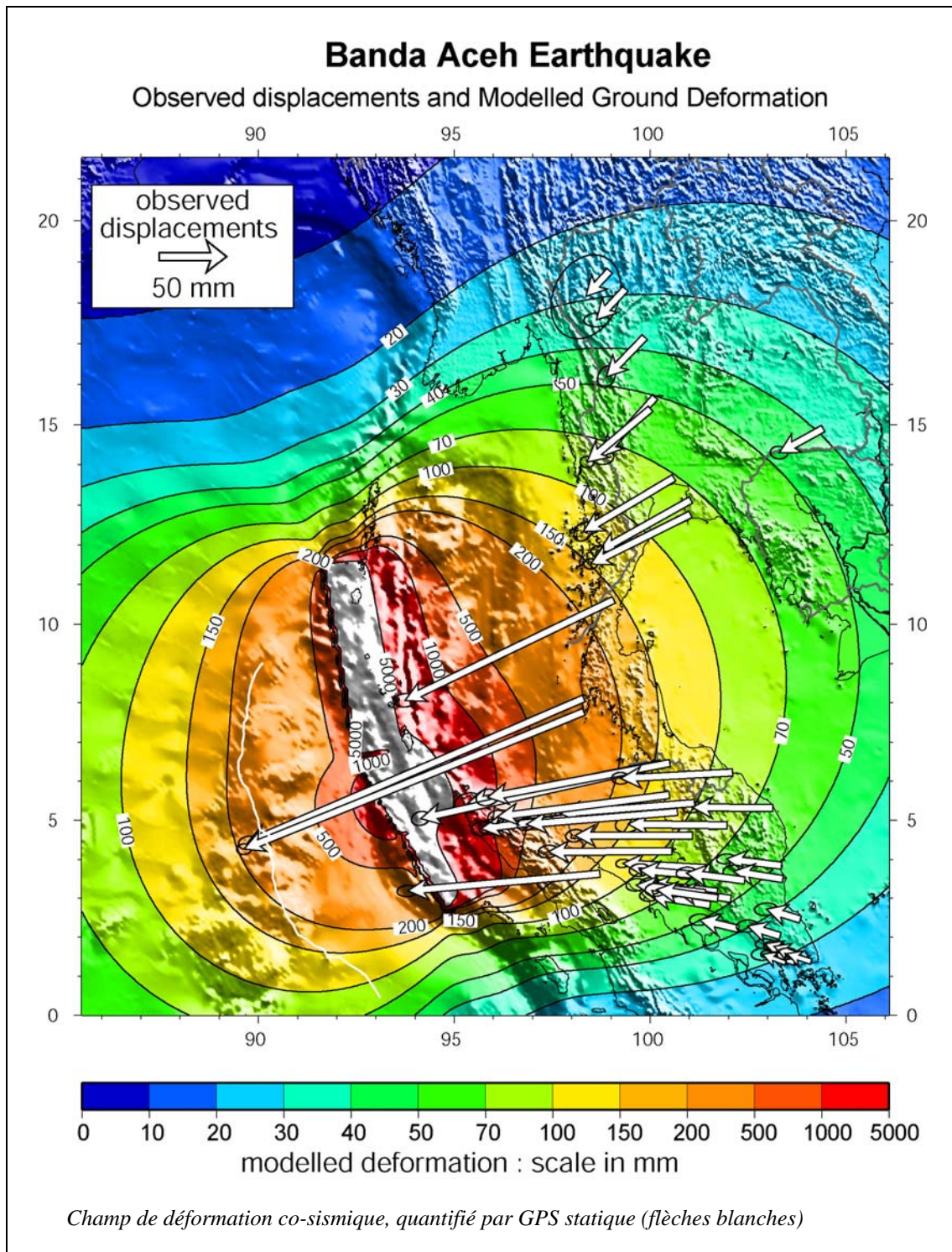
J'ai également installé des stations permanentes dans l'archipel, la première en 1999 en bordure de la subduction Minahassa, puis deux autres en 2003 et 2004, nos partenaires Hollandais en ayant installé 3 sur un profil prépendiculaire à la faille de Palu en 2002-2003 (voir figure). Cette subduction a produit un séisme de magnitude 7.9 en 1996, qui donne lieu à des déformations post-sismiques encore aujourd'hui comme l'attestent la série temporelle du point de Tomini (figure 9, p14). La série temporelle de la station permanente (ToliToli) est complexe à analyser.



Elle montre sans équivoque un phénomène de glissement qui s'est produit après un séisme de magnitude 6.5 sur la subduction en mars 2001. La modélisation en dislocation élastique (Okada) du mouvement co-sismique lié à ce séisme ne prévoit pas de déplacement détectable à ToliToli. Ce glissement aurait donc une autre origine, difficile à modéliser avec une seule série temporelle. Par contre, ce qui est certain, c'est que la vitesse de la station ne semble pas stable: elle est toujours en train de décroître aujourd'hui. En effet, le profil perpendiculaire à la subduction ne montre pas *à l'heure actuelle*, l'accumulation de déformation attendue en arrière d'une zone bloquée. Au contraire, des vitesses à peu près constantes démontrent un couplage essentiellement nul, correspondant à un fluage sans blocage en profondeur. Le fait que la subduction produise des séismes importants (MW 7.9 en 1996) montre bien qu'il ne peut pas en avoir été toujours ainsi. Ce couplage apparemment nul n'est donc que *transitoire*. A l'heure actuelle, la déformation post-sismique compense à peu près l'accumulation inter-sismique. Avec le temps, le post-sismique va décroître, l'accumulation inter-sismique va réapparaître. Si les prochains séismes susceptibles d'affecter la série temporelle de la station se produisent avant que le post-sismique de 1996 ait disparu, la preuve aura été faite qu'il n'y a peut être tout simplement pas de régime inter-sismique "pur", c'est à dire d'accumulation à vitesse constante, entre deux séismes.

## Le séisme de Sumatra (Banda Aceh) du 26 décembre 2004

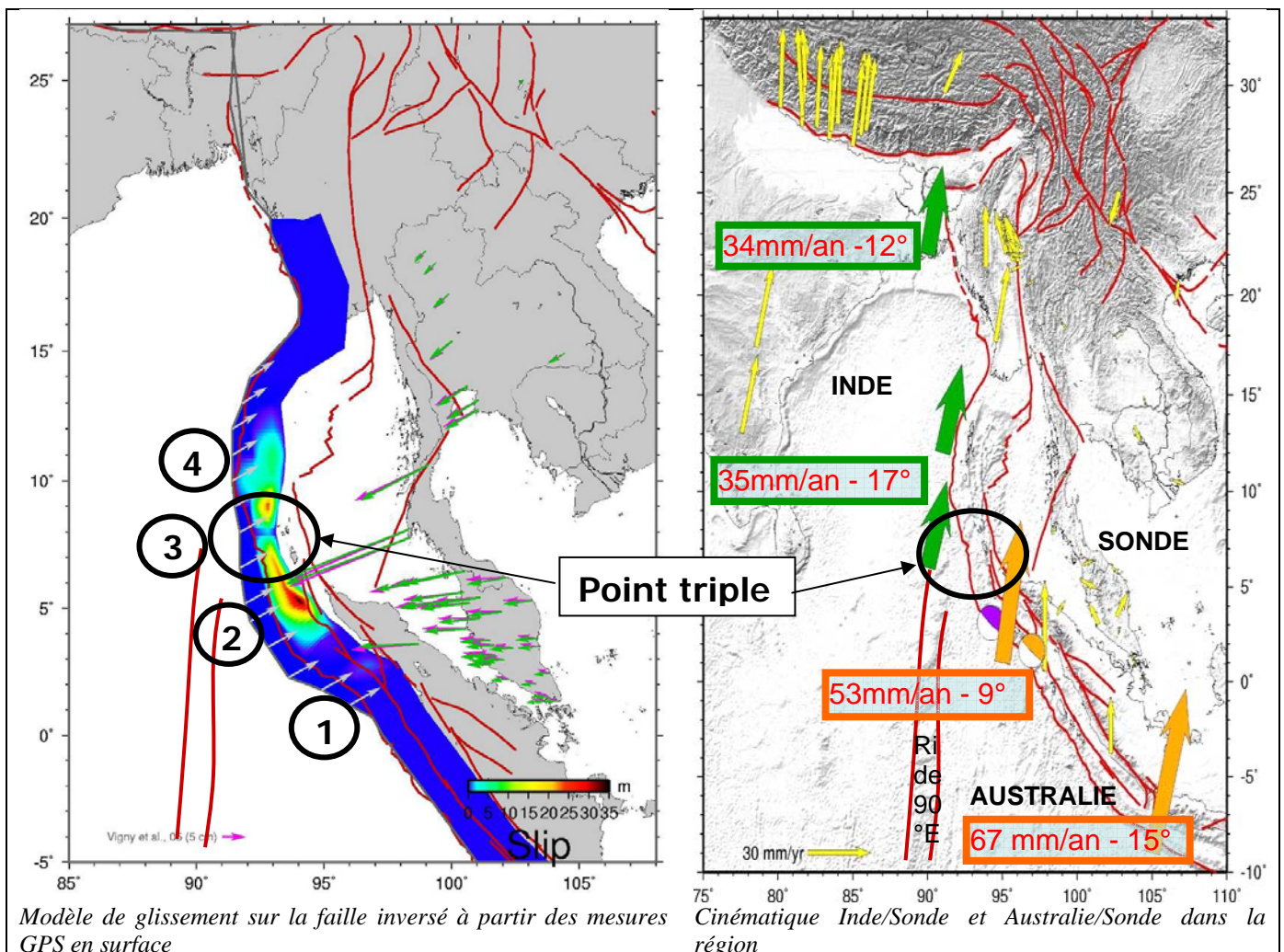
Ce séisme est le deuxième plus gros de l'époque instrumentale. Sa magnitude reste assez mal contrainte (entre 9.1 et 9.3) à cause de la grande complexité de sa rupture: la quantité de glissement sur le plan de faille est très inhomogène, et la vitesse de propagation sur ces différents segments est très différente. Les réseaux GPS permanents développés en Thaïlande, Malaisie, et Indonésie, parce qu'ils sont denses (60 stations au total), permettent non seulement de "voir" le rebond crustal associé au séisme, mais surtout de le modéliser complètement. Plus que le déplacement à un endroit donné, ce sont les gradients de déformation qui contraignent la rupture.



Grâce à la mesure de la déformation sur une zone qui s'étale depuis le sud de la Malaisie (Singapour) au nord de la Thaïlande (ChiangMai), on peut contraindre l'extension de la rupture (1200km de long) et la quantité moyenne de glissement (12m) et donc la magnitude (9.2), mais surtout la répartition du glissement sur le plan de faille. On découvre alors qu'il est très variable:

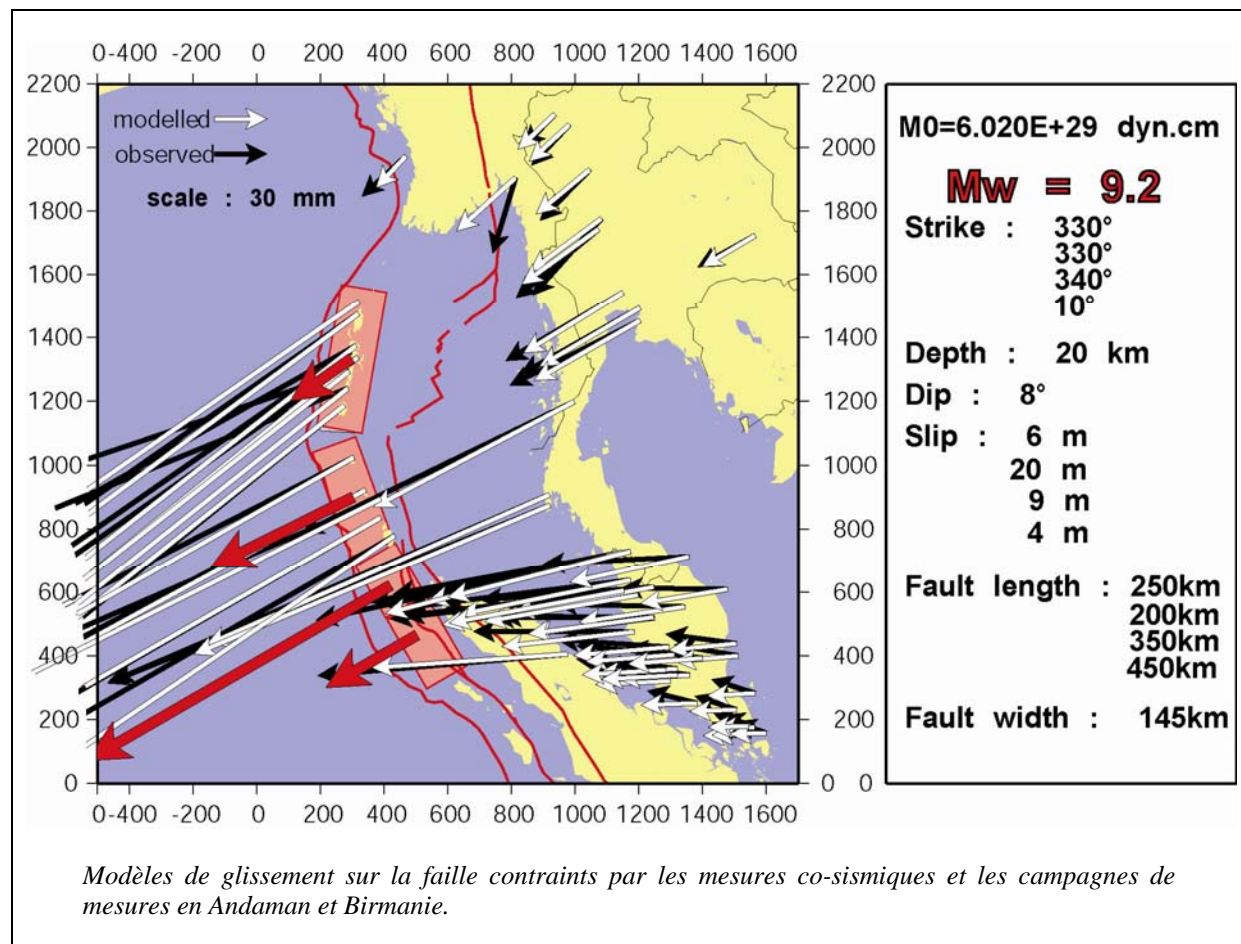
- 1 glissement de quelques mètres seulement au démarrage de la rupture près de l'épicentre
- 2 puis plus de 30m sur une large zone au nord de la pointe de Sumatra, en face de Phuket
- 3 puis une zone de près de 100km quasiment sans glissement vers 7° de latitude
- 4 puis de nouveau une zone avec un glissement important jusqu'aux îles Andaman

La zone sans glissement est particulièrement intéressante. Elle correspond plus ou moins avec la frontière de plaque (très mal connue) entre l'Inde et l'Australie dans la région. Nous pensons donc avoir la réponse à l'énigme posée par cette rupture qui traverse un point triple: loin de l'avoir traversé, elle s'est en fait arrêtée sur cette frontière, puis à déclenché un second séisme de l'autre côté (quasi instantanément) par augmentation des contraintes.



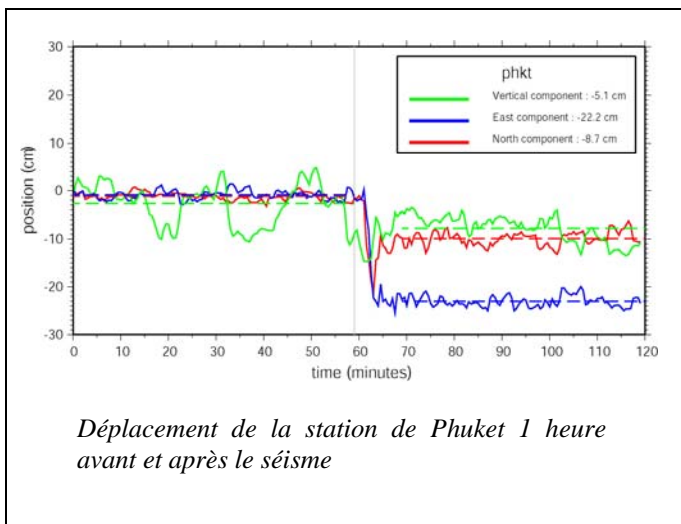
Les campagnes de mesures réalisées sur les îles Andaman (Gahalaut et al., 2006) ainsi que les remesures de la partie Sud de mon réseau en Birmanie (Maurin et al., 2006) quelques mois après le séisme montrent également très clairement que la direction du glissement n'est pas la même sur les segments Nord et Sud de la rupture (voire figure). Au sud, le glissement est bien perpendiculaire à la fosse, mais au nord il est très oblique. Or justement, en arrière de ce segment Nord de la fosse, au lieu de trouver une grande faille décrochante qui assure le partitionnement de la déformation (comme la grande faille de Sumatra au Sud), on trouve le rift de la mer d'Andaman qui accommode

la composante Nord-Sud du mouvement par son ouverture. A l'évidence, le rift n'assure qu'une partie du mouvement nécessaire, la subduction fonctionne donc de manière oblique dans cette région.



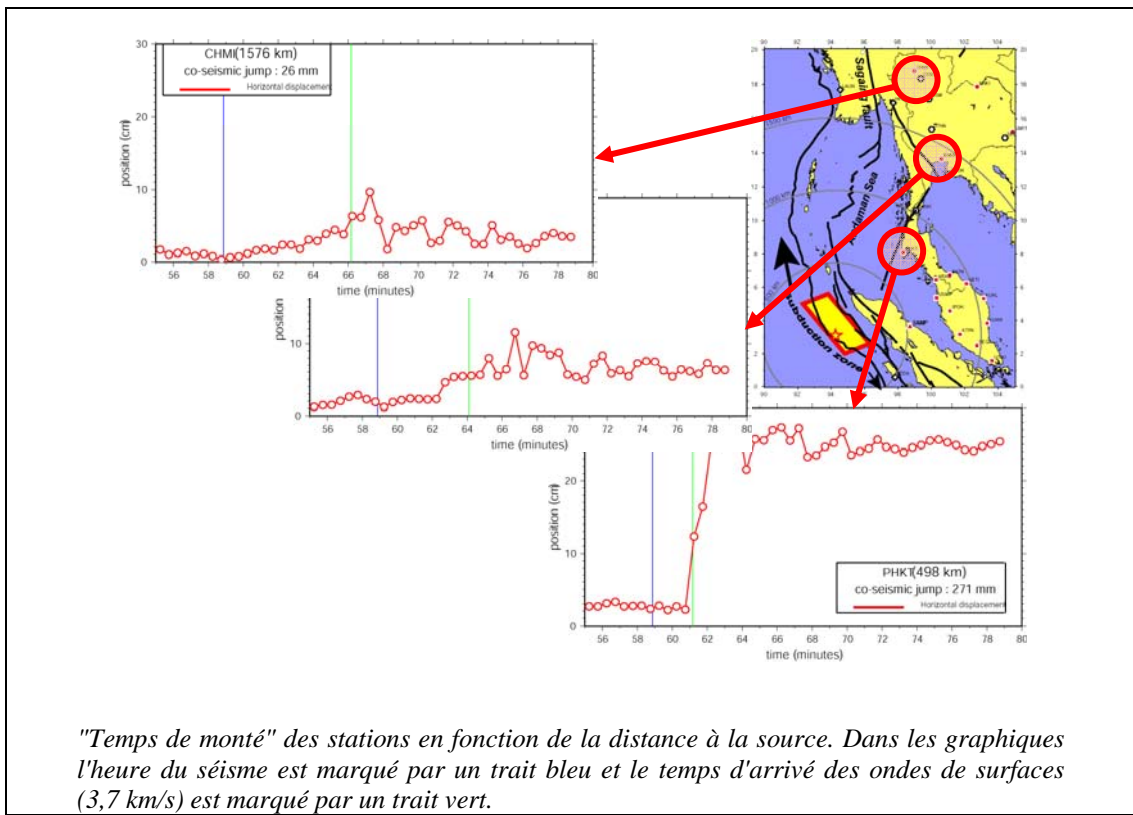
Cela corrobore nos modèles de subduction oblique encore plus au Nord sous l'Arakan. Nous arrivons donc à une solution assez simple: Au Sud, le mouvement Australie/Sonde est *complètement partitionné* (convergence pure sur la fosse, décrochement sur la grande faille de Sumatra). Au Nord, de l'autre côté du point triple, le mouvement Inde/Sonde n'est que *partiellement partitionné* (convergence oblique sur la fosse, "décrochement" sur le rift Andaman et sur la faille de Sagaing). Le mécanisme du séisme de Banda Aceh reflète cette situation.

Grâce à la méthodologie du GPS "cinématique", il est possible d'aller encore au-delà de la simple mesure du déplacement co-sismique total. Il faut pour cela disposer de stations permanentes fonctionnant en continu. Il est alors possible de mesurer leur position à chaque instant de l'acquisition sur les satellites (30s usuellement, mais facilement portable à 1s), c'est à dire *pendant* le séisme. La précision que l'on obtient alors sur la position est évidemment légèrement moins bonne que celle obtenue par le cumul de 24h de données, mais les méthodes de "Precise Point Positioning (PPP)" qui s'affranchissent de la formation explicite des doubles différences permettent d'atteindre le cm, et ce quelle que soit la distance entre les stations. Une station GPS devient alors une sorte de sismographe très basse fréquence, qui mesure directement le déplacement (ni l'accélération, ni la vitesse) et qui a l'avantage de ne jamais saturer.

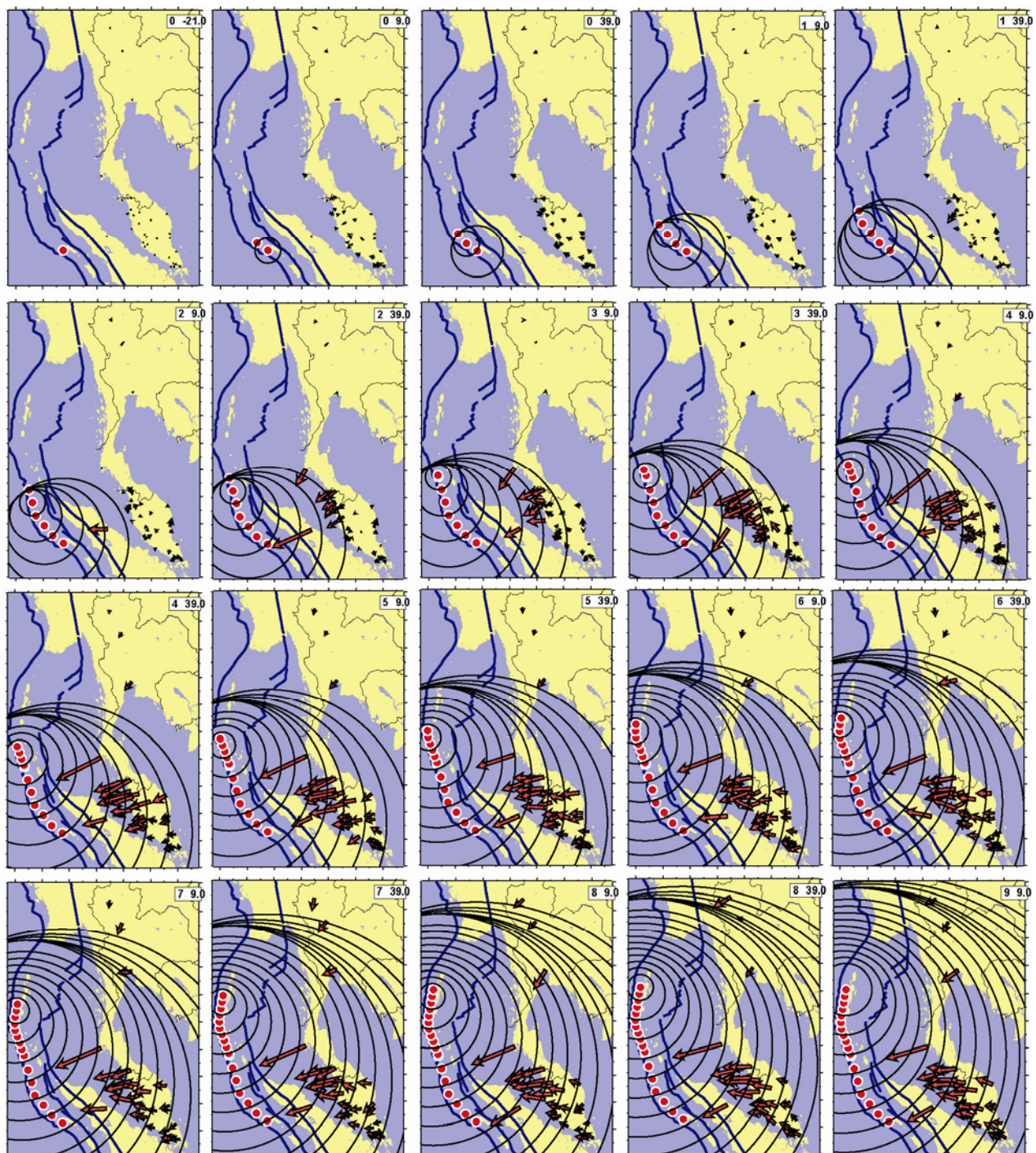


Ormis sur la composante verticale qui est assez bruitée, Il est possible de déterminer le saut co-sismique avec une assez bonne précision ( $\pm 1$  cm) sur les composantes horizontales, à l'aide d'une heure de données seulement. En théorie, avec un échantillonnage assez rapide du signal GPS (1 point/s) on devrait obtenir un "sismogramme" tout à fait comparable à celui obtenu par une sismographe large bande au passage des ondes de surface. Ce test a été réalisé pour les ondes du séisme de Denali (Alaska) traversant le réseau GPS Californien, et montre une correspondance parfaite.

Avec des données à 30s uniquement, on voit malgré tout le "temps de monté" des stations, qui diffère en fonction de la distance à la faille et à la source sismique. Les stations proches du départ de la rupture (comme Phuket) voient un maximum d'énergie sismique arriver en un laps de temps assez court. Cela correspond à la zone de glissement très fort (de l'ordre de 30m) qui se produit en face de Phuket. Elles "montent" donc à leur nouvelle position assez rapidement: 3-4 époques, soit moins de 2 minutes à Phuket. Les stations plus au Nord reçoivent de l'énergie d'une manière plus étalée dans le temps. Elles montent à leur nouvelle position en 5-6 minutes à Bangkok et 7-8 minutes à Chiang Mai. Cela correspond à l'énergie rayonnée par une source mobile qui se déplace un peu plus lentement que les ondes sismiques.



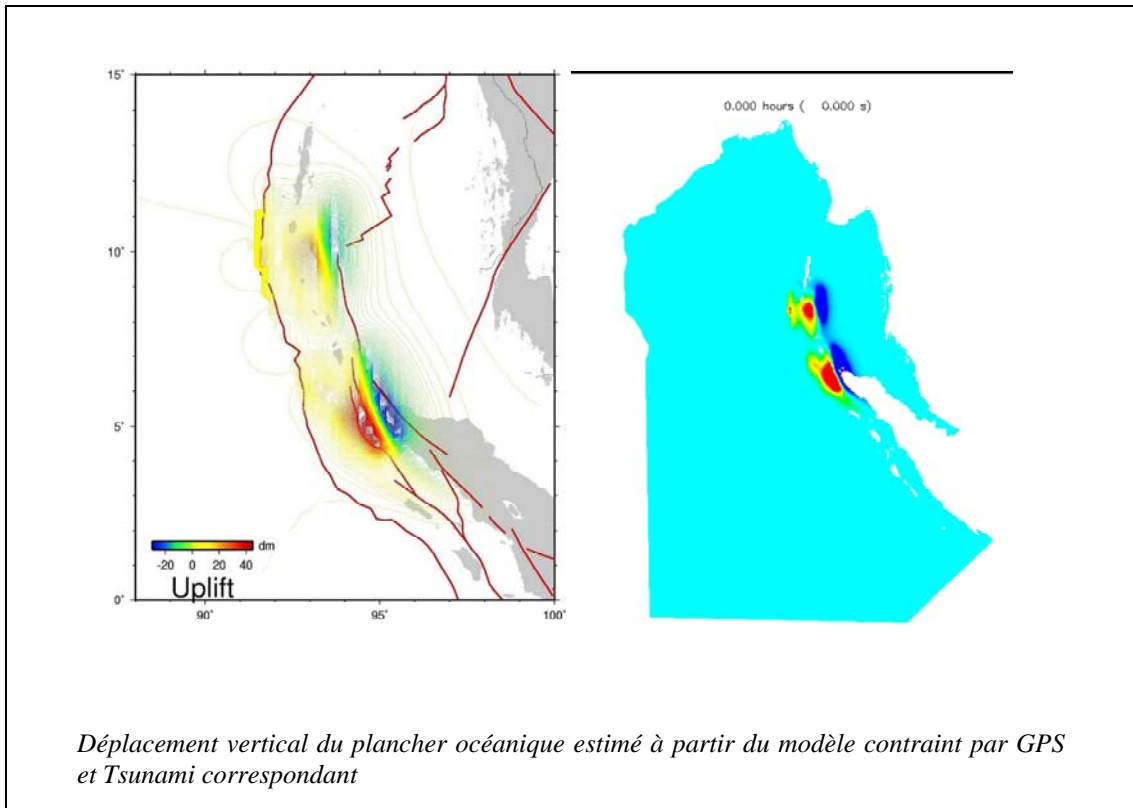
Il est donc possible de calculer la vitesse de propagation de la rupture le long de la faille à partir de ces temps d'arrivée aux stations et du "temps de monté" de chaque station.



*Propagation de la rupture et des ondes de surfaces. Chaque panneau montre la situation de 30s en 30s. Le temps à partir du début de la rupture (épicentre USGS) est donné en (minutes secondes) en haut à droite.*

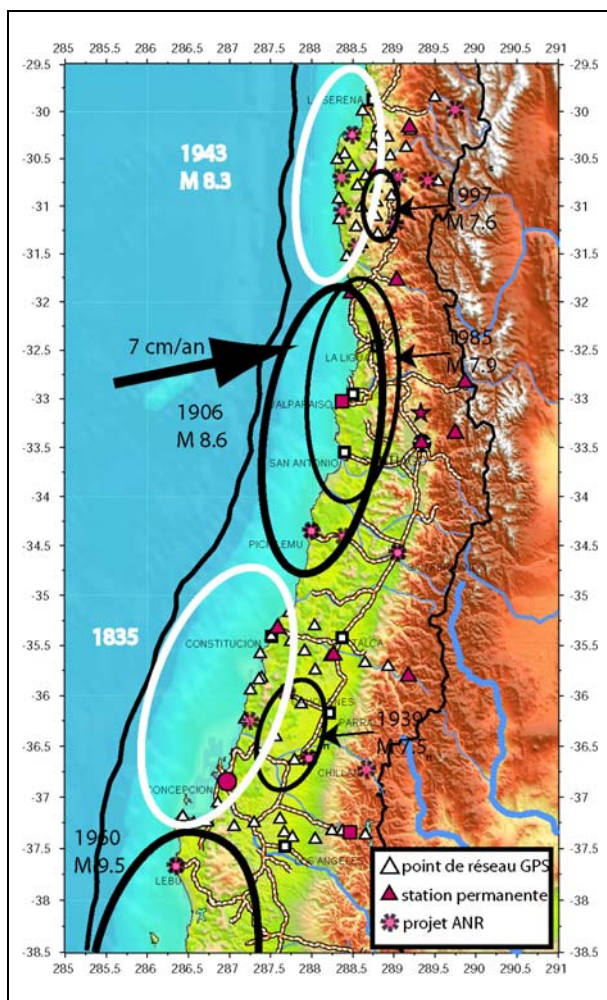
Les résultats montrent que la vitesse de propagation de la rupture est plus lente sur le segment Nord (~2 km/s) que sur le segment Sud (~3.5 km/s). Ils montrent également qu'une "pause" de la rupture au passage du point triple est nécessaire pour ajuster les temps d'arrivées aux stations. Cette pause est évidemment mal contrainte par des mesures chaque 30s, elle correspond à  $1\pm1$  époque, soit 30s à 1 minute près. Cette incertitude est suffisante pour que l'on ne puisse déterminer si le déclenchement sur le segment nord se fait par augmentation des contraintes statiques ou dynamiques, très probablement la somme des deux.

Finalement, les modèles de rupture contraints par la déformation horizontale en champs lointains permettent d'estimer le mouvement vertical au plus près de la faille, c'est à dire le déplacement du plancher océanique qui génère le Tsunami. Là aussi, on obtient une explication de l'amplitude exceptionnelles des vagues qui ont touché Phuket et le SriLanka. Elles résultent de l'interférence constructive (justement dans ces deux directions) des deux trains d'ondes générés par les deux ruptures.



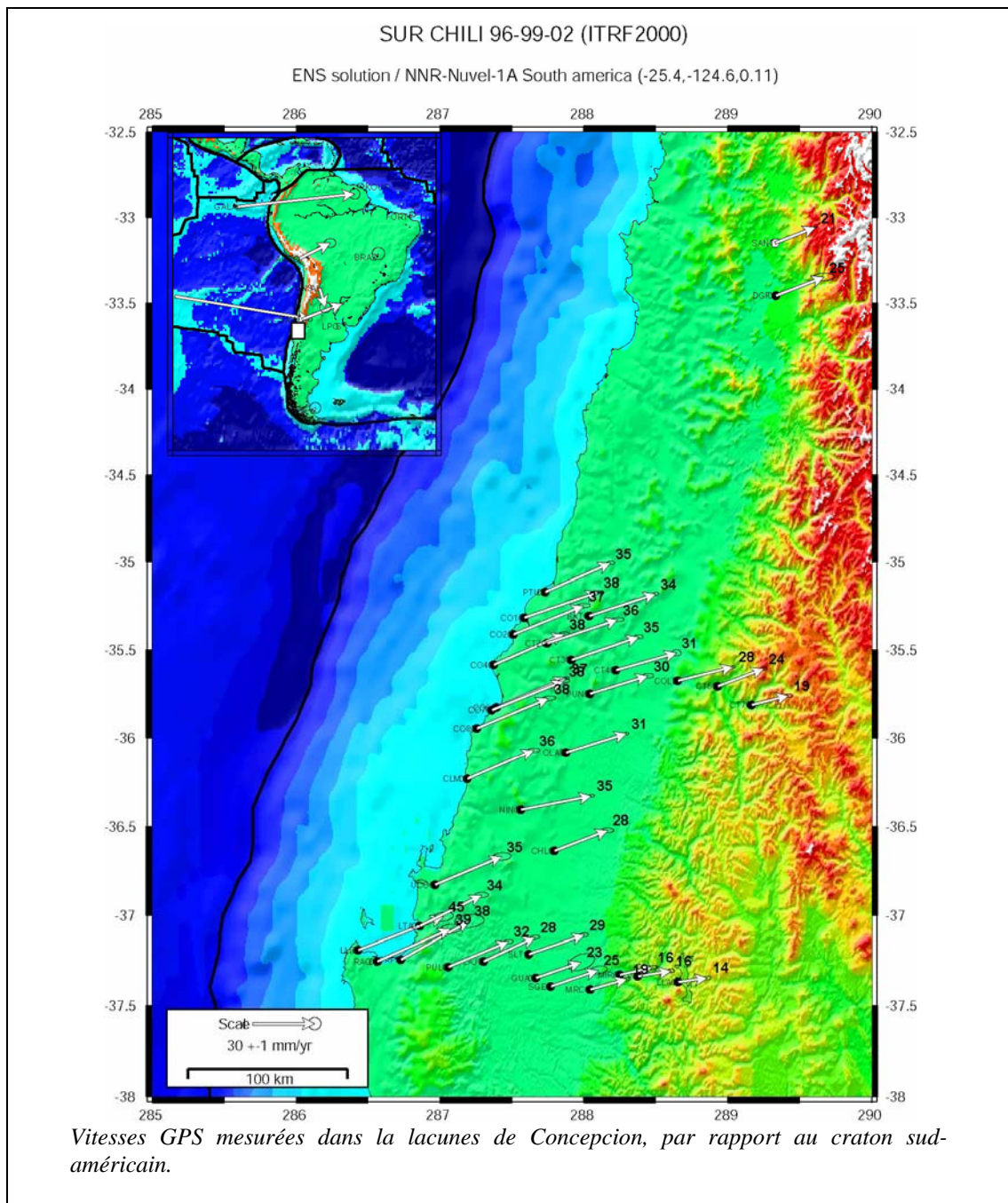
## La subduction Chilienne

Contexte : En conséquence de la subduction Nazca/Amérique du Sud, le Chili est une zone d'activité sismique intense. Le long de la côte chilienne l'interface de subduction est fragmentée en zones élémentaires de l'ordre de 100 à 200 km de long et de 50 à 100 km de large, susceptibles de produire des grands séismes lors de la relaxation des contraintes accumulées. Un séisme majeur ( $Mw > 8$ ) a lieu tous les dix ans en moyenne au Chili et la plupart des segments de faille dans la région ont produit un séisme de magnitude 8 lors du 20eme siècle. La plupart des séismes majeurs correspondent à des glissements "en faille inverse" sur l'interface de subduction dans la zone qui est habituellement bloquée lors de la période inter-sismique. Trois lacunes (zones dans lesquelles le dernier grand séisme est ancien, encadrées par des séismes plus récents) ont été clairement identifiées: la zone du coude d'Arica au Nord, la zone de Coquimbo au centre Nord, et la zone de Concepcion au centre sud.



La zone de Concepcion est une lacune typique: le dernier séisme ici c'est produit en 1835 et les segments adjacents ont rompus en 1985 au nord (séisme de Valparaiso,  $Mw 7.9$ ) et en 1960 au Sud (séisme de Valdivia  $Mw 9.5$ ). Le chantier a été initialisé en 1995 par JC. Ruegg, R. Madariaga et R. Armijo à l'IPGP. Depuis le départ à la retraite de JC Ruegg, j'ai repris la responsabilité des mesures GPS dans la région. J'ai ouvert en 2003 un second chantier dans la lacune de Coquimbo (centre Nord). Cette lacune sismique présente des signes de "maturité": en 1997 le séisme de Punitaqui (intraplaque,  $Mw 7.7$ ) a "réveillé" une sismicité relativement calme. Aujourd'hui, plus d'une dizaine de séismes de magnitude supérieure à 7 se sont produits et le nombre cumulé de petits séismes est 100 fois plus élevé qu'avant 1997. Par Ailleurs des points visiblement anormaux dans les mesures géodésiques à très grande échelle réalisée par les allemands en Amérique du Sud, pourraient indiquer des glissements transitoires sur certaines portions de la subduction.

Afin de quantifier l'aléa sismique dans la lacune de Concepcion (déterminer l'activité sismique de la zone, la possibilité d'un déficit de moment sismique, et la géométrie du champ de déformation et de contrainte) un réseau de 32 points a été installé et mesuré en 1996, puis complété (45 points) et remesuré partiellement (15 points) en 1999. En collaboration avec l'équipe de l'IPGP, j'ai donc repris le programme GPS de J.C. Ruegg sur cette région. J'ai réalisé une remesure totale du réseau en mars 2002, complétée en 2003. Grâce à la grande précision de cette campagne et grâce au doublement de la période de temps sur laquelle les vitesses sont déterminées, on obtient un champ de vitesse remarquablement cohérent sur l'ensemble des 45 points du réseau.

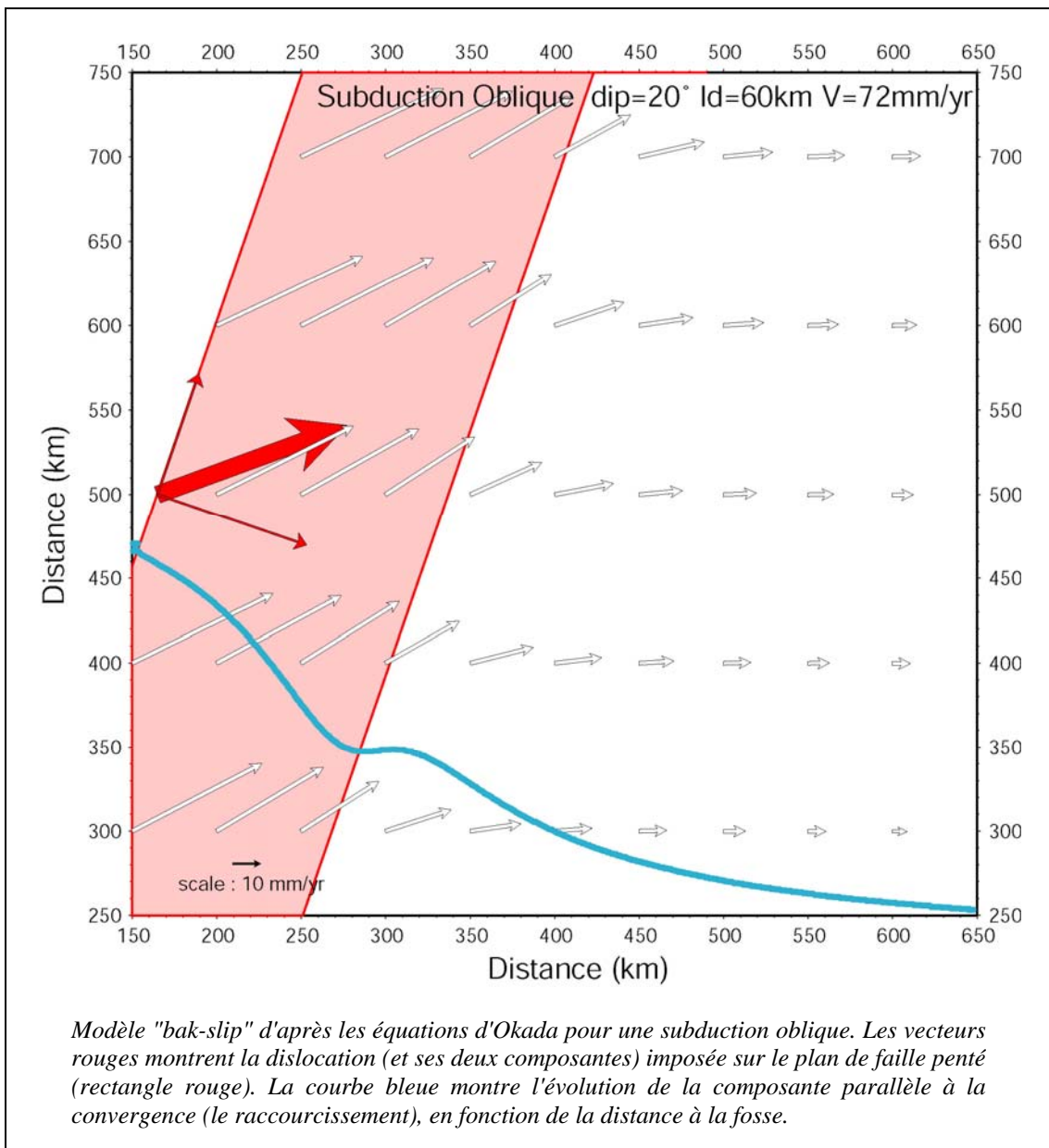


A grande échelle, les points importants sont les suivants :

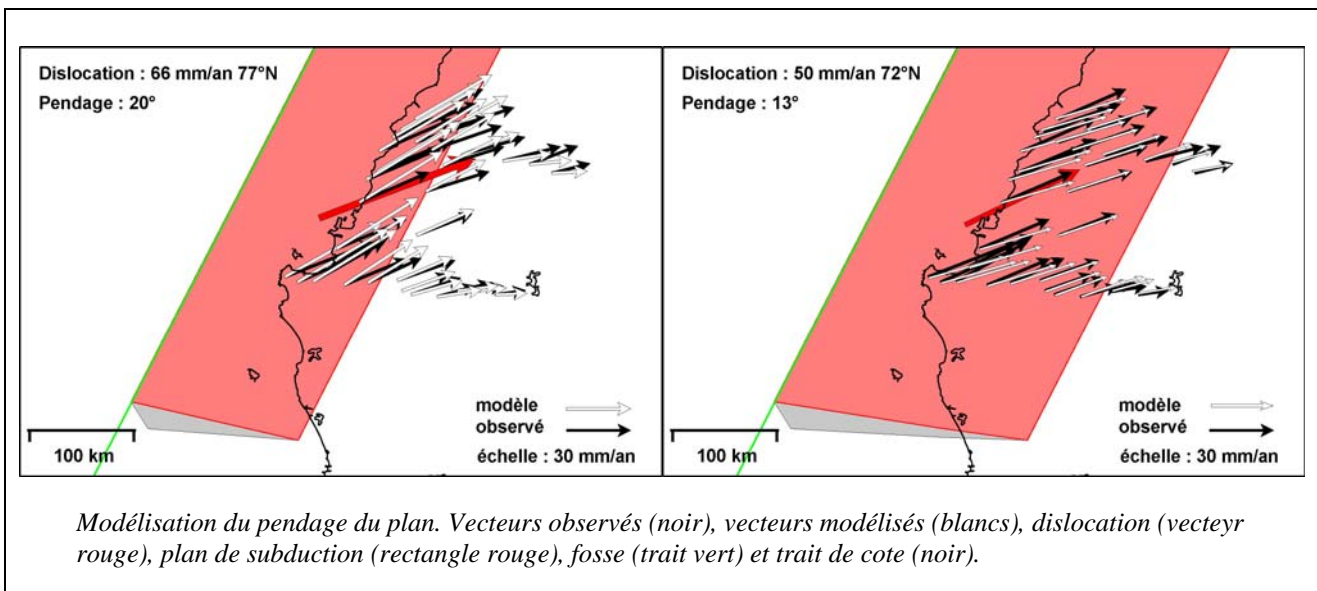
- La plaque Amérique du Sud est bien contrainte, en effet les vitesses des stations fiducielles sont très faibles sur la partie stable de l'Amérique du Sud, < 2 mm/an.
- On trouve pour Nazca (Galapagos et Ile de Pâques) des vitesses sensiblement plus lentes que celles définies par Nuvel-1a : 7 cm/an (au lieu de 8) à l'Ile de Pâques, et 6 cm/an (au lieu de 7) aux Galapagos. On en déduit que le pôle de rotation rigide Nazca/SAmérique de Nuvel-1A n'est pas compatible avec les déformations GPS mesurées actuellement. Nos mesures indiquent une diminution de la vitesse de rotation de la plaque Nazca de l'ordre de -15% (*conformément à Larson et al. 1997, Angermann et al. 1999, et Norabuena et al. 1998*). On prédit alors sur la fosse une vitesse de la plaque Nazca de 72 mm/an (10% de moins que NUVEL1A), avec un azimut N70°, parallèle aux vitesses mesurées sur la côte.

A petite échelle, on voit l'accumulation de déformation élastique entre la côte et la cordillère. La déformation est toujours significative plus de 350km en arrière de la fosse, il faut probablement passer en Argentine pour trouver le zéro.

La modélisation (dislocation en "backslip") montre que malgré l'obliquité de la convergence, il n'y a pas forcément partitionnement de la déformation.



Les paramètres qui contrôlent la propagation de la déformation dans une couche élastique sont le module d'Young et le coefficient de Poisson. Ils transmettent les contraintes normales et les contraintes cisailantes dans un milieu à 3 dimensions. De manière générale donc, les déformations tangentialles ne se propagent pas à la même distance que les déformations axiales. De ce fait, lorsque l'on applique une dislocation oblique sur un plan, la composante en raccourcissement se propage plus loin que la composante décrochante. Il se produit donc une rotation des vecteurs déformation que l'on observe en surface, au fur et à mesure que l'on s'éloigne de la fosse. Cette rotation est maximum à l'endroit où la composante décrochante "s'éteint". Cet endroit se trouve à l'aplomb du bout du plan bloqué en profondeur. La composante de déformation parallèle à la convergence (courbe bleue sur la figure) présente un plateau à cet endroit. Le champ de vecteur en surface peut donc donner l'impression de correspondre à du partitionnement avec un décrochement parallèle à la fosse à cet endroit. Les deux situations ne peuvent être différencierées qu'à l'aide d'un réseau de points assez dense, en particulier dans cette région, mais tout de même assez étendu pour échantillonner complètement la déformation.

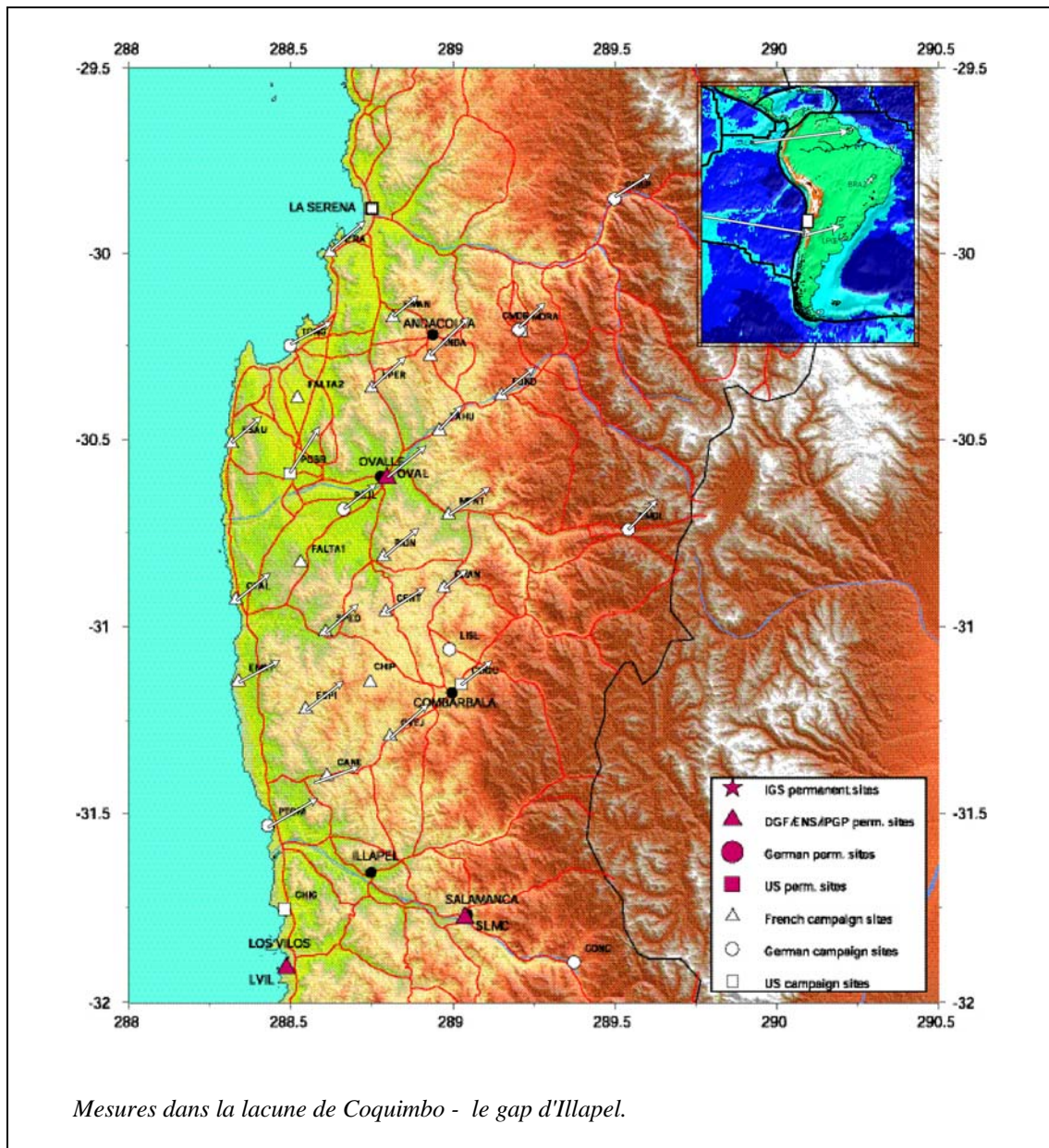


Un modèle satisfaisant de la subduction est obtenu avec un plan bloqué jusqu'à 60km de profondeur (la profondeur de transition entre blocage et glissement continu) et un pendage de  $20^\circ$ , sur lequel on applique une dislocation de 66 mm/an orientée  $77^\circ\text{N}$  (figure de gauche). Un tel plan de subduction explique bien la déformation observée dans le sud du réseau (Concepcion). Par contre, elle prédit une rotation des vitesses plus rapide que celle qui est réellement observée dans le nord du réseau (Constitucion). En effet, le long de ce profil, les vecteurs restent parallèles quasiment jusqu'au bout du profil, près de 300 km en arrière de la fosse. Pour obtenir un modèle qui corresponde à cette observation il faut diminuer le pendage du plan de manière à ce qu'il génère de la déformation beaucoup plus loin de la fosse. On arrive alors à un pendage de l'ordre de  $13^\circ$  (figure de droite). Il est à noté que cette valeur convient également à la déformation mesurée dans la région de Santiago. Il est alors nécessaire de diminuer la dislocation que l'on impose sur le plan (de 66 m/an à 50 mm/an) afin de conserver une norme compatible avec celle qui est observée. Cette vitesse est très différente de la vitesse de la plaque Nazca ( $\sim 7$  cm/an). Il faudrait donc imaginer soit de la déformation intraplaque avant la fosse, soit que le couplage sur la subduction n'est que partiel, la plaque inférieure glissant de manière a-sismique de la quantité manquante, soit environ 2 cm/an. En tout état de cause, il semble établit que le pendage varie significativement du Sud ( $20^\circ$ ) au Nord ( $13^\circ$ ) de notre réseau, c'est à dire sur 250 km environ. Des variations de couplage ou de profondeur de blocage sont certainement associées à des variations de pendage.

En termes d'aléa sismique, en prenant les valeurs les plus conservatives (5 cm/an), on calcule aisément que plus de 8m de déformation ont été accumulés dans la zone depuis le dernier séisme de 1835. Un glissement de cet ordre de grandeur sur toute la longueur de la lacune (environ 300 km) produirait un séisme de magnitude au moins 8.5. Les lois d'échelle indiquant un glissement moyen de l'ordre de 3-4 m pour un tel séisme, il semble que celui-ci soit déjà très en retard.

Les tout premiers résultats des mesures sur la lacune de Coquimbo (3 époques de mesures sur 1 an en 2005-2005) montrent également l'accumulation de déformation élastique liée au blocage sur la fosse. Les différences avec la lacune de Concepcion sont notables:

- L'amplitude de la convergence (les points sur la côte) est réduite à presque la moitié (2.5 cm/an au lieu de 4.5 cm/an)
- La direction de la compression reste constante, ce qui implique un plan sub-horizontal qui se prolonge donc très loin à l'Est



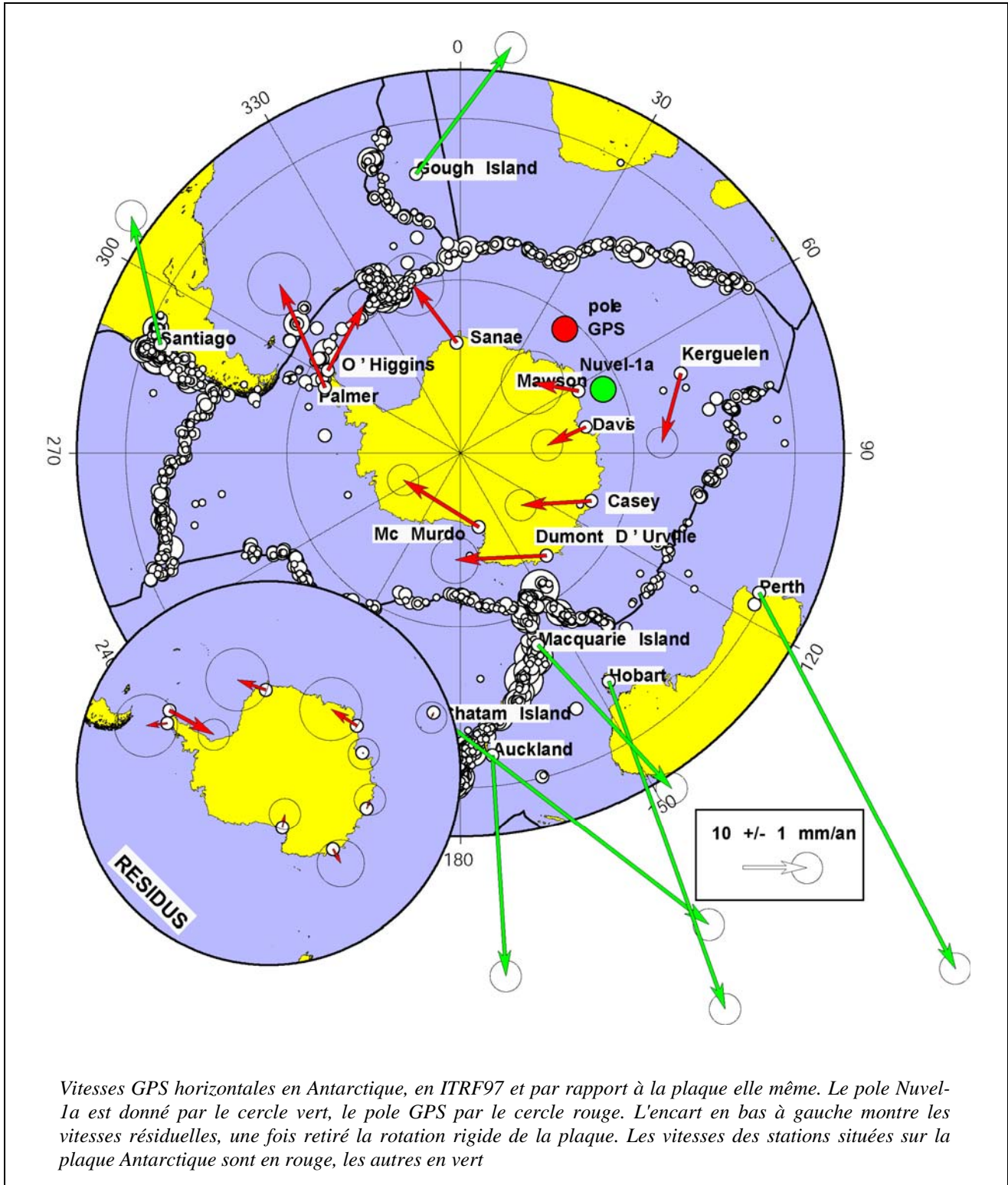
Ces deux observations sont à priori contradictoires. En effet, un pendage faible implique à priori une zone de couplage très large, et donc un effet élastique maximum. Seul un couplage faible (non total) permet d'expliquer les mesures. L'intensité du couplage varie-t-elle dans le temps? Est-ce ainsi (par diminution progressive du couplage) qu'une rupture se prépare?

Pour répondre à ces questions, nous travaillons sur deux axes :

- réaliser des campagnes de mesures fréquentes (deux fois par an) sur un réseau assez dense (maille de 20-30km) et couvrant l'aplomb du bout du plan de subduction. L'objectif est de réaliser des séries temporelles longues (au moins une décennie) qui permettraient de détecter une variation temporelle du couplage à cette échelle de temps. J'ai donc installé en 2004 un tel réseau de 30 points, auxquels j'ajoute quelques points supplémentaires chaque année, et je l'ai mesuré 4 fois depuis.
- Installer un réseau de stations GPS permanentes (7 aujourd'hui, plusieurs dizaines à terme) afin de détecter et quantifier d'éventuels glissements asismiques en profondeur (le trémor des subductions mis en évidence par *Rogers et al.* Sur la zone des Cascades) et bien sûr de "capturer" le glissement lors d'un prochain séisme sur ce segment de la subduction.

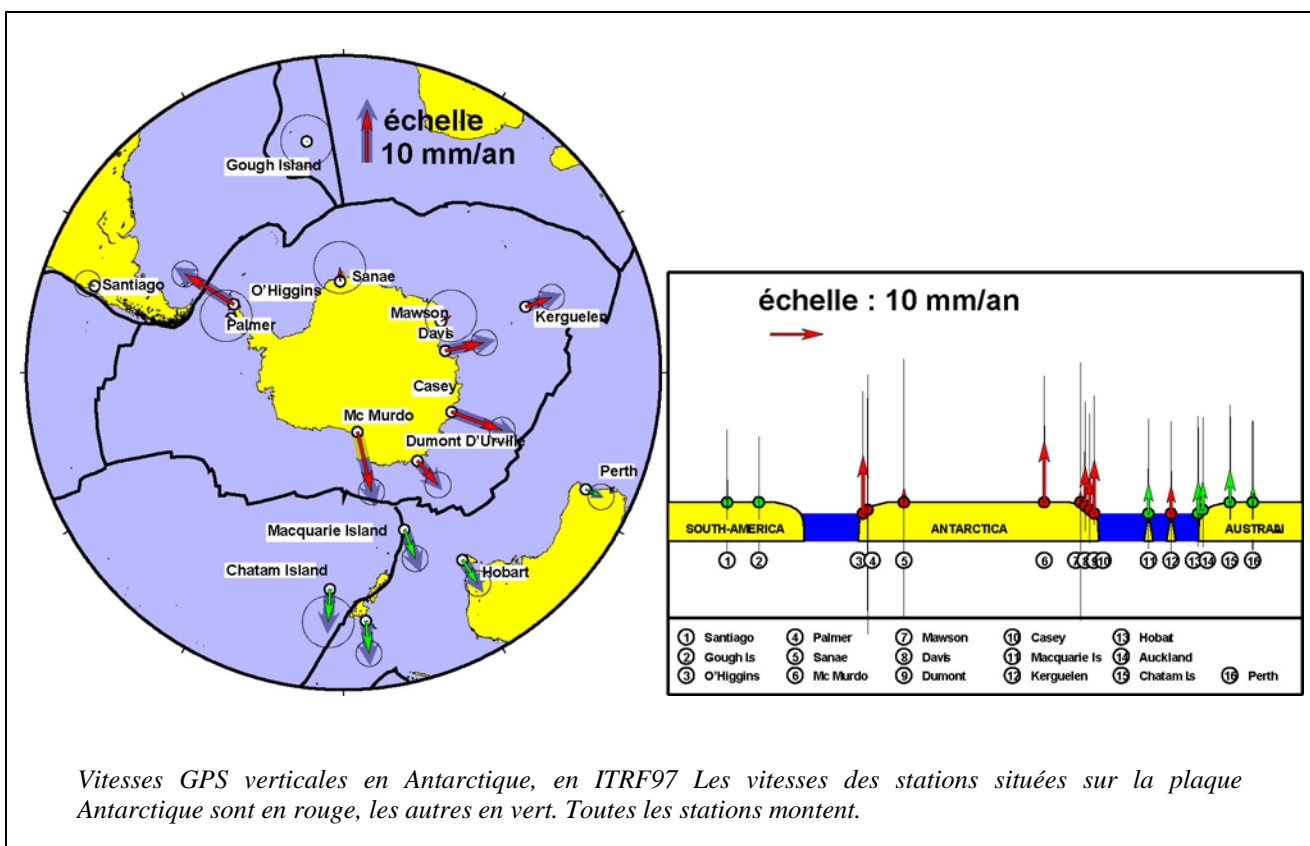
## Antarctique: rebond post-glaciaire

Contexte: J'ai réalisé mon projet d'installation d'une station GPS continue à la base française de Dumont d'Urville en Antarctique lors de la campagne d'été austral (Janvier 1998). Le but de ces mesures, associées aux mesures provenant des autres stations GPS permanentes du continent) est de détecter un éventuel rebond de celui ci, lié à une possible diminution actuelle de la masse de la calotte glaciaire, elle même due au réchauffement planétaire. Ce programme est financé par l'IFRTP.



Là encore, nous avons montré qu'un contrôle rigoureux du système de référence permettait de définir un nouveau pôle de rotation pour la plaque Antarctique (en accord avec les nouveaux pôles Indiens car là aussi il faut conserver le mouvement relatif Inde/Antarctique tel que définit par Nuvel-1a). La particularité de la plaque Antarctique est qu'étant pratiquement entourée de dorsales, la plaque tourne sur elle-même. Le pôle GPS pour ce mouvement est significativement différent du pôle Nuvel-1a, mais l'essentiel n'est pas là. Plus important: mis à part la péninsule (au sud de l'Amérique du Sud), la plaque antarctique est très rigide: les résidus par rapport à la rotation rigide de la plaque sont très faibles, de l'ordre du mm/an. Malgré tout, les bordures de cette plaque peuvent aussi être affectées par de la déformation élastique, comme l'atteste le déplacement de quelques centimètres de la station de Dumont d'Urville lors du séisme des îles Balleny en 2000. Ce n'est qu'après correction de ce déplacement co-sismique que nous trouvons le mouvement tectonique de la plaque.

Une comparaison menée avec la technique DORIS montre également que la solution GPS est beaucoup moins bruitée. De manière plus surprenante, cela est vrai aussi pour les vitesses verticales. Les résultats GPS tendent à montrer un rebond important sur les sites situés sur la péninsule Antarctique (où la fonte des glaces est très élevée et attestée par les glaciologues), et un rebond plus faible, mais néanmoins détectable sur la partie "Est" pourtant dite stable à-priori. Par comparaison, les sites sur les continents adjacents (Amérique du Sud, Afrique, Australie) ne montrent pas de mouvement verticaux significatifs, ce qui est rassurant sur la réalité de la surrection généralisée mise en évidence en Antarctique : il ne s'agit à-priori pas d'une erreur dans le système de référence.



Sur la péninsule, le rebond vertical est associé à un mouvement horizontal de "retrait", qui montre que les modèles standards (lithosphère élastique mince, sur asthénosphère visqueuse) ne fonctionnent pas très bien (ils prédisent une divergence associée à un rebond) et que donc la fonte est très importante actuellement: il ne s'agit pas seulement d'une réponse tardive à une déglaciation ancienne. Des modèles globaux en harmoniques sphériques, utilisant des stratifications verticales

de la viscosité, confirment que, contrairement aux modèles standards (James et Ivins, Sauber et al.) il est possible de changer à volonté le signe des déformations horizontales associée à un rebond. Ces différences proviennent de l'approche utilisée dans les modèles. En effet, les modèles standards considèrent un changement de masse ponctuel, appliqué sur une couche élastique mince, posée sur un manteau visqueux. La réponse à une charge ponctuelle sur une couche mince est toujours une convergence horizontale quand la charge augmente, et une divergence quand la charge diminue (c'est le modèle du ballon de baudruche). Mais quand la charge prend une grande extension latérale, l'approximation en couche mince n'est plus valide. On doit alors considérer le manteau dans son ensemble (sur toute sa hauteur) comme un milieu à propriété visco-élastique. Le mouvement horizontal local en réponse à une décharge peut alors prendre n'importe quel signe suivant la présence ou l'absence de saut(s) de viscosité en profondeur.

Enfin les séries temporelles de certaines stations (en particulier celles qui montrent une surrection importante comme O'Higgins) montrent des cycles annuels de forte amplitude (+/- 3 cm). Nous sommes toujours en train d'analyser ces séries afin de déterminer si ces cycles sont des artefacts dus aux conditions météo ou aux oscillations libres de la Terre par exemple, ou s'ils correspondent vraiment à des mouvements du sol.

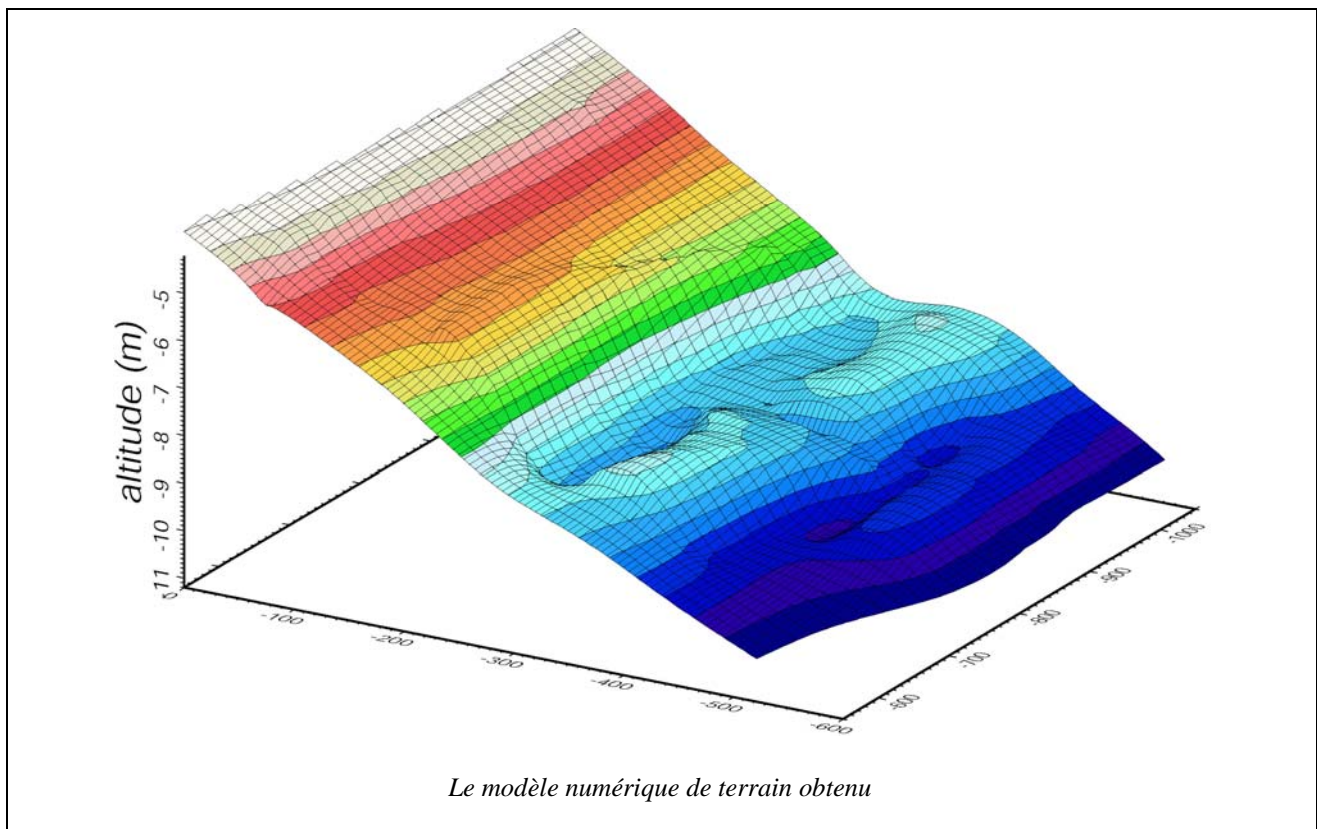
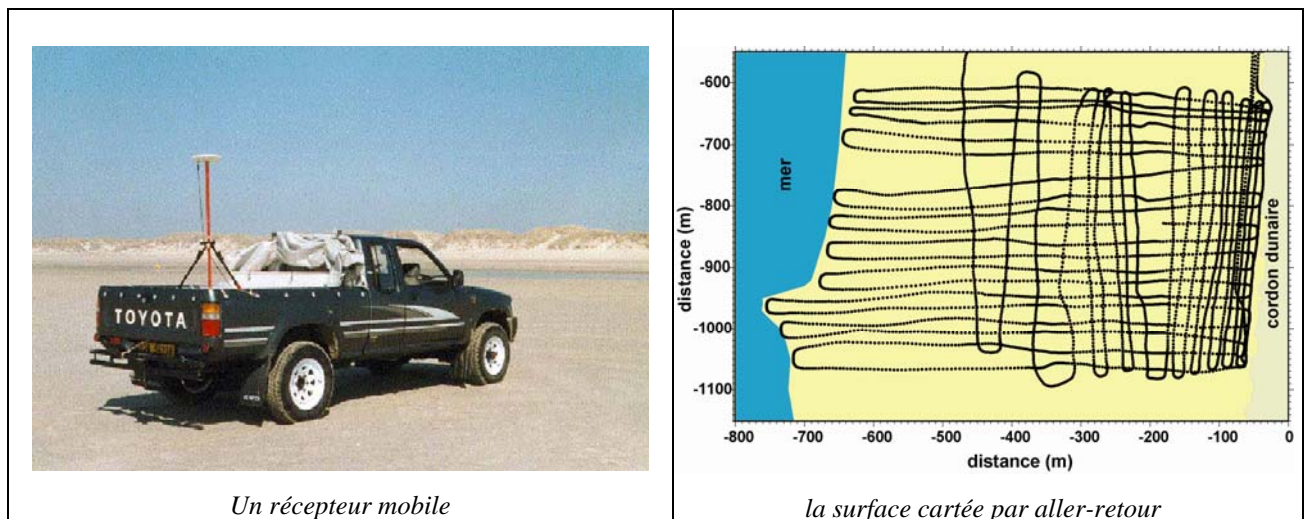
Il est clair que les incertitudes sur les mouvements verticaux déterminés sont élevées. Il est certain aussi que des biais inconnus, comme la dérive du système de référence (son échelle en particulier) peuvent sensiblement affecter ces mesures. Il convient donc de rester prudent. Malgré tout, il semble bien que toutes les stations en Antarctique montent, ce qui plaide pour une diminution générale de la masse de la calotte. Attention: diminution de masse ne veut pas nécessairement dire fonte. Il est clair que les constantes de temps longues associées à la diffusion de la chaleur dans la glace, ne peuvent conduire à une fonte rapide d'un énorme volume de glace dont la température moyenne est très largement en dessous de 0° Celsius. Ce sont d'autres phénomènes, sensibles à une variation de quelques degrés de la température, qui conduisent à la décharge.

- en premier lieu la vitesse d'écoulement des glaciers dépend fortement de la température. Si celle-ci augmente un tant soit peu, alors les glaciers peuvent accélérer énormément. Ce phénomène est connu, mais peu quantifié à l'heure actuelle. Il est donc difficile de savoir s'il suffit à expliquer les chiffres mesurés aujourd'hui.
- Ce phénomène est d'autant plus instable, qu'il est contrôlé par ce qui se passe au bout du glacier, au niveau de son arrivée dans la mer. Un bouchon de glace bloquera tout le glacier, au contraire de l'eau libre qui laissera le fleuve de glace s'écouler avec sa propre dynamique. Une débâcle locale, amplifiée par les phénomènes de circulation thermo-aline (l'eau de mer qui "grignote" les icebergs, peut donc avoir des conséquences à grande échelle très importantes.
- Enfin, compte tenu de l'énorme épaisseur de la calotte glaciaire (4 km) Il existe une épaisse couche d'eau liquide sous pression à la base de la calotte. Cette eau peut s'échapper si des fissures apparaissent aux bords de la calotte.

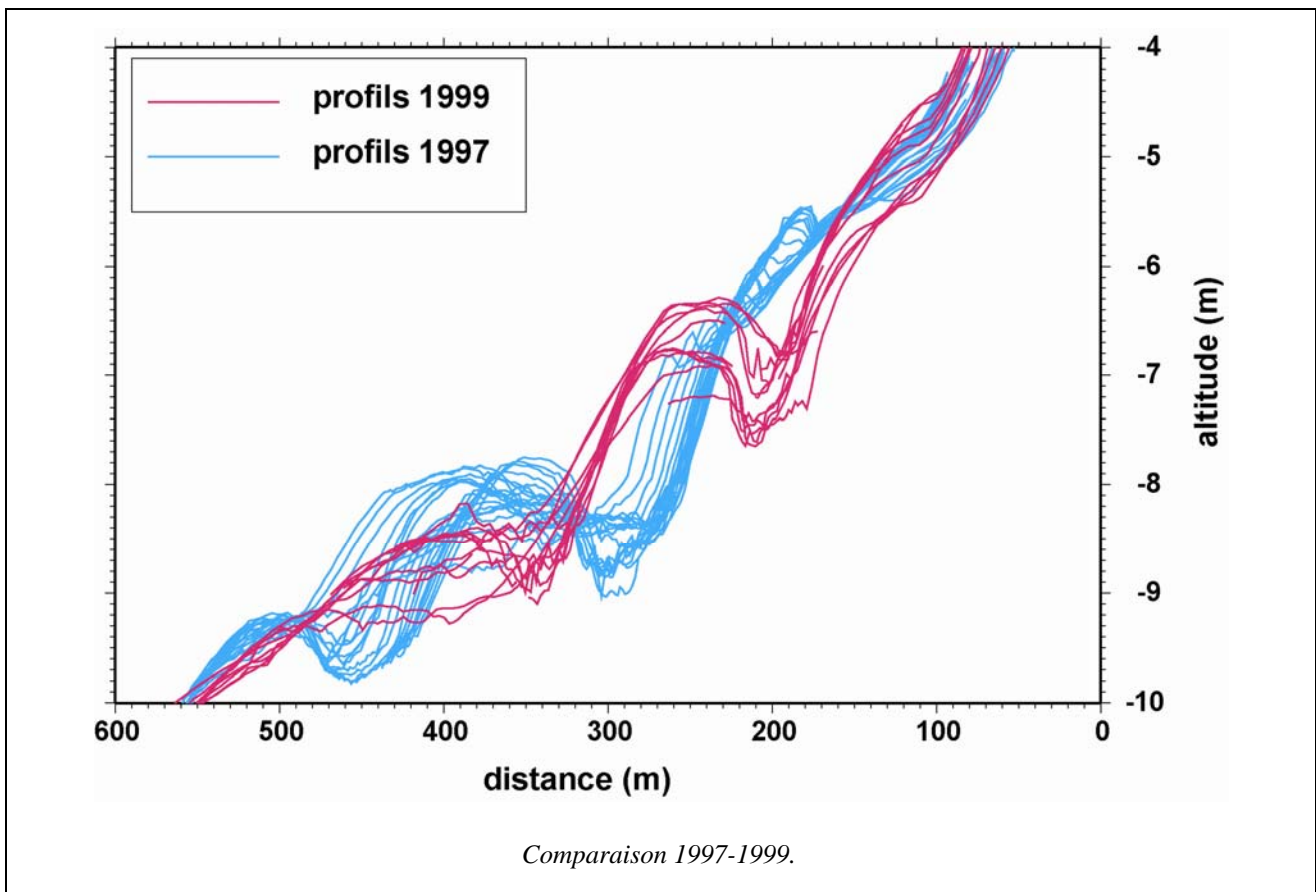
En tout état de cause, il est certain que beaucoup d'indices corroborent une décharge glaciaire actuelle importante, dont le plus spectaculaire est la désagrégation totale de la plateforme Larsen A en quelques années.

## Erosion: GPS cinématique sur un plage du nord (Merlimont)

J'ai inventé en 1995 la méthode du "GPS cinématique" pour réaliser un MNT précis d'une surface: l'idée est simple: il suffit de déplacer un récepteur GPS qui enregistre à haute fréquence sur la surface que l'on veut carter. Le calcul de la position en 3-D du récepteur mobile, relativement à une station fixe, en fonction du temps donne également l'altitude en fonction de la position horizontale: c'est un MNT. Il suffit de régler le pas d'acquisition et la vitesse de déplacement pour obtenir la grille de points avec la maille souhaitée. J'ai effectué un test de cette méthode et de son application à la mesure quantitative de l'érosion sur une zone de la plage de Merlimont (Pas de calais). Pour ce faire, j'ai réalisé une première mesure en mars 1997 puis une seconde en avril 1999, et enfin une troisième en avril 2000. A chaque fois, j'ai couvert une zone de 500m x 500m environ en une série de profils parallèles puis perpendiculaires au trait de côte, distants de 20m environ et avec un pas d'une dizaine de mètres.



La comparaison entre les deux premiers MNT effectués en Mars 1997 et Avril 1999 permet d'évaluer et de quantifier les phénomènes d'érosion et de transport sur cette surface.



On voit sur la carte des profils ci-contre que si le pied et le haut de plage n'ont pas variés en 2 ans, la surface de la plage évolue rapidement avec le temps. La comparaison des surfaces cartées en 97 et 99 montre l'évolution morphologique de celle-ci. La barre sableuse de 1 à 2 m de haut qui traverse la plage vers 250 m en 97 s'est avancée de presque 100 m en 2 ans. La bâche présente devant s'est comblée, alors que la rigole derrière s'est creusée. Il est donc à priori possible de suivre la surface d'érosion en continu en réitérant cette mesure régulièrement. Il est également possible de calculer des volumes et donc des flux de sables, à intégrer dans les modèles de transports et d'ensablement régionaux.

Lors de la mesure d'Avril 2000, j'ai mis en place une nouvelle méthodologie dans le but d'améliorer encore la précision de la mesure de l'altitude par GPS. En effet, à cause de l'évolution des orbites au cours de la mesure, on constate qu'il apparaît du bruit à basse fréquence (avec une période de l'ordre de la dizaine de minutes à 1 heure) dans l'altitude du mobile. Ce bruit apparaît clairement lorsque l'on traite les données de la station fixe comme s'il s'agissait d'une mobile. En utilisant une deuxième base fixe, on peut calculer son altitude relative par rapport au premier récepteur fixe (qui devrait être constante donc) et soustraire le signal observé de l'altitude de la station mobile. Ce faisant, on élimine complètement le bruit à basse fréquence et la dérive du système pour ne conserver que les variations réelles d'altitude de la surface. Cette méthode donne de bons résultats qui sont encore en cours de développement.

**Christophe VIGNY**  
Né le 02 Mars 1964 à Lyon, France

Baccalauréat	série C, Lycée International de St Germain en Laye
DEUG	A (Math/Physique) Université Paris XI Orsay
Licence	Physique – Option Astronomie Université Paris XI Orsay
Maîtrise	Physique – Option Mécanique des fluides Université Paris XI Orsay
Doctorat	en Sciences de la Terre Paris XI -- ORSAY / ENS Ulm Titre: Le Géoïde et la dynamique interne de la Terre. Jury: Froidevaux, Woodhouse, Ricard, Montagner, Rabinowicz, Sotin.
Post-Doc 1	à l'ONERA, équipe de P. Touboul, Modélisation des mesures gravimétriques par satellite (accéléromètres spatiaux) pour le projet ARISTOTELES/GRADIO
Post-Doc 2	au MIT, équipe de B. Hager Géodesie spatiale et tectonique des plaques

Service militaire actif effectué en 1989-1990

**Situation actuelle :** Chargé de recherches au CNRS (depuis 1991) au laboratoire de Géologie de l'Ecole Normale Supérieure (ENS), Paris, France

**Autres expériences professionnelles/administratives**

- Responsable de l'équipe de géophysique du laboratoire de 1999 à 2004
- Chargé de mission à l'INSU pour l'observation de la Terre par satellite de 1999 à 2003
- Directeur du GDR « Géodesie-Géophysique » de 2002 à 2006
- Encadrement de 4 thèses

**langues**

- Anglais : lu, écrit parlé couramment
- Portugais : courant (vécu 4 ans au Portugal, section portugaise du Lycée International)
- Italien : courant (2 ans scolaires)
- Espagnol : courant (nombreuses (6) missions au Chili depuis quelques années)
- Indonésien : notions (presque un an de missions cumulées en Indonésie et Malaisie depuis 1994)

**prix et distinctions**

- lauréat du concours général en Portugais, 1981
- médaille de bronze au championnat de France windsurfer 1984 (Brest)

## Enseignements et encadrement de recherches

### a) Bien que CNRS, j'assume une **charge d'enseignement importante : ~50h/an**

- Cours de mécanique des fluides dans le module "Géophysique" du magistère de sciences de la Terre de l'ENS
  - 20h Cours (en 2eme année) en 92, 93, 94, 95
- Cours et TD du module "champs géophysiques" du magistère de sciences de la Terre
  - 40h Cours + 40h TD (en 1ere année) en 96, 98, 99
  - 40h de cours (en 2eme année) en 2000, 2001, 2002
  - 20h de Cours (en M1) depuis
- Option « Science de la Terre » au magistère de physique de l'ENS (20 h).
  - 24h de Cours (en L3) depuis 2003
- Cours en DEA (maintenant M2)(divers modules)
  - entre 5h et 10h par an tous les ans depuis 1991
- Cours et T.D. dans le cadre de notre programme international Europe/ASEAN SEAMERGES
  - 30h Cours + 30h TD à Bangkok, Thaïlande en 2004
  - 30h Cours + 30h TD à Bandung, Indonésie en 2005
- Séminaires dans le cadre de la préparation à l'agrégation de l'ENS et de la formation des professeurs agrégés et certifiés
- conférences « grand-public » dans le cadre de la semaine de la science (palais de la découverte, collèges et lycées, Université du temps libre, séminaires Pour la Science, ...).

### b) j'ai encadré 3 thèses

- 1) L'observation de la tectonique active en Asie du sud-est par géodésie spatiale: un projet GPS." (1993/1997) (Andrea Walpersdorf)
- 2) Vitesses GPS en Antarctique et rebond post-glaciaire (1995/1999) (Marie-Noëlle Bouin)
- 3) Accommodation du mouvement relatif entre l'Inde et la Sonde depuis la Faille de Sagaing (Myanmar) jusqu'à la Syntaxe Est Himalayenne. (2000/2003) (Anne Socquet)

et j'encadre en ce moment **une autre thèse :**

- 4) GPS continu sur des grandes failles tectoniques (Chili, Indonésie) (2003-) (Alain Rudloff)

- c) Je suis membre de trois **commissions de spécialistes** (ENS TAO, ENS Géographie, et université de Versailles), du bureau scientifique de l'IERS, et du conseil scientifique de l'IGN (président de la section géodésie).

- d) j'ai été pendant 4 ans **chargé de mission à l'INSU** (ST et OA, puis SIC) pour l'observation de la Terre par satellite. Ce travail représentait une **charge à mi-temps** avec le suivi de différents programmes nationaux (PNTS, PNP, ACI « obs Terre »), l'expertise des dossiers de demandes de bourses (docteurs-ingénieurs, co-financées CNRS-régions, ...), la participation au nom de l'INSU à bon nombre de comités d'expert, de conseils scientifiques, etc...
- e) J'ai également été pendant 4 ans **responsable de l'équipe de Géophysique** (8 chercheurs – 1 ITA) du laboratoire de Géologie de l'ENS.
- f) Actuellement, après avoir démissionné des charges administratives mentionnées ci-dessus, je continue à diriger le **GDR G2« Géodésie-Géophysique »** lancé à mon initiative en 2003, dont le but est de fédérer les recherches thématiques autour du positionnement spatial précis en sciences de la Terre en rapport avec les développements récents en géodésie fondamentale (systèmes de référence ou multi-techniques par exemple).

## Bibliographie

### A] Communications à des congrès internationaux (33)

1. Geoide et dynamique interne de la Terre.  
**Vigny, C.**, Y. Ricard, et C. Froidevaux.  
*Comptes rendus de la 12<sup>e</sup> réunion des sciences de la Terre*, 1988
2. Mantle Heterogeneities, Geoid, and Plate Motion : a Monte-Carlo Inversion.  
**Vigny, C.**, Y. Ricard, and C. Froidevaux.  
*Annales Geophysicae trans. EGS*, 1988
3. From Seismic Tomography to Plate Motion.  
**Vigny, C.**, Y. Ricard, and C. Froidevaux.  
*Annales Geophysicae trans. EGS*, 1989
4. Mantle Dynamics in the Presence of Rigid Lithospheric Plates  
Ricard Y., **C. Vigny** and C. Froidevaux.  
*Annales Geophysicae trans. EGS*, 1989
5. Mantle Dynamics in the Presence of Rigid Lithospheric Plates  
**Vigny, C.**, and Y. Ricard.  
*Terra abstracts trans. EUG*, 1989
6. From Seismic Tomography to Plate Motion.  
Froidevaux C., Y. Ricard, and **C. Vigny**.  
*Terra abstracts trans. EUG*, 1989
7. Precision of the 1990 Fort Davis Site Stability Survey.  
Bell, L., G. Mader, M. Schenewerk, **C. Vigny**, R. King, B. Shutz, C. Wilson, M. Bryant, E. Pavlis, and V. Nelson.  
*EOS trans. AGU*, 1991
8. Analysis of the 1990 GPS Fort Davis Footprint.  
**Vigny, C.** and R. King.  
*Annales Geophysicae trans. EGS*, 1992
9. First Epoch Geodetic GPS Measurements across the Afar Plate Boundary Zone  
**Vigny C.**, J.C. Ruegg, P. Briole, K.L. Feigl, A. Orsoni.  
*EOS trans. AGU*, 1993
10. Two years of GPS measurements on the Arta-Sana'a line across the Afar plate boundary  
Walpersdorf, A., and **C. Vigny**  
*Annales Geophysicae trans. EGS*, 1994
11. First GPS Measurements Over the Alps 1993-1994.  
**Vigny, C.**, J. Chery, and G. Ferhat.  
*EOS Trans. IUGG*, 1995.
12. GEODYSSSEA -- A Network for Geodynamics Across South-East Asia.  
Wilson P., X. LePichon, M. Kasser, E. Reinhart, B. Ambrosius, N. Vlaar, D.P. Zakaria, I. Bahar, S. Sutisna, A. Majid, R. Almeda and F. Wasu, on behalf of the GEODYSSSEA working group.  
*EOS trans IUGG*, 1995
13. First results from the GEODYSSSEA 1994 GPS campaign  
Angerman, D., G. Baustert, P. Wilson, M. Becker, C. Bruijninx, P.A. Cross, L. Pezzoli, **C. Vigny**, and A. Walpersdorf.  
*Annales Geophysicae trans. EGS*, 1996
14. Modélisation 3D de surfaces Géologiques à partir de données spatiales : apport de la fusion d'information MNT-SPOT & GPS.  
Vidal, G., **C. Vigny**, F. Thoué, et P. Leturmy.  
*Comptes rendus de la 17<sup>e</sup> réunion des sciences de la Terre*, 1997
15. Geodetic Evidence for the Seismic Behaviour of the Great Sumatran Fault, Indonesia.  
Duquesnoy, T., O. Bellier, M. Sebrier, M. Kasser, **C. Vigny**, I. Bahar, E. Putranto, F. Ego, and I. Effendi.  
*Terra Nova V9, abstracts trans. EUG*, 1997
16. Landslide Slip Surfaces Computation from High Resolution DEM Registered on GPS Control Points.  
Vidal, G., F. Thoué, **C. Vigny**, and M. Méminier.  
*Terra Nova V9, abstracts trans. EUG*, 1997
17. GPS observations of the tectonic activity in the triple junction area in Indonesia.  
Walpersdorf, A., **C. Vigny**, P. Manurung, C. Surbarya and S. Sutisna.  
*EOS trans. AGU*, 1997

18. Instantaneous and finite kinematics in the northern arm of Sulawesi.  
Walpersdorf, A., **C. Vigny**, C. Rangin, H. Bellon, B. Priadi.  
*GEODYSSSEA Concluding International Symposium, Penang, Malaysia, 1997*
19. The Error Budget of the GEODYSSSEA GPS Solution  
**Vigny, C.**, and A. Walpersdorf.  
*GEODYSSSEA Concluding International Symposium, Penang, Malaysia, 1997*
20. Interpretation of GPS Observations in the Triple Junction Area in Indonesia.  
Walpersdorf, A., W. Simmons, B.A.C Ambrosius, D. VanLoon, J. Kahar, **C. Vigny**, and C. Stevens.  
*Annales Geophysicae trans. EGS , 1998*
21. Deformation in the Palu-Koro fault region (Sulawesi) observed by GPS.  
Walpersdorf, A., W. Simmons, B.A.C Ambrosius, D. VanLoon, J. Kahar, **C. Vigny**, and C. Stevens.  
*Annales Geophysicae trans. EGS , 1998*
22. GPS Data Processing in Antarctica : a Geodetic Measurement of Glacial Rebound.  
Bouin, M.N, and **C. Vigny**.  
*Annales Geophysicae trans. EGS , 1999*
23. GPS Data Analysis in Antarctica : Crustal motions, GPS Data Processing, and Reference Systems.  
Bouin, M.N, and **C. Vigny**.  
*EOS trans. AGU , 1999*
24. Tectonic Deformation near the Triple Junction in S.E. Asia : Results and Outlook.  
Simons, W., D. Van Loon, B. Ambrosius, **C. Vigny**, A. Walpersdorf, J. Kahar, H. Abidin, C. Subarya, and P. Manurung.  
*trans. GPS99, Tsukuba, 1999, invited*
25. Migration of Seismicity and Earthquake Interractions in S.E. Asia Triple Junction.  
**Vigny, C.**, A. Walpersdorf, H. Perfettini, W. Simons, D. Van Loon, B. Ambrosius, C. Subarya, P. Manurung, J. Kahar, and H. Abidin.  
*trans. GPS99, Tsukuba, 1999*
26. GPS network monitors Sagaing Fault, Myanmar.  
**Vigny, C.**, C. Rangin, M. Pubellier, A. Socquet, N. Chamot-Rooke  
*EOS trans. AGU , 2001*
27. Thermo-Mechanical modeling of seismic cycle and Quaternary Deformation of the Asal Rift, Djibouti, Africa:  
Implication for the Rheology of the Lithosphere  
Cattin, R., J.B. de Chabalier, G. King, **C. Vigny**, J.P. Avouac, J.C. Ruegg  
*EOS trans. AGU , 2001*
28. Crustal motion and block behaviour in S.E.-Asia from GPS Measurements  
Simons, W., D. Van Loon, B. Ambrosius, **C. Vigny**, A. Lemoine, C. Subarya, R.W. Mattindas, J. Kahar, S.H. Abu, M.A. Kadir, H. Wongissares, and P. Burinrwatana.  
*Western Pacific Geophysics meeting, Wellington NZ, trans. AGU, 2002, invited*
29. Active deformation in SE Asia documented by regional and local GPS networks  
Rangin, C., K. Le Pichon, M. Pubellier, C. Kreemer, and **C. Vigny**  
*Western Pacific Geophysics meeting, Wellington NZ, trans. AGU, 2002, invited*
30. Accommodation Of The Relative Motion Between India And Sundaland  
Socquet, A., **C. Vigny**, N. Chamot-Rooke, M. Pubellier, C. Rangin  
*Western Pacific Geophysics meeting, Wellington NZ, trans. AGU, 2002*
31. Monitoring of the December 26<sup>th</sup> 2004 mega-thrust earthquake in SE Asias by GPS  
**Vigny, C.**, W. Simons, S. Abu, R. Bamphenyu, C. Satirapod, M. Hashizume, C. Subarya, P. Tregoning, B. Ambrosius  
*Geophysical Research abstracts, trans. EGU, EGU05-A-10732, 2005, invited*
32. Status of GPS based investigations on the 26 December 2004 mega-thrust earthquake  
**Vigny, C.**, W. Simons, S. Abu, , Chaiwat Promthong, C. Satirapod, A. Socquet, R. Cattin, J. Pietrzak, Kee Tuan Chew, D. Sarsito, B. Ambrosius  
*Geophysical Research abstracts, trans. EGU, EGU06-A-?????, 2006*
33. *Geohazards: the example of Dec. 2004 mega thrust earthquake*  
**Vigny, C.**, W. Simons, S. Abu, , Chaiwat Promthong, C. Satirapod, A. Socquet, R. Cattin, J. Pietrzak, Kee Tuan Chew, D. Sarsito, B. Ambrosius  
Nederlands .Aardwetenschappelijk Congress (NAC) 8, Veldhoven, The Netherlands, 24-25 April 2006, invited

**B] Publications dans des revues sans comité de lecture (11)**

34. Le champ de gravité de trois planètes telluriques : la Terre, Mars et Venus.  
Ricard, Y., et C. Vigny.  
*revue interne du CNES*, 1988
35. GPS: How and what for ?  
**Vigny C.**  
*Sciences and Research, special volume on Franco-Nepalese geophysical research*, 3, 1-7, 1996
36. GPS compared to Long-Term Geologic Motion of the northern arm of Sulawesi.  
Walpersdorf A., C. Rangin, and C. Vigny.  
*The GEODYSSSEA project, Scientific Technical Report STR98/14 to the Europ. Com.*, 1998
37. GPS Observation of the Triple Junction, Indonesia.  
Walpersdorf A., C. Vigny, P. Manurung, C. Surbarya and S. Sutisna.  
*The GEODYSSSEA project, Scientific Technical Report STR98/14 to the Europ. Com.*, 1998
38. The Final Geodetic results of the GEODYSSSEA Project : The Combined Solution  
Simons, W., B.A.C Ambrosius, R. Noomen, D. Angermann, P. Wilson, M. Becker, E. Reinhart, A. Walpersdorf, and C. Vigny.  
*The GEODYSSSEA project, Scientific Technical Report STR98/14 to the Europ. Com.*, 1998
39. Quantitative Estimation of Plate Convergence Across the Sundaland/Philippine Sea-Plate Boundary from GPS results (GEODYSSSEA).  
Rangin, C., M. Pubellier, N. Chamot-Rooke, C. Vigny, X. LePichon, M. Aurelio, and R. Quebral.  
*The GEODYSSSEA project, Scientific Technical Report STR98/14 to the Europ. Com.*, 1998
40. Sundaland motion in a global reference frame detected from GEODYSSSEA GPS measurements : implications for relative motions at its boundaries with the Australian-Indian plates and the South-China block.  
Chamot-Rooke, N., X. LePichon, C. Rangin, P. Huchon, M. Pubellier, C. Vigny, and A. Walpersdorf.  
*The GEODYSSSEA project, Scientific Technical Report STR98/14 to the Europ. Com.*, 1998
41. Earthquake induced Tsunami awareness : initiatives toward plate tectonic monitoring in the southeast asian region using space geodetic techniques.  
Ses, S., M. Kadir, K. Omar, G. Desa, F. Nordin, S. Abu, A. Mohamed, S. Nordin, W. Simons, C. Vigny  
*The Malaysian Surveyor, Inst. Survey. Malaysia, ISSN 0127-4937, pp735/2/2005, pp9-19*, 2005
42. The 26 December 2004 Sumatra Earthquake and Tsunami seen by Satellite Altimeters and GPS  
Ambrosius, B., R. Scharro, C. Vigny, E. Schrama and W. Simons  
*Geo-information for Disaster Management, Springer-ISBN: 3-540-24988-5, pp 323-336*, 2005
43. Mesures GPS continues et tectonique des plaques  
**Vigny, C.**, A. Socquet, A. Rudloff  
*Géochronique*, publication BRGM/SGF, juillet 2005
44. Le séisme de Sumatra vu par GPS  
**Vigny, C.**, A. Socquet  
*Pour la Science*, mai 2006

**C] Publications dans des revues à comité de lecture : rang B (4)**

45. Global Positioning System Network Monitors the Western Alps.  
Chery, J., **C. Vigny**, B. Meyer, G. Ferhat, M. Anzidai, R. Bayer, L. Boloh, P. Briole, A. Deschamps, K.L. Feigl, J.F. Gamond, A. Geiger, F. Jouanne, M. Kasser, M. Leppape, J. Martinod, G. Menard, J.C. Ruegg, J.M. Scheubel, and J.J. Walch.  
*EOS, Vol. 76, 48*, November 28, 1995
46. Study Provides Data on Active Plate Tectonics in South-East Asia Region.  
Wilson et al. on behalf of the **GEODYSSSEA working group**.  
*EOS, Vol 79, n 45*, Nov. 10, 1998.
47. Etude géodésique d'un segment sismique de la Grande Faille de Sumatra (Indonésie).  
*"Geodetic study of a seismic segment of the Great Sumatran Fault (Indonesia)"*.  
Duquesnoy T., O. Bellier, M. Sébrier, M. Kasser, **C. Vigny**, F. Ego, I. Bahar, E. Putranto, et I. Efendi.  
*Bull. Soc. Géol. France, t. 170, N 1*, pp. 25-30, 1999.
48. REGAL: réseau GPS permanents dans les Alpes occidentales. Configuration et premiers résultats.  
Calais, E., R. Bayer, J. Chéry, F. Cotton, E. Doerflinger, M. Flouzat, F. Jouanne, M. Kasser, M. Laplanche, D. Maillard, J. Martinod, F. Mathieu, P. Nicolon, J.M. Nocquet, O. Scotti, L. Serrurier, M. Tardy, **C. Vigny**  
*C. R. Acad. Sci., 331*, pp435-442, 2000.

D] Publications dans des revues à comité de lecture : rang A (30)

49. Mantle heterogeneities, geoid and plate motion: a Monte Carlo inversion.  
Ricard, Y., **C. Vigny**, and C. Froidevaux.  
*J. Geophys. Res.*, **94**, 13739-13754, 1989
50. Mantle dynamics with induced plate tectonics.  
Ricard, Y., and **C. Vigny**.  
*J. Geophys. Res.*, **94**, 17543-17559, 1989
51. The driving mechanism of plate tectonics.  
**Vigny**, C. and C. Froidevaux.  
*Tectonophysics*, **187**, 345-360, 1991
52. On the origin of deviatoric stresses in the lithosphere.  
Bai Wuming, **C. Vigny**, Y. Ricard, and C. Froidevaux.  
*J. Geophys. Res.*, **97**, 11,729-11,737, 1992
53. First Epoch Geodetic GPS Measurements Across the Afar Plate Boundary Zone.  
Ruegg, J.C., P. Briole, K. Feigl, **C. Vigny**, M. Anis Abdallah, O. Bellier, P. Huchon, S. Al Khirbashi, A. Laike, N. d'Oreye, and M. Prevot.  
*Geophys. Res. Lett.*, **20**, 1899-1902, 1993
54. Insights on the Fort Davis - Mc Donald Site Stability : a GPS Footprint.  
**Vigny C.**  
*Journal of Geodesy*, **70**, 300-306, 1996
55. Deformation related to the 1994 Liwa Earthquake derived from Geodetic Measurements.  
Duquesnoy T., O. Bellier, M. Kasser, M. Sebrier, **C. Vigny**, I. Bahar.  
*Geophys. Res. Lett.*, **21**, 3055-3058, October 1996
56. GPS measurements of present-day convergence across the Nepal Himalaya.  
Bilham R., K. Larson, J. Freymuller, and **Project Idylhim members**  
*Nature*, **386**, 61-63, March 1997
57. Determining the Sula Block kinematics in the triple junction area in Indonesia by GPS  
Walpersdorf A. and **C. Vigny**.  
*Geophysical Journal International*, **Vol 135, Issue 2**, pp351-361, 1998.
58. GPS compared to long-term geologic motion of the North arm of Sulawesi.  
Walpersdorf A., C. Rangin, and **C. Vigny**.  
*Earth and Planetary Science Letter*, **Vol 159**, pp47-55, 1998.
59. Monitoring of the Palu-Koro Fault (Sulawesi) by GPS.  
Walpersdorf A., **C. Vigny**, C. Subarya, and P. Manurung.  
*Geophysical Research Letters*, **Vol 25, N 13**, pp 2313-2316, 1998.
60. 5 Years of GPS Observations in the Afar Triple Junction Area.  
Walpersdorf A., **C. Vigny**, J.-C. Ruegg, P. Huchon, L. M. Asfaw and S. Al Kirbashi.  
*Journal of Geodynamics*, **Vol. 28, issue 2-3**, pp. 225-236, 1999.
61. Convergence in the Himalayas of western Nepal deduced from preliminary results of GPS measurements.  
Jouanne, F. , Mugnier J. L., Pandey M.R. , Gamond J.F. , Le Fort P., Serrurier L., **Vigny C.**, Avouac J.P. and Idylhim members.  
*Geophysical Research Letters*, **Vol 26, N 13**, pp 1933-1936, 1999.
62. Observing Plate motions in S.E. Asia : Geodetic results of the GEODYSSSEA project.  
Simmons W., B Ambrosius, R. Noomen, D. Angermann, P. Wilson, M. Becker, E. Reinhart, A. Walpersdorf, and **C. Vigny**.  
*Geophysical Research Letters*, **Vol 26, N 14**, pp 2081-2084, 1999.
63. Rapid rotations about a vertical axis in a collisional setting revealed by the Palu fault, Sulawesi, Indonesia.  
C. Stevens, R. McCaffrey, Y. Bock, J. Genrich, Endang, C. Subarya, S.S.O. Puntodewo, Fauzi, and **Vigny C.**  
*Geophysical Research Letters*, **Vol 26, N 17**, pp 2677-2680, 1999.
64. Plate convergence measured by GPS across the Sundaland-Philippines Sea Plate deformed boundary (Philippines and Eastern Indonesia).  
Rangin C., M. Pubellier, N. Chamot-Rooke, A. Walpersdorf, **C. Vigny**, X. Le Pichon, M. Aurelio, and R. Quebral.  
*Geophysical Journal International*, **139**, pp 296-316, 2000.
65. New constraints on Antarctic plate motion and deformation from GPS data.  
M-N Bouin and **C. Vigny C**  
*J. Geophys. Res.*, **105**, pp 28279-28294, 2000.
66. Crustal motion and block behavior in SE-Asia from GPS measurements.

- Michel, G., Y. Yu, S. Zhu, C. Reigber, M. Becker, E. Reinhart, W. Simons, B. Ambrosius, **C. Vigny**, N. Chamot-Rooke, X. LePichon, P. Morgan, S. Matheussen.  
*Earth and Physics Science letters*, **187**, pp 289-244, 2001.
67. GPS network monitor the western Alps over a five year period : 93-98.  
**C. Vigny**, J. Chery, T. Duquesnoy, F. Jouanne, J. Ammann, M. Anzidei, J.P. Avouac, F. Barlier, R. Bayer, P. Briole, E. Calais, F. Cotton, F. Duquenne, K. Feigl, G. Ferhat, M. Flouzat, J.F. Gamond, A. Geiger, A. Harmel, M. Kasser, M. Laplanche, M. Le Pape, J. Martinod, G. Menard, B. Meyer, J.C. Ruegg, J.M. Scheubel, O. Scotti, G. Vidal.  
*Journal of Geodesy*, **76**, pp 63-76, 2002
68. Migration of seismicity and earthquake interactions monitored by GPS in S.E. Asia triple Junction : Sulawesi, Indonesia.  
**C. Vigny**, H. Perfettini, A. Walpersdorf, A. Lemoine, W. Simons, D. Van Looon, B. Ambrosius, C. Stevens, R. McCaffrey, P. Morgan, Y. Bock, C. Subarya, P. Manurung, J. Kahar, H. Abidin, S. Abu.  
*J. Geophys. Res.*, **107**(B10), 2231, doi:10.1029/2001JB000377, 2002.
69. GPS network monitors the Arabia-Eurasia collision deformation in Iran.  
Nilforoushan, F., P. Vernant, F. Masson, **C. Vigny**, J. Martinod, M. Abbasi, H. Nankali, D. Hatzfeld, R. Bayer, F. Tavakoli, A. Ashtiani, E. Doerflinger, M. Daignières, P. Collard, J. Chéry.  
*Journal of Geodesy*, **77**:422-441, doi:10.1007/s00190-003-0326-S, 2003.
70. Present day crustal deformation around Sagaing fault, Myanmar  
**Vigny**, C., A. Socquet, C. Rangin, N. Chamot-Rooke, M. Pubellier, M.N. Bouin, G. Bertrand, M. Becker.  
*J. Geophys. Res.*, **108**(B11), 2533, doi:101029/2002JB001999, 2003.
71. Present day crustal deformation and plate kinematics in Middle East constrained by GPS measurements in Iran and northern Oman  
Vernant, P., F. Nilforoushan, D. Hatzfeld, M. Abbasi, **C. Vigny**, F. Masson, H. Nankali, J. Martinod, A. Ashtiani, R. Bayer, F. Tavakoli, J. Chéry.  
*Geophysical Journal International*, **157**, 381-398, 2004.
72. Numerical modeling of quaternary deformation and post-rifting displacement in the Asal-Ghoubbet rift (Djibouti, Africa)  
Cattin, R., C. Doubre, J.B. DeChabalier, G. King, **C. Vigny**, J.P. Avouac, and J.C. Ruegg  
*Earth and Physics Science letters*, **239**, 352-367, 2005.
73. Insight into the 2004 Sumatra-Andaman earthquake from GPS measurements in southeast Asia  
**Vigny**, C., W. Simons, S. Abu, R. Bamphenyu, C. Satirapod, N. Choosakul, C. Subarya, A. Socquet, K. Omar, H. Abidin and B.A.C. Ambrosius  
*Nature*, vol 436, 14/07/05, pp201-206, doi:10.1038/nature03937, 2005
74. Confirmation of Arabia plate slow motion by new GPS data in Yemen.  
**Vigny**, C., P. Huchon, J.C. Ruegg, K. Khanbari, and L. Asfaw  
*J. Geophys. Res.*, **111**, B02402, doi:10.1029/2004JB003229, 2006.
75. 25 years of geodetic measurements along the Tadjoura-Asal rift system, Djibouti, East Africa  
**Vigny**, C., J.B. DeChabalier, J.C. Ruegg, P. Huchon, K. Feigl, R. Cattin, L. Asfaw and K. Khanbari  
*J. Geophys. Res.*, accepted, 2006.
76. GPS determination of the relative motion between India and Sunda, and its accommodation in Myanmar  
Socquet, A., **C. Vigny**, W. Simons, N. Chamot-Rooke, C. Rangin, B. Ambrosius  
*J. Geophys. Res.*, in press, 2006.
77. A decade of GPS measurements in SE Asia: (Re)Defining Sundaland motion and boundaries  
Simons, W., A. Socquet, **C. Vigny**, S. Matheussen, B. Ambrosius, C. Subarya, R. Mattindas, D. Sarsito, J. Kahar, S. Abu, H. Ali, C. Promthong, P. Swangnet, M. Iwakuni, T. Kato, P. Morgan, and W. Spakman  
*J. Geophys. Res.*, submitted, 2004.
78. Kinematic behaviour, crustal block rotations and plate coupling in the triple junction area in SE Asia from inversion of GPS and slip vector data (Sulawesi, Indonesia)  
Socquet, A., W. Simons, **C. Vigny**, R. McCaffrey, B. Ambrosius, W. Spakman, C. Subarya and D. Sarsito  
*J. Geophys. Res.*, accepted, 2006.



# A Decade of GPS Measurements in S.E. Asia: (Re)Defining Sundaland Motion and its Boundaries

W.J.F. Simons,<sup>1</sup> A. Socquet,<sup>1</sup> C. Vigny,<sup>2</sup> S. Matheussen,<sup>1</sup> B.A.C. Ambrosius,<sup>1</sup> C. Subarya,<sup>3</sup> R.W. Matindas,<sup>3</sup> D.A.C. Sarsito,<sup>4</sup> J. Kahar,<sup>4</sup> S. Haji Abu,<sup>5</sup> H. Bin Ali,<sup>5</sup> Chaiwat Promthong,<sup>6</sup> Phanusak Swangnet,<sup>6</sup> M. Iwakuni,<sup>7</sup> T. Kato,<sup>7</sup> P. Morgan<sup>8</sup> and W. Spakman<sup>9</sup>

**Abstract.** An updated geodetic solution on crustal velocities in S.E. Asia is presented. Parts of the existing GEODYSSSEA network in S.E. Asia were re-measured, and episodic and/or permanent data from new GPS points in Indonesia, Malaysia, Myanmar and Thailand were added. The expanded GPS database on S.E. Asia now provides more than 100 velocity estimates with horizontal accuracies of 0.5–2.5 mm/yr. To achieve this, both the GIPSY GPS software package and the International Terrestrial Reference Frame solution of 2000 (ITRF-2000) were used, thereby using improved processing and mapping strategies. Based on 28 velocity vectors on its rigid part, a refined pole for Sundaland in ITRF-2000 was computed, located at 48.9° S and 85.8° E and with a clockwise rotation rate of 0.341°/Myr. The Sundaland block is composed of a rigid core, characterized by very slow strain rates and residual velocities < 3 mm/yr, which covers the Indochina and Malaysian peninsulas in the North and West, the Sunda shelf, the major part of Borneo in the East and extends to the South almost until Java. However, strain rates increase from the core of Sundaland outwards, with significant deformation occurring close to its boundaries. With respect to GPS Eurasia, Sundaland rotates clockwise at 0.106°/Myr around a pole located at 108°E, 36°S. The predicted Sundaland / Eurasia motion confirms an Eastward motion, increasing from south to north, of Sundaland with respect to Siberia. With respect to South China, the motion is small but significant and increases from very small values within the South China Sea in the pole area, to higher strain rates in the Red River area.

## 1. Introduction

The plate tectonics concept [McKenzie and Parker, 1967; Morgan, 1968; Le Pichon, 1968; Chase, 1972, 1978; Minster and Jordan, 1978] was a fundamental advance in understanding global Earth behavior, however it still lacks in complexity to describe continental area's kinematics and deformation. For example, the NUVEL-1A model [DeMets *et al.*, 1990, 1994] presents a global plate motion model, averaged for the last 3 Myrs, based on geological constraints. For Eurasia, this kinematic model predicts a rigid plate from Western Europe until South-East Asia. However, it was recognized early that the spectacular Asiatic relief pattern attests for intra-continental deformation extending from the Himalayas to the Baikal rift zone to the North, and until the Red River Fault in the South East, resulting from the collision between India and Eurasia [Argand, 1924].

Deformation of Asia has been extensively studied from the 70's by

analysis of satellite imagery [Tapponnier and Molnar, 1977, 1979], geological and seismological studies [Molnar and Tapponnier, 1978; Molnar and Lyon-Caen, 1989]. To explain the geological features and the geophysical data set, end-members models assume that continents deform either by viscous flow of a continuously deforming medium [England and Houseman, 1985, 1986; Houseman and England, 1986, 1993] or by motion of rigid lithospheric blocks along narrow fault zones [Tapponnier *et al.*, 1982; Tapponnier, 1986; Peltzer and Tapponnier, 1988; Avouac and Tapponnier, 1993; Peltzer and Saucier, 1996; Meyer *et al.*, 1998]. Discriminating these end-members models requires spatially dense measurements of surface strain rate. High accuracy GPS measurements can constrain models for a better understanding of the mode of deformation of the lithosphere and of the plates kinematics.

The Sundaland block, making up a large part of South-East Asia, has been the subject of discussions whether or not it has a significant motion with respect to the Eurasian plate and how the deformation is distributed between Siberia and South-East Asia.

Initial GPS results in S.E. Asia (eg. [Tregoning *et al.*, 1994; Genrich *et al.*, 1996]) led to the conclusion that this region seemed rigidly connected to the Eurasian plate. However, this conclusion was obtained from using mostly local GPS data, many of which are located in deformation zones (Sumatra, Java, Sulawesi, Banda Arc) and hence not belong anymore to rigid Sundaland. Later, the results of the GEODYSSSEA project [Wilson *et al.*, 1998; Chamot-Rooke *et al.*, 1998; Simons *et al.*, 1999; Michel *et al.*, 2001] showed clearly that the Sundaland block presents a rigid motion with respect to Eurasia and is separated from the Siberian platform through a series of deforming and moving blocks, invalidating by the way the NUVEL-1A model [DeMets *et al.*, 1994] for present-day deformation. This project, led between 1994 and 1998, used a GPS network systematically distributed over Sundaland, which is most suited to accurately determine a rigid plate motion.

Since then, the GPS database on South-East Asia has been expanded by including new high-quality GPS measurements of both episodically and continuously operated sites. Besides actively carrying out GPS surveys through international cooperation, this was

<sup>1</sup>Department of Earth Observation and Space Systems (DEOS), Delft University of Technology, Delft, The Netherlands

<sup>2</sup>École Normale Supérieure (ENS), Paris, France

<sup>3</sup>National Coordination Agency for Surveys and Mapping (BAKOSURTANAL), Cibinong, Indonesia

<sup>4</sup>Institute of Technology Bandung (ITB), Bandung, Indonesia

<sup>5</sup>Department of Survey and Mapping Malaysia (DSMM), Kuala Lumpur, Malaysia

<sup>6</sup>Royal Thai Survey Department (RTSD), Bangkok, Thailand

<sup>7</sup>Earthquake Research Institute, University of Tokyo, Tokyo, Japan

<sup>8</sup>University of Canberra (UC), School of Computing, Canberra, Australia

<sup>9</sup>Faculty of Earth Sciences, University of Utrecht, Utrecht, The Netherlands

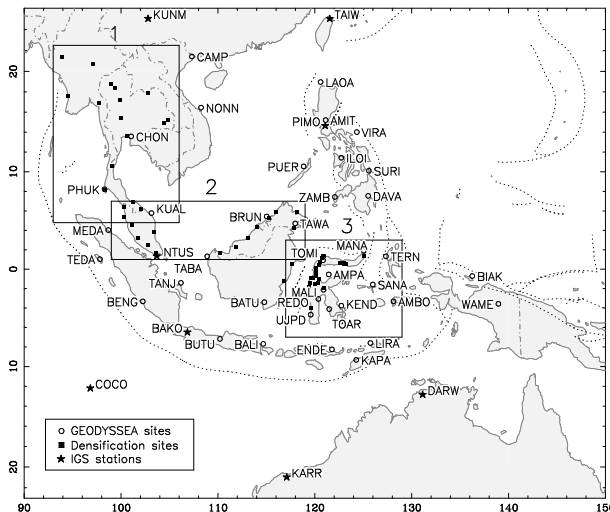


**Figure 1.** Regions densified in the GEODYSSSEA GPS network since 1997.

mostly done by sharing data from European, Indonesian, Japanese, Malaysian and Thai sources. This has resulted in an exclusive GPS data set, which spans almost a decade, and includes data from 100+ GPS sites, that were almost all at least observed 3 times, and of which 30 are continuously operating GPS stations that up to present are not available to the international GPS community. All this data was (re)processed, using the latest state-of-the-art processing techniques, and up to 30 (global+regional) IGS sites were included in this network. Moreover, with the International Terrestrial Reference Frame (ITRF) 2000 [Altamimi *et al.*, 2002] becoming available in 2001, the ITRF velocities of relatively recent sites located in S.E. Asia became more accurate, allowing a better mapping into the ITRF. With more than 40 sites now available on Sundaland, a further refinement of the Sundaland can be given.

The aim of this paper is to present a redefinition of the Sundaland block and its boundaries.

We first describe the expansion of the GPS data in S.E. Asia, then explain the applied processing and mapping strategy and the geodetic results. Next attention is given to an update of the Sundaland pole in ITRF-2000 and to the description of the Sundaland boundaries, as well as observed deformation in and around the Sundaland block. The updated Sundaland motion with respect to the neighbouring plates will then be discussed. Enlightened by the latest results on Eurasian plate [Calais *et al.*, 2003], we will especially focus on the relative motion between these two plates and on the intra-continental deformation between Siberia and South East Asia.

## 2. Densified GPS network in S.E. Asia

The GEODYSSSEA network shown in Fig. 1 covers an area of about 4000 by 4000 km in South and South-East Asia, and has resulted in velocity estimates at about 40 geodetic points between 1994 and 1998 [Michel *et al.*, 2001]. Although the network provides a good coverage of the major tectonic blocks in the region, further densification and additional geodetic measurements were required to update, expand and improve the existing geodetic results within Sundaland. Important is also to further study the complex geodynamics near the boundaries on this block. A complete densification and simultaneous (continuous) measurement of the existing GEODYSSSEA network would not be efficient and expensive to realize. Therefore only selected parts of the network have been expanded (the rectangular regions 1, 2 and 3 shown in Fig. 1) in/near Thailand, Malaysia and on/near the island of Sulawesi, Indonesia. More detailed figures on each region can be viewed at <http://www.deos.tudelft.nl/~wims/sunda.html>. Where possible,

continuously operating stations were included in the network, which were setup separately from the GEODYSSSEA project, namely in Malaysia, Thailand and Indonesia. Care was taken to only introduce the best available geodetic GPS data (3-5 days per episodical measurement), resulting in highly accurate motions suitable for detailed geophysical interpretations and derived models.

The densification in/near Thailand (Region 1 in Fig. 1 resulted from the addition of the complete THAICA and GAME-T networks in Thailand, and part of the ENS network in Myanmar. The THAICA network [Mingsamor *et al.*, 1998] is the first order network of Thailand, and was established and designed by the Royal Thai Survey Department (RTSD). This network, consisting out of 5 sites, was (partly) measured in 1994 and 1996 alongside with the GEODYSSSEA network, and again in 2000, 2001 and 2002. The GAME-T (GEWEX Asia Monsoon Experiment Tropics) [Takiguchi *et al.*, 2000; Iwakuni *et al.*, 2003] GPS network was setup to understand the role of the Asian monsoon. The data of the 6 permanent sites that were operational from 1998 to 2001 is also very suited to study the tectonics in this region. In 1998, coinciding with the 1998 GEODYSSSEA GPS campaign, the École Normale Supérieure (ENS) has measured a GPS network in Myanmar [Vigny *et al.*, 2003], including a transect of the Sagaing fault. Four reference sites were included in the GEODYSSSEA-98 data set, and the Myanmar net-

**Table 1.** Overview of the available sites in the 1994-2003 GPS database. The table shows the size of all the (sub-)networks in each region, followed by the number of sites observed in each year. Numbers marked with \* indicate that all the available permanent data was daily processed for that particular year.

Description	Size	Year									
		94	96	97	98	99	00	01	02	03	
GEODYSSSEA	<b>40</b>	39	40	14	38	4	10	4	9	6	
<b>Region 1</b>											
THAICA	<b>5</b>	5	3	-	-	-	1	5	5	-	
ENS	<b>4</b>	-	-	-	4	-	4	-	-	-	
GAME-T	<b>6</b>	-	-	-	6*	5*	5*	5*	-	-	
<b>Region 2</b>											
MASS	<b>17</b>	-	-	-	9	15*	15*	17*	17	14	
<b>Region 3</b>											
GEODYSSSEA Sec.	<b>14</b>	-	6	7	7	4	8	7	12	12	
BAKO monuments	<b>6</b>	-	-	1	1	4	5	5	6	6	
BAKO permanent	<b>7</b>	-	1	2	2	3*	5*	4*	7	7	
<b>IGS</b>											
Local (S.E. Asia)	<b>3</b>	-	-	1	2*	3*	3*	3*	3	3	
<b>Subtotal</b>	<b>102</b>	44	50	25	69	38	56	50	59	48	
<b>IGS</b>											
Regional+global	<b>28</b>	21	25	26	28*	28*	27*	27*	26	25	
<b>Total</b>	<b>130</b>	67	75	51	97	66	83	77	85	73	

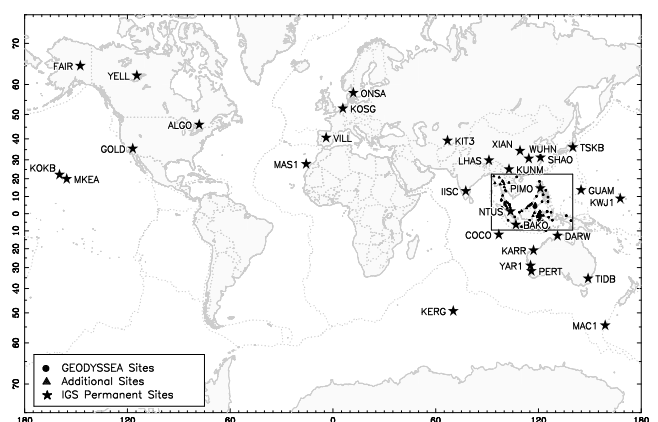


**Figure 2.** The included IGS GPS sites.

work was re-measured by ENS in 2000. These 3 additional networks increase the available GPS points in this region by 15.

In Malaysia, (Region 2 in Fig. 1) the included Malaysia Active GPS System (MASS) consists presently of 17 permanent GPS tracking stations situated at strategic locations, some at tide gauge stations. The MASS network was setup by the Department of Survey and Mapping, Malaysia (DSMM) at the end of 1998. The MASS network has a good spacing on both the Peninsula and East Malaysia. While the largest part of Malaysia is located on the stable part of Sundaland, the network is very suited to investigate any intra-block deformations in Malaysia, especially near/in the Sundaland boundaries in the eastern part of East-Malaysia (Sabah province). Three full years of permanent GPS data (1999-2001) were included in this paper, as well as 2-3 weeks of MASS data in 1998, 2002 and 2003. In this region, the addition of the MASS network increases the number of available geodetic points from 5 to 22.

The island of Sulawesi, Indonesia, together with the surrounding region (Region 3 in Fig. 1, is more complex from a geodynamic viewpoint [Walpersdorf *et al.*, 1998; Simons *et al.*, 2000; Vigny *et al.*, 2002]. Therefore the existing GEODYSSSEA network was most densified here and re-measured yearly since 1996. The observed network also includes 2 fault transects (Palu-Koro and the Gorontalo fault). Since 1999 permanent stations have also been installed in Sulawesi, mainly to study the behavior of the Palu-Koro fault (at present 6 stations), in both east-west and north-south direction. Although all Sulawesi GPS network data was processed along with the other data on S.E. Asia, a detailed treatment of the results for Sulawesi is beyond the scope of this paper. Hence, mainly the motion of the western part of Sulawesi with respect to Sundaland will be discussed later on. The Sulawesi GPS network was densified from the original 8 GEODYSSSEA sites in 1994, up to more than 30 in 2003, plus an additional 25 fault transect points.

Since 1997, 3 new sites (NTUS, BAKO and PIMO) from the IGS became operational in S.E. Asia. These sites have also been included in the network described here. The BAKO site was also observed as part of the GEODYSSSEA network, and the velocity estimates of these IGS sites were not constrained to those of ITRF solution of 2000. The time series included for these sites in the ITRF-2000 solution are relatively short, and hence the velocity estimates given are not sufficiently accurate for our study. Finally, data was included from 1 permanent site in Sumatra, Indonesia.

In total, data from about 100 (125 including Sulawesi fault transect points) GPS points in South and South-East Asia was uniformly (re)processed, along with an additional data set of about 30 IGS stations. A summary of the available GPS network sites is given in Table 1.

The campaign-style GPS data from the Asia Pacific Regional Geodetic Project (APRGP), which is also available for S.E. Asia since 1997, was not included in this paper. Near almost all APRGP sites located on Sundaland, the GPS database used in this paper contains permanent GPS data. In addition tests conducted with this part of the APRGP data indicate that the quality of the data (contributed separately by each Asian APRGP participant) is not always consistent and sometimes noisier. This can also be noticed in Socquet *et al.* [2003, subm.] where 1997-2000 APRGP data on Indochina was included to a GPS network similar to Table 1, and relatively higher velocity residuals with respect to Sundaland at these APRGP sites can be observed.

Because one of the goals of this paper is to present the velocity estimates in ITRF-2000, a number of permanent IGS GPS stations needed to be included. Previous experience with mapping local networks in S.E. Asia into ITRF, has shown that if only regional IGS stations are selected the mapping may not always be optimal, and position, and hence velocity errors may occur. The main reason is that even today, the available IGS network with valid ITRF-2000 solutions in S.E. Asia is still limited. A number of new IGS sites in the region have become available since 1996, but their time series are relatively short, and the data quality sometimes lower than average (e.g. IISC, GUAM, LHAS, NTUS and BAKO). Moreover, some stations have been affected by nearby earthquakes (e.g. COCO), and hence they don't always fit the linear velocity trend given by

ITRF, nor are official position jumps made available. Some stations had such short time series at the time they were included in an ITRF solution, that their listed coordinates and velocity estimates were much less accurate (e.g. KARR in ITRF-97 and PIMO in ITRF-2000). Because ITRF gives a velocity estimate together with position at a certain reference epoch (01-01-97 in the last two ITRF solutions), any errors in the predicted position become larger as the analyzed GPS data lies further away from the actual time series used in ITRF-2000. This might not always become clearly visible in the mapping process, because with few regional IGS sites available, part of the position misfits can be absorbed by the Helmert transformations, which are commonly used in the transformation of network solutions.

If beside regional IGS stations, also a number of well determined global IGS sites are included in the analysis, the above mapping problems can be avoided. Furthermore, some of these included IGS stations can be excluded from the mapping process, and used to check/validate the quality of the ITRF transformation and/or provide more accurate ITRF velocities for these sites in the analyzed time period. Therefore, IGS data from 14 regional and 17 global stations (Fig. 2) were retrieved from the IGS databases (<http://igscb.jpl.nasa.gov>, [Beutler *et al.*, 1994]). The global IGS sites were selected upon their availability from 1994 until the end of 2003, and because the majority of them are 'long-running' permanent IGS stations. This ensures that these sites have very well determined coordinates and velocity estimates, with the most recent ones provided by ITRF-2000 (<http://lareg.ensg.ign.fr>).

### 3. GPS Data Analysis

In this section the results of the GPS data analysis with the GIPSY-OASIS II v2.6.1 [Blewitt *et al.*, 1988] software are discussed. The software includes a processing method that allows permanent GPS networks (up to 100 stations) to be processed in relatively short time periods, including ambiguity fixing for the whole network.

For the complete data set from 1994 to 2003, daily fiducial-free network solutions were computed with the GIPSY precise point positioning (PPP) strategy. With this strategy, each station can be solved for individually, using precise (JPL) satellite orbits, satellite clocks and corresponding earth rotation parameters (<ftp://sideshow.jpl.nasa.gov>). Because the orbits and clocks are held fixed in this technique, all correlations among the different stations are not explicitly computed. Therefore a network can be processed in a much more computationally efficient way, as opposed to the traditional technique where the complete network is processed simultaneously.

The individual PPP station coordinate solutions were computed using the ionosphere-free linear combination of the zero-differenced GPS phase and pseudorange data at 5 minute intervals with an elevation cut-off angle of 15 degrees. To account for tropospheric effects, the zenith path delay (using Niell's model [Niell, 1991]) and gradients are estimated at each time interval. If required, the default apriori value of the wet tropospheric delay (10 cm) and the apriori station coordinates are iterated upon. Data from GPS satellites that were undergoing maintenance during part of the processed day (<ftp://tycho.usno.navy.mil/pub/gps/>) were removed. Ocean loading parameters for all site locations were obtained from H.-G. Scherneck and M.S. Bos ([http://www.oso.chalmers.se/~loading/\[Scherneck, 1991\]](http://www.oso.chalmers.se/~loading/[Scherneck, 1991])) and ocean loading modeling was applied to each site in the network. Finally, because different antennae were used in the network, the NGS relative antenna phase center corrections (<http://www.ngs.noaa.gov/ANTCAL> [Mader, 1998]) were applied. In previous analyses, the IGS antenna phase center corrections [Rothacher and Mader, 1996] were used. Unfortunately, the GPS network in this analysis contains GPS antennae that were not included in the original official table provided by IGS (igs01.pcv). As these new GPS antennae became available, IGS included the NGS antenna phase center corrections for most of these antennae. However, differences can be observed between the IGS and NGS tables for some (older) antenna types also used in this network.

**Table 2.** Daily Coordinate Repeatabilities 1994-2003. The tables shows the number of sites observed yearly in each region, along with the number of daily solutions used (and the number of outliers) in the multi-day averaging, followed by the RMS of the residuals w.r.t. each multi-day averaged solution. Regions marked with \*, indicate that permanent data was daily processed in those years.

Year	Description	Sites Observed	Daily Solutions	RMS Residuals (mm)		
			North	East	Up	
<b>1994</b>	GEODYSSSEA	39	189 (- 15)	2.4	5.5	11.7
	Region 1	5	19 (- 2)	2.8	3.4	13.7
	IGS	21	274 (- 18)	3.1	5.7	11.1
<b>1996</b>	GEODYSSSEA	40	224 (- 14)	2.2	5.7	13.3
	Region 1	3	15 (- 0)	2.7	6.5	18.9
	Region 3	7	27 (- 1)	2.9	6.6	11.2
	IGS	25	325 (- 16)	3.1	6.8	11.5
<b>1997</b>	GEODYSSSEA	14	96 (- 5)	2.1	4.3	9.5
	Region 3	10	55 (- 2)	2.1	3.5	9.1
	IGS	27	352 (- 7)	2.5	4.0	9.0
<b>1998</b>	GEODYSSSEA	38	186 (- 4)	1.7	3.5	8.6
	Region 1*	10	1036 (- 2)	1.9	2.8	8.1
	Region 2	9	54 (- 10)	1.5	3.8	8.1
	Region 3	10	56 (- 4)	1.9	5.0	8.7
	IGS*	30	7630 (- 78)	2.4	4.0	8.9
<b>1999</b>	GEODYSSSEA	4	20 (- 2)	2.2	5.2	9.1
	Region 1*	5	1204 (- 8)	1.7	2.8	7.9
	Region 2*	15	3189 (- 11)	2.0	3.0	8.8
	Region 3*	11	183 (- 16)	2.4	5.7	10.1
	IGS*	31	9092 (-141)	2.5	4.6	9.7
<b>2000</b>	GEODYSSSEA	10	44 (- 2)	1.9	3.5	9.5
	Region 1*	10	782 (- 13)	2.1	4.4	8.5
	Region 2*	15	4419 (- 30)	2.1	4.0	8.9
	Region 3*	18	592 (- 22)	2.2	7.1	9.9
	IGS*	30	9718 (-240)	2.6	5.3	10.3
<b>2001</b>	GEODYSSSEA	4	19 (- 0)	2.0	4.3	12.7
	Region 1*	10	500 (- 9)	1.9	3.8	9.0
	Region 2*	17	5438 (- 33)	1.9	3.9	9.5
	Region 3*	16	1243 (- 27)	1.8	4.1	9.5
	IGS*	30	9287 (-142)	2.3	4.5	9.2
<b>2002</b>	GEODYSSSEA	9	57 (- 6)	2.6	3.3	8.0
	Region 1	5	68 (- 0)	2.4	3.8	9.8
	Region 2	17	412 (- 12)	2.5	4.1	10.8
	Region 3	25	433 (- 6)	2.0	3.4	8.7
	IGS	29	1514 (- 20)	2.2	3.7	7.6
<b>2003</b>	GEODYSSSEA	6	20 (- 1)	2.5	2.7	7.7
	Region 2	14	200 (- 1)	1.7	3.4	8.1
	Region 3	24	272 (- 11)	1.8	3.4	8.6
	IGS	28	1033 (- 3)	1.7	2.5	6.3

Because consistency among the phase corrections is an important issue and NGS provides more regularly updates when new GPS antennae become available, preference to the NGS calibration tables was given in this analysis. It is possible to directly map the daily PPP coordinate solution(s) into (at present) the ITRF-2000, using Helmert transformation parameters from JPL which are compatible with the JPL precise orbits and satellite clocks. Although this approach works well, the parameters sometimes are not directly available, and they need to re-computed at JPL each time a new ITRF solution becomes available.

In a final step, the solutions of each station can be simply merged into one daily covariance band matrix (no correlations between different stations) for the complete network, after which the ambiguities can be resolved. This is the only stage at which GIPSY relies on double-differences from the ionosphere-free combined GPS phase and pseudorange measurements. Current software memory

requirements prevent that ambiguities can all be solved in one step for big networks. Therefore the ambiguities are resolved in successive iterations, where the shortest baselines are solved for first (boot-strapping), using a sequential wide- and narrow-laning approach to fix the phase biases to the correct integers. This works for both short (< few 100 km, most ambiguities fixed) and long baselines (up to 8000 km, few ambiguities fixed). When the iterations are completed, the daily covariance matrix is updated, and has now become a full matrix, due to the correlations introduced in the ambiguity fixing procedure. Throughout the following computations of multi-day averaged coordinate solutions, their transformation into the ITRF, and the final velocity estimation, full covariance matrices can be used.

### 3.1. Multi-day averaged solutions

The daily PPP coordinate solutions were combined into weekly or campaign averaged coordinate solutions whereby any systematic differences between the various daily network solutions are eliminated by computing optimized 7-parameter Helmert transformations using a least squares adjustment. In this process, any daily station solutions identified as outliers are downweighted (all components, or only the vertical component). The (default) criteria used to detect these outliers can be automatically scaled up, if the daily positions for a given site exhibit a lot of noise. This is done to prevent almost all solutions for a given site to become marked as outliers. The above procedure only removes extreme outliers from

**Table 3.** Residuals IGS sites after ITRF-2000 transformations.

Year	IGS sites used	RMS Residuals (mm)		
		North	East	Up
<b>1994</b>	15	1.7	2.3	8.8
<b>1996</b>	20	2.7	3.1	9.2
<b>1997</b>	20	1.8	2.5	6.4
<b>1998</b>	19-23	2.3	2.7	7.2
<b>1999</b>	15-22	2.2	2.9	8.3
<b>2000</b>	15-21	2.2	3.1	8.6
<b>2001</b>	13-19	2.0	2.9	8.2
<b>2002</b>	15-17	2.0	2.4	7.7
<b>2003</b>	13-14	2.2	1.7	8.2

**Table 4.** Residuals stations w.r.t. linear trend fitting. Shown first are the number of velocity estimates obtained for each S.E. Asia and IGS (sub)network, along with the number of multi-day averaged solutions used (and rejected) in the velocity estimation. The last 3 columns give the RMS of the residuals between the multi-day averaged position components in ITRF-2000 and the fitted linear trend for each site. These values are not available for the ENS site as they were only measured twice.

Description	Sites	Solutions	RMS Residuals (mm)		
			North	East	Up
GEODYSSSEA	38	141 (- 17)	2.9	3.3	8.3
<b>Region 1</b>					
THAICA	5	16 (- 2)	2.6	4.9	3.9
ENS	4	8 (- 0)	N/A	N/A	N/A
GAME-T	6	518 (- 7)	2.5	3.3	9.3
<b>Region 2</b>					
MASS	17	2063 (- 28)	2.3	3.2	8.0
<b>Region 3</b>					
GEODYSSSEA Sec.	14	54 (- 10)	2.6	2.5	7.7
BAKO monuments	6	24 (- 4)	4.0	2.6	7.4
BAKO permanent	7	319 (- 8)	2.5	3.8	9.1
<b>IGS</b>					
Local	3	456 (- 28)	3.3	3.6	10.3
Regional+global	29	4922 (- 98)	2.0	3.0	7.5
<b>Total</b>	129	<b>8521 (-202)</b>	<b>2.3</b>	<b>3.1</b>	<b>8.0</b>

the multi-day averaged (local) solutions, and hence the daily coordinate repeatabilities shown in Table 2, give a realistic indication of the internal accuracy of the network processed. In a final stage, the formal errors, which typically are underestimated in the GIPSY PPP strategy, are scaled using the overall repeatability of each averaged solution. This results in realistic errors, which in turn, will result in more realistic formal errors in the site velocity estimation, and automatically weighs the contribution of each campaign/weekly averaged solution. Therefore it is not required to 'artificially' scale up the formal errors as sometimes is done.

The daily station coordinate repeatabilities, together with the number of final and removed station coordinate solutions, are given in Table 2 as the Root-Mean-Square (RMS) of the daily station coordinate residuals for each campaign and/or year of the permanent data processed. The daily repeatabilities are in general better than respectively 2 and 4 mm for the horizontal positions and around 9 mm for the height. A clear improvement can be seen since 1997, mainly due to an improvement in the GPS orbits and the amount of GPS satellites available. The measurements of 1996 exhibit the highest residuals, and are probably caused by a poorer quality of the GPS orbits in the observation time window of this year.

An overview of the daily coordinate repeatabilities for the IGS stations can also be seen in Table 2. These show similar values as for the S.E. Asia network, and also here the 1996 positions show higher daily offsets. The east component is sometimes a bit larger, because the ambiguity resolving works less well for the global IGS sites included (baselines > 2000 km to the nearest site). It is interesting to notice that (relatively) more outliers were removed between 1999 and 2001, mainly for stations located in the equatorial region. All these sites used Rogue SNR-8000 receivers, which had problems with tracking GPS satellites during periods of increased solar activity (higher ionospheric delays). All these receivers have been replaced in the past 4 years with upgraded or new GPS receivers.

### 3.2. Mapping solutions in ITRF-2000

Each (weekly/campaign) multi-day averaged solution was projected onto ITRF-2000 coordinate sets, each containing the positions of the 31 IGS stations at the middle epoch of each analyzed week/campaign. The ITRF-2000 GPS SINEX file (<http://lareg.ensg.ign.fr>) is propagated to each of these epochs, and contains the full covariance matrix for the IGS stations subset.

In the mapping process, any multi-day averaged IGS coordinate solutions, identified as (horizontal and/or vertical) clear outliers with respect to the propagated ITRF-2000 solution were downweighted. The coordinate residuals of the IGS sites for all epoch transformations are shown in Table 3.

The coordinate residuals of all IGS stations are small and consistent, with RMS values of 2 to 3 mm for the horizontal and about 8 mm for the vertical position. These numbers correspond with the repeatabilities for the IGS sites in the above section, and hence confirms (only stable and linearly moving stations were used) the internal accuracies. From the total of 31 included stations, 13-23 were used in the mapping of all weekly/campaign solutions from 1994 to 2003. The ITRF positions of BAKO, NTUS, PIMO (all in S.E. Asia), MKEA, KARR, SHAO and KUNM (mapping quality check) were estimated along with the S.E. Asia network. Since DARW and XIAN are relatively new in IGS and ITRF-2000, these stations were also not considered in the mapping. Finally, a number of sites, in chronological order COCO, KOKB, TSKB, GUAM, GOLD, FAIR and KOSG were automatically rejected from the mapping between 1999 and 2003. This was due to jumps in the time series, which all could be traced back to seismic events, antenna changes and/or changes in the site marker/antenna setup. This GPS analysis allowed the detection of horizontal jumps larger than 2 mm and about 10 mm in the height in the time series of the permanent sites.

The results of Table 3 together with the daily coordinate repeatabilities of the S.E. Asia and IGS sites (Table 2), indicate that the global accuracy with respect to ITRF-2000 of each multi-day averaged solution is in the range of 2-4 and 4-6 mm for the horizontal position components, and around 9-15 mm for the height.

### 3.3. Velocity estimates in ITRF-2000

In this paper only steady state site velocities are given, and these can be easily estimated by computing a (linear) fit through all ITRF-2000 mapped weekly site coordinates, and checking the residuals at

each point in the time series. Also the velocity differences between this solution and the ITRF-2000 will be verified, for both sites that were and were not used in the mapping process.

A linear velocity model was fitted through all the available ITRF-2000 mapped coordinates for each individual site making use the GIPSY software utilities. In this process, combined coordinate solutions in ITRF-2000 identified as clear outliers with respect to the linear velocity trend are downweighted. Jumps in site position can also be estimated, but this is primarily useful for time series of continuously operated stations, unless a campaign site was measured many times, both before and after a jump in position.

The coordinate residuals for all the S.E. Asia and IGS sites w.r.t. to their estimated velocity trend are given in Table 4 for each of the

**Table 5.** Residuals IGS stations w.r.t. linear trend fitting. Conform Table 4 the RMS of the residuals from the linear trend fitting are shown, but this time for individual IGS stations that were not used in the mapping into the ITRF-2000

IGS Station	Weekly Solutions	RMS Residuals (mm)		
		North	East	Up
BAKO / Indonesia	189 (- 5)	3.2	3.4	9.7
NTUS / Singapore	145 (- 7)	2.9	3.6	9.2
PIMO / Phillipines	122 (-16)	3.9	4.0	12.4
KUNM / China	157 (- 1)	2.5	3.6	8.5
XIAN / China	79 (- 0)	2.5	1.9	6.8
DARW / Australia	156 (- 8)	2.2	3.3	8.6
KARR / Australia	200 (- 1)	1.5	2.6	8.1
MKEA / Hawaii	184 (- 5)	1.7	3.4	8.4

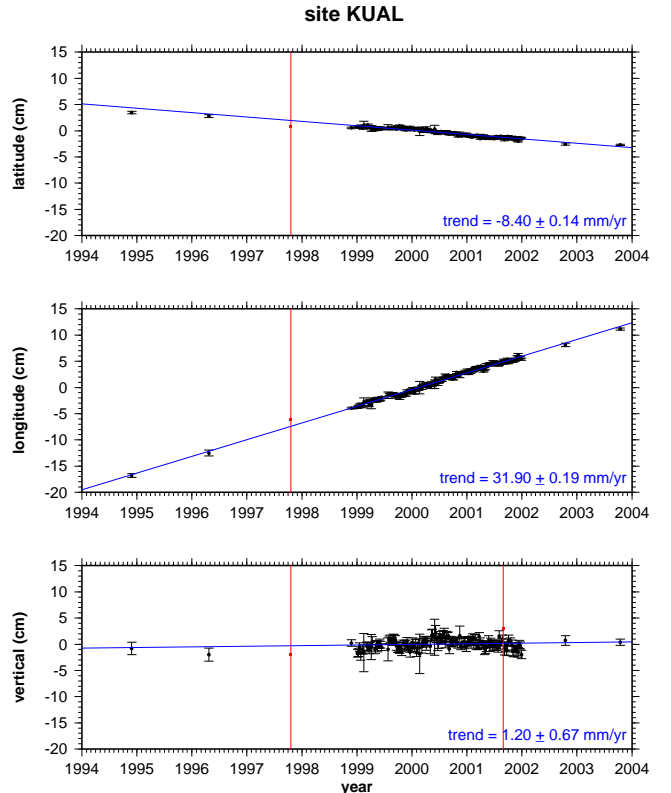


**Figure 3.** MASS site KUAL: Coordinate time series in ITRF-2000. This site in Malaysia was originally a GEODYSSSEA site, and became a permanent station at the end of 1998. The figure shows a marked outlier in 1997, and a vertical only outlier in 2001. The errors on the velocity component are  $1-\sigma$  values, which do not require any further scaling.

sub-networks, conform to Table 1. For the campaign style observations, most position outliers were due to seismic events, especially in the Sulawesi region. The residuals are well within the range of absolute accuracy indication given in the previous section. All of the sites use a fixed antenna-setup, with the exception of the BAKO monuments in Sulawesi, which were observed using tripods. Many of these sites have poorer visibility and are located in/near deformation zones, and therefore the residuals at these sites are slightly higher w.r.t. to the linear trend fitted.

For the IGS sites used in the mapping, the residuals will be almost identical to the ones of Table 3 (they were projected onto their ITRF-2000 positions at each epoch, and only the weighting is slightly different in the velocity estimation step). It is interesting to look at the IGS sites in and near S.E. Asia that were not included in the mapping, shown in Table 5. This gives another indication on the quality of the mapping. Indeed, the IGS stations in Table 5, located in and around the S.E. Asia network show good linear fits with few outliers, and their performance is similar to that of other regional and global sites. Only PIMO performs less well, caused by the receiver problems due to the increased solar activity around 2000.

To illustrate the velocity estimation process, the result for MASS station KUAL is shown in Figure 3, and demonstrates the robustness and accuracy of the GPS data analysis presented here. Station

KUAL initially was a GEODYSSSEA site, which was equipped with a permanent receiver by DSMM at the end of 1998. One outlier can be clearly noticed, for the 1997 measurement, due to a different antenna used and/or a misalignment of the antenna setup. The error estimates are  $1-\sigma$  values, as they come out of the GPS data analysis. The time series for the complete network are given at <http://www.deos.tudelft.nl/~wims/sunda.html>

In order to get more grip on the accuracy of the station velocities, the obtained velocities for the IGS sites can be compared with their velocities in ITRF-2000. The results are shown in Table 6. It should be pointed out that in the GPS data analysis, the IGS sites were nowhere constrained to both their ITRF-2000 positions and velocities. The included IGS sub-network was only projected onto its predicted positions using the ITRF-2000 for each campaign/weekly averaged solution. Table 6 confirms that the mapping strategy was stable throughout the time period the data was analyzed for. The

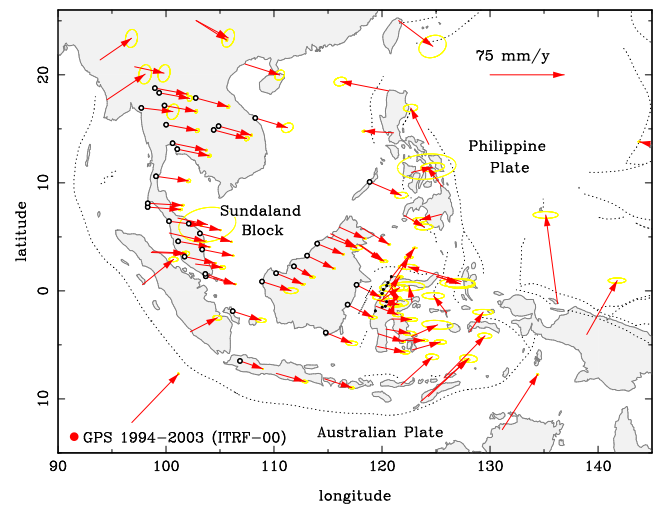


**Figure 4.** S.E. Asia 1994–2003 Velocities in ITRF-2000. The error ellipses are  $3-\sigma$  values, and also the sites considered to be located on rigid Sundaland are shown (open black dots).

**Table 6.** Differences Obtained/ITRF-2000 IGS Station Velocities. Shown are the velocity differences after subtracting the ITRF-2000 velocity values from the ones estimated in this paper. The top part is for IGS stations used in the mapping process, while the bottom part is for IGS sites that were projected onto the ITRF-2000 along with the S.E. Asia sites. In the remark section, important events in the analyzed time series are given, and also if a position jump was estimated during the linear trend fitting.

IGS Station	Velocity differences (mm/yr)			Remarks
	North	East	Up	
<b>Used</b>				
ALGO	-0.1	-0.1	-0.5	
COCO	0.8	-0.6	0.4	before seismic event
FAIR	-0.6	-0.3	2.0	seismic event / jump
GOLD	0.9	1.9	-6.2	seismic event / jump
GUAM	-0.1	0.4	1.5	unknown event / jump
IISC	-0.1	-0.3	0.1	
KERG	0.9	0.2	2.8	
KIT3	0.3	0.2	-1.7	
KOKB	-0.1	0.8	-1.1	antenna event / jump
KOSG	-0.6	-0.6	1.6	antenna event / jump
KWJ1	-0.2	0.8	0.6	
LHAS	-0.3	1.7	2.7	relative new / noise
MAC1	-0.9	0.1	-2.4	
MAS1	0.5	0.3	1.3	
ONSA	-0.7	-0.3	2.1	
PERT	0.4	-0.1	3.3	
TIDB	0.8	0.9	-4.7	
TSKB	-1.0	-0.1	-0.3	antenna event / jump
VILL	0.3	-0.2	1.5	
WUHN	-0.6	-0.7	-0.9	
YARI	-0.2	-0.3	-4.4	
YELL	0.5	-0.4	0.6	
<b>Average</b>	<b>0.0</b>	<b>0.2</b>	<b>-0.1</b>	
<b>RMS</b>	<b>0.6</b>	<b>0.7</b>	<b>2.5</b>	
<b>Not used</b>				
BAKO	2.2	0.8	-8.1	improved wrt ITRF-2000
NTUS	3.7	0.3	0.7	improved wrt ITRF-2000
PIMO	29.1	-17.3	3.9	wrong in ITRF-2000
MKEA	-0.4	0.1	-0.1	validation site
KARR	0.9	-0.5	2.8	validation site
SHAO	-0.5	-0.1	-4.5	validation site
KUNM	-0.5	0.5	5.3	validation site
DARW	2.9	-1.3	10.0	improved wrt ITRF-2000
XIAN	-2.1	0.1	-2.3	new and few data

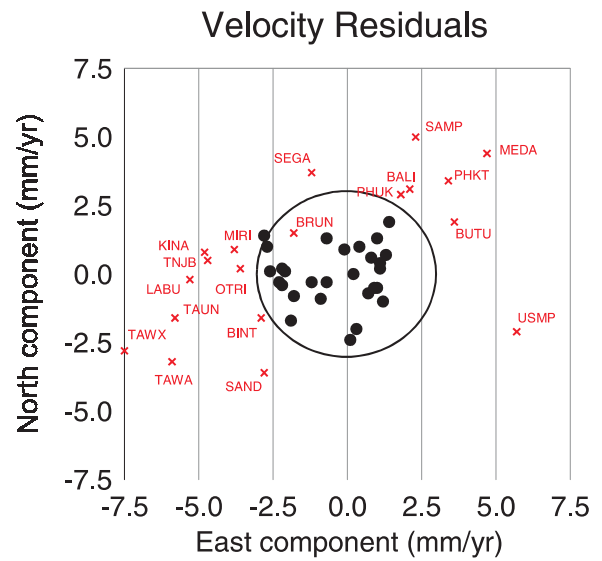


**Figure 5.** Velocity residuals Sundaland sites w.r.t pole. The velocity residuals are shown for both the (28) sites that are located on rigid Sundaland (black dots) and the sites (19) that are located in deformation zones near the Sundaland boundaries (red crosses). The circle is drawn with a 3 mm/yr radius, which was the threshold value to accept sites on rigid Sundaland.

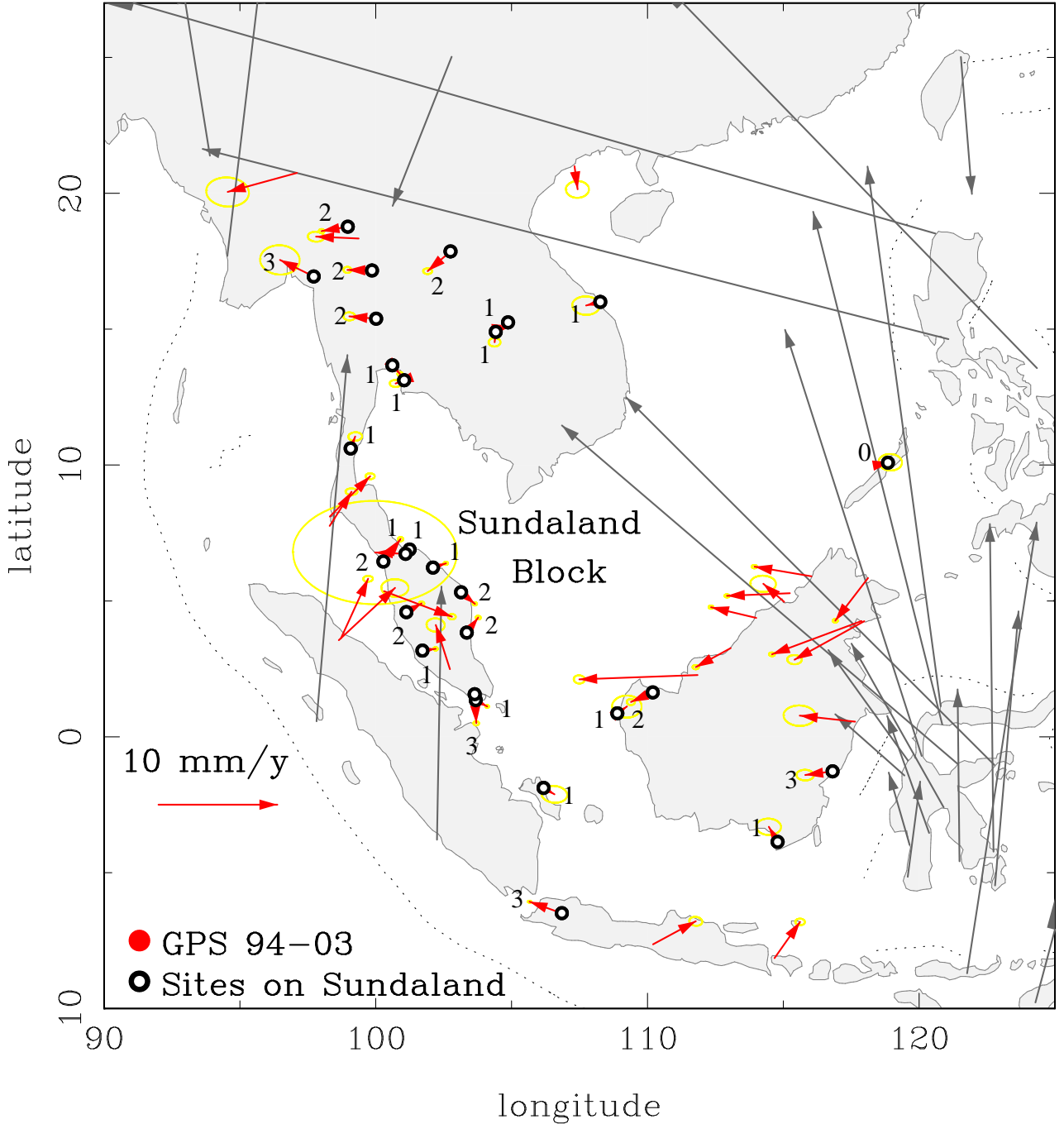


**Figure 6.** GPS Velocities w.r.t. Sundaland. Shown are the residual velocities w.r.t. to the updated Sundaland pole for the 28 sites used (open dots with black vectors).

differences between the estimated and the ITRF-2000 velocities for IGS sites used in the mapping are typically below 1 mm/yr for the horizontal and a few mm/yr for the vertical components. The IGS sites that were mapped along with the S.E. Asia network, are also within these differences. For stations BAKO, NTUS, PIMO and DARW the velocities computed in this analysis are more accurate than in ITRF-2000, since they are based on longer time series.

Based upon the results in Table 6, taking into account the velocity differences for IGS sites closest to the S.E. Asia network as well as the internal accuracy of this network, it can be concluded that the S.E. Asia computed velocities have absolute accuracies, which are in agreement with the formal errors ( $1-\sigma$ ) obtained in the final step in this section. The horizontal velocity vectors have ( $1-\sigma$ ) errors range from about 0.3 mm/yr for the permanent stations to 0.5 to 2.5 mm/yr (depending on the number of observations/time elapsed)

for the episodically observed sites. A number of new sites have larger errors because they were only observed twice in the past year (mainly Sulawesi sites and 1 THAICA site in South-Thailand). The velocity vectors along with their ( $3-\sigma$ , for more clearness) uncertainties are shown in Fig. 4. The velocity field is available from the first author upon request and it can be used as a reference solution, or to connect to other regional network solutions.

## 4. Sundaland Motion and deformation

### 4.1. Pole estimation

In this paper, we present an updated Sundaland pole in ITRF-2000 derived from the velocity field obtained by processing GPS data described in the previous section. This pole was carefully es-

timated by using a small velocity residual criteria (3 mm/yr) and a well-balanced choice out of over 40 sites in both the core and the boundary zones of Sundaland. Although the GPS vector field presented here provides good coverage on S.E. Asia, there is a higher density of GPS points in Thailand and Malaysia. Therefore in a first pole estimation, 17 sites with similar spacing within Sundaland were selected. Initially, also all stations were equally weighted to minimize the effect of any bad fitting site(s) with small velocity sigmas (eg. permanent GPS sites). Only sites that had horizontal (normalized) residuals smaller than 3 mm/yr were kept into the computations. In subsequent steps, additional sites that fit well the initial pole(s) were added to the pole estimations. This led to a Sundaland pole based on 28 of the 40+ available GPS velocities. Almost all the rejected points were located in the boundary zones of Sundaland with its neighboring plates. In a final step, the computation was repeated, only this time the selected points were weighted according to their individual velocity errors. This is also necessary to get a realistic error estimate on the pole location and rotation rate. Furthermore, the more accurate velocities should be allowed to contribute relatively more to the pole estimation. In any case, the pole location and rotation rate remained stable throughout all the subsequent software runs.

With the expanded GPS vector field, the Sundaland block rotates clockwise at a rate of 0.341 °/Myr about a pole located 48.9 ° S and 85.8 ° E in ITRF-2000. The (3- $\sigma$ ) error on this pole is 2.01 ° for the long axis of the ellipse, oriented 21 ° NNW and 0.24 ° for the short one. The uncertainty on the rotation rate is 0.006 °/Myr. The ellipse error is obtained using the method described by *DeMets et al.* [1994]. The residual velocities of all Sundaland sites with respect to this pole are shown in Figures 5 in 6. For the 28 sites included in the pole estimation, the residual velocities are all below 3 mm/yr (circle radius in Fig. 5), and more than half are smaller than 2 mm/yr. The excluded sites are almost all located in deforming regions near the Sundaland boundaries (Sabah province in East-Malaysia, Central Java, Bali, Sumatra and northwest Thailand/Myanmar).

#### 4.2. Pole comparison and history

Although the initial results of the GEODYSSSEA project [*Wilson et al.*, 1998; *Simons et al.*, 1999] were plagued by not-well

constrained mapping issues into ITRF-94/96, an adjustment of the velocity vectors after only 2 measurements campaigns already confirmed and provided some good insights in the relative motion of Sundaland with respect to Eurasia [*Chamot-Rooke et al.*, 1998]. [*Michel et al.*, 2001] included the 3rd observation round of the GEODYSSSEA project, and provided a further refined Sundaland pole vector in ITRF-97.

In the last 2 years, 3 papers have been published which present a 'new' Sundaland pole. The *Sella et al.* [2002] paper does this by using only 3 IGS sites (BAKO, NTUS, KUNM), of which 2 not yet have very accurate velocities in ITRF-97 and 1 is not even located on Sundaland. The second paper is by *Kreemer et al.* [2003], which has made use the geodetic solution of *Michel et al.* [2001], and considered 8 GEODYSSSEA sites on Sundaland and added the IGS station Singapore. A third paper by *Bock et al.* [2003], presents results on the Indonesian archipelago, and thereby also defines a Sundaland (there named Sunda Shelf) motion, based on Indonesian data for 10 sites, IGS stations BAKO/NTUS/TAIW in/near S.E. Asia and 3 IGS sites located in South-China (SHAO/WUHN/XIAN).

The history of the angular velocities for Sundaland published both by the GEODYSSSEA project and others is given in Table 7.

In order to determine if these other Sundaland poles provide a better (geodetical) description of the Sundaland motion than *Michel et al.* [2001], it first is important to know how much different the predicted velocities are within Sundaland. For 3 geographically spread locations within Sundaland, the differences of the predicted velocities with respect to the updated Sundaland pole presented in this paper are shown in Table 8. Also included are the previous Sundaland poles computed during the GEODYSSSEA project.

In Table 8, clearly the mapping problems in ITRF-94 and ITRF-96 can be observed. The *Wilson et al.* [1998] solution shows almost constant offsets w.r.t. the solution in this paper which is taken as reference. Mainly Helmert translations have offset the velocity vectors that were used to compute the angular velocities. The second GEODYSSSEA solution by *Simons et al.* [1999] has already a better mapping, but still the north velocity component generated by the Sundaland pole presented there is off by about 15 mm/yr. These offsets were caused by the use of only 5 IGS sites (YAR1, TIDB, TSKB, TAIW, KIT3) for the mapping into the ITRF. At least 2 of these sites (TAIW and KIT3) didn't follow the linear ITRF-94/96 trend during the first 2 GEODYSSSEA campaigns, thereby affecting the mapping. The final geodetic GEODYSSSEA paper by *Michel et al.* [2001], the Sundaland pole appears to have stabilized quite well, as the differences with the 'newer' Sundaland poles are within 3-5 mm/yr. This was achieved by adding one more observation round, data from additional IGS stations, and mapping the velocity field into the ITRF-97. The predicted velocities using the 3 Sundaland poles from the other 3 papers [*Sella et al.*, 2002; *Kreemer et al.*, 2003; *Bock et al.*, 2003] are within a few mm/yr (roughly the size of their velocity errors) of the reference values that are obtained with the Sundaland pole derived in this paper.

Furthermore, also the amount, location and the produced velocity residuals of sites within Sundaland are an important factor to determine the quality of the previously published poles. In combination with the discussion about the final GEODYSSSEA and the 'newer' 3 Sundaland poles given above, the pole of *Sella et al.* [2002] is based on the weakest velocity constraints. The *Kreemer et al.* [2003] pole for Sundaland has predicted offsets that are similar to the ones of *Michel et al.* [2001], but they are larger in the east component throughout the longitudinal range. Probably the reference frame (NNR) is not fully compatible with ITRF-2000 for the Sundaland block, as the majority of the velocity estimates is identical to *Michel et al.* [2001]. The *Bock et al.* [2003] paper underestimates the east velocity component by 1-2 mm/yr, and the pole stability appears to depend mostly on the inclusion of IGS sites in N-S direction up to South-China, as the N-S spread of the local Indonesian data is only a few hundred kilometers and most of the Indonesian sites are in/near the Sundaland deformation zones. This is confirmed by the relatively higher velocity residuals in the east components up to 1 cm/yr for the Indonesian sites (including the

**Table 7.** Overview of published Sundaland poles.

Reference	Reference frame	Sites used	Pole	Rotation parameters	
			Lat(° S)	Lat(° E)	°/Myr
<b>GEODYSSSEA</b>					
<i>Wilson et al.</i> [1998]	ITRF-94	12	31.8°	134.0°	-0.280°
<i>Simons et al.</i> [1999]	ITRF-96	12	43.0°	119.0°	-0.370°
<i>Michel et al.</i> [2001]	ITRF-97	10	56.0°	77.0°	-0.339°
This paper	ITRF-00	28	48.9°	85.8°	-0.341°
<b>Others</b>					
<i>Sella et al.</i> [2002]	ITRF-97	3	38.9°	93.1°	-0.393°
<i>Kreemer et al.</i> [2003]	NNR	9	47.3°	89.8°	-0.392°
<i>Bock et al.</i> [2003]	ITRF-00	16	49.8°	84.1°	-0.320°

**Table 8.** Differences in predicted motions w.r.t. previous poles.

Reference	Differences horizontal motions (mm/yr)					
	Indochina		Sunda Shelf		South Borneo	
	15°N105°E	5°N110°E	5°N115°E	North	East	North
This paper (ref. val.)	-8.2	31.8	-10.2	30.5	-12.2	26.6
<b>GEODYSSSEA</b>						
<i>Wilson et al.</i> [1998]	+21.1	-11.9	+21.0	-12.0	+20.8	-12.4
<i>Simons et al.</i> [1999]	+15.5	+0.9	+15.0	+0.1	+14.2	-1.3
<i>Michel et al.</i> [2001]	-1.7	+1.3	-1.3	+2.2	-0.8	+3.1
<b>Others</b>						
<i>Sella et al.</i> [2002]	+1.2	+1.4	+0.3	-0.3	-0.5	-2.0
<i>Kreemer et al.</i> [2003]	+0.5	+4.6	-0.1	+3.9	-0.4	+3.0
<i>Bock et al.</i> [2003]	+0.1	-1.9	+0.2	-1.6	+0.4	-1.2

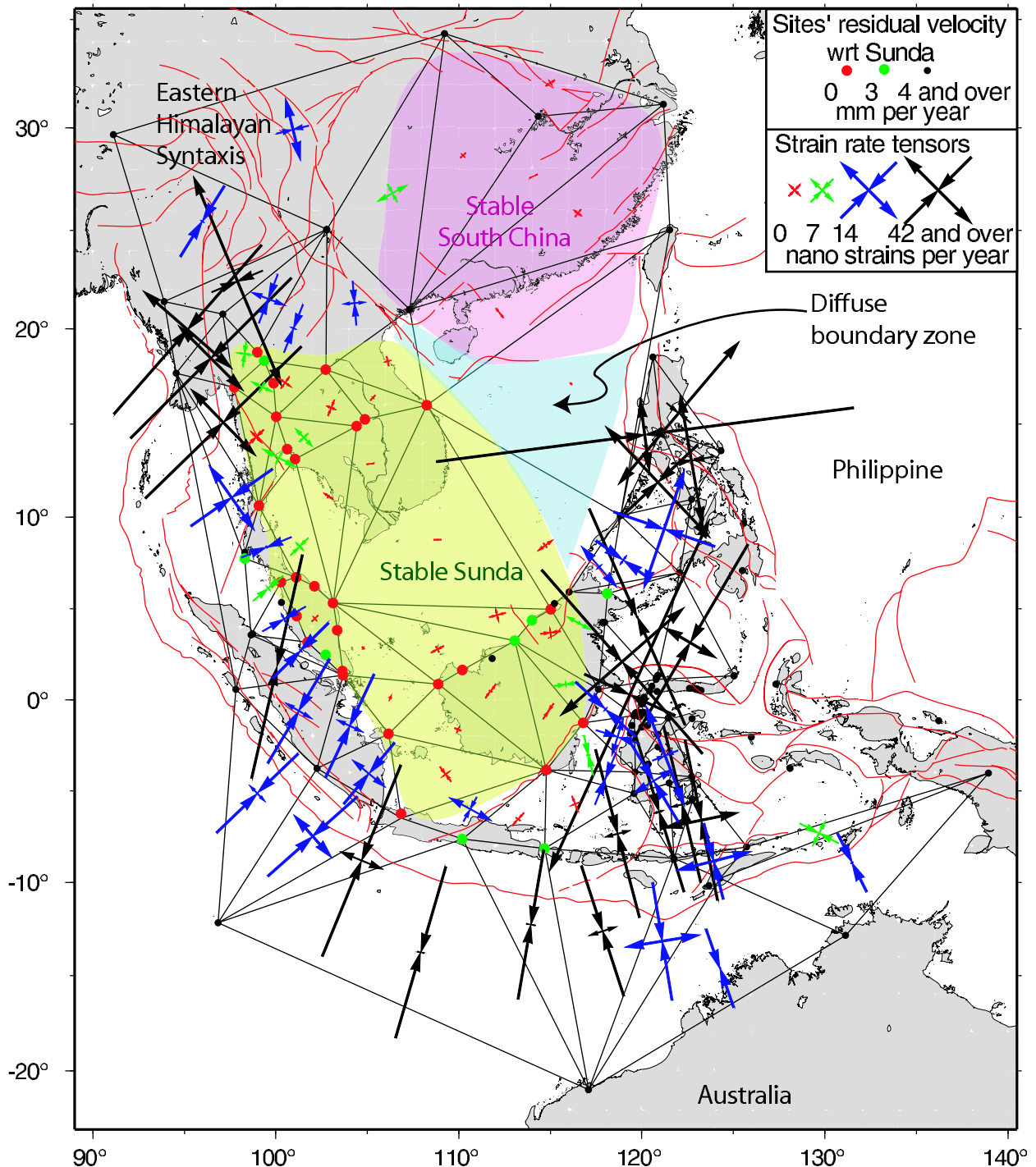


**Figure 7.** Deformation in and around Sunda plate. The strain rate tensors have been computed from the velocity solution presented in this paper, except for TAIW station whose velocity was taken in ITRF-2000. Different colors for the strain rate crosses indicate different level of deformation. The dots localise the GPS stations processed in this solution. Red dots represent stations with a residual velocity with respect to Sunda below 3 mm/year, green ones between 3 and 4 mm/yr, and black ones above 4 mm/yr.

south-west of Sulawesi) that were concluded to be on Sundaland [Bock *et al.*, 2003]. This pole implicates that the so-called Sunda Shelf extends all the way to South China (and therefore underestimates the Sundaland east velocity components since the IGS sites in South China have an eastward motion which is 2-3 mm/yr smaller than their Sundaland-like predicted motions). This is not the case in the results that will be presented here, since the relative motion be-

tween South-China and Sundaland could very well be small when computed at these site locations (e.g. clockwise Sundaland and a counter-clockwise South-China rotating blocks).

Finally it is clear that although the pole location and rotation rate can differ significantly (Table 8), the final GEODYSSSEA and other predicted motions are still within 2 to 4 mm/yr at the studied locations. Although the Sundaland poles of all sources are converging and now in reasonable agreement with each other, there certainly was room for further improvement. However, it is important to note

that any revision of the Sundaland pole needs to be based on both more AND more accurate velocity estimates on the rigid part of Sundaland. If in this paper the same selection of 10 sites would be used as in *Michel et al.* [2001], which also included GEODYSSSEA sites in Central Java and in Bali, the pole rate would slow down slightly and its location would shift towards the one of *Michel et al.* [2001].

Therefore only with the significantly expanded, more accurate and well spread velocity field presented in this paper it made scientific sense to update the Sundaland motion, thereby clearly identifying and/or removing sites that are in deforming regions.

#### 4.3. Stable Sundaland rigidity and boundaries deformation

Fig. 7 focuses on both the intra- and inter-plate deformation in South-East Asia. The strain rate tensors have been computed from the velocity solution presented in this paper, except for TAIW station whose velocity was taken from ITRF-2000 because there are only 2 epochs with poor data quality and relatively short time span included in our data analysis.

##### 4.3.1. Stable Sundaland definition

From the analysis of the strain rates tensors, it is possible to localize a zone of very low strain rate (red crosses) which constitutes the rigid core of Sundaland. This stable core of the Sundaland block can also be defined from the stations with a residual velocity with respect to Sundaland smaller than 3 mm/yr (red dots), almost all of which have been used to compute the pole. Hence, there is a very good agreement between the analysis of the residual velocities and the one of the strain rate tensors.

The core of the Sundaland block (green area) covers the Indochina peninsula to the North, the Malaysian peninsula to the West, the Sunda shelf, the major part of Borneo to the East and extends to the South almost until the Java island.

Another zone of small strain rates is the stable South China block, outlined by a pink area.

Around the Sundaland block, inter-plate deformation rates can reach very high values (Fig. 7, black crosses) due to the motion of Sundaland block relative to its neighboring plates. It is possible to see a progressive increase in the deformation rate from the core of Sundaland (red crosses) to its boundaries (green and blue crosses). These zones of medium deformation rate surrounding the rigid core seem to indicate that high-rate inter-plate deformation is not completely localized at the boundaries but extends a bit inside the Sundaland block. However, it is not possible to determine whether the origin of these medium strain rates is due to elastic coupling on a single fault accommodating the major part of inter-plate motion or to a distribution of the deformation on several smaller scale faults in the boundary areas. Discriminating these two deformation modes needs locally densified GPS measurements in order to constrain the mechanical models.

##### 4.3.2. Deformation at the Sundaland boundaries

The highest strain rates are located along the eastern border of the Sundaland block, in the Philippine belt and Sulawesi island (Fig. 7). In the latest area, the main compressive strain axis rotates anti-clockwise from NNE-trending at the NE of the island to NNW-trending North of the island (Minahassa trench) and until WNW-trending East of the island (Palu left-lateral strike-slip fault). To the West, deformation seems to extend, at smaller rates, in the eastern part of Borneo island. To the south of Sulawesi island the main compressive strain axis trends generally NNW.

To the South, the Sundaland block is bounded by the arcuate Sunda trench. There, the main compressive strain axis remains normal to the subduction axis (fig. 7), and hence rotates slightly clockwise from NNW-trending to the East (South of Sulawesi and Flores islands) to NE-trending to the West, in the Sumatra area.

To the West, the Sundaland block is bounded by a right-lateral strike-slip zone extending from Sumatra to Myanmar. The Sumatra shear zone is affected by deformation compatible with right-lateral strike-slip on the Great Sumatran Fault. Further to the North, our results confirm a right-lateral strike-slip on the Sagaing fault in Myanmar [Vigny et al., 2003]. Deformation of this area is detailed in Socquet

*et al.* [2003, subm.] in order to understand how the relative motion between India and Sundaland is accommodated in Myanmar. The Northern boundary of Sundaland extends from the Eastern Himalayan Syntaxis until the South China sea, through the Red River Fault. There, the main compressive strain directions rotates from NE-trending to the West, to N-trending to the East. Strain tensors are compatible with right-lateral shear across the Red River Fault, the boundary between the Sundaland and the South China blocks. To the SE, this fault ends in the South China Sea Basin, characterized by very slow present-day strain rate and that may be considered as a diffuse boundary zone (fig. 7).

#### 4.4. Motion relative to Eurasia and other plates

The motion of Sundaland with respect to Eurasia is the subject of discussions since the first GPS measurements in S.E. Asia [e.g. Tregoning et al., 1994; Genrich et al., 1996; Wilson et al., 1998; Chamor-Rooke et al., 1998; Simons et al., 1999; Michel et al., 2001].

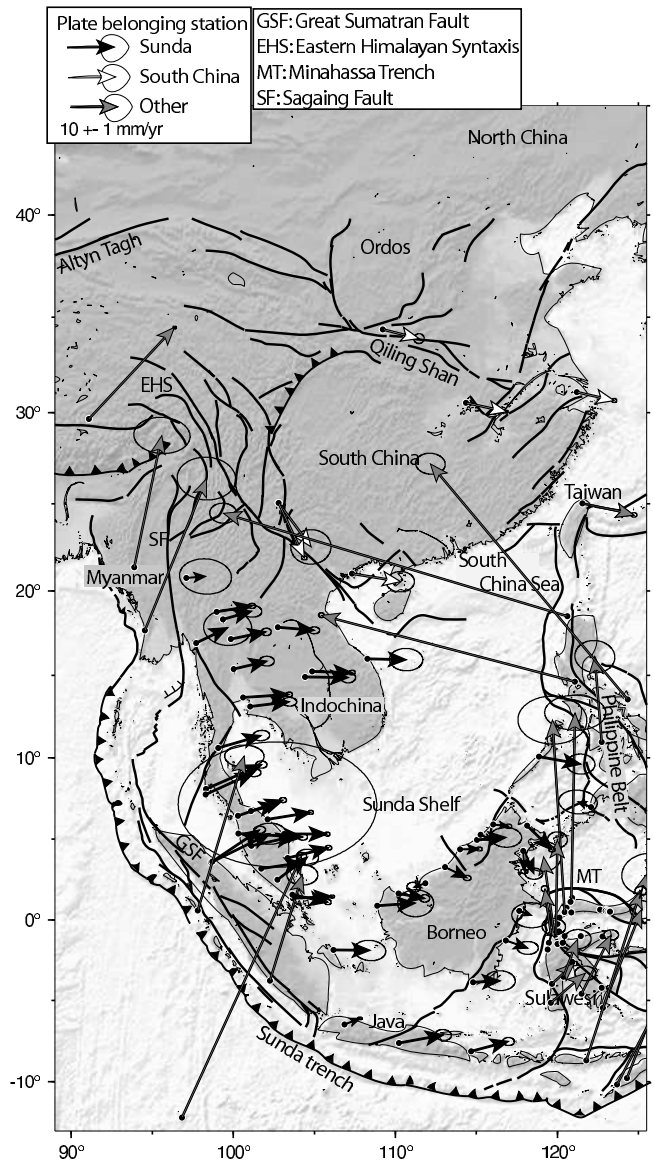


**Figure 8.** Velocities in South-East Asia, with respect to Eurasia of *Calais et al.* [2003]. Black arrows are for sites belonging to Sunda, white ones for South China and gray ones for other areas. the major tectonic structures of the area are also shown as black lines.

The latest determination of *Michel et al.* [2001] showed clearly that the Sundaland block presents a rigid motion with respect to Eurasia and is separated from the Siberian platform through a series of deforming and moving blocks. In *Michel et al.* [2001]'s paper, Sundaland motion is described with respect to NUVEL-1A Eurasia, which is an averaged motion for Eurasia over the last 3 Myrs.

In order to compare the latest motion description [*Michel et al.*, 2001] with the updated Sundaland motion in ITRF-2000 presented here, it is necessary to be in the same reference frame. The motion with respect to Eurasia (NUVEL-1A NNR) are 11 mm/yr oriented ENE in Indochina, decreasing to about 8 mm/yr E in the south of Borneo. This confirms the second of 2 possible interpretations given by [*Michel et al.*, 2001], which stated that Sundaland rotates clockwise with respect to (NUVEL-1A NNR) Eurasia at a velocity (in ITRF-97) increasing from  $10 \pm 3$  mm/yr in the south to  $14 \pm 3$  mm/yr in the north. The obtention of a slightly slower motion with the new solution presented here, can be attributed to the use of many more stations to define Sundaland and to the use of a different and refined ITRF.

Although getting a Sundaland/NUVEL1A-Eurasia pole is important to compare our pole determination with previous studies, it is not the most correct way of describing the relative motion between these two plates. A fully consistent relative pole determination would imply a geodetic determination of the Eurasian pole, using GPS stations located on this plate. The motion of the Eurasian plate, has been extensively studied with GPS in the last decade [Argus and Heflin, 1995; Larson et al., 1997; Heki et al., 1999; Kogan et al., 2000; Nocquet et al., 2001; Fernandes et al., 2003; Nocquet and Calais, 2003; Steblow et al., 2003]. However, given the fact that stations are extremely unevenly spread on this very wide plate, the geodetic definition of Eurasia is an extremely difficult task, and it remained long time a very controversial topic. Indeed, Western Europe is covered by hundreds of stations whereas only a few of them cover Central Eurasia and Asia (Siberia), and the estimation of a rigid pole for Eurasia can result in the estimation of a European pole. Recently, the introduction of more GPS data in Siberia allowed a geodetic redefinition of the entire Eurasian plate [Calais et al., 2003]. Hence, this new pole constrains better the motion of the Siberian part of Eurasia, which is particularly important when focusing on Eastern Asia kinematics and deformation.

The velocities are plotted with respect to the recently GPS derived Eurasia pole of *Calais et al.* [2003] in Fig. 8.

The motion of Sundaland with respect to GPS Eurasia of *Calais et al.* [2003] is described by a pole located at  $108^\circ\text{E}$ ,  $36^\circ\text{S}$  with a clockwise rotation rate of  $0.106^\circ/\text{Myr}$ . The predicted motion of Sundaland block with respect to the GPS derived Eurasia pole of *Calais et al.* [2003] is 9 mm/yr oriented  $N85^\circ$  in Indochina, down to 6 mm/yr  $100^\circ$  in the south of Borneo. Although this relative motion is slightly smaller than the one with respect to NUVEL1A-Eurasia, it confirms an Eastward motion and a clockwise rotation of the Sundaland with respect to Siberia.

Although the relative motion between South China block and Sundaland block is small, these two blocks seem to be individualized. The velocity field in Fig. 8 shows that South China stations (in white) move toward the East-South-East while Sundaland stations move toward the East. Also the South China stations move 2-3 mm/yr slower to the East (well beyond their velocity uncertainties) than their predicted Sundaland-like motions. These results do not confirm the existence of a single Sundaland-South China block, as proposed by *Bock et al.* [2003].

Unfortunately, stations in South China are missing to model its motion by a rigid rotation. *Calais et al.* [2003] have performed an analysis on this region, and they concluded that the South and North China blocks may behave as a single East China block. The relative pole between this East China block defined by *Calais et al.* [2003] and our Sundaland block is located at  $120^\circ\text{E}$ ,  $20^\circ\text{N}$ , south of Taiwan island and rotates anti-clockwise at  $0.15^\circ/\text{Myr}$ . The location of this relative pole helps to understand the complex boundary between Sundaland and South China, described in section 4.3: the Red River Fault is affected by right-lateral shear and the South China Sea is a zone of low strain rate. Indeed, the relative East China/Sundaland pole being located in the South China sea, motions are very slow in this area and increase with the distance to the pole. It is then easily understandable why the South China Sea is a diffuse boundary zone.

## 5. Conclusion

The GPS database in S.E. Asia was significantly expanded by including new high-quality GPS measurements of both episodically and continuously operated sites. This resulted in a densified network in S.E. Asia with over 40 sites now available on Sundaland. Moreover, the availability of ITRF-2000 allows a refinement of the Sundaland pole. Based on 28 velocity vectors on stable Sundaland, a refined pole for Sundaland in ITRF-2000 was computed, located at  $48.9^\circ\text{S}$  and  $85.8^\circ\text{E}$  and with a clockwise rotating rate of  $0.341^\circ/\text{Myr}$ .

From the coupled analysis of the strain rates tensors and residual velocities, it was possible to localize a zone of very low strain rate and residuals smaller than 3 mm/yr, which constitutes the rigid core of Sundaland block. The core of stable Sundaland hence covers the Indochina peninsula to the North, the Malaysian peninsula to the West, the Sunda shelf, the major part of Borneo to the East and extends to the South almost until the Java island.

It is possible to see a progressive increase in the deformation rate from the core of Sundaland to its boundaries, indicating that high-rate inter-plate deformation is not completely localized at the boundaries but extends a bit inside the Sundaland block. The origin of this intra-plate deformation close to boundary areas may as well be due to elastic coupling on a single fault accommodating the major part of inter-plate motion as to a distribution of the deformation on several smaller scale faults in the boundary areas. Discriminating between these two deformation modes would need locally densified GPS measurements in order to constrain mechanical models.

Around the Sundaland block, inter-plate deformation rates can reach very high values due to the motion of Sundaland block relative to its neighboring plates. Our pole estimation confirms the second plausible interpretation given by *Michel et al.* [2001], which stated that Sundaland rotates clockwise with respect to Eurasia at a velocity increasing from the south to the north, although our refined pole predicts a slightly smaller relative motion.

With respect to South China, the Sundaland motion is small but significant and increases from very small values within the South China Sea in the pole area, to higher strain rates in the Red River area.

### Acknowledgments.

This work is a continuation of the joint research activities in S.E. Asia, which were initiated by the participation in the GEODYSSSEA project. Thanks and appreciation are extended to all people not visible in the author list, but whom have contributed significantly in expanding the GPS data base on S.E. Asia. We would like to thank especially all the staff/students at the Geodesy department of the Institut Teknologi Bandung and the Geodynamics division of the National Coordination Agency for Surveys and Mapping (BAKOSURTANAL) in Indonesia for their contribution to the GPS measurements in Sulawesi. We also are grateful for the support we got (with measurements and/or providing data) from the Scripps Institute for Oceanography (SCRIPPS) and the Rensselaer Polytechnic Institute (RFI), US. We especially would like to thank the Dutch Integrated Solid Earth Science (ISES) research program for their financial support in our GPS activities since 1999. Finally the authors also wish to thank the Jet Propulsion Laboratory (JPL), who developed GIPSY-OASIS GPS software, for their support and advice.

## References

- Altamimi, Z., P. Sillard, and C. Boucher (2002), ITRF2000: A new release of the International Terrestrial Reference Frame for earth science applications, *J. Geophys. Res.*, 107(B10), 2114, doi:10.1029/2001JB000561.

- Argand, E. (1924), La tectonique de l'Asie, *Congrès Géologique International, Comptes Rendus de la 13ème session*, 1, 596.

- Argus, D. F., and M. B. Heflin (1995), Plate motion and crustal deformation estimated with geodetic data from the global positioning system, *Geophysical Research Letters*, 22(15), 1973–1976, article.
- Aouac, J. P., and P. Tapponnier (1993), Kinematic Model of Active Deformation in Central-Asia, *Geophysical Research Letters*, 20(10), 895–898, article.
- Beutler, G., I. I. Mueller, and R. E. Neilan (1994), The International GPS Service for Geodynamics (IGS): Development and start of official service on January 1, 1994, *Bull. Géod.*, 68, 39–70.
- Blewitt, G., et al. (1988), GPS geodesy with centimeter accuracy, in *Lecture Notes in Earth Sciences*, edited by E. Groten and R. Strauss, Springer-Verlag, New York.
- Bock, Y., L. Prawirodirdjo, J. Genrich, C. Stevens, R. McCaffrey, C. Subarya, S. Puntodewo, and E. Calais (2003), Crustal motion in Indonesia from Global Positioning System measurements, *J. Geophys. Res.*, 108 (B8), 2367, doi:10.1029/2001JB000324.
- Calais, E., M. Vergnolle, V. San'kov, A. Lukhnev, A. Miroshnichenko, S. Amarjargal, and J. Deverchere (2003), GPS measurements of Crustal Deformation in the Baikal-Mongolia Area (1994–2002): Implications for Current Kinematics of Asia, *Journal of Geophysical Research-Solid Earth*, 108(B10).
- Chamot-Rooke, N., X. L. Pichon, C. Rangin, P. Huchon, M. Pubellier, C. Vigny, and A. Walpersdorf (1998), Sundaland Motion in a Global Reference Frame Detected from GEODYSSA GPS Measurements: Implications for Relative Motions at its Boundaries with the Australo-Indian Plates and the South China Block, in *GEODYSSA final report to the Commission of the European Community*, GFZ Scientific Technical Report STR98/14, Potsdam, Germany.
- Chase, C. (1972), The N problem of plate tectonics, *Geophys. J. Roy. Astron. Soc.*, 29, 117–122.
- Chase, C. (1978), Plate Kinematics: the Americas, East Africa and the rest of the world, *Earth Planetary Science Letters*, 37, 355–368.
- DeMets, C., R. G. Gordon, D. F. Argus, and S. Stein (1990), Current plate motions, *Geophysical Journal International*, 101, 425–478.
- DeMets, C., R. G. Gordon, D. F. Argus, and S. Stein (1994), Effect of recent revisions to the geomagnetic reversal timescale on estimates of current plate motions, *Geophys. Res. Lett.*, 21, 2191–2194.
- England, P., and G. Houseman (1985), Role of Lithospheric Strength Heterogeneities in the Tectonics of Tibet and Neighboring Regions, *Nature*, 315(6017), 297–301.
- England, P., and G. Houseman (1986), Finite Strain Calculations of Continental Deformation .2. Comparison With the India-Asia Collision Zone, *Journal of Geophysical Research-Solid Earth and Planets*, 91(B3), 3664–3676.
- Fernandes, R., B. Ambrosius, R. Noomen, L. Bastos, M. Wortel, W. Spakman, and R. Govers (2003), The relative motion between Africa and Eurasia as derived from ITRF2000 and GPS data, *Geophys. Res. Lett.*, 30(16), 1628, doi:10.1029/2003GL017,089.
- Genrich, J., Y. Bock, R. McCaffrey, E. Calais, C. Stevens, and C. Subarya (1996), Accretion of the southern Banda arc to the Australian plate margin determined by Global Positioning System measurements, *Tectonics*, 15, 288–295.
- Heki, K., S. Miyazaki, H. Takahashi, et al. (1999), The Amurian plate motion and current plate kinematics in eastern Asia, *J. Geophys. Res.*, 104, 29,147–29,155.
- Houseman, G., and P. England (1986), Finite Strain Calculations of Continental Deformation .1. Method and General Results For Convergent Zones, *Journal of Geophysical Research-Solid Earth and Planets*, 91(B3), 3651–3663.
- Houseman, G., and P. England (1993), Crustal Thickening Versus Lateral Expulsion in the Indian-Asian Continental Collision, *Journal of Geophysical Research-Solid Earth*, 98(B7), 12,233–12,249.
- Iwakuni, M., T. Kato, H. Takiguchi, T. Nakagawa, and M. Satomura (2003), Crustal deformation in Thailand and tectonics of Indochina peninsula as seen from GPS observations, *Geophys. Res. Lett.*, 31(11), L11,612, doi:10.1029/2004GL020,347.
- Kogan, M. G., G. M. Steblow, R. W. King, T. A. Herring, D. I. Frolov, S. G. Egorov, V. Y. Levin, A. Lerner-Lam, and A. Jones (2000), Geodetic Constraints on the Rigidity and Relative Motion of Eurasia and North America, *Geophysical Research Letters*, 27(14), 2041–2044, article.
- Kreemer, C., W. Holt, and J. Haines (2003), An integrated global model of present-day plate motions and plate boundary deformation, *Geophys. J. Int.*, 154, 8–34.
- Larson, K. M., J. T. Freymueller, and S. Philipsen (1997), Global plate velocities from the global positioning system, *Journal of Geophysical Research-Solid Earth*, 102(B5), 9961–9981, article.
- Le Pichon, X. (1968), Sea floor spreading and continental drift, *J. Geophys. Res.*, 73, 3661–3697.
- Mader, G. (1998), GPS Antenna Calibration at the National Geodetic Survey, *Technical report available at NGS website*, National Geodetic Survey, Silver Spring, US.
- McKenzie, D., and R. Parker (1967), The North Pacific: an example of tectonics on a sphere, *Nature*, 216, 1276–1280.
- Meyer, B., P. Tapponnier, L. Bourjot, F. Metivier, Y. Gaudemer, G. Peltzer, G. Shunmin, and C. Zhitai (1998), Crustal thickening in Gansu-Qinghai, lithospheric mantle subduction, and oblique, strike-slip controlled growth of the Tibet plateau, *Geophysical Journal International*, 135(1), 1–47.
- Michel, G., Y. Q. Yu, S. Y. Zhu, C. Reigber, M. Becker, E. Reinhart, W. Simons, B. Ambrosius, C. Vigny, N. Chamot-Rooke, X. L. Pichon, P. Morgan, and S. Matheussen (2001), Crustal motion and block behaviour in SE-Asia from GPS measurements, *Earth Plan. Sci. Lett.*, 187, 239–244.
- Mingsham, S., C. Boonphakdee, M. Becker, P. Neumaier, E. Reinhart, and H. Seeger (1998), Final Results of the THAICA 94/96 GPS Campaigns, in *GEODYSSA final report to the Commission of the European Community*, edited by P. Wilson and G. W. Michel, GFZ Scientific Technical Report STR98/14, Potsdam, Germany.
- Minster, J., and T. Jordan (1978), Present day plate motions, *J. Geophys. Res.*, 83, 5331–5354.
- Molnar, P., and H. Lyon-Caen (1989), Fault plane solutions of earthquakes and active tectonics of the Tibetan Plateau and its margins, *Geophysical Journal of the Royal Astronomical Society*, 99(1), 123–153.
- Molnar, P., and P. Tapponnier (1978), Active tectonics of Tibet, *Journal of Geophysical Research, A, Space Physics*, 83(B11), 5361–5375.
- Morgan, J. (1968), Rises, trenches, great faults and crustal blocks, *J. Geophys. Res.*, 73, 1959–1982.
- Niel, A. (1991), Global mapping functions for the atmospheric delay at radio wavelengths, *J. Geophys. Res.*, 101, 3227–3246.
- Nocquet, J. M., and E. Calais (2003), Crustal velocity field of western Europe from permanent GPS array solutions, 1996–2001, *Geophysical Journal International*, 154(1), 72–88, article.
- Nocquet, J. M., E. Calais, Z. Altamimi, P. Sillard, and C. Boucher (2001), Intraplate deformation in western Europe deduced from an analysis of the International Terrestrial Reference Frame 1997 (ITRF97) velocity field, *Journal of Geophysical Research-Solid Earth*, 106(B6), 11,239–11,257, article.
- Peltzer, G., and F. Saucier (1996), Present-day kinematics of Asia derived from geologic fault rates, *Journal of Geophysical Research-Solid Earth*, 101(B12), 27,943–27,956.
- Peltzer, G., and P. Tapponnier (1988), Formation and Evolution of Strike-Slip Faults, Rifts, and Basins During the India-Asia Collision - an Experimental Approach, *Journal of Geophysical Research-Solid Earth and Planets*, 93(B12), 15,085.
- Rothacher, M., and G. Mader (1996), *Combination of Antenna Phase Center Offsets and Variations: Antenna Calibration set IGS\_01*, IGS Central Bureau / University of Berne, Switzerland.
- Scherneck, H.-G. (1991), A parametrized solid Earth tide mode and ocean loading effects for global geodetic base-line measurements, *Geophys. J. Int.*, 106 (3), 677–694.
- Sella, G., T. Dixon, and A. Mao (2002), REVEL: A model for Recent plate velocities from space geodesy, *J. Geophys. Res. Solid Earth*, 107(B4), art.no.–2081.
- Simons, W. J. F., B. A. C. Ambrosius, R. Noomen, D. Angermann, P. Wilson, M. Becker, E. Reinhart, A. Walpersdorf, and C. Vigny (1999), Observing Plate Motions in S.E. Asia: Geodetic Results of the GEODYSSA Project, *Geophys. Res. Lett.*, 26(14), 2081–2084.
- Simons, W. J. F., D. L. F. van Loon, A. Walpersdorf, B. A. C. Ambrosius, J. Kahar, H. Z. Abidin, D. A. Sarsito, C. Vigny, S. H. Abu, and P. Morgan (2000), Geodynamics of S.E. Asia: First Results of the Sulawesi 1998 GPS Campaign, *IAG: Geodesy Beyond 2000*, 121, 271–277.
- Socquet, A., C. Vigny, W. Simons, N. Chamot-Rooke, C. Ranging, and B. Ambrosius (2003, subm.), GPS determination of the relative motion between India and Sunda and its accommodation in Myanmar, *J. Geophys. Res.*.
- Steblov, G., M. Kogan, R. King, C. Scholz, R. Burgmann, and D. Frolov (2003), Imprint of the North American plate in Siberia revealed by GPS, *Geophys. Res. Lett.*, 30 (18), 1924, doi:10.1029/2003GL017,805.
- Takiguchi, H., T. Kato, H. Kobayashi, and T. Nakagawa (2000), GPS observations in Thailand for hydrological applications, *Earth Plan. Sci. Lett.*, 52, 913–919.
- Tapponnier, P. (1986), A Tale of 2 Continents - the Collision of Great Landmasses and the Death of a Sea Are Parts of the Geological Drama That Created the Himalayas, *Natural History*, 95(11), 56–65, article.
- Tapponnier, P., and P. Molnar (1977), Active faulting and tectonics in China, *Journal of Geophysical Research*, 82(20), 2905–2930.

- Tappognier, P., and P. Molnar (1979), Active faulting and Cenozoic tectonics of the Tien Shan, Mongolia, and Baykal regions, *Journal of Geophysical Research*, 84(B7), 3425–3459.
- Tappognier, P., G. Peltzer, A. Y. Ledain, R. Armijo, and P. Cobbold (1982), Propagating Extrusion Tectonics in Asia - New Insights from Simple Experiments with Plasticine, *Geology*, 10(12), 611–616, article.
- Tregoning, P., F. Brunner, Y. Bock, S. Puntodewo, R. McCaffrey, J. Genrich, E. Calais, J. Rais, and C. Subarya (1994), First geodetic measurement of convergence across the Java trench, *Geophys. Res. Lett.*, 21, 2135–2138.
- Vigny, C., H. Perfettini, A. Walpersdorf, A. Lemoine, W. Simons, D. van Loon, B. Ambrosius, C. Stevens, R. McCaffrey, P. Morgan, Y. Bock, C. Subarya, P. Manurung, J. Kahar, H. Abidin, and S. Abu (2002), Migration of seismicity and earthquake interactions monitored by GPS in SE Asia triple junction: Sulawesi, Indonesia, *J. Geophys. Res. Solid Earth*, 107(B10), art.no.–2231.
- Vigny, C., A. Socquet, C. Rangin, N. Chamot-Rooke, M. Pubellier, M.-N. Bouin, G. Bertrand, and M. Becker (2003), Present day crustal deformation around sagaing fault, myanmar, *JGRSE*, 108(B11), 2533.
- Walpersdorf, A., C. Vigny, P. Manurung, C. Subarya, and S. Sutisna (1998), Determining the Sula block kinematics in the triple junction area in Indonesia by GPS, *Geophys. J. Int.*, 135, 351–361.
- Wilson, P., J. Rais, C. Reigber, E. Reinhart, B. A. C. Ambrosius, X. L. Pichon, M. Kasser, P. Suharto, A. Majid, P. Awang, R. Almeda, and C. Boonphakdee (1998), Study Provides Data on Active Plate Tectonics in Southeast Asia Region, *Eos Trans. AGU*, 79(45), 545–549.
- 
- W.J.F. Simons, DEOS/AS, Faculty of Aerospace Engineering, Delft University of Technology, Kluyverweg 1, 2629 HS Delft, The Netherlands, (Wim.Simons@lr.tudelft.nl)



# India and Sunda Plates motion and deformation along their boundary in Myanmar determined by GPS

Anne Socquet<sup>1\*</sup>, Christophe Vigny<sup>1</sup>, Nicolas Chamot-Rooke<sup>(1)</sup>, Wim Simons<sup>2</sup>, Claude Rangin<sup>3</sup>, Boudewijn Ambrosius<sup>2</sup>

**Abstract.** Using a regional GPS data set including ~190 stations in Asia, from Nepal to Eastern Indonesia and spanning 11 years, we update the present-day relative motion between the Indian and Sundaland Plates and discuss the deformation taking place between them in Myanmar. Revisiting measurements acquired on the Main Boundary Thrust in Nepal, it appears that points in southern Nepal exhibit negligible deformation with respect to mainland India. We show that including these points, using a longer time span than previous studies, and making an accurate geodetic mapping in the newest reference frame allow to refine the present day Indian motion.

Not only we confirm a current motion of India slower than predicted by the Nuvel-1A model, but our India-Eurasia motion is significantly (~5mm/yr) slower than previous geodetic determinations. This new Indian motion combined with a refined determination of the Sundaland motion gives way to a relative India-Sunda angular velocity of 20.2°N, 26.1°E, 0.370°/My in ITRF2000, predicting a relative motion of 35 mm/yr oriented N10° at the latitude of Myanmar. There, about half of the shear component of motion is taken along the Sagaing Fault that accommodates only 18 mm/yr of right-lateral strike-slip. We present two models addressing how and where the remaining deformation may occur. A first model of distributed deformation implies convergence on the Arakan subduction (the northern continuation of the now famous Sumatra-Andaman trench) and wrench faulting in the Arakan wedge. The second model uses localized deformation, where deformation observed west of the Sagaing fault is entirely due to elastic loading on a faster and oblique Arakan subduction (23 mm/yr). This latter model predicts that a major earthquake of Mw=8.5 may occur every century on this segment of the subduction.

## 1. Introduction

The India and Sundaland plates share a common boundary in Myanmar. Due to sparse geodetic networks in this region of the world, the present day relative motion between those two plates remained poorly known. Hence, the amount of right-lateral shear and associated style of active deformation in Myanmar has not been quantified so far. The 26 December 2004 Banda Aceh earthquake and the inherent damages strengthened the urgent need to study active deformation and seismic hazard along adjacent segments of the subduction. The mega-earthquake

ruptured a 1200 km-long portion of the trench, starting from the northern edge of the Sumatra Island, and ending offshore the Andaman Islands, only a few hundred kilometers south of Myanmar shores (Fig.1) [e.g. *de Groot-Hedlin*, 2005; *Ishii, et al.*, 2005; *Lay, et al.*, 2005; *Lomax*, 2005; *Vigny, et al.*, 2005]. This earthquake likely increased stress on adjacent segments of the subduction, raising seismic hazard at both ends of the rupture. The March 2005 Mw=8.7 Nias earthquake, which occurred just south of the previous rupture, is a case example of the triggered seismicity we can now fear further north on the Arakan Trench, along the Myanmar / Bangladesh border.

The aim of this paper is to study how the relative India / Sunda motion is accommodated in Myanmar, and in particular the style and rate of deformation along the two main active structures, the Arakan Trench and the Sagaing fault. We first present our new regional GPS processing and determine the current motion of the Indian Plate with respect to the Sunda Plate. We then focus on the active deformation in Myanmar and discuss the possible distribution of slip along the main faults. Although different models

<sup>1</sup>Laboratoire de Géologie de l'Ecole normale supérieure, UMR 8538, Paris, France

<sup>2</sup>Department of Earth Observation and Space Systems (DEOS), Delft, The Netherlands

<sup>3</sup>Collège de France - Chaire de Géodynamique, Europôle de l'Arbois, Aix en Provence, France

\*Now at the Department of Earth and Space Sciences, UCLA, USA

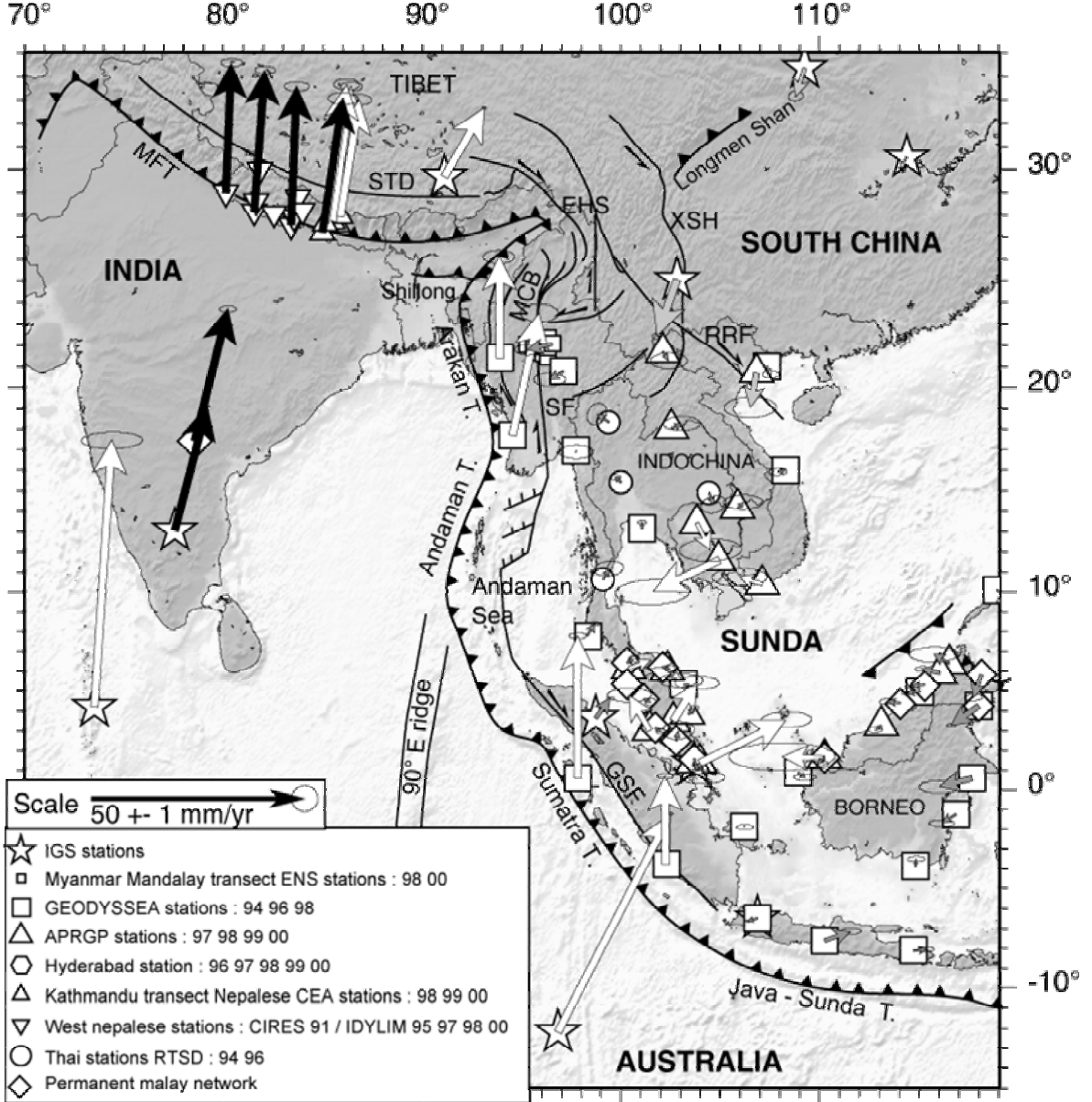


**Figure 1:** SE Asia GPS velocity vectors with respect to Sunda plate. Error ellipses show the 99% confidence level. Black arrows belong to Indian plate, dark grey arrows belong to South China block and light grey arrows belong to Sunda. Different symbols indicate data source. The major SE Asian faults and plates are also represented on the GTOPO-30 shaded topography. Abbreviations are as follow: EHS: Eastern Himalayan Syntaxis, GSF: Great Sumatran Fault, MFT: Main Frontal Thrust, MCB: Myanmar Central Basins, SF: Sagaing Fault, RRF: Red River Fault, STD: Southern Tibet Detachment, XSH: Xianshuihe Fault.

equally fit the data we have in hand, we show that a simple locked-trench model is plausible and discuss the implications in terms of yearly accumulation of deformation in Myanmar and seismic hazard.

## 2. Geodynamic setting

Southern Asia is constituted by three major plates: the Indian Plate, the Australian Plate and the Sunda

Plate (Fig. 1). The Indian Plate extends on the Indian continent and the western part of the Indian Ocean. The Australian Plate extends on the eastern part of the Indian Ocean and the Australian Craton. The Sunda Plate involves the Indochinese and Malaysian peninsulas, the Sunda Shelf, Borneo, Sumatra and Java Islands. Western Indonesia was early recognized as a consistent tectonic entity [Hall, 2002; Hamilton, 1972]. Geodetic measurements confirmed this point and showed that the Sunda plate is currently moving eastward with respect to the Eurasian Plate [Bock, et al., 2003; Chamot-Rooke and Le Pichon, 1999; Michel, et al., 2001; Simons, et al., 1999].

The triple junction between India, Australia and Sunda plates is located at the intersection between the Andaman Trench, the Sumatra Trench and the 90° E Ridge (Fig. 1), where the December 26<sup>th</sup> 2004 earthquake occurred. The 90°E Ridge can be approximated as being the boundary between the Indian and Australian plates, although this limit is most probably diffuse. In this area, the Indian oceanic crust consists of three component plates (India, Australia and Capricorn) and multiple diffuse plate boundaries [DeMets at al., 2005; Gordon et al., 1990; Royer and Gordon, 1997]. The boundary between the Indian and Australian plates is a wide region affected by NW-SE compressive deformation of the oceanic lithosphere [Chamot-Rooke, et al., 1993] and by active left-lateral strike-slip along north-trending paleo transform faults [Abercrombie, et al., 2003; Deplus, 2001; Deplus, et al., 1998]. To the north, the limit between the Indian Plate and the actively deforming Asian continent is the Main Frontal Thrust (Fig. 1 and 2) [Cattin and Avouac, 2000; Lave and Avouac, 2000]. To the east, the Himalayan thrusts connect, in the inner part of the Eastern Himalayan Syntaxis, to the north-trending Myanmar structures [e.g. Burg, et al., 1998; Holt, et al., 1991; Mitchell, 1993; Ratschbacher, et al., 1996]. At the latitude of Myanmar, the Indian Plate slides northward past the Sunda Plate. There, the 1200 km-long right-lateral strike-slip Sagaing Fault is classically considered

**Table 1:** India / South Nepal stations baselines variations in mm/yr.

Baseline	Length variation
IISC - HYDE	2.1
IISC - MAHE	2.4
IISC - BHAI	1.9
IISC - NEPA	1.2
IISC - SIMR	1.1
HYDE - MAHE	0.1
HYDE - BHAI	-1.1
HYDE - NEPA	-0.7
HYDE - SIMR	-1.6

as being the main boundary between the Indian Plate and the Sunda Plate [Ledain, et al., 1984; Michel, et al., 2001; Peltzer and Saucier, 1996; Tapponnier and Molnar, 1975, 1977] although the Andaman and Arakan trenches seem to constitute the eastern limit of the Indian Plate (Fig. 1 and 2) [Curay, 1989; Nielsen, et al., 2004; Mitchell, 1993]. South of Myanmar, the Andaman Trench becomes the Sumatra Trench. East of this trench system, the Andaman Basin opens in a pull-apart setting between the Sagaing Fault to the north and the West Andaman and Great Sumatran Fault to the south. The Sumatra Trench runs parallel to the Great Sumatran Fault (Fig. 1). These two structures accommodate by partitioning the oblique Australia - Sunda motion e.g. [Curay, 1989; Fitch, 1972; Genrich, et al., 2000; McCaffrey, 1991; McCaffrey, et al., 2000; Prawirodirdjo, et al., 1997].

In Myanmar, east of the Arakan trench, the Arakan accretionary wedge is affected by shallow seismicity [Dasgupta, et al., 2003; Rao and Kumar, 1999; Satyabala, 2003] along large N/S strike-slip faults [Bender, 1983; Guzman-Speziale and Ni, 1996; Socquet, et al., 2002]. The Myanmar Central Basins bound this mountain belt to the east [Bender, 1983; Pivnik, et al., 1998; Rangin, et al., 1999]. The major tectonic break between the Arakan range and the basins is the Kabaw Fault (or Eastern Boundary Thrust). About 200 km to the East, the North-trending Sagaing Fault cuts through the central basins and follows a zone of topographic gradient, the Shan Scarp, along which the Mogok metamorphic belt outcrops [Bertrand, et al., 2001; Bertrand, et al., 1999]. The Sagaing Fault presently ends in a compressional horsetail toward the North in the Himalayan Syntaxis area, and an extensional horsetail toward the South in the Andaman pull-apart (Fig. 1) [Curay, 2005; Guzman-Speziale and Ni, 1993; Ledain, et al., 1984].

### 3. Data processing

The velocity solution presented here is a reprocessing of a mix of campaign and continuous GPS data covering South and Southeast Asia. The solution includes ~190 stations spanning 11 years of data from 1991 to 2002. We processed new data — the

**Table 2:** Plate pairs rotation parameters used in this study

Plate pair	reference	Rotation parameters		
		Lat(°N)	Lon(°E)	$\omega$ (°/My)
India/ITRF	This study	50.9	-12.1	0.486
	This study	27.5	12.9	0.398
India/Euras	Nuvel-1a	24.4	17.7	0.51
	Paul et al	25.6	11.1	0.44
India/Sunda	This study	20.2	26.1	0.370

permanent Malaysian network acquisitions from 1999 to 2001, the Asia Pacific Regional Geodetic Project campaigns from 1997 to 2000 [Govind, et al., 1999], the first order Thai network measurements in 1994-1996-2000 and data from Hyderabad GPS station in India from 1996 to 2000 — as well as already published data — GEODYSSSEA data [Chamot-Rooke and Le Pichon, 1999; Michel, et al., 2001; Simons, et al., 1999], GPS campaigns in Sulawesi from 1999 to 2002 [Simons, et al., 2000; Vigny, et al., 2002; Walpersdorf, et al., 1998; Walpersdorf, et al., 1998], Myanmar campaigns in 1998 and 2000 [Vigny, et al., 2003], West Nepal network measurements in 1991-1995-1997-1998-2000 [Bilham, et al., 1997; Jouanne, et al., 1999; Larson, et al., 1999], the Kathmandu transect campaigns from 1998 to 2000 [Avouac, et al., 2001; Jouanne, et al., 2004] and data from 30 IGS stations world wide spread (Fig. 1). The raw GPS measurements were analyzed in 24-hours daily solutions with GAMIT [King, 1999]. Velocities were estimated and mapped in ITRF-2000 [Altamimi, et al., 2002] using GLOBK/GLORG softwares [Herring, 1999]. A slightly different data set (80% common stations in SE Asia) was also processed independently with GIPSY OASIS II software [Blewitt et al., 1988] and published separately [Simons et al., submitted]. We combined these data with ours, again using GLOBK. The GAMIT processing, the combinations, the reference frame mapping and the error analysis are detailed in the electronic supplement. Fig. 1 depicts the velocity field we obtain with respect to the Sunda Plate.

## 4. India / Sunda motion

### 4.1. India deformation and motion

From a geodetic point of view, the Indian plate remains undeformed up to the foothills of the Himalaya. Actually, and contrary to what one would expect from simple elastic coupling theories, stations in southern Nepal hardly show any motion with respect to India. Baselines lengths between points located in Southern Nepal (MAHE, NEPA, BHAI and SIMR) and points located further south in continental India (HYDE and IISC) vary by less than 2 mm/yr (Table 1, Fig.2). Since the residuals do not show any systematic trend, we conclude that these small numbers are representative of the data uncertainties rather than the actual rate of deformation. [Jouanne, et al., 2004; Larson, et al., 1999; Paul, et al., 2001] found similar results since their south Nepalese points move at less than 2 mm/yr with respect to IISC. We thus consider in the following that velocities of South Nepal stations are indeed representative of the motion of the Indian plate. A new geodetic rotation pole for the India Plate in ITRF-2000 was thus determined using two Indian stations (IISC and HYDE) and four southern Nepalese stations (MAHE, NEPA, BHAI, SIMR) located south of the Main Frontal

Thrust. The Maldives station was not used because we processed only two sets of measurements separated by a year interval only, explaining its poor velocity determination. In any case, Maldives Island is located into the diffuse zone of deformation between India and Australia. In ITRF-2000, our pole determination for the Indian Plate is  $50.9^{\circ}\text{N}$ ,  $-12.1^{\circ}\text{E}$ ,  $0.486 \pm 0.01^{\circ}/\text{Myr}$  (Table 2). The computed error ellipse was constructed from variance-covariance matrix describing uncertainties, linearly propagated from the errors assigned to the data, following the method described by [DeMets et al., 1994]. Its semi-major axis is oriented  $110^{\circ}$  and is  $5.11^{\circ}$  long and its semi-minor axis is  $0.61^{\circ}$  long. The shape of the ellipse (ratio between long and short axes and ellipse orientation) is mainly constrained by the geographical distribution of the stations. Here, the longitudinal uncertainty is larger because there is a trade-off between the angular speed and the distance pole / plate. Residual velocities for the stations used for the pole determination are below 2 mm/yr with an rms of 1.29 mm/yr (Figure 2). In order to compare our pole with previous studies, we rotate our India/ITRF-2000 pole with respect to the Eurasian Plate defined by [Calais, et al., 2003]. With respect to

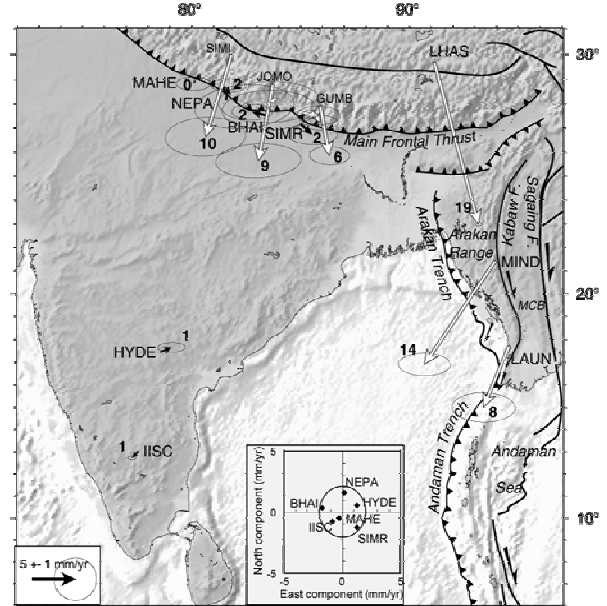


**Figure 2:** GPS velocities in India, Nepal and Western Myanmar with respect to the Indian Plate. Error ellipses show the 95% confidence level. Black arrows belong to Indian plate. The main tectonic structures are also represented on the GTOPO-30 shaded topography. MCB: Myanmar Central Basins. Inset: Vector components of the residual velocities used for the India / ITRF-2000 pole determination. Units are in mm/yr. Indian stations display residual velocities below 2 mm/yr (circle).

Eurasia, the Indian Plate rotates anticlockwise about a pole located at  $27.5^\circ\text{N}$ ,  $12.9^\circ\text{E}$  at a rate of  $0.398^\circ/\text{Ma}$ . Our pole determination predicts a velocity at Bangalore (IISC) of  $39\text{ mm/yr}$  oriented  $N25^\circ$ . This is  $20\%$  slower than the  $48\text{ mm/yr}$  oriented  $N21^\circ$  predicted by NNR-Nuvel1A model [DeMets, et al., 1990; DeMets, et al., 1994]. It is also  $\sim 5\text{ mm/yr}$  slower than the  $44\text{ mm/yr}$  oriented  $N22^\circ$  at IISC given by the latest previous geodetic study [Paul, et al., 2001]. This difference is probably due to the use of a different reference frame for the two GPS solutions (ITRF-2000 versus ITRF-96). Also, the technique used by [Paul et al., 2001] to map their velocities in ITRF-96 (by applying tight constraints to the coordinates of IISC, KIT3 and POL2) may have forced IISC velocity. Indeed IISC velocity is slower by  $2\text{ mm/yr}$  northward and faster by  $2\text{ mm/yr}$  eastward in ITRF-2000 than in ITRF-96. It is quite noticeable that as the determination of the ITRF is refined, the geodetic estimate of the India/Eurasia motion decreases and becomes more oblique.

#### 4.2. Sunda – India relative pole determination

To determine the rotation pole between Indian and Sunda plates, we rotate our velocities with respect to the previously defined Indian Plate and minimize, in the least square sense, the velocities of the stations located on the Sunda Plate. The stations located close to the block boundaries, potentially affected by significant elastic deformation or located in seismically active regions were not selected for the pole determination

(Eastern margin of Borneo, Java Island, south Sumatran shore). Stations displaying a residual velocity higher than  $10\text{ mm/yr}$  have been removed too. These non-consistent velocities are mainly the APRGP stations, most of which have been measured only twice with a year interval, and thus display important uncertainties (Table S4). This leaves us with 33 stations used for the pole determination (PHON, TAUN, OTRI, VIEN, HPAA, NONN, UTHA, SRIS, KHON, CHON in Indochina, BANH, PHUK, ARAU, IPOH, KTPK, GETI, DOP4, SEGA, KUAL, KUAN, UTMJ, NTUS, TANJ in the Malaysian peninsula, TABA, KUCH, BINT, MIRI, BATU, BRUN, LABU, KINA, D005, PUER in Borneo). The relative rotation pole between the Sunda Plate and the Indian Plate is located in North Africa ( $20.2^\circ\text{N}$ ,  $26.1^\circ\text{E}$ ) and rotates clockwise at a rate of  $0.370^\circ/\text{Ma}$ . The error ellipse is oriented  $N158^\circ$ , has a  $2.11^\circ$ -long semi-major axis and a  $0.39^\circ$ -long semi-minor axis, which means that the longitude of the pole is better constrained than its latitude. The residual velocities of Sunda stations with respect to this pole are listed in Table S4. As shown in Fig. 3, the residual velocities at stations used for the pole determination are small ( $50\% < 2\text{ mm/yr}$ ) and have no preferential orientation. Therefore, we consider that we reached a robust estimate of the relative India/Sunda motion, more accurate than previous solutions since it includes far more stations over rigid Sunda, and takes into account the slower motion of India –  $5\text{ mm/yr}$  slower than [Paul et al., 2001]. Our new pole predicts a relative India / Sunda motion along the Arakan Trench of  $35\text{ mm/yr}$  with a  $N11^\circ$  azimuth in central Myanmar ( $22^\circ\text{N}$ ), and of  $36\text{ mm/yr}$  with a  $N14^\circ$  azimuth in southern Myanmar ( $17^\circ\text{N}$ ).

### 5. Deformation at the plate boundary

#### 5.1. GPS velocity field in Myanmar

Myanmar GPS velocities are shown in Fig. 4 in the new Sunda reference frame, together with the active fault traces and the available earthquake focal mechanisms. At the latitude  $\sim 22^\circ\text{N}$  and east of the Sagaing Fault, YWEN station moves at  $6\text{ mm/yr}$  with respect to the Sunda Plate. The motion of YWEN is possibly affected by elastic strain loading due to coupling on the Sagaing Fault. The westward component of motion is however best explained by intracontinental deformation at the northern edge of the Indochinese peninsula, due to clockwise rotations evidenced around the Eastern Himalayan Syntaxis [Holt, et al., 1991; Ratschbacher, et al., 1996; Wang, et al., 1998]. This rotational pattern generates shear on the northern edge of the Indochinese peninsula (in Yunnan, China) that is accommodated along E-W left-lateral strike-slip faults [Lacassin, et al., 1998; Socquet

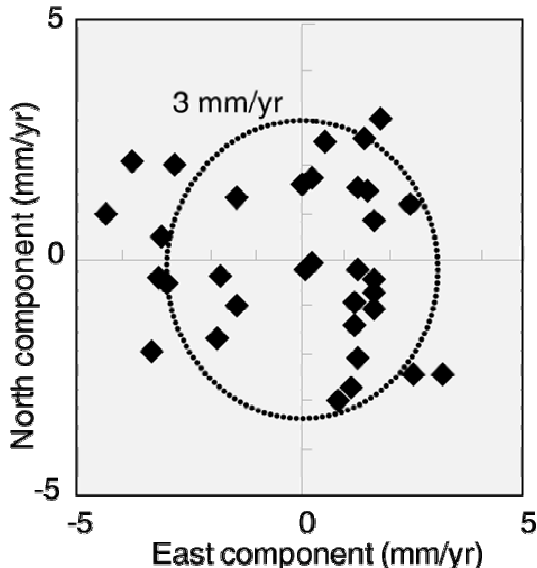


**Figure 3:** Vector components of the residual velocities used for the India / Sunda pole determination. Units are in  $\text{mm/yr}$ .  $73\%$  of the stations display residual velocities below  $3\text{ mm/yr}$  (circle), the remaining ones being located close to the plate's boundaries.

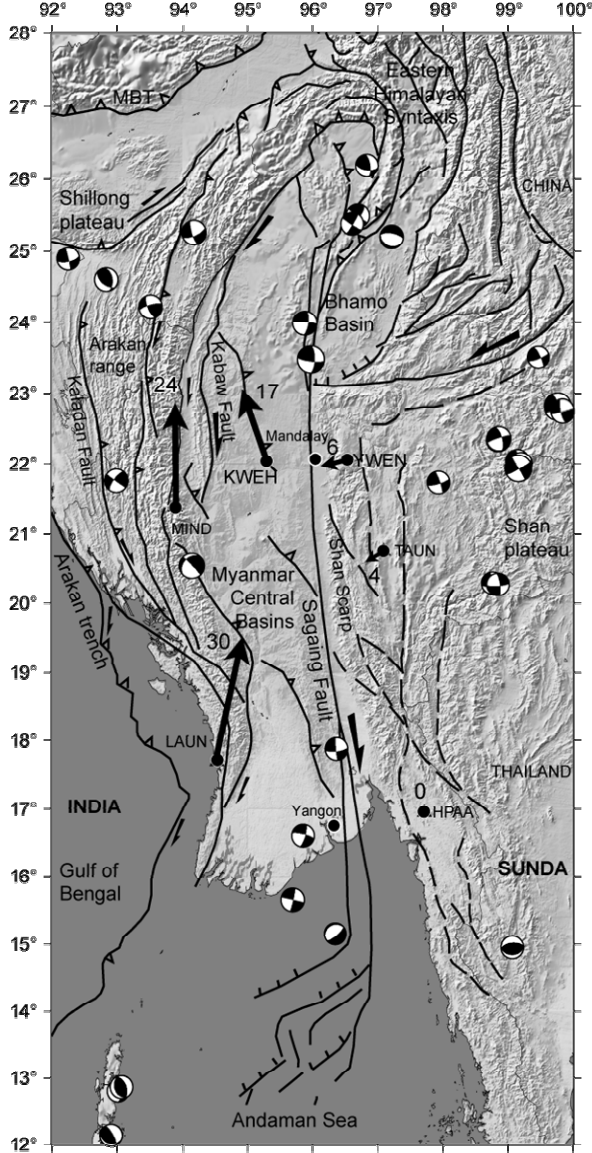


**Figure 4:** Main Myanmar structures, shallow CMT focal mechanisms, GPS velocities with respect to the Sunda Plate (black arrows). The motion to be accommodated between the GPS points is also reported.

and Pubellier, 2005; Wang and Burchfiel, 1997; Wang, et al., 1998]. East of YWEN, the shallow seismicity of strike-slip type attests that this intracontinental strain probably extends to the Shan Plateau (Fig. 4). West of the plateau, the relative motion between KWEH and YWEN indicates that the Sagaing fault accommodates about 18 mm/yr of right-lateral strike-slip. This slip amount agrees with the previous geodetic solution [Vigny, et al., 2003] and the neotectonic studies [Bertrand, et al., 1998]. In the Arakan Range (western Myanmar), MIND station moves 24 mm/yr north with

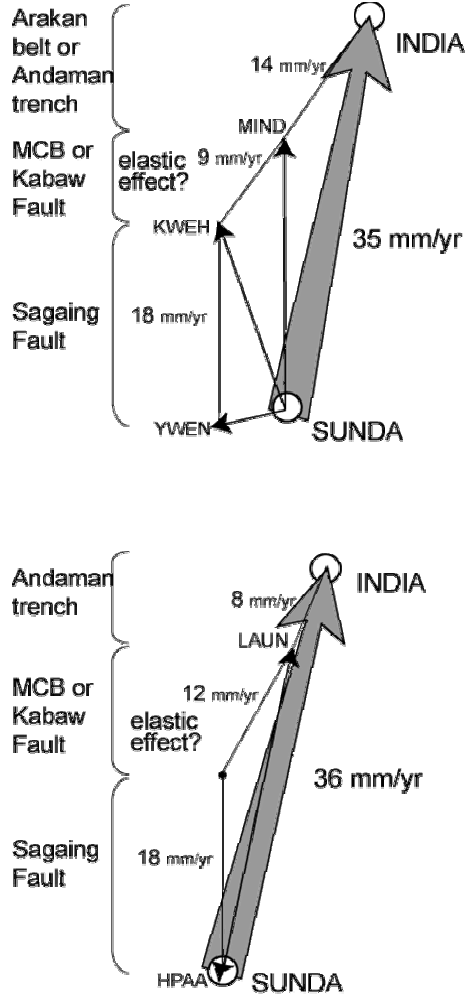


**Figure 5:** Velocity diagrams showing the distribution of deformation across central (top) and southern (bottom) Myanmar. The plain grey arrows represent India / Sunda motion, small circles represent the plates location in the velocity space, black arrows represent the measured GPS velocities with respect to the Sunda Plate, and the numbers show the amount of motion to be accommodated between the points of the velocity diagram (GPS stations or tectonic plate).

respect to Sunda (Fig. 4). With respect to India, this station moves 14 mm/yr toward the south-west (Fig. 2). We summarize in Fig. 5 the various GPS constraints in the form of synthetic velocity diagrams. In the velocity vector diagram constructed at this latitude (Fig. 5, top), the three heads of the vectors describing the motion of the Indian Plate, KWEH and MIND sites with respect to the Sunda Plate are aligned. This implies that the motion to be accommodated between the Indian Plate and the Myanmar central basins (KWEH point) has a constant azimuth. LAUN

station is located in south-western Myanmar south of the Arakan range ( $17^{\circ}\text{N}$ ), close to the trace of the Arakan trench (Fig. 4). In this area, offshore data revealed that the trench has a dog-leg shape with strike-slip segments oriented  $N\ 30^{\circ}$ , and thrusts segments oriented  $N\ 120^{\circ}$  [Nielsen et al., 2004]. In our solution, LAUN moves 8 mm/yr to the azimuth  $N203^{\circ}$  in the Indian reference frame (Fig. 2) and up to 30 mm/yr with respect to Sunda (Fig. 4). Assuming that the estimated slip rate on the central Sagaing Fault can be extrapolated to its southern end, i.e. 18 mm/yr oriented N-S, and further considering that HPAA station belongs to the Sunda Plate (no residual velocity with respect to Sunda), then 20 mm/yr oriented  $\sim N30^{\circ}$  must be accommodated west of the Sagaing fault (Fig. 5, bottom). At this latitude, no major fault exists between the trench and the Sagaing Fault, so that this motion is likely to be accommodated obliquely along the trench itself as suggested by marine surveys [Nielsen et al., 2004].

With respect to Sunda, India moves around 35 mm/yr NNE. The Sagaing fault only accounts for 18 mm/yr N. The remaining motion must be taken elsewhere. The question we raise is whether the remaining motion is localized entirely at the trench, as suggested at least for the southernmost segment, or distributed within the Arakan belt. We thus examine quantitatively two models: one where the deformation is distributed onto several faults and one where the motion is localized on two major faults only – the Arakan Trench and the Sagaing Fault, hereafter the two-fault model – with accumulation of interseismic elastic deformation at their locked interfaces.

## 5.2. Distribution of the deformation in Myanmar

Seismicity and faults mapping in Myanmar support the possibility of distributed deformation. Immediately above the Arakan subduction slab, and possibly within it, both strike-slip and reverse focal mechanisms are observed [Dasgupta, et al., 2003; Rao and Kumar, 1999; Satyabala, 2003]. At surface, the Arakan range is an active fold-and-thrust-belt, also affected by large N-S strike-slip faults. Shallow seismicity occurs both as strike-slip and thrust events [Guzman-Speziale and Ni, 1996]. Hence both the Arakan Trench and the structures affecting the Arakan wedge might account for strike-slip and thrust deformation necessary to accommodate the 14 mm/yr that occurs between the Indian Plate and MIND station (Fig. 4 and 5 top). In this hypothesis, the remaining 9 mm/yr oriented  $N36^{\circ}$  must occur between the Myanmar Central Basin (KWEH) and the Arakan range (MIND) (Fig. 4 and 5 top). Directions of the tectonic structures there are mainly N/S [Pivnik, et al., 1998; Rangin, et al., 1999]. The major fault between the Arakan range and the basins is the Kabaw Fault (also

called Eastern Boundary Thrust). [Hla Maung, 1987] reported transcurrent motion on this fault before the Miocene. If this structure is still active, it would be a good candidate to accommodate part of the right-lateral wrench faulting [Nielsen et al., 2004]. As in the Arakan range, folding is observed within the Neogene sediments of the Myanmar Central Basins, although folding is much gentler in the lowlands [Ledain, et al., 1984]. If still actively growing, these en echelon NW-SE folds could also accommodate part of the motion (Fig. 4), but it is unlikely that the cumulated motion on them is large. The difficulty in testing more quantitatively the distributed model is that on one hand, it does not rule out the possibility of elastic loading onto a few discrete faults – including the trench itself – and on the other hand, the network we use is clearly not dense enough to recognize narrow high straining zones.

## 5.3. Elastic modeling

The alternative is to test whether our geodetic solution is compatible with a simple locked-trench and locked-Sagaing fault model. The rationale is that the observed deformation at our Myanmar GPS stations may be purely transient and related to the combination of interseismic elastic coupling on the Sagaing Fault and the Arakan Trench only. In this case, the Sagaing fault would be affected by pure strike-slip deformation along its entire length while oblique convergence would be accommodated on the Arakan subduction from southern Myanmar up to the Shillong. Although the distribution of GPS sites may be insufficient and constraints on the detailed geometry of the subduction locked interface are obviously lacking, the assumptions are simple enough to perform a first order test. We constructed a model using DEFNODE software [McCaffrey, 1995, 2002, 2005] considering rigid blocks separated by faults modeled as locked dislocations in an elastic half space [Okada, 1985]. The two-fault model is schematized in Fig. 6. The surface traces of the faults follow the mapping of the Arakan trench and the Sagaing Fault [Nielsen, et al., 2004; Vigny, et al., 2003]. The Sagaing fault is a vertical strike-slip fault locked at 15 km depth [Vigny, et al., 2003]. We consider a dip of  $15^{\circ}$  at shallow depths (< 50 km) for the Arakan Trench, constrained by seismicity cross sections [Dasgupta, et al., 2003; Satyabala, 2003]. The model is composed of four independent blocks: the Indian and Sunda plates, the Myanmar sliver microplate and the Yunnan block. This last block is a feature used to "mimic" the intracontinental deformation around the Himalayan syntaxis which results in the 6 mm/yr westward motion of YWEN in this area. Obviously, this kind of intracontinental distributed strain is difficult to model properly with elastically deforming blocks, but it still

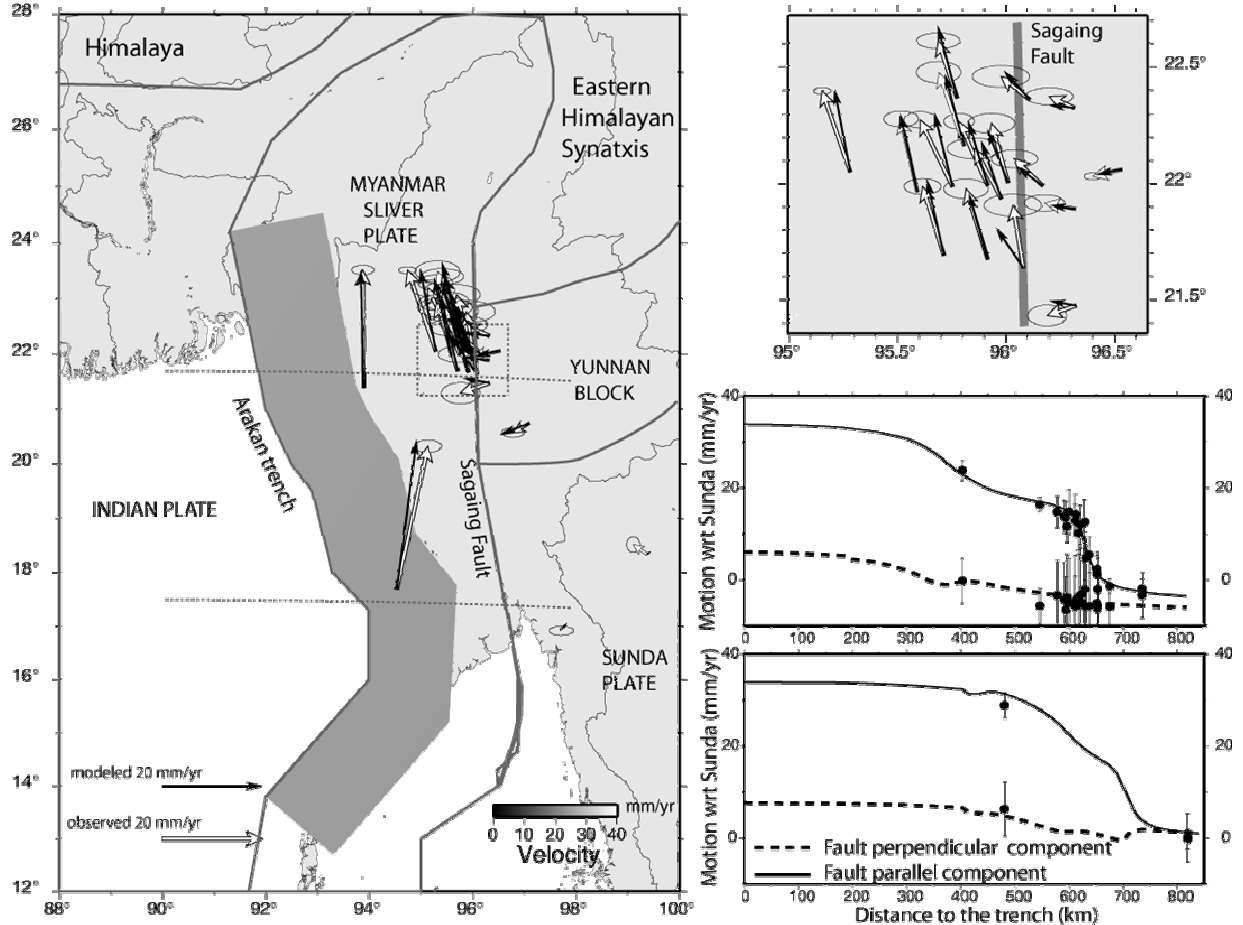


**Figure 6:** Two-fault (Arakan trench and Sagaing Fault) elastic loading model of the deformation in Myanmar. The slip on these faults was inverted and its amount is represented with a grey scale. Observed GPS vectors are in white while the modelled ones are black. The reference frame is the Sunda Block. The left regional map show the geometry and the results of the model. The top right inset shows the detail of the velocities within the Mandalay network, across the Sagaing Fault. The two right lower insets are E-W cross sections performed at 21.5°N (upper one) and at 17.5°N (lower one). They show both the fault normal component (dashed line) and the fault parallel component (continuous line) of the velocity. Observed data are represented by dots while the curve depicts the modelled velocity.

needs to be taken into account. This is done by allowing a small westward motion of a block located on the Shan Plateau, and called here the Yunnan Block. While fixing the India/Sunda total motion, we invert the GPS data for the rotation pole of the Myanmar sliver, allowing us to estimate possible rates of slip on the Sagaing Fault and the Arakan trench. Coherently with [Vigny, et al., 2003] our best fit model finds that the Sagaing fault is locked and slips at 18 mm/yr (Fig. 6, right). Moreover it shows that the velocities at MIND and LAUN (west of the Sagaing fault) are well explained by elastic loading on the Arakan Trench. The trench would then be locked at 50 km and would accommodate an oblique slip varying from 20 mm/yr oriented N30° in southern Myanmar

(around 17° of latitude) to 23 mm/yr oriented ~N35° in central Myanmar (around 22° of latitude). MIND station is located ~200 km away from the trench. There, the calculated elastic deformation reaches 5–6 mm/yr for the perpendicular component and 7 mm/yr for the strike-slip component. Thus, elastic loading on the Arakan subduction interface could be responsible for the motion observed at MIND station (Fig. 5 top: MIND to KWEH). Likewise, the motion observed at LAUN station, located at ~50 km from the trench, can be modeled as the addition of the rigid rotation of the Myanmar sliver and 12 mm/yr oriented N30° of elastic strain due to the loading on the trench (Fig. 5 bottom: LAUN to sliver).

This second hypothesis implies that deformation in Myanmar is partitioned on two main structures: the Sagaing Fault and the Arakan trench. Such a partitioning mechanism was described a long time ago for the western Sunda Arc where convergence occur on the Sunda trench and strike slip on the Great Sumatran Fault [Curray, 1989; Fitch, 1972]. Here, the deformation would be partially partitioned with 18 mm/yr of pure right-lateral strike-slip on the Sagaing Fault and still oblique convergence on the Arakan trench accommodating about 23 mm/yr oriented N 35° (~18 mm/yr of right-lateral strike-slip and ~13 mm/yr of convergence).

#### 5.4. Discussion

While earlier seismologic studies suggested cessation of subduction in Myanmar [Rao and Kumar, 1999], our new data confirm the more recent interpretations of a still active subduction [Dasgupta, et al., 2003; Satyabala, 2003; Nielsen, et al., 2004]. However, the localized versus distributed end-members models remain difficult to discriminate, since structural and geophysical arguments may support each hypothesis. Argument against the distribution hypothesis is that no large straining zone was recognized west of the main Sagaing fault. [Hla Maung, 1987] postulates transcurrent motion along the Kabaw Fault, but no geologic nor geophysical evidence was reported to indicate such movement [Khin Zaw, 1990]. Moreover, the folds affecting the Myanmar Central Basins did not accumulate significant shortening since their formation. [Pivnik, et al., 1998] interpret the en-echelon pattern of the fold axes and reverse faults affecting the basins as the result of internal shear within the sliver, as described by the models of deformation in fore-arc sliver terranes bounded by an oblique subduction zone on one side and a trench-parallel strike-slip fault on the other side [Jarrard, 1986]. [Nielsen, et al., 2004] proposed partitioning onto the Sagaing fault and the Arakan trench in southern Myanmar (around 18°N), evolving to full partitioning at higher latitudes (around 25°N): the shear motion taken on the trench would be progressively transferred to several strike-slip and thrust structures within the Arakan wedge. Shallow seismicity north of 20°N indeed supports current activity along the strike-slip faults and thrusts affecting the external part of the Arakan wedge, but seems to be restricted to the west of station MIND (Fig. 4). If we acknowledge that no significant motion is accommodated between this station and the Sagaing Fault – neither on the Kabaw Fault nor within the Myanmar Central Basins – then the measured velocity at MIND station can only be explained by elastic deformation. This pleads for a significant part of the motion being accommodated on the locked subduction plane.

This localized two-fault model yields a high seismic hazard on the Arakan trench. If we consider a locked plane 400 to 600 km long and 200 km wide – which corresponds to a plane locked at 50 km depth with 15° dip – with an accumulation of 23 mm/yr and a mean crustal shear modulus of  $3.3 \cdot 10^{10}$  Pa, it is due to produce a magnitude 8.5 earthquake every century or a magnitude 9 every 500 years [Kanamori, 1977; Wells and Coppersmith, 1994].

#### 6. Conclusion

Our extensive regional GPS velocity field allows us to determine both the relative plate motions and the intra-continental deformation in the region of interaction between India, Eurasia and Sunda plates. Thanks to long time series, numerous measurements in Nepal and the availability of ITRF-2000, our new rotation pole for the Indian Plate yields an India/Eurasia convergence rate significantly slower (~5 mm/yr) than estimated by previous geodetic determination [Paul et al., 2001]. Combining with our refined estimation of Sunda motion, we predict around 36 mm/yr of right-lateral N/S strike-slip and 7 to 9 mm/yr of E-W convergence in Myanmar. Distribution of active deformation in Myanmar is constrained by far-field plate motion (India / Sunda motion), near-field GPS measurements (stations in Myanmar), active tectonics on land and at sea (faults style and rate) and seismological data (focal mechanisms). In southern Myanmar (17°N), the relative India / Sunda motion is partitioned between the right-lateral Sagaing Fault slipping at 18 mm/yr and the Andaman trench accommodating 20 mm/yr of oblique convergence oriented N30°. A similar two-faults partitioning process probably prevails in central Myanmar (22°N), the shear component west of MIND (about 23 mm/yr) being mainly accommodated as oblique convergence (oriented N35°) along the Arakan trench. A significant portion of the Arakan trench is thus presently elastically locked and accumulating significant motion. Moreover, this trench portion is localized in a major seismic gap: to the north, two Mw 8.7 earthquakes occurred in 1897 in the Shillong Plateau and in 1950 in Assam, when to the south, the rupture of the Mw 9.2 earthquake of December 2004 extended up to the Andaman Islands but not beyond. This has important implications for seismic hazards along the Burma subduction front. The 26 December 2004 earthquake on the Sumatran trench showed that the northern part of the subduction (Andaman trench) was locked and had accumulated enough elastic deformation to produce a Mw 8.9 earthquake by itself [Vigny, et al., 2005]. Our partitioned elastic model with oblique slip on the trench is a simple continuation of this system to the North and yields high probability for one great

subduction earthquake of magnitude 8.5 every century in this area.

## 7. Acknowledgements

The Myanmar program was initiated in the framework of the GEODYSSSEA project between the European commission and the GFZ in Germany. The bulk of the Myanmar campaigns was sponsored by TMEP (GIAC project) and CNRS/INSU contribution. Thanks and appreciations are extended to RTSD for making the THAICA 1994 and 1996 data available, to LDG-CEA, Cires and IDYLLIM for making the Nepalese data available. We are indebted to Kristine Larson (Department of Aerospace Engineering Sciences, University of Colorado, USA) for providing her re-estimated orbits for the period of 1991 campaign in Western Nepal, and to François Jouanne (LGCA, Université de Savoie, France) for providing SINEX file for the West Nepal 1995 campaign. Asia Pacific Regional Geodetic Project (APRGP) raw GPS data used in this processing were distributed by Geosciences Australia. HYDE station was measured by the National Geophysical Research Institute in Hyderabad (NGRI, India) and data were kindly provided by James Campbell (Geodetic Institute der Universität Bonn, Germany). We are very grateful to Rob McCaffrey for allowing us to use DEFNODE software he developed at RPI and to R.W. King (MIT) for his numerous advices. This paper benefited from very constructive reviews of Paul Tregoning and five anonymous reviewers. The maps in this paper were produced using the public domain Generic Mapping Tools (GMT) software [Wessel and Smith, 1995].

## References

- Abercrombie, R. E., et al. (2003), The June 2000 Mw 7.9 earthquakes south of Sumatra: Deformation in the India – Australia Plate, *J. Geophys. Res.*, **108**, 2018.
- Altamimi, Z., et al. (2002), ITRF2000: A new release of the International Terrestrial Reference frame for earth science applications, *Journal of Geophysical Research-Solid Earth*, **107**, art. no.-2214.
- Avouac, J. P., et al. (2001), Seismic cycle in the Himalayas, *Comptes Rendus Acad. Sci. Ser II-A*, **333**, 513-529.
- Bender, F. (1983), *Geology of Burma*, Borntraeger, Stuttgart.
- Bertrand, G., et al. (2001), Diachronous cooling along the Mogok Metamorphic Belt (Shan scarp, Myanmar): the trace of the northward migration of the Indian syntaxis, *J. Asian Earth Sci.*, **19**, 649-659.
- Bertrand, G., et al. (1999), Cenozoic metamorphism along the Shan scarp (Myanmar): evidences for ductile shear along the Sagaing fault or the northward migration of the eastern Himalayan syntaxis? *Geophys. Res. Lett.*, **26**, 915-918.
- Bertrand, G., et al. (1998), The Singu basalts (Myanmar): new constraints for the amount of recent offset on the Sagaing Fault, *Comptes Rendus Acad. Sci. Ser II-A*, **327**, 479-484.
- Bilham, R., et al. (1997), GPS measurements of present-day convergence across the Nepal Himalaya, *Nature*, **386**, 61-64.
- Blewitt, G., et al. (1988), {GPS} geodesy with centimeter accuracy, in *Lecture Notes in Earth Sciences*, edited by E. G. a. R. Strauss, Springer-Verlag, New York.
- Bock, Y., et al. (2003), Crustal motion in Indonesia from Global Positioning System measurements, *Journal of Geophysical Research-Solid Earth*, **108**, 2367.
- Burg, J. P., et al. (1998), The Namche Barwa syntaxis: evidence for exhumation related to compressional crustal folding, *J. Asian Earth Sci.*, **16**, 239 -252.
- Calais, E., et al. (2003), GPS measurements of crustal deformation in the Baikal-Mongolia area (1994-2002): Implications for current kinematics of Asia, *Journal of Geophysical Research-Solid Earth*, **108**.
- Cattin, R., and J. P. Avouac (2000), Modeling mountain building and the seismic cycle in the Himalaya of Nepal, *Journal of Geophysical Research-Solid Earth*, **105**, 13389-13407.
- Chamot-Rooke, N., et al. (1993), Intraplate shortening in the central Indian Ocean determined from a 2100-km-long north-south deep seismic reflection profile, *Geology*, **21**, 1043-1046.
- Chamot-Rooke, N., and X. Le Pichon (1999), GPS determined eastward Sundaland motion with respect to Eurasia confirmed by earthquakes slip vectors at Sunda and Philippine trenches, *Earth Planet. Sci. Lett.*, **173**, 439-455.
- Curry, J. R. (1989), The Sunda Arc - a Model for Oblique Plate Convergence, *Netherlands Journal of Sea Research*, **24**, 131-140.
- Curry, J. R. (2005), Tectonics and history of the Andaman Sea region, *Journal of Asian Earth Sciences*, **25**, 187-232.
- Dasgupta, S., et al. (2003), The geometry of the Burmese-Andaman subducting lithosphere, *Journal of seismology*, **7**, 155 -174.

- de Groot-Hedlin, C. D. (2005), Estimation of the rupture length and velocity of the Great Sumatra earthquake of Dec 26, 2004 using hydroacoustic signals, *Geophys. Res. Lett.*, 32, L11303.
- DeMets, C., et al. (1990), Current plate motions, *Geophysical Journal International*, 101, 425-478.
- DeMets, C., et al. (1994), Effect of recent revisions to the geomagnetic reversal time scale on estimates of current plate motions, *Geophys. Res. Lett.*, 21, 2191-2194.
- DeMets, C., et al. (2005), Motion between the Indian, Capricorn and Somalian plates since 20Ma: implications for the timing and magnitude of distributed lithospheric deformation in the equatorial Indian ocean, *Geophysical Journal international*, 161, 445-468.
- Deplus, C. (2001), Plate tectonics - Indian ocean actively deforms, *Science*, 292, 1850-1851.
- Deplus, C., et al. (1998), Direct evidence of active deformation in the eastern Indian oceanic plate, *Geology*, 26, 131-134.
- Fitch, T. J. (1972), Plate Convergence, Transcurrent Faults, and Internal Deformation Adjacent to Southeast Asia and Western Pacific, *Journal of Geophysical Research*, 77, 4432-&.
- Genrich, J. F., et al. (2000), Distribution of slip at the northern Sumatran fault system, *Journal of Geophysical Research-Solid Earth*, 105, 28327-28341.
- Gordon, R., et al. (1990), Kinematic constraints on distributed lithospheric deformation in the equatorial Indian Ocean from present motion between the Australian and Indian plates, *Tectonics*, 9, 409-422.
- Govind, R., et al. (1999), Combination of high precision space geodetic techniques: The Asia and Pacific Regional Geodetic Project 1997, in *Satellite Dynamics, Orbit Analysis and Combination of Space Techniques*, edited, pp. 797-807.
- Guzman-Speziale, M., and J. F. Ni (1993), The Opening of the Andaman Sea - Where Is the Short-Term Displacement Being Taken Up, *Geophys. Res. Lett.*, 20, 2949-2952.
- Guzman-Speziale, M., and J. F. Ni (1996), Seismicity and active tectonics of the western Sunda Arc, in *The tectonic evolution of Asia*, edited by A.Y.H., pp. 63-84.
- Hall, R. (2002), Cenozoic geological and plate tectonic evolution of SE Asia and the SW Pacific: computer-based reconstructions, model and animations, *J. Asian Earth Sci.*, 20, 353-431.
- Hamilton, W. B. (1972), Plate Tectonics of Southeast Asia and Indonesia, *American Association of Petroleum Geologists Bulletin*, 56, 621-&.
- Herring, T. A. (1999), Documentation for the GLOBK software version 5.01, Mass. Inst. of Technol., Cambridge.
- Hla Maung (1987), Transcurrent Movements in the Burma-Andaman Sea Region, *Geology*, 15, 911-912.
- Holt, W. E., et al. (1991), The active tectonics of the eastern Himalayan syntaxis and surrounding regions, *Journal of Geophysical Research, B, Solid Earth and Planets*, 96, 14,595-514,632.
- Ishii, M., et al. (2005), Extent, duration and speed of the 2004 Sumatra-Andaman earthquake imaged by the Hi-Net array, *Nature*, 435, 1127-1133.
- Jarrard, R. (1986), Terrane Motion by Strike-slip Faulting of Fore-arc Systems, *Geology*, 14, 780-783.
- Jouanne, F., et al. (2004), Current shortening across the Himalayas of Nepal, *Geophysical Journal International*, 157, 1-14.
- Jouanne, F., et al. (1999), Oblique convergence in the Himalayas of western Nepal deduced from preliminary results of GPS measurements, *Geophys. Res. Lett.*, 26, 1933-1936.
- Khin Zaw (1990), Geological, Petrological and Geochemical Characteristics of Granitoid Rocks in Burma: With Special Reference to the Associated W-Sn Mineralization and their Tectonic Setting, *J. Southeast Asian Earth Sci.*, 4, 293-335.
- King, R. W., and Y. Bock (1999), Documentation for the GAMIT GPS software analysis version 9.9, Mass. Inst. of Technol., Cambridge.
- Lacassin, R., et al. (1998), Hairpin river loops and slip-sense inversion on southeast Asian strike-slip faults, *Geology*, 26, 703-706.
- Larson, K. M., et al. (1999), Kinematics of the India-Eurasia collision zone from GPS measurements, *Journal of Geophysical Research-Solid Earth*, 104, 1077-1093.
- Lave, J., and J. P. Avouac (2000), Active folding of fluvial terraces across the Siwaliks Hills, Himalayas of central Nepal, *Journal of Geophysical Research-Solid Earth*, 105, 5735-5770.
- Lay, T., et al. (2005), The great Sumatra-Andaman earthquake of 26 December 2004, *Science*, 308, 1127-1133.

- Ledain, A. Y., et al. (1984), Active Faulting and Tectonics of Burma and Surrounding Regions, *Journal of Geophysical Research*, 89, 453-472.
- Lomax, A. (2005), Rapid estimation of rupture extent for large earthquakes: Application to the 2004, M9 Sumatra-Andaman mega-thrust, *Geophys. Res. Lett.*, 32, L10314.
- McCaffrey, R. (1991), Slip Vectors and Stretching of the Sumatran Fore Arc, *Geology*, 19, 881-884.
- McCaffrey, R. (1995), DEFNODE users' guide, (<http://www.rpi.edu/~mccaffr/defnode>), edited, Rensselaer Polytechnic Institute, Try, NewYork.
- McCaffrey, R. (2002), Crustal block rotations and plate coupling, in Plate Boundary Zones, AGU.
- McCaffrey, R. (2005), Block kinematics of the Pacific - North America plate boundary in the southwestern United States from inversion of GPS, seismological, and geological data, *J. Geophys. Res.*, 110.
- McCaffrey, R., et al. (2000), Strain partitioning during oblique plate convergence in northern Sumatra: Geodetic and seismologic constraints and numerical modeling, *Journal of Geophysical Research-Solid Earth*, 105, 28363-28376.
- Michel, G. W., et al. (2001), Crustal motion and block behaviour in SE-Asia from GPS measurements, *Earth Planet. Sci. Lett.*, 187, 239-244.
- Mitchell, A. H. G. (1993), Cretaceous-Cenozoic Tectonic Events in the Western Myanmar (Burma) Assam Region, *J. Geol. Soc.*, 150, 1089-1102.
- Nielsen, C., et al. (2004), From partial to full strain partitioning along the Indo-Burmese hyper-oblique subduction, *Marine Geology*, 209, 303-327.
- Okada, Y. (1985), Surface deformation due to shear and tensile faults in a half-space, *Bull. Seism. Soc. Am.*, 75, 1135-1154.
- Paul, J., et al. (2001), The motion and active deformation of India, *Geophys. Res. Lett.*, 28, 647-650.
- Peltzer, G., and F. Saucier (1996), Present-day kinematics of Asia derived from geologic fault rates, *Journal of Geophysical Research-Solid Earth*, 101, 27943-27956.
- Pivnik, D. A., et al. (1998), Polyphase deformation in a fore-arc/back-arc basin, Salin subbasin, Myanmar (Burma), *AAPG Bull.-Am. Assoc. Petr. Geol.*, 82, 1837-1856.
- Prawirodirdjo, L., et al. (1997), Geodetic observations of interseismic strain segmentation at the Sumatra subduction zone, *Geophys. Res. Lett.*, 24, 2601-2604.
- Rangin, C., et al. (1999), Cenozoic pull-apart basins in central Myanmar; the trace of the path of India along the western margin of Sundaland, paper presented at European Union of Geosciences conference; EUG 10, Strasbourg, France, March 28-April 1, 1999.
- Rao, N. P., and M. R. Kumar (1999), Evidences for cessation of Indian plate subduction in the Burmese arc region, *Geophys. Res. Lett.*, 26, 3149-3152.
- Ratschbacher, L., et al. (1996), Cenozoic deformation, rotation and stress patterns in eastern Tibet and western Sichuan, China, in *The tectonic evolution of Asia*, edited by A. Y. H., pp. 227-249.
- Royer, J. Y., and R. Gordon (1997), The motion and boundary between the Capricorn and Australian plates, *Science*, 277, 1268-1274.
- Satyabala, S. (2003), Oblique plate convergence in the Indo-Burma (Myanmar) subduction region, *Pure Appl. Geophys.*, 160, 1611 -1650.
- Simons, W. J. F., et al. (1999), Observing plate motions in Southeast Asia; geodetic results of the GEODYSSSEA Project, *Geophys. Res. Lett.*, 26, 2081-2084.
- Simons, W. J. F., et al. (submitted), A Decade of GPS Measurements in S.E. Asia: (Re)Defining Sundaland and its Boundaries, *J. Geophys. Res.*
- Simons, W. J. F., et al. (2000), Geodynamics of S.E. Asia; first results of the Sulawesi 1998 GPS campaign; IAG general assembly, *IAG general assembly*, 121, 271-277.
- Socquet, A., et al. (2002), Late Cretaceous to Eocene metamorphism of the internal zone of the Indo-Burma range (western Myanmar): geodynamic implications, *Comptes Rendus Geoscience*, 334, 573-580.
- Socquet, A., and M. Pubellier (2005), Cenozoic deformation in Western Yunnan (China-Myanmar border), *Journal of Asian Earth Sciences*, 24, 495-515.
- Tapponnier, P., and P. Molnar (1975), Major strike-slip faulting in China; its significance for Asian tectonics, *Seismological Society of America, annual meeting*, 7, 425-426.
- Tapponnier, P., and P. Molnar (1977), Rigid plastic indentation; the origin of syntaxis in the Himalayan Belt Himalaya; sciences de la terre, paper presented at Ecologie et geologie de l'Himalaya, Paris, France, Dec. 7-10, 1976.

- Vigny, C., et al. (2002), Migration of seismicity and earthquake interactions monitored by GPS in SE Asia triple junction: Sulawesi, Indonesia, *Journal of Geophysical Research-Solid Earth*, 107, art. no.-2231.
- Vigny, C., et al. (2005), GPS unveils actual impact of the mega thrust earthquake in SE Asia, *Nature*, 24, 495-515.
- Vigny, C., et al. (2003), Present day crustal deformation around Sagaing fault, Myanmar, *Journal of Geophysical Research-Solid Earth*, 108(B11), 2533.
- Walpersdorf, A., et al. (1998), GPS compared to long-term geologic motion of the north arm of Sulawesi, *Earth Planet. Sci. Lett.*, 159, 47-55.
- Walpersdorf, A., et al. (1998), Determining the Sula block kinematics in the triple junction area in Indonesia by GPS, *Geophysical Journal International*, 135, 351-361.
- Wang, E., and B. C. Burchfiel (1997), Interpretation of Cenozoic tectonics in the right-lateral accommodation zone between the Ailao Shan shear zone and the eastern Himalayan syntaxis, *International Geology Review*, 39, 191-219.
- Wang, E., et al. (1998), Late Cenozoic Xianshuihe-Xiaojiang, Red River, and Dali fault systems of southwestern Sichuan and central Yunnan, China, *Special Paper - Geological Society of America*, 327, 108.

# Electronic supplement to : India and Sunda Plates motion and deformation along their boundary in Myanmar determined by GPS

## 1. Data processing

The solution presented here is a combination of two different solutions performed independently with different softwares (GAMIT / GLOBK and GIPSY-OASIS II). The data sets are also different, having only 60% of the sites in common, and different measurements history at some sites. The main difference in processing strategies is that GAMIT explicitly forms double differences and solves for all baselines in a given network, while GIPSY uses the precise point positioning (PPP) strategy. The second important difference is the strategy used to estimate velocities. GLOBK combines all measurements to estimate positions and velocities in an unconstrained reference frame (the so called free network solution) and map them into a given reference frame (here ITRF2000) in a second stage. GIPSY estimates positions in a given reference frame (again ITRF2000) at every epoch, and velocities are then estimated by linear trend fitting of the position time series.

### 1.1. Details on the GAMIT/GLOBK processing

The solution computed using the GAMIT / GLOBK software [Herring, 1999; King, 1999] includes more than 150 stations spread over Southern Asia spanning 11 years of data processed simultaneously. The data located in SE-Asia are GEODYSSSEA (GEODYnamics of South and Southeast Asia) project (1994-1996-1998) [Michel et al., 2001], APRGP (Asia Pacific Regional Geodetic Project) (1997-1998-1999-2000) [Govind, et al., 1999], THAICA (first order network of Thailand established by the Royal Thai Survey Department) (1994-1996-2000), Myanmar campaigns performed in 1998-2000 [Vigny, et al., 2003] and Sulawesi (ENS/DEOS densification of the GEODYSSSEA network in Sulawesi, Indonesia) (1999-2000-2001-2002) campaigns [Walpersdorf et al., 1999; Simons et al., 2000; Vigny et al., 2002; Socquet et al., 2005]. Data located on the Indian plate include the West Nepal network measured in 1991-1995-1997-1998-2000 within the CIRES and IDYLHIM projects [Bilham, et al., 1997; Larson, et al., 1999; Jouanne, et al., 1999], the Kathmandu transect measured in 1998-1999-2000 by the LDG-CEA (Commissariat à

l'Energie Atomique) [Avouac, et al., 2001] and HYDE station (Hyderabad) measured by the National Geophysical Research Institute in Hyderabad (NGRI, India) and the Geodaetisches Institut der Universitaet Bonn (Germany) in 1996-1997-1998-1999-2000.. Finally, all IGS stations available in the area at the time of any of our measurements are included

Twenty-four-hour measurement sessions are reduced to daily positions. For every daily session theoretical values for phase and pseudorange observables are modelled. The model parameters such as stations coordinates, phase ambiguities and tropospheric zenith delay (one every 3 hours) are adjusted by least squares method. The observations are sampled every 30 seconds with an elevation cut-off angle of 15 degrees. We use the "LC" or "L3" Ionosphere free combination of the two-phase data and explicitly form the double differences (between every pairs of satellites and stations). During a first step the integer ambiguities are allowed to take decimal values. They are assigned to integer values in a second step, using the method developed by [Dong and Bock, 1989]. We also used IGS tables for modelling of antenna phase centre variations. Finally, we used precise orbits from the International GPS Service for Geodynamics (IGS) [Beutler, et al., 1993] that we did not re-estimate, except for the West Nepal data of 1991 where we used the orbits computed by [Larson, et al., 1997]. IGS orbits are fixed in different reference frames as time passes. This is taken into account by simply estimating the translation and rotation parameters of the reference frame at each epoch when combining the epoch solutions to estimate linear velocities at all sites. This is a standard procedure which gives similar results to the "relax" orbit kind of solutions.

One of the ways to assess the internal quality of a solution is to estimate daily repeatabilities, i.e. the scatter of the baseline measurements about their campaign average. This is done for every campaign and gives a higher bound of its noise level, provided that sufficient repetition generates significant repeatabilities. Baseline component repeatability values for each campaign are summarized in Table S1 for fixed ambiguities. Repeatabilities vary for

each campaign, depending on the quality of measurements, the quality and homogeneity in the type of antennae used, the mean length of baselines for the considered campaign (the dispersion increases with the length of the baselines essentially due to uncertainties in satellites orbits) and the number of stations processed simultaneously. Values range between 1 and 4 mm for the north component and between 3 and 8 mm for the east component, whereby more recent data generally show better repeatabilities.

The solution vectors and associated variance/covariance matrices of the independent daily solutions have been combined by GLOBK, based on a Kalman filtering approach, to obtain a multi-session free-network solution for each campaign with loose constraints on positions and velocities. Long term repeatabilities (i.e. the scatter of independent campaign determinations about their detrended average) have been performed for this solution and average values are about 1.8 mm for the north component and 2.9 mm for the east component for baselines of about 1000 km (Fig S1). Velocities are not estimated at this stage but rather after the combination with the GIPSY solution.

## 1.2. Details on GIPSY processing

The solution computed with the GIPSY-OASIS II v2.6.1 [Blewitt, *et al.*, 1988] software uses a data set spanning 1994-2002. Again, GEODYSSSEA (1994-1996-1998), THAICA (1994-1996-2000) and Sulawesi (1999-2002) campaigns have been re-processed independently from the GAMIT solution. These are the data common to the GAMIT/GLOBK solution, and represent 60% of the sites used in the final combination. Three years of the permanent Malaysian (MASS) network (1999-2000-2001), Sulawesi (1996-1997-1998) and THAICA (2001) data have been added. Also, up to 30 IGS stations world wide spread have been included in the processing to allow an accurate mapping in the ITRF.

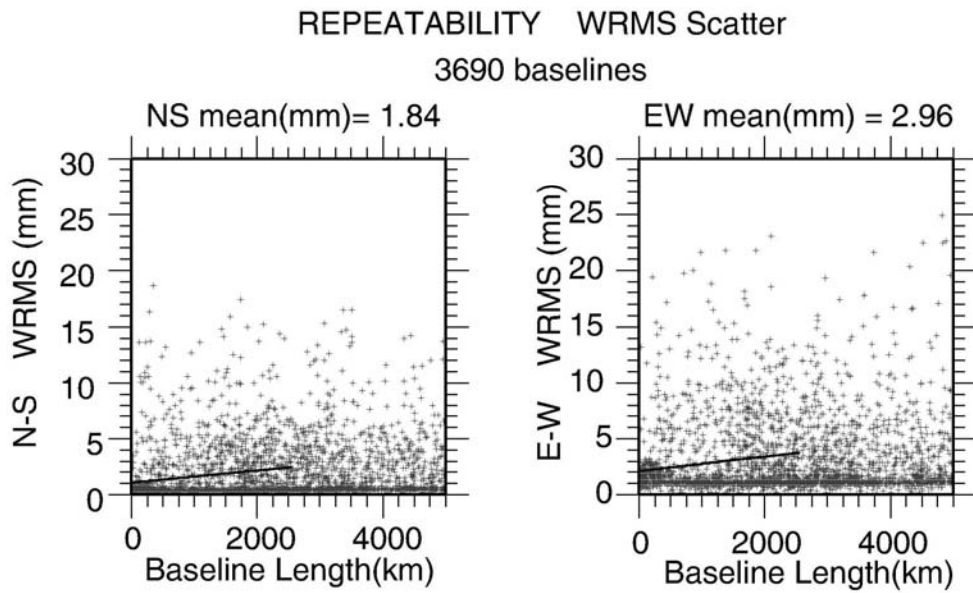
The precise point positioning (PPP) strategy has been chosen, using fixed satellite orbits and clocks distributed by JPL (Jet Propulsion Laboratory). As in the GAMIT processing, the ionosphere-free linear combination of GPS phase and pseudorange data is used, here with a sample rate of 5 minutes and an elevation cut-off angle of 15 degrees. Tropospheric delay parameters (zenith path delay and gradients) are also estimated. Ocean loading parameters are included

for each GPS location [Scherneck, 1991], and to account for the different GPS antennae, the NGS relative antenna phase centre corrections [Mader, 1998] are applied.

Each campaign solution is projected on ITRF-2000 using up to 25 IGS stations. Then, velocities are obtained by fitting a linear trend through station's position by a mean square minimization. At that stage, no adjustments of the station positions are allowed. Outliers (positions differing by more than 2mm from their estimated value) are removed from the linear trend estimation. Those can be due to measurements errors of any kind or co-seismic induced displacements for example. A detailed description on the GIPSY solution and discussion of its uncertainties are given in [Simons, *et al.*, submitted].

## 1.3. Combination

A combined solution was made from the GAMIT and GIPSY processing. It spans the entire region from India and Nepal up to the south-eastern tip of the Indonesian archipelago. This solution was generated by combining loosely constrained variance-covariance matrices from the two independent solutions with the GLOBK Kalman filter. Common sites (the regional IGS stations we use and 60% of our campaign sites) enable a strong unification of the two solutions. The final mapping in the International Terrestrial Reference Frame (ITRF) 2000 is done by minimizing (in a mean square procedure) the departure of a selected list of IGS stations positions and velocities from their a priori values in the ITRF2000 [Altamimi, *et al.*, 2002]. On these stations, the velocity misfits range between 0 and 2 mm/yr, indicating an accurate mapping in the reference frame (Table S2). A comparison of velocities determined independently (GAMIT/GLOBK vs. GIPSY) at common sites is also made (Table S3). They differ by no more than 2 mm/yr at most sites, and these differences should probably be attributed to the usage of different orbits (IGS vs. JPL) and the slightly different antenna phase centre corrections (IGS vs. NGS) that were applied. Velocities in ITRF2000 of most sites involved in the combined solution with their 1- $\sigma$  uncertainties are given in Table S4. The velocities are plotted with respect to the Sunda block on Fig. 2 in the paper.

**Figure S1:** Long term repeatabilities of the GAMIT solution.**Table S1:**  
Repeatabilities of GAMIT "campaign like" solutions

Year	Campaign	Repeatabilities (mm)		
		biases fixed		
		Nort h	East	Up
20 02	Sulawesi	4.4	7.8	16
20 01	Sulawesi	4.3	8.0	21.8
20 00	Myanmar / Hyde / East Nepal	0.8	3.1	7.3
	West Nepal	3.7	9.1	21.4
	APRGP	1.7	5.1	13.8
20 00	Global processing	2.2	5.0	11.0
19 99	Hyde	3.5	7.5	18.0
	APRGP / East Nepal	3.6	7.1	17.7
19 99	Global processing	3.8	6.4	17.0
19 98	Geodyssea / APRGP	4.1	6.9	15.9
	Myanmar / Hyde / Nepal	3.4	5.0	10.4
19 98	Global processing	4.0	6.4	14.3
19 97	Hyde / APRGP / West Nepal	3.2	5.6	13.7
19	Hyde	2.2	8.0	15.8

<b>96</b>	Geodyssea / RTSD	3.9	8.0	16.4
<b>19 96</b>	Global processing	3.8	7.9	16.3
<b>19 94</b>	RTSD	1.1	7.8	7.9
	Geodyssea	4.8	7.2	15.8
<b>19 94</b>	Global processing	3.8	6.8	15.6
<b>19 91</b>	West Nepal	5	15	30

**Table S2:**

Residual velocities of IGS stations used for mapping the combined solution with respect to the ITRF 2000.

Stations	Lat	Lon	Res N mm/yr	Res E mm/yr
<b>BAKO</b>	-6.49	106.85	-1.29	-0.90
<b>GUAM</b>	13.59	144.87	-0.77	-1.84
<b>IISC</b>	13.02	77.57	-0.11	-1.27
	-			
<b>KARR</b>	20.98	117.10	-0.74	-1.08
<b>KIT3</b>	39.13	66.89	-0.21	0.44
<b>KUNM</b>	25.03	102.80	0.67	-1.28
<b>LHAS</b>	29.66	91.10	0.74	-0.97
	-			
<b>PERT</b>	31.80	115.89	-0.39	-0.07
<b>POL2</b>	42.68	74.69	0.52	0.26
<b>SHAO</b>	31.10	121.20	0.09	0.58
	-			
<b>TIDB</b>	35.40	148.98	-0.08	-0.18
<b>TSKB</b>	36.11	140.09	1.80	0.29
<b>URUM</b>	43.81	87.60	1.66	0.97
<b>WUHN</b>	30.53	114.36	1.22	0.72
<b>XIAN</b>	34.37	109.22	-0.66	1.79
	-			
<b>YAR1</b>	29.05	115.35	-0.61	-0.43
	-			
<b>DARW</b>	12.84	131.13	-1.57	1.19

**Table S3:**

Velocity comparison for common sites between GAMIT and GIPSY solutions.

Network	# Sites	RMS	RMS	# Sites
		Diff. North mm/yr	Diff. East mm/yr	Diff. >2mm/yr
GEODYSSSEA	38	1.15	1.43	8
THAICA (Thailand)	4	1.94	0.20	2
Sulawesi (Indonesia)	10	1.62	2.33	4
<b>Total</b>	<b>69</b>	<b>1.23</b>	<b>1.46</b>	
IGS (for mapping)	9	0.68	0.89	0

**Table S4 :**Stations velocities in the ITRF 2000,  $1-\sigma$  uncertainties<sup>(\*)</sup> and residual velocities with respect to belonging plates.

	Station	Long (E)	Lat (N)	ITRF 2000 (mm/yr)				Residual <sup>†</sup> (mm/yr)	
				V <sub>E</sub>	V <sub>N</sub>	$\sigma_{VE}$	$\sigma_{VN}$	V <sub>E</sub>	V <sub>N</sub>
<b>INDIA PLATE</b>									
INDIA	IISC	77.57	13.021	40.02	33.32	0.19	0.08	-0.8	-0.76
	HYDE	78.551	17.417	41.44	34.66	0.65	0.23	1.31	0.58
	MAHE	80.148	28.963	37.17	33.59	0.81	0.31	0.17	-0.47
	NEPA	81.575	28.134	38.28	35.67	0.8	0.32	0.27	1.66
	BHAI	83.418	27.507	37.04	34.32	0.94	0.37	1.67	0.4
	SIMR	84.984	27.165	40.57	32.6	1.17	0.48	1.34	-1.22
NEPAL	SURK	81.635	28.586	33.42	36.16	1.96	0.9	4.47	2.15
	SIMI	81.826	29.967	34.49	24.57	1.88	0.91	3.01	-9.43
	RANJ	82.573	28.063	37.91	33.42	2.33	1.03	-0.4	-0.55
	TANS	83.554	27.874	38.59	33.51	2.2	0.93	0.05	-0.41
	JOMO	83.718	28.781	36.74	25.1	2	0.8	1.68	-8.81
	POKH	83.978	28.199	37.58	33.48	2.37	0.97	1.09	-0.41
	DAMA	85.108	27.608	40.87	33.52	1	0.44	1.73	-0.29
	NAGA	85.521	27.693	40.12	32.43	0.84	0.34	0.89	-1.35
	GUMB	85.877	27.91	40.33	28.01	0.93	0.43	1.06	-5.74
*	MALD	73.526	4.189	33.47	68.49	2.36	0.66	8.17	34.51
<b>SUNDA PLATE</b>									
MYANM	WETL	95.778	22.367	30.91	7.82	2.36	0.87	3.84	11.55
	BODA	96.111	22.36	28.95	0.8	3.13	1.19	5.79	4.67
	KUNT	96.317	22.324	29.63	-1.61	2.61	0.94	5.09	2.35

	THIT	95.809	22.162	29.6	11.07	2.44	1.2	5.10	14.82
	YWEN	96.535	22.06	28.78	-5.44	0.98	0.39	5.88	-1.39
	KWEH	95.286	22.049	29	12.83	0.96	0.38	5.69	16.36
*	MDPG	96.097	22.009	7.21	2.13	0.84	0.37	27.45	6.00
	LEPA	96.011	22.003	31.33	8.13	2.57	1.1	3.34	11.96
	SAYE	95.919	21.991	28.84	9.15	1.65	0.87	5.83	12.94
	YANG	96.172	21.989	28.86	1.57	2.55	0.98	5.80	5.47
	LEGY	95.757	21.986	28.12	9.76	1.8	0.9	6.55	13.49
	HTIS	95.595	21.962	31.33	11.13	1.9	0.87	3.34	14.79
	TNYO	95.981	21.934	29.21	6.3	2.99	1.14	5.44	10.12
	ZIBI	96.321	21.89	28.4	-2.76	2.2	0.9	6.23	1.20
	MYOT	95.716	21.691	30.32	10.13	2.03	0.87	4.29	13.84
	CHAU	95.919	21.672	30.2	10.46	2.44	1.08	4.40	14.25
	NYAN	96.081	21.636	32.48	8.77	3.15	1.22	2.11	12.63
	KINV	96.323	21.473	28.76	-5.99	2.13	1.17	5.79	-2.03
	MIND	93.897	21.383	34.35	20.91	1.22	0.53	0.23	23.86
	LAUN	94.537	17.692	39.97	25.62	1.48	0.69	6.26	28.84
	<b>TAUN</b>	97.094	20.75	31.06	-6.24	1.24	0.52	3.31	-1.96
	<b>HPAA</b>	97.715	16.938	33.55	-4.77	1.31	0.52	0.09	-0.23

INDOCHINA	<b>PHON</b>	102.101	21.684	35.7	-8.43	1.44	0.61	1.3	-2.09	
	<b>OTRI</b>	99.371	18.335	30.95	-3.23	0.74	0.86	-2.81	1.99	
	<b>VIEN</b>	102.516	18.026	36	-5.37	1.44	0.56	2.42	1.14	
	<b>NONN</b>	108.263	16.004	31.08	-9.17	0.74	0.27	-1.79	-0.36	
	<b>UTHA</b>	100.013	15.384	31.55	-4.17	0.4	0.18	-1.44	1.32	
	<b>SRIS</b>	104.416	14.901	33.83	10.04	0.98	0.67	1.09	-2.76	
	<b>KHON</b>	105.852	14.119	33.74	-6.36	1.51	0.56	1.26	1.5	
	<b>CHON</b>	101.045	13.121	32.34	-4.33	0.37	0.15	0	1.58	
	<b>BANH</b>	99.076	10.61	33.02	-2.53	1.14	0.6	1.4	2.57	
	*	SIEM	103.815	13.409	35.42	13.41	2.4	0.86	3.07	-6.37
	*	PENH	104.918	11.574	16.17	15.03	2.9	0.95	15.62	-7.55
	*	QT04	107.087	10.353	26.03	-6.63	2.15	0.7	-5.33	1.72
		BENG	102.252	-3.786	26.04	14.34	0.65	0.2	-0.09	20.75
		TEDA	97.82	0.571	27.99	29	0.68	0.22	0.02	33.58
MALAYSIA	<b>PHUK</b>	98.304	7.759	32.49	-1.83	0.36	0.14	1.81	2.95	
	<b>ARAU</b>	100.28	6.45	31.83	-4.81	0.42	0.27	1.63	0.79	
	<b>IPOH</b>	101.126	4.588	31.14	-6.62	0.47	0.27	1.62	-0.67	
	<b>KTPK</b>	101.718	3.171	30.21	-7.08	0.36	0.2	1.22	-0.89	
	<b>GETI</b>	102.105	6.226	31.76	-6.76	0.38	0.24	1.66	-0.41	
	<b>DOP4</b>	102.321	6.039	33.22	-8.91	1.7	0.55	3.18	-2.48	
	<b>SEGA</b>	102.732	2.486	29.3	-4.12	1.25	0.68	0.58	2.48	
	<b>KUAL</b>	103.139	5.319	31.05	-7.01	0.22	0.09	1.28	-0.24	
	<b>KUAN</b>	103.35	3.834	30.71	-5.38	0.37	0.17	1.49	1.47	
	<b>UTMJ</b>	103.64	1.566	29.22	-9.94	0.45	0.23	0.86	-2.97	
	<b>NTUS</b>	103.68	1.346	29.45	-8.39	0.33	0.13	1.18	-1.4	
	<b>TANJ</b>	106.176	-1.881	27.25	-8.07	0.67	0.2	0.28	-0.08	
	<b>MEDA</b>	98.638	3.555	32.71	-0.15	0.28	0.1	3.56	4.77	
	<b>SAMP</b>	98.715	3.622	32.64	-0.22	0.28	0.1	3.46	4.73	
	*	USMP	100.304	5.358	37.28	-9	0.56	0.34	7.47	-3.39
	*	DOP5	100.385	6.14	35.17	-3.81	1.68	0.57	5.08	1.83
	*	DOP1	101.446	3.025	24.02	2.08	1.71	0.52	-4.91	8.16
	*	DOP3	102.622	3.464	34.6	2.37	1.72	0.53	5.51	8.93

	*	DOP2	103.608	1.377	30.49	10.55	1.7	0.51	2.21	-3.59
	*	CCBS	103.959	1.342	48.48	3.1	1.96	0.61	20.21	10.2
BORNEO		<b>TABA</b>	108.891	0.863	29.71	10.13	0.89	0.22	1.64	-1.07
		<b>KUCH</b>	110.195	1.632	26.49	11.25	0.92	0.37	-1.87	-1.68
		<b>BINT</b>	113.067	3.262	27.54	11.67	0.56	0.2	-1.39	-1
		<b>MIRI</b>	114.002	4.372	26.17	10.56	0.56	0.22	-3.13	0.46
		<b>BATU</b>	114.791	-3.867	26.48	-9.6	0.68	0.21	0.25	1.72
		<b>BRUN</b>	115.031	4.966	26.43	11.76	0.44	0.15	-3.05	-0.35
		<b>LABU</b>	115.245	5.283	26.4	-11.8	0.44	0.15	-3.18	-0.31
		<b>KINA</b>	116.039	5.905	25.41	-10.8	0.53	0.19	-4.35	0.98
		<b>D005</b>	116.486	6.394	26.15	-9.84	1.92	0.59	-3.76	2.11
		<b>PUER</b>	118.851	10.086	33.43	15.23	0.75	0.23	2.53	-2.43
	*	T030	110.219	1.586	18.33	-9.19	4.1	1.1	10.01	0.39
	*	SIBU	111.843	2.27	16.94	-9.47	2.42	0.93	11.64	0.73
		<b>BLKP</b>	116.815	-1.272	23.94	14.06	0.98	0.28	-3.32	-1.99
		<b>TNJB</b>	117.641	0.558	20.2	14.39	1.58	0.5	-7.74	-2.02
		<b>MTAW</b>	117.882	4.263	22.76	17.07	0.35	0.11	-6.44	-4.62
		<b>TAWA</b>	117.979	4.251	22.74	17.09	0.35	0.11	-6.46	-4.6
		<b>SAND</b>	118.121	5.842	27.72	18.01	0.7	0.26	-1.98	-5.47
JAV		<b>ZAMB</b>	122.073	6.973	18.1	11.53	0.77	0.24	11.83	2.41
		<b>BAKO</b>	106.849	-6.491	22.73	-8.88	0.21	0.07	-2.26	-0.63
		<b>BUTU</b>	110.208	-7.635	30.8	-7.37	0.82	0.23	6.26	2.2
		<b>BALI</b>	114.68	-8.147	27.49	10.94	0.61	0.2	3.07	0.34

SOUTH CHINA	CC06	125.445	43.791	29.6	11.44	1.37	0.67	-3.52	3.64
	TSKB	140.087	36.106	-4.53	-8.53	0.18	0.1	35.48	10.84
	XIAN	109.221	34.369	33.41	15.88	0.58	0.41	-2.12	-6.69
	SHAO	121.2	31.1	31.94	14.29	0.19	0.1	-2.13	-0.66
	WUHN	114.357	30.532	33.22	13.72	0.15	0.09	-1.58	-2.56
	KUNM	102.797	25.03	30.29	19.76	0.36	0.21	-4.69	13.13
	TAIW	121.537	25.021	38.67	19.72	1.22	0.44	5.12	-5.97
	CAMP	107.313	20.999	35	10.28	0.68	0.28	0.98	-1.84
	*	QT02	106.791	20.696	32.53	16.37	2.02	0.8	-1.46

Stations are grouped by regions. Sites names in bold were used to calculate rotation parameters for India and Sunda Plates.

\* Stations rejected from the solution.

<sup>1</sup> Residual velocities are relative to the respective plate.

(\*) It is notorious that GPS positions determination are affected by biases which are not modelled in the processing (seasonal variations, tribach offsets, mismounting of antennas, monuments erratic motion, etc...). It is possible to accurately quantify and analyse these biases with permanent stations providing continuous and long time series. Then a proper model of noise can be adjusted to the data. And then an accurate uncertainty can be inferred. For obvious reasons, it is much more difficult to do with campaign data, especially when only 2 or 3 campaigns determine the velocity.

However, stochastic noise on the campaign positions, by the mean of a random walk process (known as Markov process to the GLOBK users) can be applied to the sites. Using a value of 2 mm/sqrt(yr) (which gives a maximum of 6mm for two positions 10 years apart) leads to a realistic estimation of their velocity uncertainty, but also loosen the definition of the reference frame and the tie between regional and local stations measured not simultaneously (there's no free lunch). Doing so, we obtain a solution in which our local and regional stations exhibit velocity uncertainties typically around 1 mm/yr (1 sigma). The velocities themselves don't change by more than 1-2 mm/yr, which is within this range of uncertainty, depending on one's preference for 1, 2 or 3-sigma level. Even more important, these slight changes are randomly distributed and don't affect much the pole determinations.

## References:

- Altamimi, Z., et al. (2002), ITRF2000: A new release of the International Terrestrial Reference frame for earth science applications, *Journal of Geophysical Research-Solid Earth*, 107, art. no.-2214.
- Avouac, J. P., et al. (2001), Seismic cycle in the Himalayas, *Comptes Rendus Acad. Sci. Ser II-A*, 333, 513-529.
- Beutler, G., et al. (1993), Combining the orbits of IGS processing centers, in *Proceedings of IGS analysis center workshop*, edited by K. J., pp. 20-56.
- Bilham, R., et al. (1997), GPS measurements of present-day convergence across the Nepal Himalaya, *Nature*, 386, 61-64.
- Blewitt, G., et al. (1988), {GPS} geodesy with centimeter accuracy, in *Lecture Notes in Earth Sciences*, edited by E. G. a. R. Strauss, Springer-Verlag, New York.
- Chamot-Rooke, N., and X. Le Pichon (1999), GPS determined eastward Sundaland motion with respect to Eurasia confirmed by earthquakes slip vectors at Sunda and Philippine trenches, *Earth Planet. Sci. Lett.*, 173, 439-455.
- Dong, D. N., and Y. Bock (1989), Global Positioning System Network Analysis With Phase Ambiguity Resolution Applied to Crustal Deformation Studies in California, *Journal of Geophysical Research-Solid Earth and Planets*, 94, 3949-3966.
- Govind, R., et al. (1999), Combination of high precision space geodetic techniques: The Asia and Pacific Regional Geodetic Project 1997, in *Satellite Dynamics, Orbit Analysis and Combination of Space Techniques*, edited, pp. 797-807.
- Herring, T. A. (1999), *Documentation for the GLOBK software version 5.01*, Mass. Inst. of Technol., Cambridge.
- Jouanne, F., et al. (1999), Oblique convergence in the Himalayas of western Nepal deduced from preliminary results of GPS measurements, *Geophys. Res. Lett.*, 26, 1933-1936.
- King, R. W., and Y. Bock (1999), *Documentation for the GAMIT GPS software analysis version 9.9*, Mass. Inst. of Technol., Cambridge.
- Larson, K. M., et al. (1999), Kinematics of the India-Eurasia collision zone from GPS measurements, *Journal of Geophysical Research-Solid Earth*, 104, 1077-1093.
- Larson, K. M., et al. (1997), Global plate velocities from the Global Positioning System, *Journal of Geophysical Research-Solid Earth*, 102, 9961-9981.
- Mader, G. L. (1998), GPS Antenna Calibration at the National Geodetic Survey, Technical report available at NGS website, National Geodetic Survey, Silver Spring, US.
- Michel, G. W., et al. (2001), Crustal motion and block behaviour in SE-Asia from GPS measurements, *Earth Planet. Sci. Lett.*, 187, 239-244.
- Scherneck, H.-G. (1991), A parametrized solid Earth tide mode and ocean loading effects for global geodetic base-line measurements, *Geophysical Journal International*, 106, 677-694.
- Simons, W. J. F., et al. (1999), Observing plate motions in Southeast Asia; geodetic results of the GEODYSSSEA Project, *Geophys. Res. Lett.*, 26, 2081-2084.
- Simons, W. J. F., et al. (submitted), A Decade of GPS Measurements in S.E. Asia: (Re)Defining Sundaland and its Boundaries, *J. Geophys. Res.*
- Simons, W. J. F., et al. (2000), Geodynamics of S.E. Asia; first results of the Sulawesi 1998 GPS campaign; IAG general assembly, *IAG general assembly*, 121, 271-277.

- Socquet, A., et al. (2005), Micro block rotations and fault coupling in SE Asia triple junction (Sulawesi, Indonesia) from GPS and Earthquake Slip Vector data, *Journal of Geophysical Research-Solid Earth, submitted.*
- Vigny, C., et al. (2002), Migration of seismicity and earthquake interactions monitored by GPS in SE Asia triple junction: Sulawesi, Indonesia, *Journal of Geophysical Research-Solid Earth, 107*, art. no.-2231.
- Vigny, C., et al. (2003), Present day crustal deformation around Sagaing fault, Myanmar, *Journal of Geophysical Research-Solid Earth, 108(B11)*, 2533.
- Walpersdorf, A., et al. (1998), GPS compared to long-term geologic motion of the north arm of Sulawesi, *Earth Planet. Sci. Lett., 159*, 47-55.
- Walpersdorf, A., et al. (1998), Determining the Sula block kinematics in the triple junction area in Indonesia by GPS, *Geophysical Journal International, 135*, 351-361.

## ARTICLES

# Insight into the 2004 Sumatra-Andaman earthquake from GPS measurements in southeast Asia

C. Vigny<sup>1</sup>, W. J. F. Simons<sup>2</sup>, S. Abu<sup>3</sup>, Ronnachai Bamphenyu<sup>4</sup>, Chalermchon Satirapod<sup>5</sup>, Nithiwatthn Choosakul<sup>6</sup>, C. Subarya<sup>7</sup>, A. Socquet<sup>2</sup>†, K. Omar<sup>8</sup>, H. Z. Abidin<sup>9</sup> & B. A. C. Ambrosius<sup>2</sup>

Data collected at ~60 Global Positioning System (GPS) sites in southeast Asia show the crustal deformation caused by the 26 December 2004 Sumatra-Andaman earthquake at an unprecedented large scale. Small but significant co-seismic jumps are clearly detected more than 3,000 km from the earthquake epicentre. The nearest sites, still more than 400 km away, show displacements of 10 cm or more. Here we show that the rupture plane for this earthquake must have been at least 1,000 km long and that non-homogeneous slip is required to fit the large displacement gradients revealed by the GPS measurements. Our kinematic analysis of the GPS recordings indicates that the centroid of released deformation is located at least 200 km north of the seismological epicentre. It also provides evidence that the rupture propagated northward sufficiently fast for stations in northern Thailand to have reached their final positions less than 10 min after the earthquake, hence ruling out the hypothesis of a silent slow aseismic rupture.

The 26 December 2004 Sumatra-Andaman megathrust earthquake is associated with the continuing subduction process along the Sumatran trench. However, in this particular region, the subducting plate is neither entirely Australia nor entirely India. Therefore it is quite difficult to determine the exact relative motion on the subduction zone. According to the latest geodetic determination of plate tectonics in southeast Asia, the relative motion between Australia and Sundaland is  $5 \pm 0.3 \text{ cm yr}^{-1}$  oriented  $8 \pm 2^\circ\text{N}$  at the northern tip of Sumatra<sup>1,2</sup>. Relative to the Indian plate, the motion has a slightly different azimuth ( $20^\circ\text{N}$ ) and a lower velocity of  $4 \text{ cm yr}^{-1}$  (ref. 3). Previous GPS measurements in this area showed accumulation of elastic deformation in the overriding plate (Sundaland) owing to the locking of the subduction interface<sup>4</sup>. Dip angle and precise locking depths were difficult to estimate accurately, but the extent of residual deformation in the Malaysian peninsula and southern Thailand pointed towards a very large coupling zone. The 26 December 2004 earthquake corresponds to the elastic rebound of this large region. From initial seismological data and tsunami observations it was not clear whether the seismic rupture was confined to a length of ~450 km or continued 500 km to the north in either a seismic mode or in a slow (and 'silent') mode. Recent, new GPS data shared in the framework of the EU-ASEAN 'South-East Asia: Mastering Environmental Research Using Geodetic Space Techniques' (SEAMERGES) project enable us to quantify the widespread surface deformation and hence to determine the size of the rupture.

## GPS-observed co-seismic deformation

The GPS observations used in this study provide a data set that is unique because it provides dense coverage of the surface displacements at intermediate and large scale. Publicly available GPS data in

this region (from the International GPS Service) are limited to only 3 stations at large distances from the earthquake. Our (SEAMERGES) GPS network comprises 49 continuously operating stations in Indonesia (6), Malaysia (38) and Thailand (5). In addition, data from 7 campaign sites in Thailand, observed in October 2004 and in February 2005, are incorporated in the analysis. Furthermore, the network is extended with 9 regional and 21 global stations of the International GPS Service (IGS). The combined co-seismic displacement field is presented in Fig. 1 (and Supplementary Table 1). Only stations located more than 4,000 km away from the epicentre (for example, KIT3 in Uzbekistan and KARR in Australia) are unaffected by the earthquake. Small, but significant, co-seismic jumps between 5 and 10 mm are detected even at stations more than 3,000 km away from the earthquake epicentre—for example, in southern China (Kunming), continental India (Bangalore, Hyderabad) and eastern Malaysia (Sabah). Even stations at Diego Garcia island in the Indian Ocean and in the Philippines were displaced by more than 5 mm. The nearest sites, more than 400 km away from the epicentre, show very large co-seismic displacements: 27 cm in Phuket, Thailand, 17 cm on Langkawi island, Malaysia, and 15 cm in Sampali, Indonesia.

Overall, the deformation field points inward towards the earthquake epicentre. East–west-trending displacements at mid-latitudes (between  $0^\circ$  and  $15^\circ$ ), north–south-trending displacements at higher latitudes (below  $0^\circ$  or above  $15^\circ$ ), and absence of significant displacements north (LHAS) and south (BAKO) of the rupture are due to a thrust focal mechanism, aligned with the Sumatran trench west of the west coast of Sumatra. Large displacements in northern Thailand (8 cm in Bangkok and almost 3 cm in Chiang Mai) imply a rupture extending far north into the Andaman Sea, in agreement with the distribution of aftershocks. On the other hand, the very strong increase of displacements detected along the Malaysian

<sup>1</sup>Laboratoire de Géologie, ENS/CNRS, 75231 Paris, France. <sup>2</sup>DEOS, Delft University of Technology, 2629 HS Delft, The Netherlands. <sup>3</sup>Department of Survey and Mapping Malaysia (DSMM), 50578 Kuala Lumpur, Malaysia. <sup>4</sup>Royal Thai Survey Department (RTSD), Bangkok 10200, Thailand. <sup>5</sup>Department of Survey Engineering, Chulalongkorn University, Bangkok 10330, Thailand. <sup>6</sup>Department of Geology, Chulalongkorn University, Bangkok 10330, Thailand. <sup>7</sup>National Coordination Agency for Surveys and Mapping (BAKOSURTANAL), Cibinong 16911, Indonesia. <sup>8</sup>University of Technology Malaysia (UTM), 81310 Johor, Malaysia. <sup>9</sup>Institute of Technology Bandung (ITB), Bandung 40132, Indonesia. <sup>†</sup>Present address: ESS Department, University of California Los Angeles (UCLA), 90095-1567 California, USA.

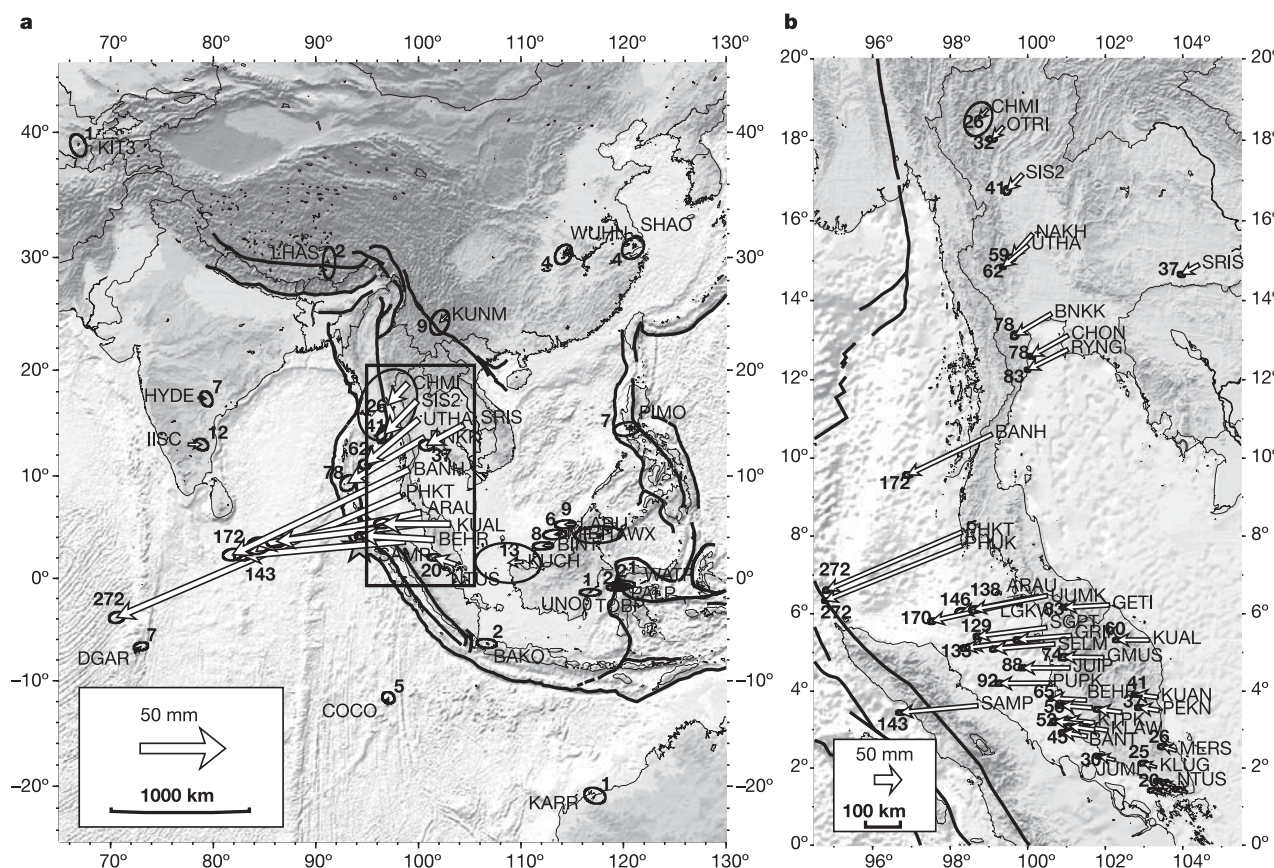


**Figure 1 | Co-seismic displacement field derived from GPS observations at more than 60 sites.** Panel a shows a large scale overview from a low-density subset. Panel b provides more detail, zooming in on a smaller area (rectangular box in a). Note the high-density sub-network on the Malaysian peninsula. Bold numbers next to arrow heads give the displacement in mm.

Ellipses depict the 90% confidence level. Thin black lines depict major faults<sup>8</sup>. The USGS earthquake epicentre location is portrayed by the star symbol, near bottom left of box. ETOPO-5 and GTOPO-30 Digital Elevation Models were used to generate the background topography and bathymetry.

peninsula (2 cm in Singapore, 17 cm in Langkawi island) suggests a limited amount of slip on the southern section of the fault.

#### Elastic co-seismic modelling

Observed surface displacements are modelled using Okada's formulation of a dislocation buried in an infinite elastic half-space<sup>5</sup>. A first model (model A) was constructed using the USGS<sup>6</sup> and CMT<sup>7</sup> parameters: localization, depth, focal mechanism and magnitude.

To match these parameters, we assume a rectangular dislocation plane of 450 km length and 145 km width, dipping with an angle of 8° and emerging at the surface roughly along the trench. Assuming a rigidity coefficient of  $4 \times 10^{11}$  GPa, a uniform slip of 12 m perpendicular to the trench direction gives a total seismic moment of  $3 \times 10^{22}$  N m and a moment magnitude  $M_w = 9.0$ , in agreement with the CMT value. With an average misfit of 27 mm this model matches well the observed deformation in northern Sumatra

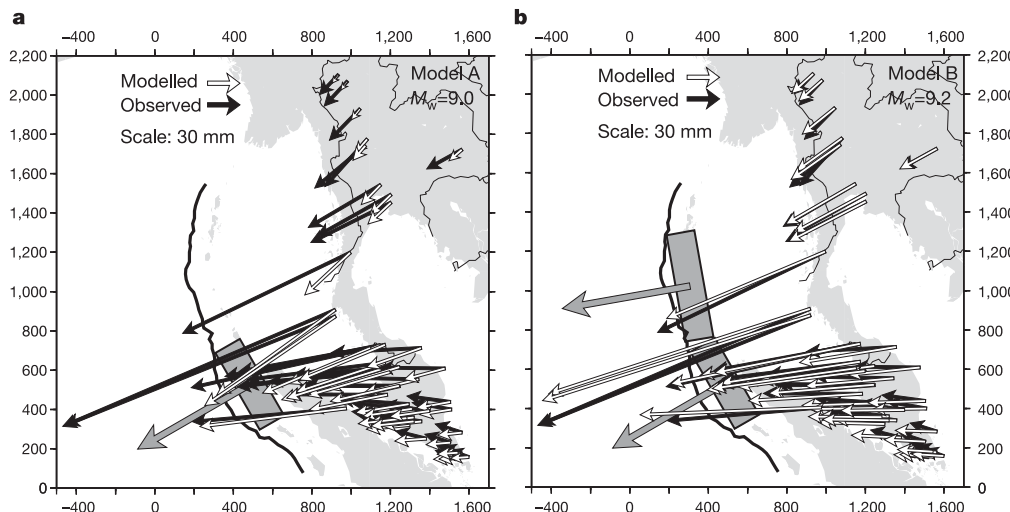


**Figure 2 | Elastic modelling of co-seismic deformation.** GPS results (black arrows) and model predictions (white arrows) are shown. Grey rectangles depict models for rupture planes buried at depth (see text for details). Grey arrows show the modelled direction and amount of slip. Model A (panel a) uses a 450-km-long rupture and model B (panel b) uses a 1,000-km-long rupture, curved along the trench in two segments. x and y axes show distance (km) in a UTM (Universal Transverse Mercator) projection.

(SAMP) and the Malaysian peninsula, but fails to predict the large deformation observed in the northern part of the network (Fig. 2). Only half of the observed deformation (15 cm instead of 27 cm) is predicted at Phuket island (PHKT). Only one-third of the observed deformation (3 cm instead of 8 cm) is predicted at Bangkok (BNKK). Finally, insignificant displacements are predicted further north in China and further west in continental India, which is in contradiction with the observations. Therefore, we can conclude that a much longer rupture must be considered.

A second model (not shown) was then constructed by simply prolonging the rupture plane further north to a total length of 1,000 km. All other parameters were kept identical to those of model A. Although this simple model fails to predict the details of the observed deformation field (in particular, the directions in continental Malaysia), it matches better the observed far-field deformation, both in amplitude and direction, with an average misfit reduced to 12 mm. The corresponding seismic moment is increased to  $7 \times 10^{22}$  N m and the magnitude to  $M_w = 9.2$ . However, it is very clear that such a rupture plane does not follow the trench direction in this area. The trench is curved to an almost north–south azimuth above a latitude of 5° N. Therefore, we constructed a third model (model B) by simply cutting the previous plane into two planes: the southernmost one with a length of 450 km and the original strike of 330°, and the second one with a length of 550 km and striking 350°. The total length and the slip being identical to those of the previous model, the seismic moment and the magnitude remained unchanged. The better alignment with the trench leads to a better

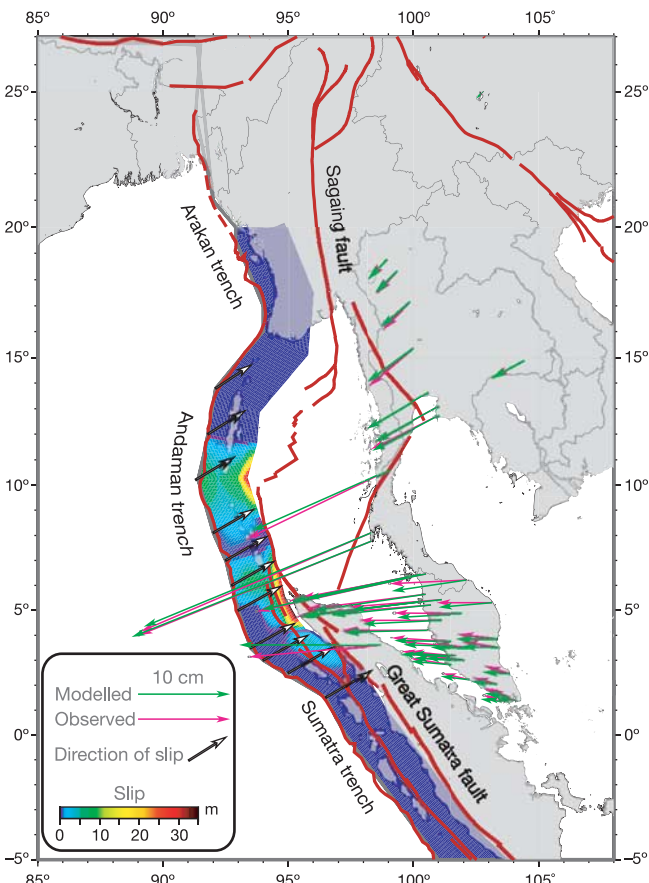


**Figure 3 | Best-fit elastic model of the co-seismic displacements using non-homogeneous slip along the rupture plane.** Colour code indicates the amount of slip from 0 (dark blue) to 35 m (dark red). Note that the area with significant slip is approximately 1,100 km long. Measured displacements (purple vectors) and modelled deformation (green vectors) are also depicted. Thin red lines depict major faults<sup>8</sup>.

fit with the observed deformation (the average misfit is now reduced to 10 mm), mostly in the predicted deformation direction, as expected (Fig. 2). This is true in particular in the central part of the network, in northern Malaysia and Thailand. As good as it is, this model still predicts too much deformation in the southern part of the Malaysian peninsula. Here, the observed displacements are consistently smaller (by 1 cm on average) than the predicted ones and point more to the north. Reduction of predicted deformation in south Malaysia can only be achieved by reducing the amount of slip on the southern part of the rupture. In fact, a fourth model (not shown)—in which we impose a reduced slip of only 3 m on the first half of the southern plane, balanced by an increased slip on the second half—yields an even better fit, with an average misfit reduced to 8 mm.

In order to investigate the effect of non-homogeneous slip on the fault, we construct a model with a grid of multiple nodes on which we invert the amount of slip, keeping its direction fixed. The surface fault geometry follows the mapping of ref. 8, the dip angle is fixed to 13° according to USGS determination<sup>6</sup>, and the maximum depth is 50 km. All models providing a good fit require a very small amount of slip on the southernmost part of the rupture (which starts around Simelue island, Indonesia), a very localized patch of very large slip (>20 m) in front of Phuket, Thailand, and a third patch of slip more spread out further north. All models also require that slip stops

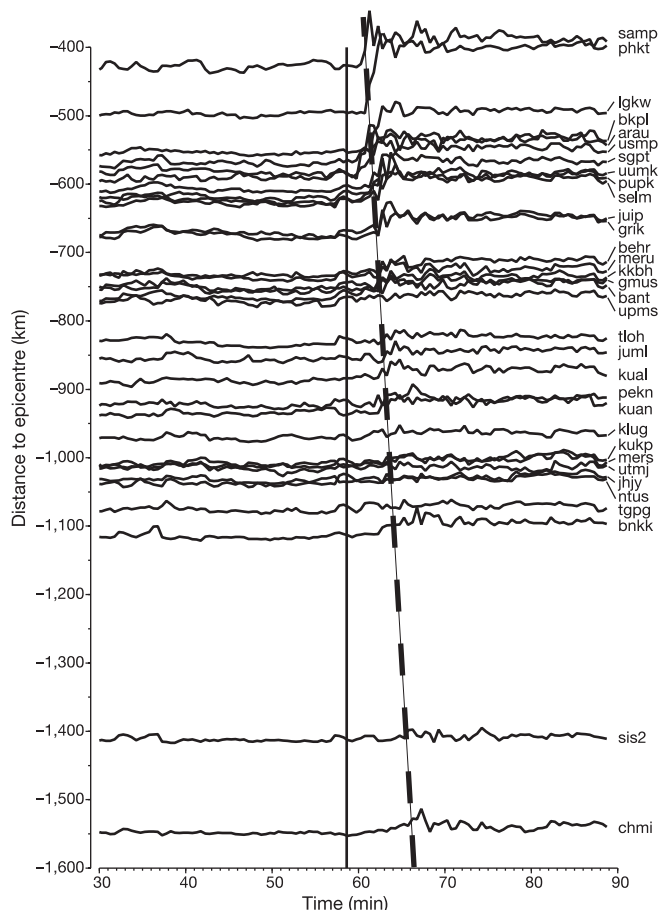


**Figure 4 | Kinematic solution of the co-seismic displacements for 33 continuous GPS stations in southeast Asia.** Each curve shows the variation in the horizontal position of a given station during 1 h around the time of the earthquake (1 point every 30 s). Curves are sorted by distance to the earthquake epicentre, from 450 km for station SAMP (Medan, northern Sumatra, top) to 1,500 km for station CHMI (Chiang Mai, Thailand, bottom). The vertical full line indicates the time of the earthquake (0 h 59 min) and the second, oblique, dashed line indicates the expected surface wave arrival time assuming a group velocity of 3.6 km s<sup>-1</sup>.

around  $13^{\circ}$ – $14^{\circ}$  latitude, which matches very well the end of the aftershock area<sup>6</sup> and the crucial changes in the bathymetry of the trench in the area<sup>9</sup>. Also, the patch with hardly any slip between  $7^{\circ}$  and  $8^{\circ}$  is a feature that persists throughout all our inversions. The best fitting model (Fig. 3) provides a normalized  $\chi^2$  of 2.2 and an average misfit of 4 mm. It requires slip to be moderate near the surface and maximum at the bottom of the fault, possibly like the 1881 Nicobar earthquake<sup>10</sup>. Imposing more slip at the surface degrades the fit ( $\chi^2$  is increased by 50%), but is still in the range of very plausible solutions: total average misfit is 6 mm. Far-field observed displacements are also matched by our best-fit elastic model. We compute 11 mm (instead of 9 mm) at Kunming, 8 mm at Manila (instead of 7 mm), 13 mm at Bangalore (instead of 12 mm) and 7 mm (as observed) at Hyderabad. Finally, the model predicts displacements of the order of magnitude of 2–5 m near the fault itself, on the Andaman and Nicobar islands. These values will have to be matched with precise GPS surveys conducted there by Indian institutes.

There is a clear trade-off between the maximum slip and the width of the fault or the depth of the fault on which slip is distributed. Obviously, our deformation field lacks the sensitivity of near-field data to fully resolve this issue. Another limitation of our inversion is the assumed constant azimuth of the slip along the rupture plane. Although this azimuth is a reasonable average, there is a slight misalignment with the aftershocks' slip vector direction at the northern termination of the rupture. Finally, the contrast in elastic parameters east of the trench between continental crust in the south and oceanic lithosphere in the north must probably be taken into account. However, the heterogeneity and localization of slip on the southern half of the rupture is in very good agreement with independent determinations from the inversion of short-period seismic body waves (<http://iisee.kenken.go.jp/staff/yagi/eq/Sumatra2004/Sumatra2004.html>). The corresponding seismic moment and magnitude that we compute depends on the assumed rigidity coefficient. Obviously, the GPS data we present here constrain well the length of the rupture, give some insight on the slip  $\times$  fault width product, but give no information at all on the rigidity. However, our magnitude of 9.2 matches well the determination of 9.3 inferred using the longest-period normal mode of the Earth over a longer time period than CMT determination<sup>11</sup>, even if this latter determination has been slightly overestimated because of the neglect of self-gravitational effects.

### Kinematic positioning

Although only measurements averaged over 24 h give the ultimate precision of a few millimetres that are expected from GPS, it is also possible to compute each station position on an epoch-by-epoch basis, that is, at the sampling rate of the GPS signal at each station (30 s in this case). GPS stations start to move when surface waves

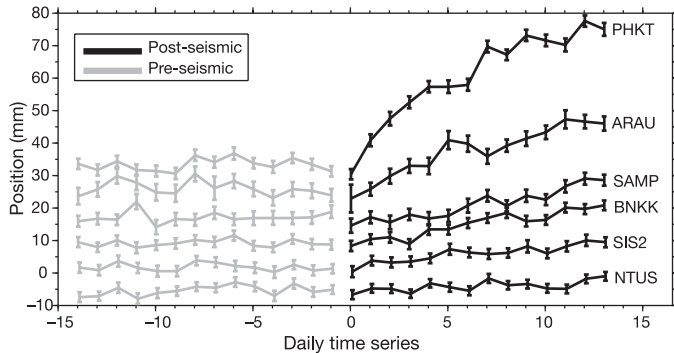


**Figure 5 | Pre- and post-seismic position variations derived from GPS observations at selected stations.** Daily solutions and  $1\sigma$  uncertainties are depicted before the earthquake (grey lines) and after the earthquake (black lines). Note the scale is in mm. Initial position is arbitrary, and co-seismic jump is removed.

emitted by the hypocentre hit their location, then within minutes they stabilize to their new position (Fig. 4). Knowing surface wave velocity, it is straightforward to predict 'arrival times' at each station and to match them to the 'jumps' in the time series. GPS records are equivalent to very-low-frequency seismograms, so that they can be used to determine the position of the centroid of deformation at the origin of the bulk of the surface wave emission. In this case, to sort arrival times, we need to move the source of the bulk of the signal almost 200 km north of the USGS-determined epicentre. This corresponds very well to the patch of high slip already determined from our co-seismic static displacements. In addition, it can be seen that stations north of the epicentre reach their final position not only later but also slower than stations in the south. Stations PHKT, SAMP or LGKW have rise times of 1 or 2 min, whereas BNKK and CHMI take up to 5 min to rise. This is due to the slow northward propagation of the rupture along the trench after the initial rupture. Phuket's initial motion (around 2 min 39 s after the earthquake time

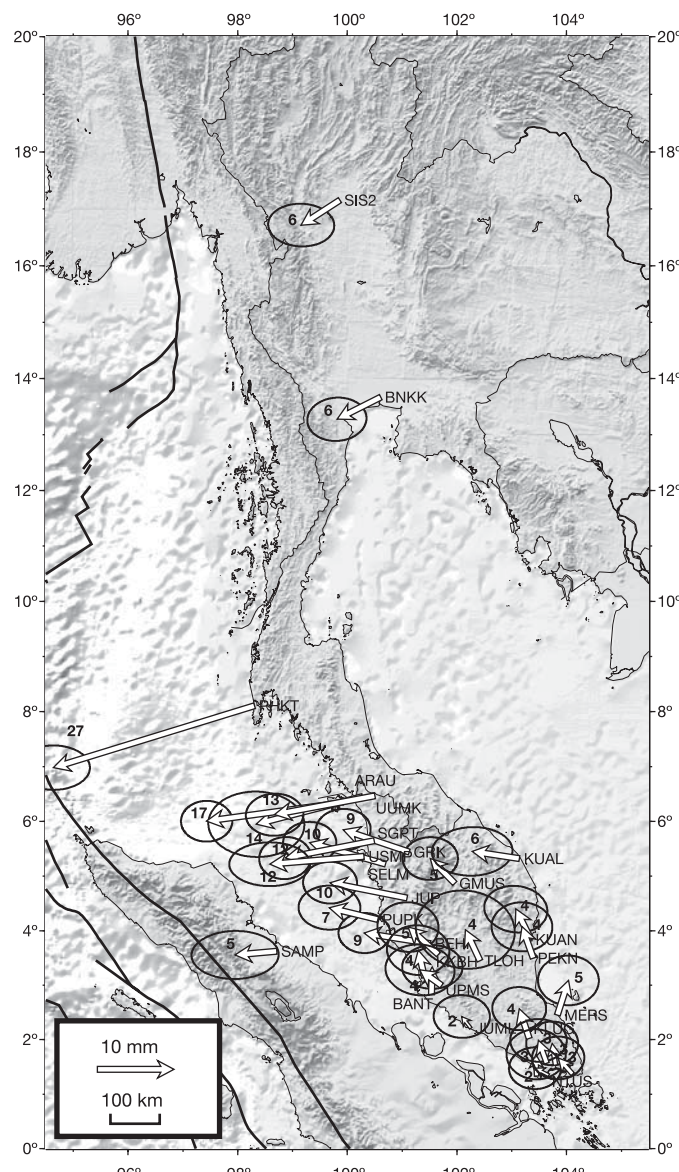


**Figure 6 | Five-day post-seismic displacement field.** Bold numbers next to arrow heads give the displacement in mm. Ellipses depict the 90% confidence level. Black lines depict major faults<sup>8</sup>. ETOPO-5 and GTOPO-30 Digital Elevation Models were used to generate the background topography and bathymetry.

tag) is towards the south-southwest, in the direction of the point where the rupture started. Three minutes later, the point stops moving and the displacement vector points towards the west-southwest, where the first rupture ended. During this elapsed time, the rupture travelled through a distance of approximately 650 km, yielding a velocity of  $3.7 \text{ km s}^{-1}$ . The second half of the rupture is slightly smaller (450 km) and is covered in around 4 min. This yields a slower rupture velocity of around  $2 \text{ km s}^{-1}$ . (A GIF animation is available; see Supplementary Information.)

Given the sampling rate of 30 s of the GPS signal, the uncertainty can be roughly estimated at  $\pm 0.5 \text{ km s}^{-1}$ . Therefore, it can be concluded that the second part of the rupture is significantly slower than the first part. Nevertheless, the fact that the northernmost stations reached their final position less than 10 min after the earthquake rules out the possibility of a completely silent aseismic rupture (that is, with a period  $>600 \text{ s}$ ).

### Post-seismic deformation

Post-seismic deformation results from a combination of different phenomena, each of which has a characteristic timescale. Deformation occurring over a period of a month represents mostly immediate after-slip, due to either aseismic slip in the poorly consolidated sediment layer overlying the fault or co-seismic slip associated with the aftershock sequences. Deformation occurring over a period of a year might be dominated by poro-elasticity, and thereafter by visco-elastic or plastic flow from low-viscosity shallow earth layers. An increasing amount of evidence indicates that after-slip follows the majority of earthquakes, particularly in subduction zones<sup>12–14</sup>. Here also, post-seismic motions started right after the co-seismic elastic displacements (Fig. 5). Additional displacements of up to 4 cm over a 15 d period after the earthquake are detected at the nearest station (PHKT). Here, the apparent logarithmic decay suggests aseismic slip in a shallow layer rather than cumulated aftershock-induced slip which should follow the well known hyperbolic trend (Omori's law)<sup>15</sup>. The pattern of after-slip cumulated 5 d after the earthquake is also more probably due to aseismic slip (Fig. 6 and Supplementary Table 2). After-slip is maximum at PHKT (3 cm) and in the same direction as co-seismic slip. The along-trench orientation of the observed vectors in south Malaysia is difficult to model with an elastic dislocation. However, the rest of the vectors point to the same patches of high slip that were identified in the co-seismic section. Finally, relative to co-seismic slip, after-slip seems to be proportionally more important in the northern section of the rupture than in the south.

Post-seismic motions continue, and will continue for a long period of time. Fifty days after the earthquake, the island of Phuket had already moved 34 cm, which is 1.25 times the initial co-seismic displacement.

### Seismic hazard in southeast Asia

An earthquake on the Sumatran trench was not unexpected. In the Sumatran subduction zone, convergence normal to the trench occurs at  $4\text{--}5 \text{ cm yr}^{-1}$ . Even near its boundaries, internal deformation of the Sundaland plate is generally small ( $<3 \text{ mm yr}^{-1}$ )<sup>16</sup>. North Sumatra was a notable exception, as both local and regional GPS networks there detected significant deformation hundreds of kilometres away from the trench<sup>2,16</sup>. This deformation was interpreted as accumulation of elastic deformation over a wide area, indicating 'high coupling' with subduction. This is in contrast with south Sumatra (south of Enggano island, approximately  $3^\circ \text{ S}$ ) and Java, where inter-seismic deformation is less intense, which is probably related to the variable dip angle and changing obliquity of the subduction. However, because it ruptured only a segment of the subduction zone, the earthquake increased stress on adjacent segments, further south on the Sumatran trench<sup>17</sup>, but also further north on the Arakan trench in Myanmar. The  $M_w 8.7$ , 28 March earthquake is a first consequence of that. In addition, strain favouring future rupture has probably been

added on the strike-slip system behind the subduction: the Great Sumatran fault in Sumatra and the Sagaing fault in Myanmar. Along-strike additional strain depends on the precise orientation of the rupture: essentially zero if exactly perpendicular to the strike-slip system, it will be increased if oriented north of this azimuth, and decreased if oriented south. In all cases, normal strain will be applied to these faults, favouring unclamping and easing slip. Because historical major earthquakes on these faults have proved that they release strain in a seismic mode<sup>18,19</sup>, the probability of large earthquakes on these structures in the near future is very high.

Finally, stress transfer has been shown to potentially trigger earthquakes on surrounding faults<sup>20</sup>. This stress transfer can be instantaneous (Coulomb stress failure) or delayed in time if associated with fluid migration in the brittle crust, and this is particularly true for the unclamping effect<sup>21</sup>. Should this effect play an important role, the foreseen time delay could be of the order of magnitude of a year. Therefore, post-seismic measurements (by GPS stations installed after the earthquake) monitoring the surface deformation for the years to come will provide crucial information on the earthquake mechanism and on possible follow-on scenarios.

### METHODS

**Static positioning.** The data are processed with the GIPSY-OASIS II software, using the (optimized) Precise Point Positioning (PPP) methodology<sup>22</sup>, including ambiguity resolution for the entire network. For the continuously operating stations, this results in a set of independent daily network solutions, covering a period from 14 d before to 14 d after the earthquake. These daily solutions are subsequently combined into two campaign-like averaged solutions (before and after the earthquake). Next, the pre-earthquake solution is mapped onto the International Terrestrial Reference Frame (ITRF) 2000<sup>23</sup> using a subset of 14 well-determined IGS global reference stations with a smooth positioning history. This is done to establish an undeformed reference solution, which is not affected by episodic jumps in the time series of some of the IGS stations. The post-earthquake solution is then projected on this reference solution using only those stations that are unaffected by co-seismic motions. The co-seismic displacements of the stations in the earthquake region then simply follow from coordinate differences between the two solutions, with a relative ( $2\sigma$ ) accuracy of about 2 mm. The GPS campaign data of the 7 additional sites in Thailand are treated in a slightly different way to compensate for the larger time difference between the two campaigns (4 months) and to remove the effects of post-seismic deformation. This is done by removing the long-term rigid plate motions predicted at these locations according to the latest geodetic models<sup>16</sup> and by correcting the total displacements with an estimation of the post-seismic motions based on the results of nearby permanent stations. For the 7 additional Thailand sites a differential horizontal positioning ( $2\sigma$ ) accuracy of 6 mm is achieved.

**Kinematic positioning.** In this approach, absolute station position are computed every 30 s with the GIPSY PPP methodology by using high-rate GPS satellite clock solutions. Each point has a higher uncertainty and is affected by biases which usually cancel out over long periods of measurement. However, the co-seismic signal is clearly detectable in these data: stations within a range of 1,500 km from the earthquake epicentre show displacements up to 3 cm, which is significantly higher than the high-frequency noise of around 1 cm typically obtained in kinematic positioning.

**Elastic modelling.** Forward models (Fig. 2a, b) are computed with RNGCHN software<sup>24</sup>. The average misfit of a given model is simply the sum of the residual displacements (difference between observed and modelled displacements) at each station, divided by the number of stations.

Inverse models are computed with DEFNODE software (<http://www.rpi.edu/~mccafri/defnode>; refs 25, 26). The inversion gets the parameters that minimizes the reduced  $\chi^2$  statistic:  $\chi_n^2 = \sqrt{\sum r^2 / s^2} / \text{dof}$ , where  $r$  is the residual,  $s$  is the standard deviation and dof is the degree of freedom. Minimization is performed using the downhill simplex technique.

Received 17 March; accepted 16 June 2005.

- Michel, G. W. et al. Crustal motion and block behaviour in SE-Asia from GPS measurements. *Earth Planet. Sci. Lett.* **187**, 239–244 (2001).
- Bock, Y. et al. Crustal motion in Indonesia from GPS measurements. *J. Geophys. Res.* **108**, doi:10.1029/2001JB000324 (2003).

3. Socquet, A. et al. Indian plate motion and deformation induced along its boundary with Sunda in Myanmar determined by GPS. *J. Geophys. Res.* (submitted).
4. Prawirodirdjo, L. et al. Geodetic observations of interseismic strain segmentation at the Sumatra subduction zone. *Geophys. Res. Lett.* **24**, 2601–2604 (1997).
5. Okada, Y. Surface deformation due to shear and tensile faults in a half-space. *Bull. Seismol. Soc. Am.* **75**, 1135–1154 (1985).
6. USGS fast moment tensor solution. ([http://wwwneic.cr.usgs.gov/neis/eq\\_depot/2004/eq\\_041226/neic\\_slav\\_q.html](http://wwwneic.cr.usgs.gov/neis/eq_depot/2004/eq_041226/neic_slav_q.html)).
7. Harvard moment tensor solution. ([http://wwwneic.cr.usgs.gov/neis/eq\\_depot/2004/eq\\_041226/neic\\_slav\\_hrv.html](http://wwwneic.cr.usgs.gov/neis/eq_depot/2004/eq_041226/neic_slav_hrv.html)).
8. Pubellier, M., Ego, F., Chamot-Rooke, N. & Rangin, C. The building of pericratonic mountain ranges: structural and kinematic constraints applied to GIS-based reconstructions of SE Asia. *Bull. Soc. Geol. Fr.* **174**, 561–584 (2003).
9. Nielsen, C., Chamot-Rooke, N., Rangin, C. & the Andaman cruise team, From partial to full strain partitioning along the Indo-Burmese hyper-oblique subduction. *Mar. Geol.* **209**, 303–327 (2004).
10. Ortiz, M. & Bilham, R. Source area and rupture parameters of the 31 December Mw = 7.9 Car Nicobar earthquake estimated from tsunamis recorded in the Bay of Bengal. *J. Geophys. Res.* **108**, doi:10.1029/2002JB001941 (2003).
11. Stein, S. & Okal, E. Speed and size of the Sumatra earthquake. *Nature* **434**, 581–582 (2005).
12. Heki, K., Miyazaki, S. & Tsuji, H. Silent fault slip following an interplate thrust earthquake at the Japan Trench. *Nature* **386**, 595–597 (1997).
13. Ruegg, J. C., Olcay, M., Armijo, R., DeChabalier, J. B. & Lazo, D. Coseismic and aseismic slip observed from continuous GPS measurements for the 2001 Southern Peru Earthquake (Mw = 8.4). *Seismol. Res. Lett.* **72**, 680–685 (2001).
14. Marquez-Azua, B., DeMets, C. & Masterlark, T. Strong interseismic coupling, fault afterslip, and viscoelastic flow before and after the Oct. 9, 1995 Colima-Jalisco earthquake: Continuous GPS measurements from Colima, Mexico. *Geophys. Res. Lett.* **29**, doi:10.1029/2002GL014702 (2002).
15. Scholz, C. Earthquakes and friction laws. *Nature* **391**, 37–42 (1998).
16. Simons, W. et al. A decade of GPS measurements in SE Asia: (Re)Defining Sundaland motion and its boundaries. *J. Geophys. Res.* (submitted).
17. McCloskey, J., Nalbant, S. S. & Steacy, S. Earthquake risk from co-seismic stress. *Nature* **434**, 291 (2005).
18. Sieh, K. & Natawidjaja, D. Neotectonics of the Sumatran fault. *J. Geophys. Res.* **105**, 28295–28326 (2000).
19. LeDain, A. Y., Tapponnier, P. & Molnar, P. Active faulting and tectonics of Burma and surrounding regions. *J. Geophys. Res.* **89**, 453–472 (1984).
20. Stein, R. S. The role of stress transfer in earthquake occurrence. *Nature* **402**, 605–609 (1999).
21. Vigny, C. et al. Migration of seismicity and earthquake interactions monitored by GPS in SE Asia triple junction: Sulawesi, Indonesia. *J. Geophys. Res.* **107**, doi:10.1029/2001JB000377 (2002).
22. Zumberge, J. M., Heflin, M., Jefferson, D., Watkins, M. & Webb, F. Precise point positioning for the efficient and robust analysis of GPS data from large networks. *J. Geophys. Res.* **102**, 5005–5017 (1997).
23. Altamimi, Z., Sillard, P. & Boucher, C. ITRF 2000: A new release of the International Terrestrial Reference frame for earth science applications. *J. Geophys. Res.* **107**, doi:10.1029/2001JB000561 (2002).
24. Feigl, K. & Dupré, E. RNGCHN: A program to calculate displacement components from dislocations in an elastic half-space with applications for modelling geodetic measurements of crustal deformation. *Comput. Geosci.* **25**, 695–704 (1999).
25. McCaffrey, R. In *Plate Boundary Zones* (eds Stein, S. & Freymueller, J.) 101–122 (Geodynamics Series 30, American Geophysical Union, Washington DC, 2002).
26. McCaffrey, R. Block kinematics of the Pacific–North America plate boundary in the southwestern US from inversion of GPS, seismological, and geological data. *J. Geophys. Res.* (in the press).

**Supplementary Information** is linked to the online version of the paper at [www.nature.com/nature](http://www.nature.com/nature).

**Acknowledgements** Thanks are extended to the different national agencies (DSMM, RTSD, BAKOSURTANAL) for sharing their regional GPS data in the framework of the SEAMERGES (<http://www.deos.tudelft.nl/seamerges>) project. We also thank M. Hashizume for contributing Thai data collected by Chulalongkorn University in cooperation with the 'Frontier Observational Research System for Global Change' (FRONTIER) project and the Earthquake Research Institute at the University of Tokyo; and we thank the Dutch research programme Integrated Solid Earth Science (ISES), the French Institut National des Sciences de l'Univers (INSU-CNRS) and the French ministry of foreign affairs (MAE) for providing equipment and financial support. Our sympathy is extended to the relatives of the Phuket GPS station operator who is still reported missing after the tsunami disaster. SEAMERGES has been funded by the ASEAN-EU University Network Programme (AUNP). The contents of this paper are the sole responsibility of the authors listed and cannot be regarded as reflecting the position of the European Union.

**Author Information** Reprints and permissions information is available at [npg.nature.com/reprintsandpermissions](http://npg.nature.com/reprintsandpermissions). The authors declare no competing financial interests. Correspondence and requests for materials should be addressed to C.V. (vigny@geologie.ens.fr).

# Micro block rotations and fault coupling in SE Asia triple junction (Sulawesi, Indonesia) from GPS and Earthquake Slip Vector data

Anne Socquet<sup>1,2</sup>, Wim Simons<sup>1</sup>, Christophe Vigny<sup>3</sup>, Robert McCaffrey<sup>4</sup>, Cecep Subarya<sup>5</sup>, Dina Sarsito<sup>6</sup>, Boudeijn Ambrosius<sup>1</sup>, Wim Spakman<sup>7</sup>

**Abstract.** The island of Sulawesi, eastern Indonesia, is located within the triple junction of the Australian, Philippine and Sunda Plates and accommodates the convergence of continental fragments with the Sunda margin. We quantify the kinematics of Sulawesi by modeling GPS velocities and earthquake slip vectors as a combination of rigid block rotations and elastic deformation around faults. We find that the deformation can be reasonably described by a small number of rapidly rotating crustal blocks. Relative to the Sunda plate, the southwestern part of Sulawesi (Makassar Block) rotates anticlockwise at  $\sim 1.4^\circ/\text{Myr}$ . The northeastern part of Sulawesi, the Bangai-Sula domain, comprises 3 blocks - the central North Sula block moves toward the NNW and rotates clockwise at  $\sim 2.5^\circ/\text{Myr}$ , the northeastern Manado Block rotates clockwise at  $\sim 3^\circ/\text{Myr}$  about a nearby axis, and East Sulawesi is pinched between North-Sula and Makassar blocks. Along the boundary between the Makassar block and the Sunda plate, GPS measurements suggest that the trench accommodates  $\sim 15 \text{ mm/yr}$  of slip within the Makassar Strait with current elastic strain accumulation. The tectonic boundary between North-Sula and Manado Blocks is the Gorontalo Fault, moving right-laterally at about  $11 \text{ mm/yr}$  and accumulating elastic strain. The  $42 \text{ mm/yr}$  relative motion between North-Sula and Makassar blocks is accommodated on the Palu-Koro left-lateral strike-slip fault zone. The data also indicate a pull-apart structure in Palu area where the fault shows a transtensive motion and may have a complex geometry involving several active strands. Sulawesi provides a primary example of how collision can be accommodated by crustal block rotation instead of mountain building.

## Introduction

Relative motions between major, fast moving plates can sometimes be accommodated within a complex deforming zone that involves microblocks rotating rapidly about nearby poles (e.g., Cascadia, Marianas, Vanuatu, Papua New Guinea, New Zealand, Tonga)

[McCaffrey *et al.*, 2000; Kato *et al.*, 2003; Calmant *et al.*, 2003; Wallace *et al.*, 2004; 2005], resulting in complex plate interactions. The boundaries between these rotating microplates are often the sites of major collisional orogenies, subduction zones, rift systems, and rapidly slipping transform faults. Accurate assessment of the kinematics of these convergent plate boundary microblocks, by using Global Positioning System (GPS) techniques for example, may help us resolve long-standing questions about the forces driving microplate rotation.

Because the triple junction between the Philippine Sea, Australian, and Sunda plates in Southeast Asia is highly seismically active and is characterized by rapid rotations of small blocks revealed by both geological and kinematic studies [Fitch and Hamilton, 1974; Hamilton, 1972; Kreemer, *et al.*, 2000; Silver, *et al.*, 1983; Silver and Moore, 1978; Simons, *et al.*, 2000; Stevens, *et al.*, 1999; Vigny, *et al.*, 2002; Walpersdorf, *et al.*, 1998; Walpersdorf, *et al.*, 1998] (Figure 1), it constitutes a type example of how a collision can be accommodated by block rotation instead of mountain building. However, to

<sup>1</sup>Department of Earth Observation and Space Systems (DEOS), Delft, Netherlands

<sup>2</sup>now at Department of Earth and Space Sciences, UCLA, USA

<sup>3</sup>Laboratoire de Géologie de l'Ecole Normale Supérieure (ENS), UMR CNRS 8538, Paris, France

<sup>4</sup>Rensselaer Polytechnic Institute (RPI), Troy, New York, USA.

<sup>5</sup>National Coordination Agency for Surveys and Mapping (BAKOSURTANAL), Cibinong, Indonesia

<sup>6</sup>Institute of Technology Bandung (ITB), Bandung, Indonesia

<sup>7</sup>Faculty of Earth Sciences, Utrecht University, Utrecht, Netherlands

## MICROBLOCK ROTATIONS IN SULAWESI, INDONESIA

more fully understand this process, a more precise description of these microblocks' motions and a better understanding of the main active structures of the area are necessary. The purpose of this paper study is to define the deformation of the Sulawesi area utilizing geodetic and seismological data. Using a decade of GPS measurements, we estimate the kinematics and likely boundaries of the micro blocks. We also examine the active faults of Sulawesi (e.g. Palu-Koro and Gorontalo strike-slip faults) in detail to quantify their interseismic behaviour and assess their contributions to seismic hazards. Toward these ends, we model our GPS velocities and earthquake slip vector azimuths with a combination of rigid block rotations [Morgan 1968; Peltzer and Saucier, 1996] and elastic deformation due to locking on the faults separating the blocks [Okada, 1985, 1992; Savage, 1983; Savage and Burford, 1973]. This simultaneous inversion results in Euler vectors describing rigid block rotation in addition to degree of coupling on the faults.

### Geodynamic setting

#### Present-day kinematics

According to the Nuvel-1A plate motion model, the triple junction of South-East Asia is a T-T-F (trench-trench-fault) type between the Eurasian (or Sunda), Australian and Philippine Plates [DeMets, et al., 1990; 1994] (Figure 1). The Australian and Philippine Plates subduct beneath the Eurasia (or Sunda) Plate at rates of 75 mm/yr and 90 mm/yr respectively. The E-W trending Australia – Philippine Sea / Pacific boundary zone that extends from eastern Indonesia through New Guinea accommodates the relative plate motion by transpressive faulting and tectonic block rotation [Tregoning et al., 1998, 1999, 2000; Stevens et al., 2002; Wallace, et al., 2004]. GPS measurement in Indonesia have helped considerably to refine the plate kinematics of South-East Asia [Puntodewo et al., 1994; Tregoning et al., 1994; Genrich et al., 1996, 2000; Prawirodirdjo et al., 1997, 2000; Michel et al., 2001; Bock et al., 2003]. In particular, GPS velocities revealed that the Eurasian Plate does not include South-East Asia, but instead the separate Sunda plate moves at about 10 mm/yr eastward relative to Eurasia [Chamot-Rooke and Le Pichon, 1999; Michel, et al., 2001; Simons, et al., 1999]. Studies based on denser GPS arrays in Sulawesi reveal even finer detail on block-like motions, for example rapid clockwise rotation of the northern part of the Sulawesi Island, named the Sula Block, with respect to the Sunda Block [Walpersdorf et al., 1998a, 1998b; Stevens et al., 1999]. The latest study, based on 100+ sites in SE Asia, shows that deformation affects both the East Borneo and Sulawesi areas, while southern Sulawesi in particular, also moves independently of the Sunda Plate [Simons et al, sub]. These studies show that Sulawesi is clearly not a

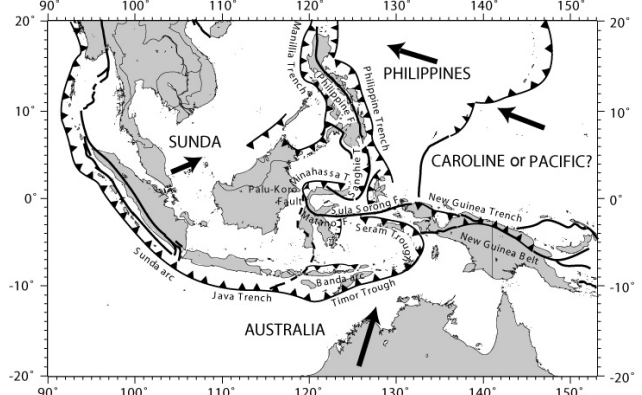


**Figure 1:** Structural map of the Sunda – Australia – Philippine - Pacific Plates junction area. Arrows depict the far field velocities of the plates with respect to Eurasia. Fault traces adapted from Hamilton (1979).

part of the Sunda plate, but instead is itself broken into multiple micro-blocks accommodating complex deformation.

#### Regional active structures

The active structures of the Sulawesi area show complex patterns of faulting [Hall, 2002; Hall and Wilson, 2000]. The Sunda plate is bounded to the south by the Sunda-Banda arc which is associated with the northward subduction of the Australian Plate. Subduction of the Australian Plate at the Java Trench evolves into collision with Australia along the Timor Trough south of Sulawesi [McCaffrey and Abers, 1991]. Highly oblique convergence (~110 mm/yr) between the Pacific (or Caroline after [Weissel and Anderson, 1978]) and the Australian Plates is accommodated in western New Guinea where shortening and left-lateral shear are distributed among several tectonic boundaries [McCaffrey and Abers, 1991; Puntodewo, et al., 1994; Stevens et al., 2002]. Faults in New Guinea continue to the west to the Seram Trough and to the Sula-Sorong Fault that continues into Sulawesi. In the Philippines, the oblique convergence between the Sunda and Philippine Plates is accommodated by partitioning of the slip between the Philippine trench and the Philippine fault [Aurelio, 2000; Fitch, 1972]. The Manilla-Philippine trench system undergoes trench-normal convergence [Rangin, et al., 1999] while left-lateral strike-slip is taken up on the Philippine Fault [Barrier, et al., 1991].

The central part of the South-East Asia triple junction coincides with Sulawesi (Figure 2). The northern part of the island, is colliding with the Sunda Plate [Rangin, 1989; Silver, et al., 1983; Silver, et al., 1983]. This relative motion is accommodated by left-lateral strike-slip motion along the Matano / Lawanopo Fault (the western

## MICROBLOCK ROTATIONS IN SULAWESI, INDONESIA

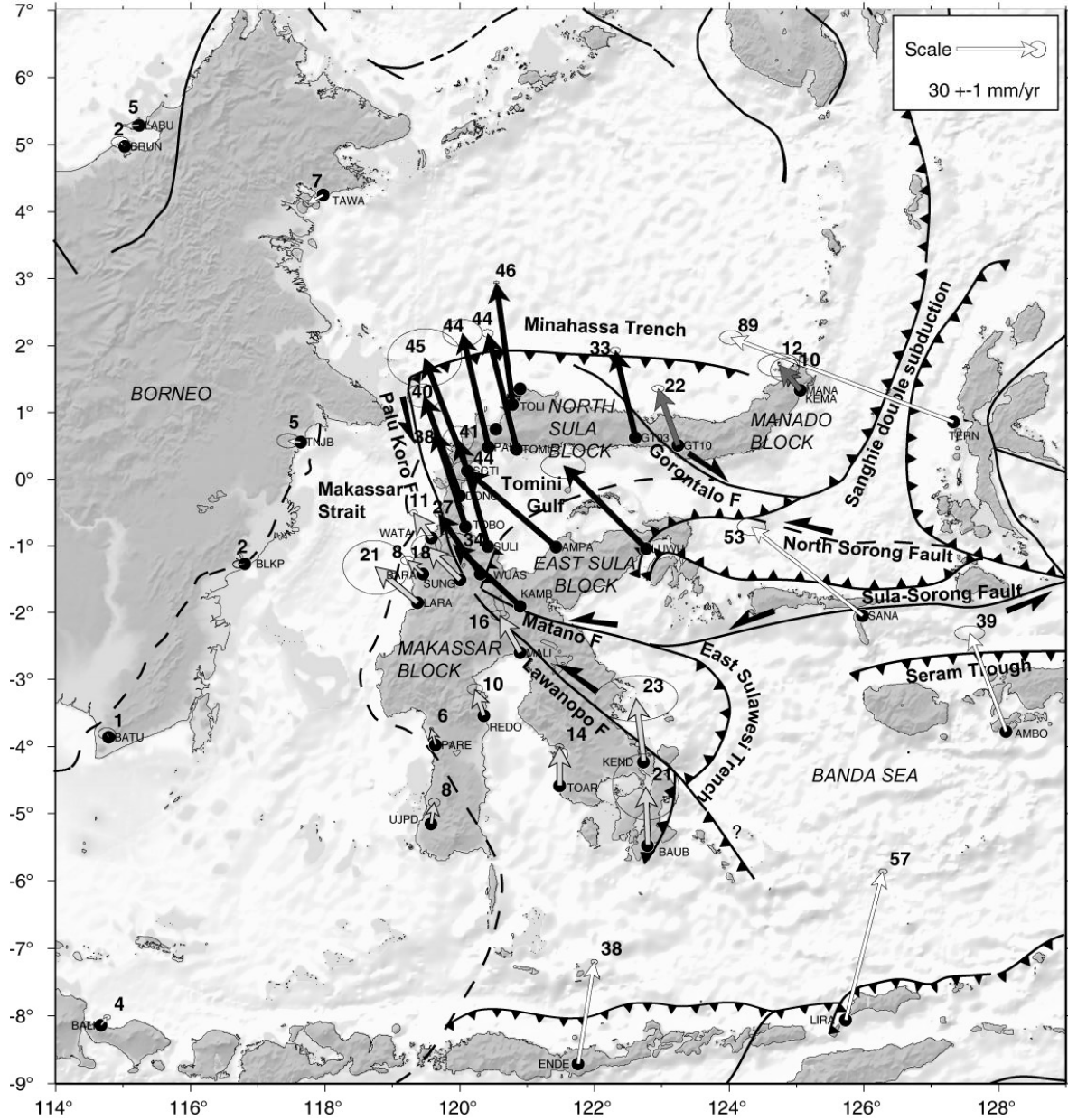


**Figure 2:** GPS velocities of Sulawesi and surrounding sites with respect to the Sunda Plate. Grey arrows belong to the Makassar Block, black ones to the northern half of Sulawesi and white ones to non-Sulawesi sites (99% confidence ellipses). Numbers near the tips of the vectors give the rates in mm/yr. The main tectonic structures of the area are shown as well.

continuation of the Sula-Sorong Fault [Hinschberger, *et al.*, 2000]) which continues to the Palu-Koro Fault in the north, which then connects to the Minahassa trench where subduction occurs (Figure 2). The Gorontalo strike-slip fault cuts the northern arm of Sulawesi and may connect to the Minahassa trench. At the Eastern termination of the Minahassa Trench, the Sangihe double subduction zone accommodates convergence between the

Philippine Plate and Sulawesi across the Molucca Sea (Figure 2).

The main active structure in Sulawesi is the Palu-Koro fault and its southeast continuation to the Matano fault and/or Lawanopo fault. The Palu-Koro fault bisects the island: the Makassar block on the southwest and the North Sula block on the northeast. GPS shows that the total motion across the fault is around 4 cm/yr. If this slip

## MICROBLOCK ROTATIONS IN SULAWESI, INDONESIA

occurs on one single fault locked at depth [Stevens, *et al.*, 1999; Walpersdorf, *et al.*, 1998], then it should produce at least one magnitude 7 earthquake every 100 years [Wells and Coppersmith, 1994]. This history of earthquakes is not seen in trenching in the Palu area [Bellier, *et al.* 2001], which poses a problem for reconciling neotectonics with the present-day geodetic rates.

### GPS velocity field of the Triple junction area

#### GPS measurements

The first GPS measurements in Sulawesi took place in 1992 [Bock *et al.*, 2003] at which time detailed transects were also established across the Palu-Koro and Gorontalo faults [Stevens, *et al.*, 1999;]. Concurrently, in the GEODYSSSEA project, a network of about 40 geodetic points covering an area of 4000 by 4000 km in South-East Asia was installed and measured between 1994 and 1998 [Michel, *et al.*, 2001]. In Sulawesi, the GPS network has been increased from the original 8 GEODYSSSEA sites in 1994 to more than 30 by 2003, plus 25 additional transect points across the Palu-Koro and Gorontalo Faults. This network has been re-measured yearly since 1996. Since 1999, 6 continuous GPS stations have been installed mainly to study the transient behaviour of the Palu-Koro Fault.

#### GPS processing

##### Regional processing

The Sulawesi GPS data (campaign and continuous measurements) have been included in regional processing covering the entire South-East Asia [Simons, *et al.*, submitted]. The station daily positions were computed with GIPSY software [Blewitt, *et al.*, 1988], applying the PPP strategy to the ionosphere-free combination of the zero-differenced GPS dual-frequency observables at 5 minute intervals, with a cut-off angle of 15 degrees. Tropospheric delays and gradients were estimated at each interval. The processing included ocean loading parameters [Scherneck, 1991], variations of the antennae phase centres (National Geodetic Survey (NGS) [Mader, 1998]), precise satellite orbits and clocks, as well as Earth orientation parameters distributed by the Jet Propulsion Laboratory (JPL). Finally, the individual PPP solutions were merged into a daily network solution after which the ambiguities were fixed to integer values. These daily network solutions were combined into weekly- or campaign-averaged solutions. The daily coordinate repeatabilities for the Sulawesi network have an internal accuracy of about 2 and 5 mm for the east and north positions and 9 mm for the height. These errors are slightly higher than those of the included IGS network, and can be explained by the less ideal site conditions (sky visibility and multipath issues) in Sulawesi. The 23 IGS stations included in the data set allowed us to project

each multi-day averaged solution onto the ITRF-2000 reference frame [Altamimi, *et al.*, 2002], by applying 7-parameter Helmert transformations to their positions. The coordinate residuals between the projected and the predicted ITRF-2000 positions at each analyzed epoch exhibit stable RMS values of about 2 to 3 mm for the east and north, and 8 mm for the vertical position. The sites velocities were estimated by computing a linear fit through all the ITRF-2000 mapped coordinate time series, while excluding any epochs that were clearly disturbed by seismic events. The coordinate residuals with respect to the linear trend at each analyzed epoch have 3-D RMS values of 2, 3 and 8 mm for east, north, and up. The differences between the estimated and the ITRF-2000 velocities for the IGS stations used for the mapping have RMS values of 0.6, 0.7 and 2.5 mm/yr, respectively, indicating that the local velocity estimates are consistently computed in a stable reference frame. The uncertainties of the horizontal velocity vectors in Sulawesi range from 0.5 to 3.0 mm/yr, depending on the number of sessions or campaigns and on the total time span between first and last occupation at each site.

##### Palu transect relative processing

The main objective of the Palu transect study is to estimate the velocity variations across the Palu-Koro fault with high relative accuracy. Therefore, we follow a different observation and processing strategy: each year the WATA station was taken as a continuously recording reference and the other transect sites were each occupied for 24 hours or more. The positions of all the network sites were computed simultaneously with respect to WATA, following a fiducial-network strategy which provides 2 important advantages. First, since the network is small (diameter of 60 km, no IGS sites included), almost all the ambiguities can be fixed. Second, there is no need to map the network into a global reference frame. The small network aperture allows for shorter observation periods and prevents loss of relative accuracy as a result of mapping errors into a global reference frame. The velocities with respect to the reference station are estimated as a linear fit through the time series of their relative positions. Daily network comparisons show small, randomly distributed residuals at each station and no systematic network rotation is found. The RMS of the daily coordinate repeatabilities with this technique is 2, 2 and 8 mm for each direction between 1998 and 2004, with slightly higher values in 1997 when some transect sites were occupied for only 3 to 4 hours. Long term uncertainties (epoch residuals relative to a linear trend) have the same amplitude (a few mm) as the short term uncertainties (daily repeatabilities). This agreement indicates that uncertainties are correctly estimated and that station positions are free of unidentified biases. Hence, the Palu transect relative processing, although based on both fewer and shorter observation periods, delivers (relative)

## MICROBLOCK ROTATIONS IN SULAWESI, INDONESIA

velocity estimates with an uncertainty ( $1-\sigma$ ) ranging from 0.3 to 1.5 mm/yr for the sites that were measured at least 3 times.

### Obtaining a consistent velocity field

The Palu transect velocities are processed relative to the westernmost station of the transect, WATA. In order to get the velocities of the transect in a global reference frame, we simply add the velocity of WATA in ITRF-2000 to all the points of the transect. In doing this we assume that the transect is affected only by translation at such a small scale (60 km at most). Indeed, the two independent determinations (relative and regional) of the velocity of the transect's easternmost site (TOBO, also continuously measured) with respect to that of WATA agree within 0.6 mm/yr. The velocities (in the ITRF2000) of this combined solution (regional + relative) are listed in the electronic supplement.

### Modelling the velocity field

#### Description of the velocities in Sulawesi area

We specify several tectonic blocks in the Sulawesi region based on the GPS velocities and the geological and seismological evidence for active faulting. Figure 2 displays the velocities relative to the Sunda plate reference frame [Simons *et al.*, subm.; Socquet *et al.*, 2006] and figure 3 shows the focal mechanisms in the same region. The first obvious pattern from the GPS velocities is the division of the island into two independent domains. In the south, the Makassar Block (grey arrows) displays a small but significant motion relative to Sunda appearing to rotate anticlockwise around a pole located near its south-western tip. The Makassar Trench (figure 4) bounds this block to the west and accommodates at least part of the Sunda / Makassar convergence. The East Sulawesi Trench constitutes the boundary of the Makassar and East Sula blocks with the Banda Sea. The northern half of Sulawesi (black arrows) moves toward the NNW and rotates clockwise around a pole located near its north-eastern tip. The northern half of Sulawesi is divided into 3 smaller blocks. The eastern part of the northern arm of Sulawesi, here named the Manado Block, has an independent motion from the North-Sula Block. These two entities are separated by the Gorontalo Fault, evident in geology. The boundary between the Makassar and North Sula blocks is the Palu-Koro fault. Lastly, the eastern arm of Sulawesi also shows independent motion from North-Sula, indicated by west trending GPS vectors at sites LUWU, AMPA and KAMB. Due to the sparseness of our network in this area, more exact boundaries of this block (here named East Sulawesi) are difficult to draw. East of Sulawesi, we define the Banda Sea as a rigid block on which we have only 2 GPS velocities: at SANA and AMBO.

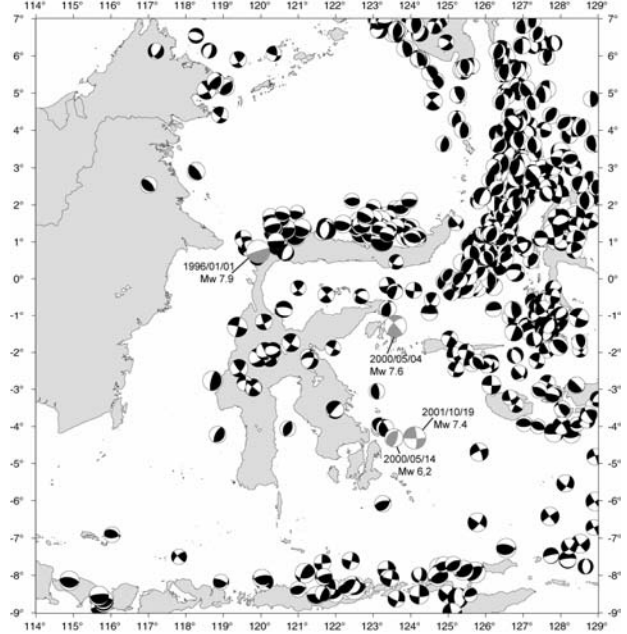


**Figure 3:** Post-1976 instrumental CMT focal mechanisms from Harvard catalogue in the Sulawesi area. The size of the symbol is proportional to the earthquake magnitude. Focal mechanisms in grey, labelled by date (YYYYMMDD) and magnitude, correspond to the earthquakes cited in the text.

### Data modelling approach

The relatively small, rotating blocks are surrounded by active faults where interseismic coupling produces elastic deformation within the blocks. In many instances, a substantial amount of the block's surface is below sea-level and inaccessible to standard GPS measurements so only a part of the block has constraints. For example, in the northern half of Sulawesi the Tomini Gulf covers the central part of the area (Figure 2). Due to the limited sampling, it is difficult to identify observation points that may indicate rigid block rotations only, i.e. no closer than 100km from any active fault. Consequently, the velocities of most points result from a combination of rigid rotations and elastic loading on faults. Therefore we use an inversion approach that simultaneously estimates the angular velocities of elastic blocks on a sphere and creep fractions (e.g., coupling coefficients) on block-bounding faults. For this purpose we use the DEFNODE software [McCaffrey, 1995, 2002, 2005] which applies simulated annealing to downhill simplex minimization [e.g., Press *et al.*, 1989] to solve for the model parameters. We minimize data misfit, defined by the reduced chi-squared statistic:

## MICROBLOCK ROTATIONS IN SULAWESI, INDONESIA

**Table 1:** Euler vectors used in this study<sup>a</sup>

Plates pairs	Euler vector				
	Long (°)	Lat (°)	$\omega$ (°/Myr)	Emax (°)	Emin (°)
Sunda / ITRF2000 [Simons et al, subm]	-48.9	85.8	-0.3		
<b>Model 1, GPS only</b>					
Makassar / Sunda	-4.5	117.4	$1.5 \pm 0.21$	0.48	0.26
North Sula / Sunda	2.4	129.9	$-2.5 \pm 0.36$	2.23	0.17
Manado / Sunda	1.9	126.6	$-3.1 \pm 0.99$	1.06	0.49
Banda Sea / Sunda	-7.1	118.1	$2.0 \pm 0.91$	6.92	1.30
East Sula / Sunda	-8.3	115.7	$2.4 \pm 1.31$	7.35	0.85
<b>Model 2, GPS + Slip Vectors</b>					
Makassar / Sunda	-4.8	117.4	$1.4 \pm 0.15$	0.42	0.21
North Sula / Sunda	2.4	129.5	$-2.6 \pm 0.38$	1.81	0.32
Manado / Sunda	1.8	126.5	$-3.2 \pm 1.99$	1.44	0.37
Banda Sea / Sunda	-9.7	113.3	$1.8 \pm 0.21$	2.55	0.63
East Sula / Sunda	-7.9	115.0	$2.2 \pm 0.55$	3.70	0.50

<sup>a</sup> $\omega$  is the rotation rate with one standard error. Euler vectors are for the first plate relative to the second one. Emax, Emin and azimuth refer to the maximum and minimum axes of the 68% confidence error ellipse and the azimuth of the major axis respectively. Positive rotation rates indicate anticlockwise motion looking from above.

$$\chi_n^2 = \left( \sum \frac{r^2}{s^2} \right) / dof$$

where  $r$  is the residual,  $s$  is the standard deviation and  $dof$  gives the degrees of freedom (number of data minus number of free parameters).

The coupling fraction (ratio of locked to total slip) on the fault is defined as a purely kinematic quantity,  $\varphi$ . If  $\varphi = 0$ , the fault is creeping at the full long-term slip rate and if  $\varphi = 1$ , the fault interface is fully locked during the interseismic period. Since the GPS data we use are sparse, we assume that this coupling fraction is uniform over large patches of the faults. However we allowed it to vary along the Palu fault and the Minahassa Trench in some inversions where the GPS arrays are denser. The relative motion on the faults is determined by the Euler vectors describing the motions of the blocks adjacent to the fault. The slip rate deficit vector on the fault is the scalar coupling value  $\varphi$  multiplied by the relative motion vector between the two blocks at a given fault. The elastic contribution to the velocity field from the fault slip rate deficit is calculated using a back-slip approach to elastic dislocation modelling [Savage, 1983], using the formulations of [Okada, 1985] for surface displacements due to dislocations in an elastic half-space.

### Results of the models

In the first model presented here, we use GPS data only (applying the 2-sigma uncertainty) to estimate the angular velocities of five blocks (North-Sula, Makassar, Manado, Banda-Sea, East-Sula) and the average coupling ratio on seven faults bounding the blocks (Palu Fault, Gorontalo Fault, Minahassa Trench, Makassar Trench,

East Sulawesi Trench, Lawanopo Fault and Tomini Gulf fault zone, Fig. 3). Given the high number of sites located near the Palu and Gorontalo Faults compared to the number of sites located on the stable blocks away from faults, we downweight the former by a factor of 4 to estimate the blocks rotations using the geographically - distributed data. We obtain  $\chi_n^2 = 8.3$  (100 observations, 78 degrees of freedom, Table 3). This model produces very large uncertainties in the estimates of some block motions and fault coupling coefficients (on the east Sulawesi Trench for example, Table 2). Therefore, in a second inversion, in addition to the GPS data, we use earthquake slip vector azimuths extracted from Harvard CMT focal mechanisms (Figures 3 and 4). We apply an uncertainty of  $10^\circ$  on the azimuth of the slip vectors except for those from the Minahassa Trench, where the uncertainty has been fixed at  $20^\circ$  for the western part and  $40^\circ$  for the eastern part because of the abundance of earthquake data in these areas. In this model, we allow the coupling ratio of the Palu fault and the Minahassa Trench to vary along strike. Although we have in this second model more parameters to estimate, the addition of these slip vector data reduces  $\chi_n^2$  to 6.4 (191 observations, 164 degrees of freedom) and reduces uncertainties on the blocks' Euler vectors by a factor of 2 to 3. The  $\chi_n^2$  obtained for the best model decreases to 3.6 if the outliers (AMBO and WUAS) are excluded from the model. The misfit to the data remains however high, indicating that the formal uncertainties derived from the GPS processing are under-evaluated and still poorly estimated. For the present data set, to obtain a realistic estimate of the error on the GPS velocities, one should take 4-sigma of the formal

## MICROBLOCK ROTATIONS IN SULAWESI, INDONESIA

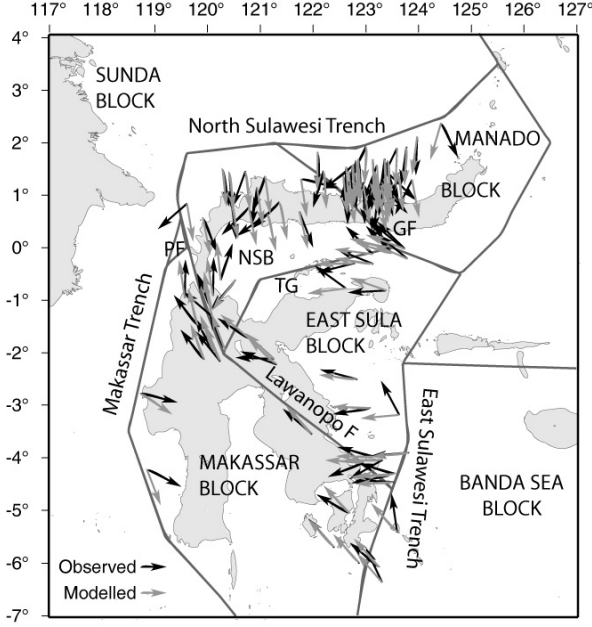


**Figure 4:** Blocks geometries used for the modelling. The observed (black) and the modelled (grey) slip vectors of model 2 are also shown. NSB: North Sula Block, PF: Palu Fault, TG: Tomini Gulf fault Zone, GF: Gorontalo Fault.

uncertainty given in the table in electronic supplement (in the inversion, uncertainties have already been scaled by 2).

Table 1 summarizes the poles of rotation we obtain for the various blocks and models. It is noticeable that the poles obtained by the two inversions are similar for the blocks that have several GPS velocities (i.e., North Sula, Manado and Makassar blocks). However slip vectors provide useful constraints for the blocks that have sparse GPS observations (East Sulawesi Block and Banda Sea block). Table 2 gives the fault geometries at depth, the estimated coupling ratios and slip rates for the 2 models. Once again, the estimation of the coupling ratio is improved by the addition of slip vector constraints for the faults that are not surrounded by GPS stations (Makassar Trench, East Sulawesi Trench, Lawanopo Fault and Tomini Gulf fault zone). However, the amount of coupling on the Palu Fault, the Gorontalo Fault and the Minahassa Trench is better determined in the model with GPS data only, since the local networks around these faults are very dense. Also note that the locking depth of the Gorontalo and Palu fault are well constrained by the width of the arctangent evident in the horizontal displacement profile of the GPS transect (Figure 7), while it has been fixed a priori for the other faults.

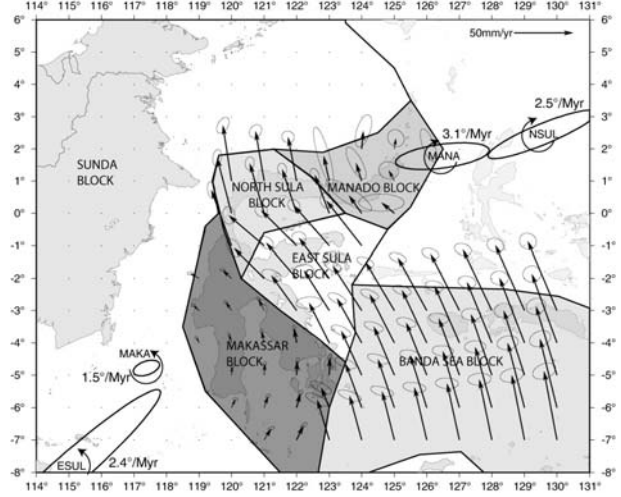


**Figure 5:** The rotational part of the inferred velocity field in the Sulawesi area (relative to the Sunda plate) as predicted by the Euler vectors of the best fit model (model 2). Error ellipses of predicted vectors show the 99% level of confidence. Also shown are poles of rotation and error ellipses (with respect to the Sunda Plate) from the best fit model. Curved arrows indicate the sense of rotation (put rotation rates on this figure). MAK: Makassar block, MANA: Manado block, ESUL: East Sula block, NSUL: North Sula block

## Discussion

### Makassar Block

The residual velocities of the sites on the Makassar Block are mainly below 3 mm/yr and display no systematic orientation (Figure 6, right) suggesting that it deforms little internally. With respect to Sunda, the Makassar block rotates anti-clockwise around a pole located near its south-western tip (Table 2, Figure 5). Due to this rotation, convergence on the Makassar Trench increases northward with a corresponding increase in slip rate deficit (Figure 6). Deformation associated with this margin may also extend into eastern Kalimantan. Stations on the eastern margin of Borneo (SAND, TAWA, TNJB, BLKP) display residual velocities of up to 7 mm/yr with respect to the Sunda plate (Figure 2). Westward motion of ~5mm/yr at the equator latitude (TNJB station, 1° north) decreases to 1-2 mm/yr at both the northern and southern ends of the island (stations of SAND at 6° north, BLKP and BATU at 1° and 4° south) implying a clockwise rotation of the eastern margin of Borneo north of the equator and an anticlockwise rotation south of it. This deformation may be distributed and can not be described in terms of rotation of rigid blocks. It might be explained by initiation of a collision in the Makassar Strait between

## MICROBLOCK ROTATIONS IN SULAWESI, INDONESIA

**Table 2:** Summary of fault parameters.<sup>a</sup>

Model 1, GPS only

Fault	Dip	Depth	$\Phi$	$\Delta\phi$	Slip rate (mm/yr)	Azimuth (°)
Palu Fault	50°	12 km	1	0.06	41 / 45	-20 / 7
Gorontalo Fault	80°	10 km	1	0.70	11 / 12	-7 / 0
Minahassa T. (west)	20°-30°	50 km	0	0.15	42 / 50	-3 / -3
Minahassa T. (east)	20°-30°	50 km	0	0.15	13 / 23	15 / -1
Makassar Trench	25-35°	20 km	1	0.54	4 / 13	-42 / -67
East Sulawesi T.	20-30°	20 km	1	1.40	9 / 19	-74 / -32
Lawanopo F.	50°	15 km	1	0.39	25 / 26	-59 / -43
Tomini F.	50°	15 km	1	0.69	28 / 18	-52 / -142

Model 2, GPS + Slip Vectors

Fault	Dip	Depth	$\Phi$	$\Delta\phi$	Slip rate (mm/yr)	Azimuth (°)
Palu Fault	50°	12 km	1 / 1	0.16 / 0.91	41 / 44	-21 / 7
Gorontalo Fault	80°	10 km	1	0.85	11 / 12	-14 / -6
Minahassa T. (west)	20°-30°	50 km	0 / 0	0.3 / 0.54	41 / 49	-3 / -4
Minahassa T. (east)	20°-30°	50 km	0 / 0	7.23 / 29.34	13 / 23	20 / 2
Makassar Trench	25-35°	20 km	1	0.50	5 / 11	-49 / -68
East Sulawesi T.	20-30°	20 km	0.64	0.43	2 / 27	-97 / -43
Lawanopo F.	50°	15 km	1	0.36	23 / 24	-51 / -36
Tomini F.	50°	15 km	1	0.79	23 / 25	-44 / -151

<sup>a</sup>Dip and depth represent the dip angle and maximum locking depth for the faults.  $\phi$  and  $\Delta\phi$  represent the coupling ratio and its 1-sigma uncertainty. In the model 1 (only GPS data used) the coupling ratio was assumed to be uniform along all faults while in the model 2 (GPS + Slip Vectors used) the coupling ratio is allowed to change along the Minahassa Trench and the Palu fault. Since slip rate and slip azimuth vary along the faults, we give the range of these values.

the eastern Borneo shelf and the westward moving Makassar and North Sula blocks.

On the eastern southside of Sulawesi, the East Sulawesi Trench is also active. Two large earthquakes occurred there: 14 May 2000 Mw 6.2 and 19 October 2001 Mw 7.4 (Figure 3). Sites BAUB and KEND are located within the elastic deformation zone associated with the trench indicated by significant displacements detected in their time series at the epoch of the earthquakes. Hence, we use only the epochs before these events (1994-1998, electronic supplement) to determine the long term inter-seismic velocities of the two sites. The 2 velocities and slip vector data are matched by a slip deficit of 15 mm/yr accommodated on a plane striking north and dipping at 20-30° fully locked down to 20 km depth (Figure 4 and 6).

### North-Sula Block

Uncertainties on the Euler vector for the North-Sula Block are high in the NE direction because the GPS data are spread in a line because of the shape of the north end of the island (Figure 2). In addition, many sites have been affected by earthquakes (Figure 2 and 3). Their time series are not linear but instead show logarithmic post-seismic decay trends making their inter-seismic velocities difficult to determine. All sites near the Minahassa trench (north side of the block) were displaced by the 1 January 1996 Mw 7.9 earthquake (Figure 3) leaving few sites on the stable part of the block (SGTI, PALA and

GT03). Other sites on the block are within the strain areas of the Palu-Koro and Gorontalo faults. In the southern part of the block, the large residual velocity of site WUAS (Figure 6) probably arises because the site is within a complex and poorly modelled junction of 3 block-bounding faults. A connection of the Palu fault to the Matano fault instead of to the Lawanopo fault may improve this fit but in this area the exact location of the fault is poorly known.

Using GPS velocities, slip vectors and a joint inversion for block rotation and fault coupling we obtain a North Sula – Sunda pole near 2.4°N and 129.5°E rotating clockwise at 2.6°/Myr (Table 1). This pole is 3-4° east of and slower than the poles estimated by previous GPS and geologic studies [Stevens, et al., 1999; Walpersdorf, et al., 1998; Silver et al., 1983]. We conclude that the North-Sula region comprises a rapidly rotating micro-block pinched between strike-slip faults (Palu, and Lawanopo and/or Matano) and subduction, revealing accumulation of both inter-seismic elastic strain and internal deformation (Figure 6).

### East Sulawesi block

The sites AMPA and LUWU show significant, large motions trending west relative to the North-Sula block and are not compatible with rotating with either the N. Sula or Manado blocks. Accordingly, we introduce another

## MICROBLOCK ROTATIONS IN SULAWESI, INDONESIA

Table 3: Probabilities derived from F Tests of block independence for various tectonic blocks/faults models<sup>a</sup>

Model	Nblocks	Ndata	Nparameters	DOF	$\chi^2$	Is model 2 better ?	Probability Answer
1, GPS only	6	100	22	78	8.3	91%	Yes
2, GPS + SV, best model	6	191	27	164	6.4		
3, MANA=NSUL	5	191	23	168	6.6	56%	Maybe
4, NSUL=ESUL	5	179	23	156	7.2	76%	Maybe
5, ESUL=MANA	5	191	24	167	8.2	94%	Yes
6, ESUL=NSUL=MANA	4	179	19	160	7.4	80%	Yes
7, MAKAKA=ESUL	5	187	24	163	12.3	99%	Yes
8, BSEA=MAKA	5	185	24	161	10.8	99%	Yes

<sup>a</sup>Except for Model 1 where only GPS data were used, all GPS and Slip Vector (SV) data were used for these models. In model 1, the coupling ratio along all the faults was uniform. In the other models, the coupling ratio is allowed to vary along the Palu Fault and the Minahassa-North Sulawesi Trench, and is uniform along the other faults. Models 3 to 8 are derived from Model 2, with fewer blocks considered. For each model, the blocks listed comprise a singlerotating unit. DOF = degree of freedom.  $\chi^2$ =Normalized Chi squared.

independent block, the East Sula Block, though the boundaries are not well defined. To the south, we bound it along the Lawanopo Fault (Figure 4) which displays moderate seismicity. However, the Matano Fault, located north of the Lawanopo, is also active. Hence, the deformation is poorly represented in the region between the Matano and Lawanopo faults. The northern boundary is taken as the roughly E-W zone of frequent seismicity beneath the Tomini Gulf (Figure 3).

Since only 3 GPS velocities are available for the East Sulawesi block, slip vectors from earthquakes located on its boundaries provide important constraints on its motion. The Euler vector that we obtain is near 7.9°S, 115.0°E (with an anticlockwise rotation rate of 2.2°/Myr) with respect to Sunda (Table 1), leading to ~25 mm/yr of left-lateral strike slip on the Lawanopo Fault and ~24 mm/yr of right lateral motion along the Tomini Gulf boundary. Inversions were run to test the independence of the East Sulawesi block from the North Sula and Makassar blocks. F-tests suggest that the East Sulawesi block is disconnected at 99% confidence from the Makassar block and at 76% confidence from the North Sula block (Table 3).

### Manado Block and Gorontalo fault

In the North-Sula Block reference frame, the sites located at the eastern termination of the northern arm of Sulawesi display residual velocities ranging from 8 to 11 mm/yr and hence belong to a different block. The Gorontalo fault, which bisects the northern arm of the island, is taken as the boundary between the Manado block and the North-Sula Block. Our best fit pole for the Manado block is near 1.8°N, 126.5°E with an anticlockwise rotation rate of 3.2°/My (Table 1). The velocity residuals are mostly less than 2 mm/yr (Figure 6, bottom right). The computed Manado / North-Sula relative Euler vector predicts 11 mm/yr of right-lateral

slip across the Gorontalo fault. Our velocity profile shows an accumulation of interseismic elastic deformation across this fault locked to about 10 km depth (Figure 7).

F-tests show that the Manado block is independent from the North Sula block (56% confidence, table 3) and the East Sula block (94% confidence). Although the F-test does not completely reject the possibility of Manado and North Sula Blocks being a single block, the gradient in the velocities across the Gorontalo Fault appears to be too large to be due to rotation of a single block, arguing the North Sula Block and the Manado Block are two different entities.

### Minahassa Trench

Very interestingly, we find no elastic deformation associated with locking on the Minahassa subduction fault (Figure 6, Table 2). While the lack of coupling is well-determined for the western Minahassa trench due to the proximity of several GPS sites, it is poorly determined for the eastern part (Table 2) because GPS sites are sparse there. In the alternative models 5 and 6, where the North Sula and Manado blocks move as one, coupling on Minahassa Trench varies along strike perhaps compensating for the lack in rotation of the Manado Block. In this case, the trench appears to be locked at its eastern part, but remains poorly locked on its western part.

The null locking observed in the western part can not represent its long term behaviour since it produced a magnitude 7.9 earthquake in January 1996 (Figure 3) that produced significant coseismic ground displacements [Gomez *et al.*, 2000]. The GPS velocities above the western end of the trench are still affected by postseismic deformation from that earthquake, which may be causing the low coupling estimate. The present day low coupling is representative of a post-seismic temporary stage during which the inter-seismic elastic deformation away from the trench is compensated by post-seismic deformation

## MICROBLOCK ROTATIONS IN SULAWESI, INDONESIA

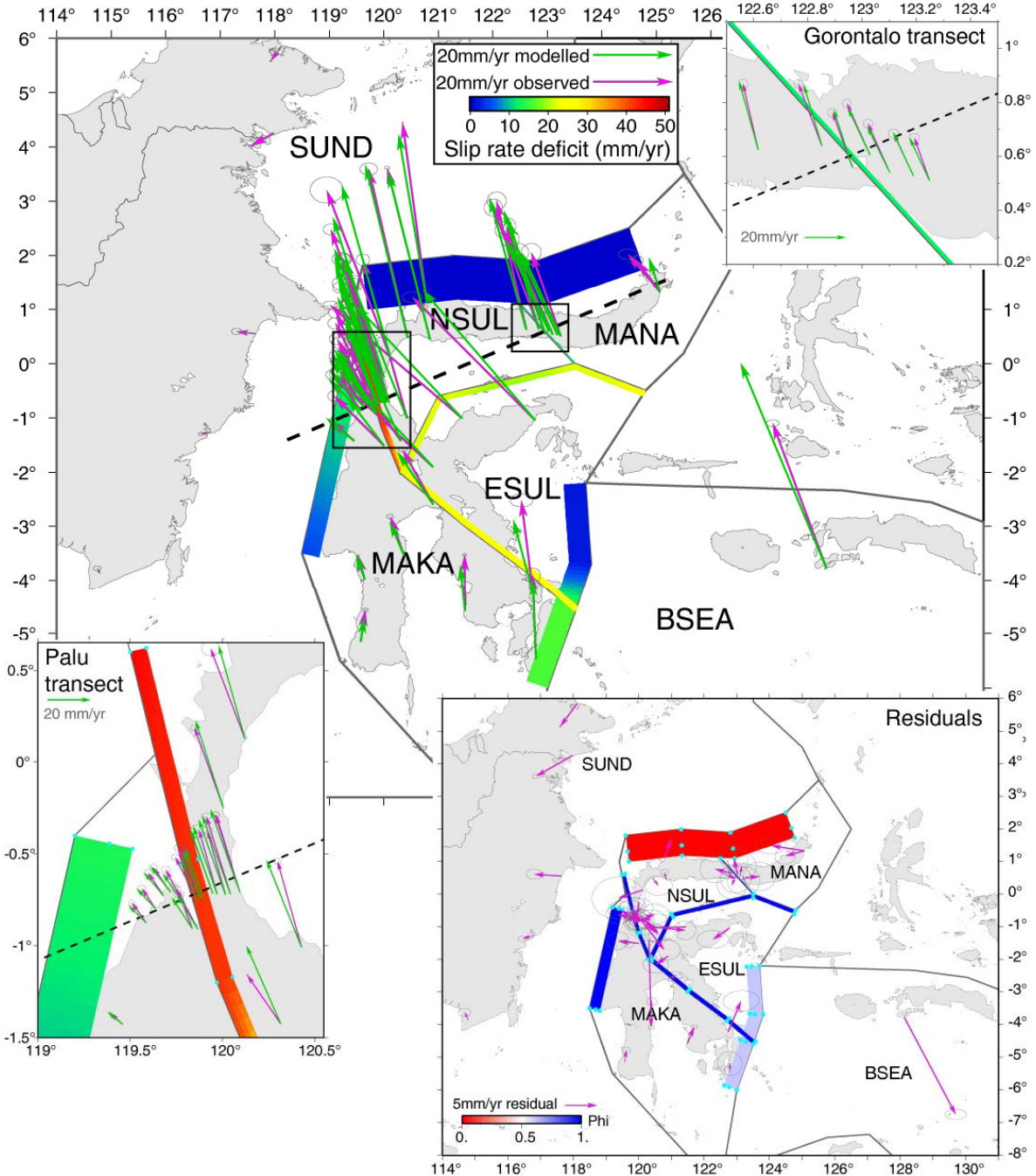


**Figure 6:** Best fit block model derived from both GPS and earthquakes slip vector azimuth data. Center: Observed (pink) and calculated (green) velocities with respect to the Sunda block (shown are 20% confidence ellipses, after GPS re-weighting; see text). The slip rate deficit (mm/yr) for the faults included in the model is represented by a color bar. The profile of figure 7 is located by the dashed black line. The black rectangles around Palu and Gorontalo fault localize the insets. Top right and bottom left insets show details of the measured and modelled velocities across the Gorontalo and Palu faults. The bottom right inset shows residual GPS velocities with respect to the model. The value of the coupling ratio,  $\phi$ , for the faults included in the model is represented by the color bar. Light blue dots represent the locations of the fault nodes where the coupling ratio is estimated. Nodes along the block boundaries are at the surface of the Earth and the others are at depth along the fault plane. In this model,  $\phi$  is considered uniform along strike and depth for all the faults, except for Palu Fault and Minahassa Trench where it is allowed to vary along strike.

## MICROBLOCK ROTATIONS IN SULAWESI, INDONESIA

(motion towards the trench), similar to what has been observed on the Japan Trench following the 1994 Sanriku-Oki Mw=7.6 earthquake [Mazzotti et al., 2000]. Presumably, full locking and accumulation of elastic strain will resume following the post-seismic deformation.

### Palu fault interseismic deformation

The computed North Sula / Makassar Euler vector predicts a slip rate of 41 to 44 mm/yr with an azimuth rotating from 21°W to 7°E, from south to north, on the Palu-Koro fault zone. For accessibility reasons, the GPS profile was installed in the vicinity of Palu city, where the fault appears to be a pull-apart structure in the morphology [Beaudouin, et al., 2003; Bellier, et al., 2001; Bellier et al., 2006].

We present two plausible models of the deformation in the pull apart area. The first model is derived from the inversion for the regional Sulawesi kinematics and involves a single fault locked at depth, while the second model involves several parallel, shallowly-locked faults.

The velocities measured across the transect fits a single dislocation model of the fault interseismically locked to a depth of 12 km, consistent with the previous studies [Stevens, et al., 1999; Walpersdorf, et al., 1998]. In the current study however, the fault appears to be dipping at 50° toward the east, accommodating ~11-14 mm/yr of extension, in addition to 39 mm/yr of strike-slip (bottom left inset in Figure 6, Figure 7, table 2). The normal component of faulting in the region of Palu inferred from the geodetic data is in agreement with triangular facets, indicating an active normal motion, observed in the morphology [Beaudouin, et al., 2003; Bellier, et al., 2001; Bellier et al., 2006].

In the alternate model, we use several parallel dislocations to explain the pull-apart geometry (Figure 8 top). The GPS data are fit best by a model of four parallel left-lateral strike-slip dislocations (Figure 8, bottom). (1) The first dislocation is located along the western side of the pull-apart, recognized by geologists as being the active Palu fault scarp [Beaudouin, et al., 2003; Bellier, et al., 2001; Bellier, et al., 2006]. It accommodates 13 mm/yr and its locking is between 2 and 5 km depth (Figure 6). (2) The second dislocation is 14 km east of this main scarp, accommodates 10 mm/yr and is locked between 1 and 5 km depth. This second dislocation, located along the eastern coast of the Palu Gulf, corresponds to the fault that bounds the Palu pull-apart to the east. It separates mio-quaternary molasses from the metamorphic bedrock [Bellier, et al., 2006] and has been activated during the February 2005 Mw=6.3 earthquake [Soehaimi et al., 2006]. (3) The third dislocation is located 28 km from the main scarp and accommodates 7 mm/yr. Its locking depth tends to zero, which is equivalent to a creeping behaviour. The dislocation is near a steep gradient in topography that could correspond to a fault scarp. The abruptness of the

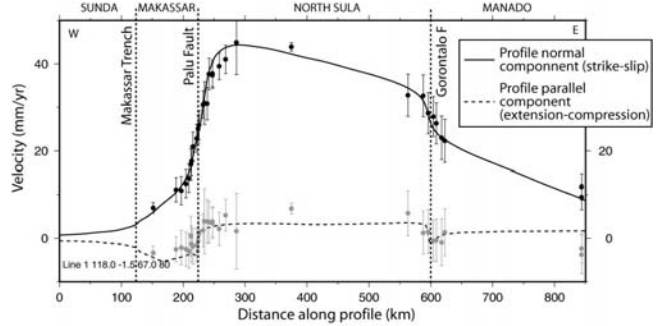


**Figure 7:** Velocity profile across Makassar Trench, Palu Fault and Gorontalo Fault (profile location in Fig. 6) in Sunda reference frame. Observed GPS velocities are depicted by dots with 1-sigma uncertainty bars while the predicted velocities are shown as curves. The profile normal component (approximately NNW) (i.e. the strike slip component across the NW-trending faults) is shown with black dots and solid line while the profile parallel component (normal or thrust component across the fault) is shown with grey dots and a dashed line. Where the profile crosses the the faults and blocks is labeled.

step in the velocities depends on the velocity determination of the sites SLBY and PL16 (measured 3 and 4 times respectively). (4) The three previous dislocations accommodate 30 mm/yr of the relative block motion. Another 8 mm/yr are missing and seem to be accommodated over a broad zone 50 km to the east. Dense GPS measurements are missing to discriminate whether these 8 mm/yr are localized on one single dislocation or are distributed. Velocities are fit well by including a fourth dislocation locked at 5-15 km depth and located ~54 km east of the main scarp. The parameters of this last dislocation are poorly constrained by three sites (DONG, SGTI, PALA) that are well to the north of Palu and span 1 degree in latitude.

The GPS inferred strike slip rate (39 mm/yr) for the Palu fault agrees with the long-term slip-rate (35 +/- 8 mm/yr) determined from stream and fan offsets, mainly seen in the quaternary deposits along the western border of the Palu basin [Bellier, et al., 2001]. This long term slip rate, ranging from 5 to 51 mm/yr [Bellier, et al., 2001], argues for the single dislocation model at its high end, although the alternate local model, that predicts 13 mm/yr on the western branch of the fault, is also within the long term range. South of the Palu basin, where the fault trace is more linear and appears to form a single trace, Bellier, et al. [2001] obtain a slip-rate of 29 +/- 5 mm/yr. This rate might either correspond to the “single strand model” or to the 30 mm/yr (13 + 10 + 7) of total amount taken on the 3 western dislocations of the “multiple strand model”.

## MICROBLOCK ROTATIONS IN SULAWESI, INDONESIA

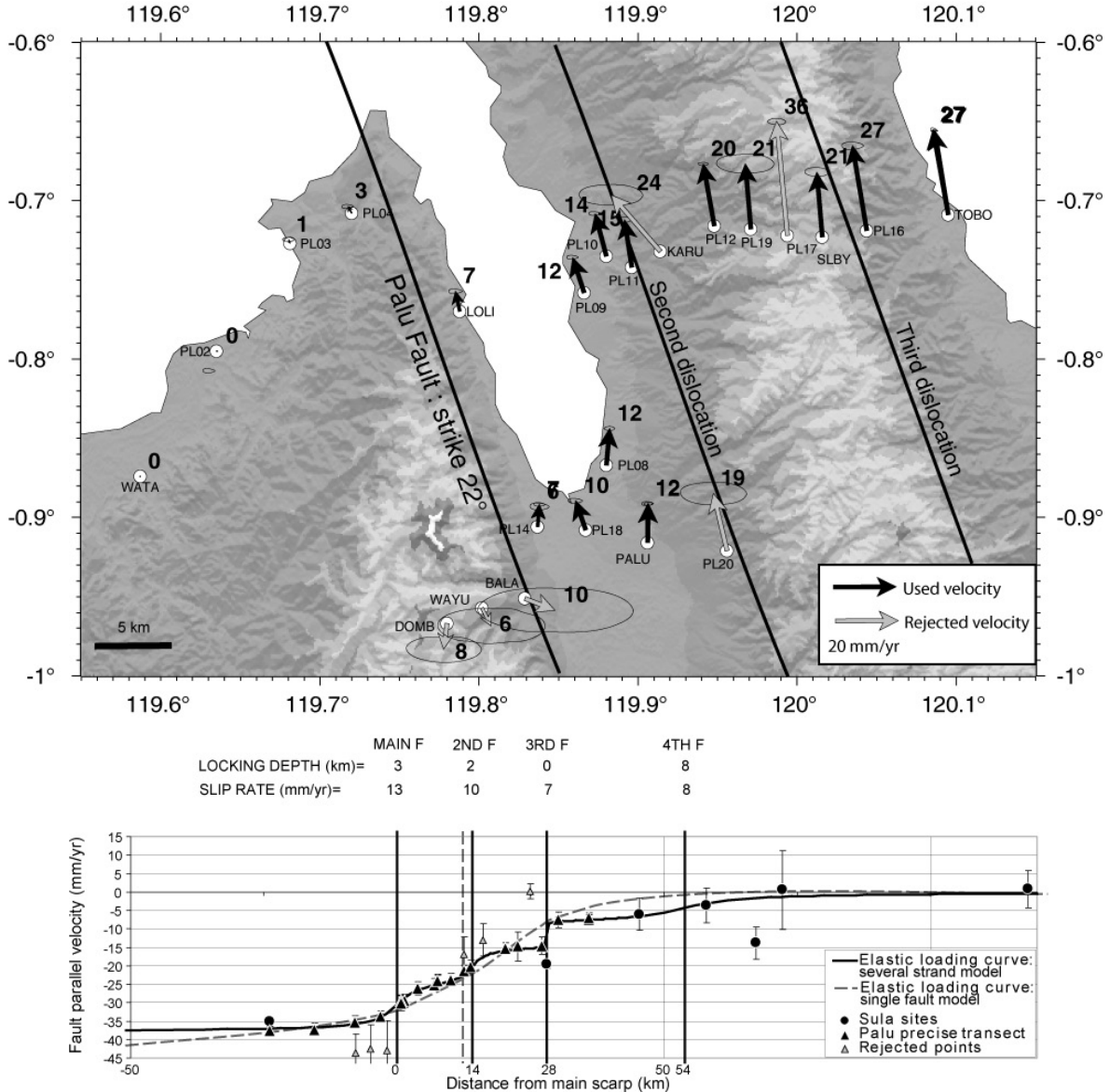


**Figure 8:** Top: GPS velocities in Palu area relative to station WATA. STRM topography is used as background. Bottom: Four parallel elastic dislocations that the velocities in the Palu fault zone. The fault parallel component of the GPS velocities (with 1-sigma error bars) is plotted with respect to their distance to the main fault scarp, in the North Sula Block reference frame.

In terms of seismicity, preliminary paleoseismological studies reveal three  $6.8 < M_w < 8$  earthquakes over the last 2000 years [Bellier, et al., 2001], implying a cumulative offset of  $\sim 30$  meters [Wells and Coppersmith, 1994]. These earthquakes occurred on the main branch of the fault, western side of the pull apart. The measured cumulative offset matches quite well the 26 meters of cumulative offset predicted by the multiple strand model on the western dislocation. Low slip on the

western strand reconciles the fact that although the paleoseismicity is small, the fault is interseismically locked and releases its strain through earthquakes. If the multiple strands model is accurate, additional paleoseismic studies on the secondary branches of the Palu Fault should be performed to sample more completely the paleoseismicity, and hence assess the complete seismic hazard of the fault zone. However, because paleoseismological studies are able to detect only

## MICROBLOCK ROTATIONS IN SULAWESI, INDONESIA

the larger earthquake events (~Mw 6.5 and above), there may be other smaller ones contributing to a slip rate. Paleoseismology is most likely slightly underestimating the rate. It is also possible that there could be periodic aseismic slip on this fault (postseismic, or episodic slow slip?), so the paleoseismology underestimates the slip rates even more if those occur. If that is the case, the single Palu fault model might be more accurate (rather than the 3-4 strands). However, small earthquakes (Mw<6) should be numerous to contribute significantly to a slip rate (one every one or two years on the 150 km long Palu segment), which is not observed in the instrumental seismicity. Strong geomorphic evidence of a pull apart in this area combined with the recent seismic activity of the east branch of the pull apart plead for the multiple strand model. Therefore we consider that the “1-dislocation” model is a good large-scale approximation (good enough when dealing with block rotations over a long period of time for example) but that a refined model with more dislocations is needed by geodetic, geomorphic and seismologic data when dealing with local fault behaviour and assessing the seismic hazard. These scenarios are not equally probable, they happen at the same time: in this area, a transtensive motion occurs on the fault system, which is probably divided into several active branches (each side of the pull-apart), that may be regarded as surface splays of a strike-slip flower structure.

### Conclusion and outlooks

#### Kinematics of the Triple junction and possible mechanisms driving the microblocks rotations

Sulawesi is located at the western termination of the boundary between Australia and Philippine/Pacific plates. This boundary accommodates the left lateral oblique convergence by rapid micro-blocks rotations in Papua New Guinea [Bock, et al., 2003; Pubellier and Ego, 2002; Pubellier, et al., 1996; McCaffrey and Abers, 1991; Stevens et al., 2002; Wallace et al., 2004] and slip partitioning further west (between normal subduction at the Timor trough and strike-slip on the Sula-Sorong fault, figure 1). Movements of crustal fragments within this E-W oriented complex boundary zone results in local collisions with the Sunda Plate in the area of Sulawesi and Borneo. Due to the rapid westward motion of the Philippine Sea Plate, the Sula-Sorong fault slips left laterally. It ends in Sulawesi (there called Matano / Palu-Koro fault), where it separates the island in two parts. The southern blocks of the study area (Makassar, Banda Sea and East Sula blocks, figure 5) rotate anticlockwise, which is consistent with a left lateral sense of shear. The northern parts of Sulawesi however (North Sula and Manado Blocks) rotate clockwise: the North Sula block rotates quickly, while the Manado Block is swept along

the latter and rotates at a slower rate (relative to the fixed Sunda block).

We suggest that the clockwise tectonic block rotation in the northern part of Sulawesi occurs due to the change in boundary condition around the North Sula block. To the west the Sulawesi Island is bound by buoyant Borneo continental crust, while oceanic crust bounds the island to the north (Celebes Sea) and to the east (Banda Sea). Because of its thick, buoyant crust, the Borneo lithosphere resists subduction below Sulawesi. Such buoyancy forces have been termed “colliding resistance” forces [Forsyth and Uyeda, 1975]. This collision inhibits rapid convergence between Borneo and Sulawesi but results in slow deformation of the eastern margin of Borneo island. Conversely, the presence of oceanic crust north and east of Sulawesi facilitates subduction. North of Sulawesi at the Makassar trench, “trench suction” forces [Elsasser, 1971; Forsyth and Uyeda, 1975; Chapple and Tullis, 1977; Chase, 1978] allow the extrusion of material toward the north. The westward motion of the northern part of Sulawesi is hence more easily accommodated by a clockwise rotation of the North Sula Block than by mountain building, since a relatively low stress boundary exists toward the north. The same kind of process has been invoked in other places (e.g. westward extrusion of the Bird’s Head block in western Papua [Pubellier and Ego, 2002; McCaffrey and Abers, 1991; Stevens et al., 2002] or extrusion models for the deformation of Asia in response to the Indian indenter [e.g. Tapponnier et al., 1982]). Similarly, the decrease of the motion from the Banda Sea Block to the Makassar Block might not only be due to a westward decreasing left-lateral shear, but also to collision of the Makassar block with Borneo continental crust. These “colliding resistance” forces would cause the E-W convergence to be instead accommodated on the East Sulawesi Trench, where the Banda Sea oceanic crust can easily subduct under the Makassar block’s continental lithosphere.

#### Interseismic behaviour of faults

The Sulawesi microblocks are surrounded by active faults that produce elastic deformation inside them. We monitored two active strike-slip faults in the region of Sulawesi using two dense local GPS networks. The Gorontalo fault appears to be active although little seismicity is evident in this area. The fault accommodates 11 mm/yr in dextral transtension and is locked to about 10 km depth. The Palu Koro Fault zone accommodates 42 mm/yr and shows a transtensive behaviour more complex than the simple strike slip commonly described (39 mm/yr of left-lateral strike-slip associated with ~11-14 mm/yr of extension). This deformation is most likely explained by the presence of a pull-apart structure that may be localized around the Palu area. We present here two models that can explain the deformation in this area. The first model is a good large-scale approximation and involves one single transtensive fault, while the second involves three closely

## MICROBLOCK ROTATIONS IN SULAWESI, INDONESIA

spaced (~14 km apart) faults with shallow locking depths accommodating a total amount of 30 mm/yr, the remaining motion being accommodated 50 km to the east. That refined three dislocation model has important consequences concerning the seismic hazard: the coexistence of three dislocations with very shallow locking depths may explain the deficit of paleoseismicity on the one studied surface trace of the fault. The GPS inferred slip-rate agrees with the long-term slip-rate determined from stream and fan offsets [Bellier, et al., 2001]. The Lawanopo/Matano Fault zone, extending from the Palu fault toward the south, is probably coupled in the interseismic period. It is still poorly known which of these faults is the southern continuation of the Palu fault. Sulawesi is surrounded by three active trenches. The East Sulawesi Trench accommodates the motion between the Banda Sea and the Makassar block. This trench is affected by periodic earthquakes between which strain is accumulated above the locked subduction plane. To explain our measured velocities properly, another locked fault must be located in the Makassar Strait. Finally, the Minahassa Trench bounds the island to the north and accommodates the motion of the North Sula block relative to the Sunda Plate. We find here a null coupling for this trench that has generated very large subduction earthquakes in the recent past [Gomez et al., 2000]. Hence, this absence of loading can not represent the regular interseismic behaviour of the trench and is certainly a transient state maybe due to afterslip following a recent seismic event [Mazzotti, et al., 2000].

### Limitations of the model

To fully represent the interseismic deformation, the time series of the sites affected by earthquakes should be analysed in terms of transient displacements, co-seismic jumps and post-seismic deformation. Beyond its crucial interest for a better understanding of the earthquake cycle, such modelling can also allow better determination of the interseismic velocity required for kinematic studies. However, constraining coseismic and postseismic deformation requires long and dense (temporally and spatially) time series (ideally those provided by permanent GPS stations) that are still missing at most sites.

The current model explains the data and describes the kinematics and the behaviour of the active structures around Sulawesi. Given the sparseness of the data, the interseismic coupling on several of the faults should only be taken as a first approximation. However, the deformation around Palu and Gorontalo faults is accurately modelled. Our detailed analysis in the Palu area revealed several subsurface splays of the fault unknown prior to this study.

### Acknowledgements

This work is a continuation of the joint research activities in SE Asia, which were initiated by the GEODYSSSEA project. Thanks and appreciation are extended to all people who have contributed significantly in expanding the GPS data base on SE Asia. We would like to thank especially all the staff and students at the Geodesy department of the Institut Teknologi Bandung and the Geodynamics division of the National Coordination Agency for Surveys and Mapping (BAKOSURTANAL) in Indonesia for their contribution to the GPS measurements in Sulawesi. GPS activities in Indonesia were supported by the Dutch Integrated Solid Earth Science (ISES) research program, the French Embassy in Indonesia (Service de Coopération et d'Action Culturelles - SCAC) and the French Ministry of Research (through the ACI "Observation de la Terre" research program). Finally the authors also wish to thank the Jet Propulsion Laboratory (JPL) for their support and advice on using the GIPSY-OASIS GPS software. This paper benefited from very constructive reviews (A.E., M. Keep, L. Wallace and an anonymous associate editor). We want to express special thanks to L. Wallace for her extremely long, detailed and thorough analysis of our work. The maps in this paper were produced using the public domain Generic Mapping Tools (GMT) software [Wessel and Smith, 1995].

### References

- Altamimi, Z., et al. (2002), ITRF2000: A new release of the International Terrestrial Reference frame for earth science applications, *Journal of Geophysical Research-Solid Earth*, 107, art. no.-2214.
- Aurelio, M. A. (2000), Shear partitioning in the Philippines: Constraints from Philippine Fault and global positioning system data, *Island Arc*, 9, 584-597.
- Barrier, E., et al. (1991), Philippine Fault - a Key for Philippine Kinematics, *Geology*, 19, 32-35.
- Beaudouin, T., et al. (2003), Present-day stress and deformation fields within the Sulawesi Island area (Indonesia): geodynamic implications, *Bull. Soc. Geol. Fr.*, 174, 305-317.
- Bellier, O., et al. (2001), High slip rate for a low seismicity along the Palu-Koro active fault in central Sulawesi (Indonesia), *Terr. Nova*, 13, 463-470.
- Bellier, O., et al. (2006), Fission track and fault kinematics analyses for new insight into the Late Cenozoic tectonic regime changes in West-Central Sulawesi (Indonesia), *Tectonophysics*, 413, 201-220.
- Blewitt, G., et al. (1988), GPS geodesy with centimeter accuracy, in *Lecture Notes in Earth Sciences*, edited by E. G. a. R. Strauss, Springer-Verlag, New York.

## MICROBLOCK ROTATIONS IN SULAWESI, INDONESIA

- Bock, Y., et al. (2003), Crustal motion in Indonesia from Global Positioning System measurements, *Journal of Geophysical Research-Solid Earth*, 108, 2367.
- Calmant, S., B. Pelletier, P. Lebellegard, M. Bevis, F. W. Taylor, and D. Phillips (2003), New insights on the tectonics along the New Hebrides subduction zone based on GPS results, *J. Geophys. Res.*, 108(B6), 2319, doi:10.1029/2001JB000644.
- Chamot-Rooke, N., and X. Le Pichon (1999), GPS determined eastward Sundaland motion with respect to Eurasia confirmed by earthquakes slip vectors at Sunda and Philippine trenches, *Earth Planet. Sci. Lett.*, 173, 439-455.
- Chapple, W. M., and T. E. Tullis (1977), Evaluation of the forces that drive the plates, *J. Geophys. Res.*, 82, 1967-1984.
- Chase, C. G. (1978), Extension behind island arcs and motions relative to hot spots, *J. Geophys. Res.*, 83, 5385-5387.
- DeMets, C., et al. (1990), Current plate motions, *Geophysical Journal International*, 101, 425-478.
- DeMets, C., et al. (1994), Effect of recent revisions to the geomagnetic reversal time scale on estimates of current plate motions, *Geophys. Res. Lett.*, 21, 2191-2194.
- Elsasser, W. M. (1971), Sea-floor spreading as thermal convection, *J. Geophys. Res.*, 76, 1101-1112.
- Fitch, T. J. (1972), Plate Convergence, Transcurrent Faults, and Internal Deformation Adjacent to Southeast Asia and Western Pacific, *Journal of Geophysical Research*, 77, 4432-&.
- Fitch, T. J., and W. Hamilton (1974), Plate Convergence, Transcurrent Faults, and Internal Deformation Adjacent to Southeast-Asia and Western Pacific - Reply, *Journal of Geophysical Research*, 79, 4982-4985.
- Forsyth, D., and S. Uyeda (1975), On the relative importance of the driving forces of plate motion, *Geophys. J. R. Astron. Soc.*, 43, 163-200.
- Genrich, J. F., Y. Bock, R. McCaffrey, E. Calais, C. W. Stevens, and C. Subarya, Accretion of the southern Banda arc to the Australian plate margin determined by Global Positioning System measurements, *Tectonics*, 15, 288-295, 1996.
- Genrich, J. F., et al. (2000), Distribution of slip at the northern Sumatran fault system, *Journal of Geophysical Research-Solid Earth*, 105, 28327-28341.
- Gomez, J. M., et al. (2000), The 1996 earthquakes in Sulawesi, Indonesia, *Bull. Seismol. Soc. Amer.*, 90, 739-751.
- Hall, R. (2002), Cenozoic geological and plate tectonic evolution of SE Asia and the SW Pacific: computer-based reconstructions, model and animations, *J. Asian Earth Sci.*, 20, 353-431.
- Hall, R., and M. E. J. Wilson (2000), Neogene sutures in eastern Indonesia, *J. Asian Earth Sci.*, 18, 781-808.
- Hamilton, W. B. (1972), Plate Tectonics of Southeast Asia and Indonesia, *American Association of Petroleum Geologists Bulletin*, 56, 621-&.
- Hinschberger, F., et al. (2000), Origin and evolution of the North Banda Basin (Indonesia): constraints from magnetic data, *Comptes Rendus De L Academie Des Sciences Serie II Fascicule a-Sciences De La Terre Et Des Planètes*, 331, 507-514.
- Kato, T., J. Beavan, T. Matsushima, Y. Kotake, J. T. Camacho, and S. Nakao (2003), Geodetic evidence of back-arc spreading in the Mariana Trough, *Geophys. Res. Lett.*, 30(12), 1625, doi:10.1029/2002GL016757.
- Kreemer, C., et al. (2000), Active deformation in eastern Indonesia and the Philippines from GPS and seismicity data, *Journal of Geophysical Research, B, Solid Earth and Planets*, 105, 663-680.
- Mader, G. L. (1998), GPS Antenna Calibration at the National Geodetic Survey, Technical report available at NGS website, National Geodetic Survey, Silver Spring, US.
- Mazzotti S., et al. (2000), Full interseismic locking of the Nankai and Japan-west Kurile subduction zones: An analysis of uniform elastic strain accumulation in Japan constrained by permanent GPS, *Journal of Geophysical Research, B, Solid Earth and Planets*, 105, 13159-13177.
- McCaffrey, R. (1995), DEFNODE users' guide, (<http://www.rpi.edu/~mccafri/defnode>), edited, Rensselaer Polytechnic Institute, Troy, New York.
- McCaffrey, R., M. D. Long, C. Goldfinger, P. C. Zwick, J. L. Nabelek, C. K. Johnson, and C. Smith (2000), Rotation and plate locking at the southern Cascadia subduction zone, *Geophys. Res. Lett.*, 27, 3117-3120.
- McCaffrey, R., Crustal block rotations and plate coupling, in *Plate Boundary Zones*, S. Stein and J. Freymueller, editors, AGU Geodynamics Series 30, 101-122, 2002.
- McCaffrey, R., Block kinematics of the Pacific - North America plate boundary in the southwestern US from inversion of GPS, seismological, and geologic data, *Journal of Geophysical Research*, 110, B07401, doi:10.1029/2004JB003307, 2005.
- McCaffrey, R., and G. A. Abers (1991), Orogeny in Arc-Continent Collision - the Banda Arc and Western New Guinea, *Geology*, 19, 563-566.
- Michel, G. W., et al. (2001), Crustal motion and block behaviour in SE-Asia from GPS measurements, *Earth Planet. Sci. Lett.*, 187, 239-244.
- Morgan, WJ (1968), Rises, trenches, great faults, and crustal blocks, *J. Geophys. Res.*, 73, p 1959-1982.
- Okada, Y. (1985), Surface deformation due to shear and tensile faults in a half-space, *Bull. Seism. Soc. Am.*, 75, 1135-1154.
- Okada, Y. (1992), Internal deformation due to shear and tensile faults in a half-space, *Bull. Seism. Soc. Am.*, 82, 1018-1040.

## MICROBLOCK ROTATIONS IN SULAWESI, INDONESIA

- Peltzer, G., and F. Saucier (1996), Present-day kinematics of Asia derived from geologic fault rates, *Journal of Geophysical Research-Solid Earth*, 101, 27943-27956.
- Prawirodirdjo, L., et al. (1997), Geodetic observations of interseismic strain segmentation at the Sumatra subduction zone, *Geophys. Res. Lett.*, 24, 2601-2604.
- Prawirodirdjo, L., Y. Bock, J. F. Genrich, S. S. O. Puntodewo, J. Rais, C. Subarya, and S. Sutisna, One century of tectonic deformation along the Sumatran fault from triangulation and GPS surveys, *J. Geophys. Res.*, 105, 28,343– 28,361, 2000.
- Press, W. H., B. P. Flannery, S. A. Teukolsky, and W. T. Vetterling (1989), Numerical Recipes, Cambridge Univ. Press, New York.
- Pubellier, M., and F. Ego (2002), Anatomy of an escape tectonic zone: Western Irian Jaya (Indonesia), *Tectonics*, 21, art. no.-1019.
- Pubellier, M., et al. (1996), Escape tectonics during and after collision in western Irian Jaya, Indonesia, *Eos, Transactions, American Geophysical Union*, 77, 654.
- Puntodewo, S. S. O., et al. (1994), Gps Measurements of Crustal Deformation within the Pacific-Australia Plate Boundary Zone in Irian-Jaya, Indonesia, *Tectonophysics*, 237, 141-153.
- Rangin, C. (1989), The Sulu Sea, a Back-Arc Basin Setting within a Neogene Collision Zone, *Tectonophysics*, 161, 119-141.
- Rangin, C., et al. (1999), Plate convergence measured by GPS across the Sundaland/Philippine Sea Plate deformed boundary; the Philippines and eastern Indonesia, *Geophysical Journal International*, 139, 296-316.
- Savage, J. C. (1983), A dislocation model of strain accumulation and release at a subduction zone, *J. Geophys. Res.*, 88, 4984–4996.
- Savage, J. C., and R. O. Burford (1973), Geodetic determination of relative plate motion in central California, *J. Geophys. Res.*, 78, 832-845.
- Scherneck, H.-G. (1991), A parametrized solid Earth tide mode and ocean loading effects for global geodetic base-line measurements, *Geophysical Journal International*, 106, 677-694.
- Silver, E. A., et al. (1983), Ophiolite Emplacement by Collision between the Sula Platform and the Sulawesi Island-Arc, Indonesia, *Journal of Geophysical Research*, 88, 9419-9435.
- Silver, E. A., et al. (1983), Collision, Rotation, and the Initiation of Subduction in the Evolution of Sulawesi, Indonesia, *Journal of Geophysical Research*, 88, 9407-9418.
- Silver, E. A., and J. C. Moore (1978), Molucca Sea Collision Zone, Indonesia, *Journal of Geophysical Research*, 83, 1681-1691.
- Simons, W. J. F., et al. (1999), Observing plate motions in Southeast Asia; geodetic results of the GEODYSSSEA Project, *Geophys. Res. Lett.*, 26, 2081-2084.
- Simons, W. J. F., et al. (submitted), A Decade of GPS Measurements in S.E. Asia: (Re)Defining Sundaland and it's Boundaries, *J. Geophys. Res.*
- Simons, W. J. F., et al. (2000), Geodynamics of S.E. Asia; first results of the Sulawesi 1998 GPS campaign; IAG general assembly, *IAG general assembly*, 121, 271-277.
- Socquet, A., et al. (2006), India and Sunda Plates motion and deformation along their boundary in Myanmar determined by GPS, *Journal of Geophysical Research*, in press.
- Soehaimi, A., et al. (2006), Geotektonik dan Kegempaan Lajur patahan aktif Palu-Koro dan dinamika Gempabumi Palolo 24 Januari 2005.
- Stevens, C., et al. (1999), Rapid rotations about a vertical axis in a collisional setting revealed by the Palu fault, Sulawesi, Indonesia, *Geophys. Res. Lett.*, 26, 2677-2680.
- Stevens, C. W., et al. (2002), Evidence for Block Rotations and Basal Shear in the World's Fastest Slipping Continental Shear Zone in NW New Guinea, in *Plate Boundary Zones*, S. Stein and J. Freymueller, editors, AGU Geodynamics Series 30, 87-99.
- Tapponnier, P., G. Peltzer, A. Y. Le Dain, R. Armijo, and P. Cobbold (1982), Propagating extrusion tectonics in Asia: New insights from simple experiments with plasticene, *Geology*, 10, 611 –616.
- Tregoning, P., F. K. Brunner, Y. Bock, S. S. O. Puntodewo, R. McCaffrey, J. F. Genrich, E. Calais, J. Rais, and C. Subarya, First geodetic measurement of convergence across the Java Trench, *Geophys. Res. Lett.*, 21, 2135–2138, 1994.
- Tregoning, P., et al. (1998), Estimation of current plate motions in Papua New Guinea from Global Positioning System observations, *J. Geophys. Res.*, 103, 12,181–12,203.
- Tregoning, P., et al. (1999), Motion of the South Bismarck Plate, Papua New Guinea, *Geophys. Res. Lett.*, 26, 3517–3520.
- Tregoning, P., et al. (2000), Present-day crustal motion in Papua New Guinea, *Earth Planets Space*, 52, 727–730.
- Vigny, C., et al. (2002), Migration of seismicity and earthquake interactions monitored by GPS in SE Asia triple junction: Sulawesi, Indonesia, *Journal of Geophysical Research-Solid Earth*, 107, art. no.-2231.
- Wallace, L. M., et al. (2004), GPS and seismological constraints on active tectonics and arc-continent collision in Papua New Guinea: Implications for mechanics of microplate rotations in a plate boundary zone, *J. Geophys. Res.*, 109, B05404, doi:10.1029/2003JB002481.
- Wallace, L. M., et al. (2005), Rapid microplate rotations and backarc rifting at the transition between collision and subduction, *Geology*, 33 (11), 857–860, doi: 10.1130/G21834.1

## MICROBLOCK ROTATIONS IN SULAWESI, INDONESIA

- Walpersdorf, A., et al. (1998), GPS compared to long-term geologic motion of the north arm of Sulawesi, *Earth Planet. Sci. Lett.*, 159, 47-55.
- Walpersdorf, A., et al. (1998), Determining the Sula block kinematics in the triple junction area in Indonesia by GPS, *Geophysical Journal International*, 135, 351-361.
- Walpersdorf, A., et al. (1998), Monitoring of the Palu-Koro fault (Sulawesi) by GPS, *Geophys. Res. Lett.*, 25, 2313-2316.
- Weissel, J. K., and R. N. Anderson (1978), Is There a Caroline Plate, *Earth Planet. Sci. Lett.*, 41, 143-158.
- Wells, D. L., and K. J. Coppersmith (1994), New Empirical Relationships among Magnitude, Rupture Length, Rupture Width, Rupture Area, and Surface Displacement, *Bull. Seismol. Soc. Amer.*, 84, 974-1002.



# Confirmation of Arabia slow motion by new GPS data in Yemen

Christophe Vigny<sup>1</sup>, Philippe Huchon<sup>2</sup>, Jean-Claude Ruegg<sup>3</sup>, Khaled Khanbari<sup>4</sup>, Laike M. Asfaw<sup>5</sup>

**Abstract.** During the last 10 years, a network of about 30 GPS sites was measured in Djibouti, East Africa. Additional points were also measured in Yemen, Oman, Ethiopia, Iran and on La Réunion island. Merged with data from the available IGS permanent stations scattered on the different plates in the area (Eurasia, Anatolia, Africa, Arabia, Somalia), this unique data set provides new insight on the current deformation in the Africa-Somalia-Arabia triple junction area and on the Arabian plate motion. Here we show that coherent motions of points in Yemen, Bahrain, Oman and Iran allow us to estimate a geodetically constrained angular velocity for the Arabian plate ( $52.59^{\circ}\text{N}$ ,  $15.74^{\circ}\text{W}$ ,  $0.461^{\circ}/\text{Myr}$  in ITRF2000). This result differs significantly from earlier determinations and is based upon our vectors in Yemen. They provide new additional data and better geometry for angular velocity determination. Combined with the African and Somalian motions, this new angular velocity results in predicted spreading rates in the Red Sea and the Gulf of Aden which are 15 to 20% lower than those measured from oceanic magnetic anomalies, and thus averaged over the last 3 Myr. With respect to Eurasia, the geodetic motion of Arabia is also about 30% slower than predicted by NUVEL-1A. Based on the kinematic results presented here and on other evidence for a similar slower geodetic rate of the Indian plate, we suggest that the whole collision zone between Africa, Arabia, India on one hand and Eurasia on the other hand has slowed down in the last 3 Ma.

## Introduction

A spectacular test of the plate rigidity hypothesis comes from the general agreement between the NUVEL-1A plate motion model [DeMets *et al.*, 1994] and space geodetic measurements [Larson *et al.*, 1997]. This agreement also suggests that the present-day motions coincide with those averaged over the last 3 Myr. However, plate velocities are known to change through time, although the reason for that remains partly unclear. For example, the dramatic decrease in the relative velocity of India with respect to Eurasia has been attributed to the India-Eurasia collision at about 50 Ma [eg. Patriat and Achache, 1984]. More subtly, the description of the Africa-Eurasia convergence also shows fluctuations [Dewey *et al.*, 1989; Rosenbaum *et al.*, 2002] that are often more difficult to interpret. Part of these variations may be due to errors in the determination of kinematic parameters, but still it appears that, at a given point, increase or decrease of the order of 5 to 20 mm/yr are predicted by plate

kinematics. Therefore there is no a priori reason for present-day plate motions to be identical to those predicted by "geological" instantaneous model such as NUVEL-1A, which is based on measured velocities averaged over the last 3 Myr, in spite space geodetic measurements have often shown a fairly good agreement with NUVEL-1A [Larson *et al.*, 1997]. Given that plate motions obviously change over time, information on how fast and often these changes occur are important for addressing plate dynamics.

Based on space geodetic measurements, McClusky *et al.* [2000] and Kreemer *et al.* [2003] first pointed out that Arabia is currently moving more slowly than predicted by NUVEL-1A. In their global kinematic model, Sella *et al.* [2002] also conclude that some plates, including Arabia and India, may move slower than predicted by NUVEL-1A. They found an angular velocity vector for Arabia ( $51.47^{\circ}\text{N}$ ,  $2.89^{\circ}\text{E}$ ,  $0.521^{\circ}/\text{Myr}$  in ITRF-97 reference frame), significantly different of the NNR-NUVEL-1A vector ( $45.20^{\circ}\text{N}$ ,  $4.40^{\circ}\text{W}$ ,  $0.545^{\circ}/\text{Myr}$ ). However, their determination for the Arabian plate is based on two geodetic sites only (one GPS in Bahrain and one SLR in Riyadh) and may thus be subject to discussion. An updated global model has been recently proposed by Prawirodirjo and Bock [2004] but unfortunately does not handle correctly the Arabia motion since it uses 5 stations which are very close to the Levant Fault or even on the western side of the fault, on the Sinai block, not on Arabia. The analysis of the same stations by Wdowinski *et al.* [2004] indeed shows they are within the zone of elastic strain accumulation. McClusky *et al.* [2003] addressed the question of the Arabia motion with four GPS sites, three

<sup>1</sup>Laboratoire de Géologie, Ecole Normale Supérieure (ENS), CNRS, Paris, France

<sup>2</sup>Laboratoire de Tectonique, Université Pierre et Marie Curie-Paris6 & Institut Océanographique, Paris, France

<sup>3</sup>Institut de Physique du Globe (IPGP), Paris, France

<sup>4</sup>Department of Geosciences, University of Sana'a, Sana'a, Yemen

<sup>5</sup>Addis Observatory, Department of Geophysics, Addis Ababa University, Addis Ababa, Ethiopia

of them (KIZI, GAZI and KRCD) close to the Bitlis suture zone and East Anatolian fault (EAF). Although they argue that the sites are far enough from the main faults to be outside the elastic strain field, using these stations is disputable because of the shortening that may occur further south within the Arabian plate, in the Palmyride fold-and-thrust belt.

A significant improvement of the kinematic constraints on the geodetic motion of Arabia comes from a regional survey performed in Iran and northern Oman [Nilforoushan *et al.*, 2003; Vernant *et al.*, 2004]. Among the 27 GPS sites measured, three (KHAS, KHOS and MUSC) are well within the Arabia plate, away enough from the plate boundary, and were used by Vernant *et al.* [2004], together with BAHR and the three stations of McClusky *et al.* [2003] mentioned above, to derive parameters of rotation for Arabia. We shall discuss their results in comparison with those presented in this paper, in which we use an improved and larger dataset, including four new sites in Yemen and several sites in Djibouti and Ethiopia, to assess the motion of Arabia with respect to neighboring plates

### GPS data set and processing

In November 1991 the first observations of a 30 points GPS network were made in the junction zone of the Somalian, Arabian and African plates around the Afar region [Ruegg *et al.*, 1993, Walpersdorf *et al.*, 1997]. During the following decade, many of those points were remeasured periodically, including a remeasurement of 4 points in Yemen in 2001. Campaigns conducted in the framework of a French-Iranian program provide data on points located in Oman and southern Iran in 1999 and 2001 [Nilforoushan *et al.*, 2003; Vernant *et al.*, 2004]. Data from the 12 Iranian sites of the Asia-Pacific Regional Geodetic Project (APRGP) (1997-2001) are included. Occasional measurement on La Réunion island were also used. As many as 42 stations from the International GPS Service for Geodynamics (IGS) network [Neilan *et al.*, 1995], spanning six plates (Eurasia, Anatolia, India, Africa, Somalia, and Arabia) are included in the processing. This allows not only to improve the spatial coverage where campaign data are scarce, but also allows to “tie” the different networks to each other. The actual number of stations used in each campaign analysis is shown in Table 1.

We analyze our GPS observations with the GAMIT/GLOBK software [King and Bock, 1999, Herring, 1999]. Twenty-four hours measurement sessions are reduced to daily positions using the LC Ionosphere free combination and fixing the ambiguities to integer values when possible. We used precise orbits from the IGS [Beutler *et al.*, 1993], except for the 1991 and 1993 campaigns for which we adjusted global orbits provided by Scripps Institution of Oceanography (SIO). We also used IGS tables for modelling of antenna phase centre variations. We do not use

externally determined meteorological data but rather use the data themselves to estimate tropospheric delay parameters (once every 3 hours). More detailed explanations concerning the older data set processing (1991 to 1995) can be found in Walpersdorf *et al.* [1999]. For most regional scale baselines, length repeatabilities (i.e. root-mean-square dispersion of baselines length about their mean value) steadily improve from around 10 mm in 1991, to standard values of around 1 to 3 mm since 1997.

Solutions in a consistent reference frame were obtained at all epochs by including data from as many IGS permanent stations available around our study area at the time of the campaigns. This list increased from the small number of 4 stations in 1991 to 42 in 2003 and include 16 stations in Europe and central Asia (BRUS, GRAZ, JOZE, KIT3, MADR, MATE, METS, NOTO, ONSA, POL2, POLV, SOFI, USUD, WSRT, WTZR, ZECK), 12 stations in and around Africa (GOUG, HARK, LAMP, MALI, MAS1, MBAR, MSKU, NKLG, RABT, SUTH, TGCV, YKRO), 9 stations in the Middle East (AMMN, ANKR, BAHR, DRAG, DYR2, NICO, NSSP, RAMO, TRAB) and 5 stations spread in the Indian Ocean (DGAR, IISC, MALD, REUN, SEY1). These daily data were combined with the daily global GAMIT solutions from SCRIPPS IGS centre (including more than 200 stations spread all over the world) into a loose system using Helmert type transformations in which translation, rotation, scale and Earth orientation parameters (polar motion and rotation) are estimated. The reference frame is then defined by minimizing, in the least-square sense, the departure from a priori values based on the International Terrestrial Reference Frame (ITRF) 2000 [Altamimi *et al.*, 2002], of the positions and velocities of a set of 22 well determined stations in and around our study area (Ankara (ANKR), Ekaterinburg (ARTU), Bahrein (BAHR), Bruxelles (BRUS), DiegoGarcia (DGAR), Kiev (GLSV), Gough Island (GOUG), Graz (GRAZ), Hartebeesthoek (HARK), Bangalore (IISC), Jozefoslaw (JOZE), Kittab (KIT3), Malindi (MALI), MasPalomas (MAS1), Matera (MATE), Metsohavi (METS), Onsala (ONSA), Bishkek (POL2), Mitzpe Ramon (RAMO), Sutherland (SUTH), Westerboork (WSRT), and Wetzell (WTZR)). The total misfit to those fiducial stations is 2.8 mm for positions (after rejection of IISC and MALI) and 1.6 mm/yr for velocities. Such small values indicate that local velocities are consistently computed in a stable reference frame.

It is long recognized that without adding a proper noise model to GPS data processing we obtain unrealistic very low uncertainties on rates determined over long periods of time. In other words, because we use many epochs the straight line which fits station positions at different epochs is determined with a very low uncertainty, but very commonly does not intersect these epoch positions with their formal uncertainties. This does not mean that the rate inferred from the time

**Table 1.** Data set used for this study<sup>a</sup>.

Site	campaigns																			
	A91	A93.1	A93.2	A93.3	R95	A95	A97	I97	R97	I98	A99	O99	I99	R99	A00	I00	A01	O01	R02	I02
BRUS	-	-	-	-	X	X	X	X	X	X	X	X	X	X	X	X	X	X	X	X
GRAZ	-	X	X	X	X	X	-	X	X	X	X	X	X	-	X	-	X	X	X	-
MADR	X	X	X	X	X	X	X	X	X	-	-	-	-	-	-	X	X	X	X	X
MATE	-	X	X	X	X	X	X	X	X	X	X	X	X	X	X	X	X	X	X	X
METS	-	X	X	X	X	-	-	X	X	-	X	X	X	X	X	X	X	X	X	X
NOTO	-	-	-	-	-	-	-	X	-	X	-	X	X	-	-	X	-	X	-	X
ONSA	X	X	X	X	X	X	X	X	X	X	X	X	X	X	X	X	X	X	X	X
SOFI	-	-	-	-	-	-	X	X	-	X	X	X	-	X	X	X	X	X	X	X
WSRT	-	-	-	-	-	-	X	X	X	X	X	X	X	X	X	X	X	X	X	X
WTZR	X	X	X	X	-	X	X	X	X	X	X	X	X	X	X	X	X	X	X	X
ARTU	-	-	-	-	-	-	-	-	-	-	X	X	X	X	X	X	X	X	X	X
GLSV	-	-	-	-	-	-	-	X	X	X	X	X	X	X	X	X	X	X	X	X
JOZE	-	-	-	X	X	-	-	X	X	X	-	X	X	X	-	X	X	X	X	X
KIT3	-	-	-	-	X	X	X	X	X	-	X	-	-	-	X	X	-	-	X	-
POL2	-	-	-	-	-	X	X	X	X	X	X	X	X	X	X	X	-	X	X	X
USUD	-	X	X	X	X	X	X	X	X	X	X	X	X	X	X	-	X	X	X	X
ZECK	-	-	-	-	-	-	X	X	X	-	X	X	X	-	X	X	X	X	X	X
ADD1	X	-	-	-	X	X	-	-	-	X	-	-	-	-	-	-	-	-	-	X
GOUG	-	-	-	-	-	-	-	-	X	X	X	X	X	X	X	X	X	X	X	X
HARK	-	-	-	-	-	-	-	X	X	X	X	X	X	X	X	X	X	X	X	X
LAMP	-	-	-	-	-	-	-	-	-	X	X	X	-	X	-	X	X	X	X	X
MAS1	-	X	X	X	X	X	X	X	X	X	X	X	X	X	X	X	X	X	X	X
MBAR	-	-	-	-	-	-	-	-	-	-	-	-	-	-	-	-	-	-	-	-
MSKU	-	-	-	-	-	-	-	-	-	-	-	-	-	-	-	-	X	X	-	-
NKLG	-	-	-	-	-	-	-	-	-	-	-	-	-	-	-	X	X	X	X	X
RABT	-	-	-	-	-	-	-	-	-	-	-	-	-	-	-	X	X	X	X	X
SUTH	-	-	-	-	-	-	-	-	X	X	X	X	X	X	X	X	X	X	X	X
YKRO	-	-	-	-	-	-	-	-	-	-	-	-	-	-	-	-	-	-	-	-
CBL0	X	-	-	-	-	X	-	-	-	X	-	-	-	-	-	X	-	-	-	X
GOR0	X	-	-	-	-	-	-	-	-	-	-	-	-	-	-	-	-	-	-	X
LLL0	X	-	-	X	-	X	X	-	-	X	-	-	-	-	-	X	-	-	-	X
MALI	-	-	-	-	-	X	X	X	X	X	X	X	X	X	X	-	X	X	X	X
REUN	-	-	-	-	-	-	-	-	-	-	-	-	X	-	-	-	X	X	X	X
SEY1	-	-	-	-	-	-	X	-	-	-	X	-	-	-	-	X	X	X	-	-
AMMN	-	-	-	-	-	-	-	-	-	-	X	X	X	-	X	-	X	X	-	-
BAHR	-	-	-	-	-	X	X	X	X	X	X	X	X	X	X	X	X	X	X	X
DHAM	X	-	-	-	-	-	-	-	-	-	-	-	-	-	-	X	-	-	-	-
HODD	X	-	-	-	-	-	-	-	-	-	-	-	-	-	-	X	-	-	-	-
JNAR	X	-	-	-	-	-	-	-	-	-	-	-	-	-	-	X	-	-	-	-
KHAS	-	-	-	-	-	-	-	-	-	X	-	-	-	-	-	X	-	-	-	-
KHOS	-	-	-	-	-	-	-	-	-	X	-	-	-	-	-	X	-	-	-	-
MUSC	-	-	-	-	-	-	-	-	-	X	-	-	-	-	-	X	-	-	-	-
SANA	X	X	X	X	-	X	-	-	-	X	-	-	-	-	-	X	-	-	-	-
DRAG	-	-	-	-	-	-	-	-	-	-	-	-	-	-	-	X	X	X	X	X
RSB0	X	-	-	-	-	-	-	-	-	X	-	-	-	-	-	X	X	X	X	X
RAMO	-	-	-	-	-	-	-	-	X	X	X	X	X	X	X	X	X	X	X	X
MALD	-	-	-	-	-	-	-	-	-	X	X	X	-	X	-	X	-	-	X	-
IISC	-	-	-	-	X	X	X	X	X	X	X	X	X	X	X	X	X	X	X	X
DGAR	-	-	-	-	-	X	X	X	X	X	X	X	X	X	X	-	-	X	-	-
ANKR	-	-	-	-	-	X	X	X	X	X	X	X	X	X	-	X	X	X	X	X
NICO	-	-	-	-	-	-	X	X	-	X	X	X	-	X	X	X	X	X	X	X
NSSP	-	-	-	-	-	-	-	X	-	-	-	-	-	-	-	X	-	X	-	X
TRAB	-	-	-	-	-	-	-	-	-	-	-	-	-	-	-	X	X	X	X	X
AHVA	-	-	-	-	-	-	-	-	-	-	-	-	-	-	-	X	-	-	-	-
LADA	-	-	-	-	-	-	X	-	X	-	X	-	X	-	X	-	-	-	-	-
MARI	-	-	-	-	-	-	X	-	X	-	X	-	X	-	-	-	-	-	-	-
MASH	-	-	-	-	-	-	-	-	-	-	X	-	-	X	-	X	-	-	-	-
MIAN	-	-	-	-	-	-	-	-	-	-	X	-	-	-	-	X	-	-	-	-
NILO	-	-	-	-	-	-	X	-	X	-	X	-	-	-	-	-	-	-	-	-
REIH	-	-	-	-	-	-	X	-	X	-	X	X	-	-	-	X	-	-	-	-
ROSE	-	-	-	-	-	-	X	-	X	-	X	-	X	-	X	-	X	-	-	-
SHIR	-	-	-	-	-	-	-	-	-	-	X	-	-	-	-	X	-	-	-	-
TEHN	-	-	-	-	-	-	-	-	-	-	-	-	-	-	-	X	-	-	-	-
YAS1	-	-	-	-	-	-	-	X	-	X	-	X	-	-	-	X	-	X	-	-
ZABO	-	-	-	-	-	-	-	-	-	-	X	-	-	X	-	X	-	-	-	-

<sup>a</sup>Crosses indicate whether a given station is available at the date of the campaign : Afar (A), Oman (O), Reunion (R), Iran (I), followed by the year final two digits. The precise denomination and dates of the GPS campaigns are : AFAR91 : 1991.9152, AFAR93-1 : 1993.0790, AFAR93-2 : 1993.2711, AFAR93-3 : 1993.9501, REUN95 : 1995.0315, AFAR95 : 1995.2479, AFAR97 : 1997.1301, IRAN97 : 1997.7959, REUN97 : 1997.9192, IRAN98 : 1998.9082, AFAR99 : 1999.1466, OMAN99 : 1999.7356, IRAN99 : 1999.8562, REUN99 : 1999.9164, AFAR00 : 2000.5150, IRAN00 : 2000.7882, AFAR01 : 2001.2233, OMAN01 : 2001.7959, REUN02 : 2002.0534, IRAN02 : 2002.7795, AFAR03 : 2003.2342

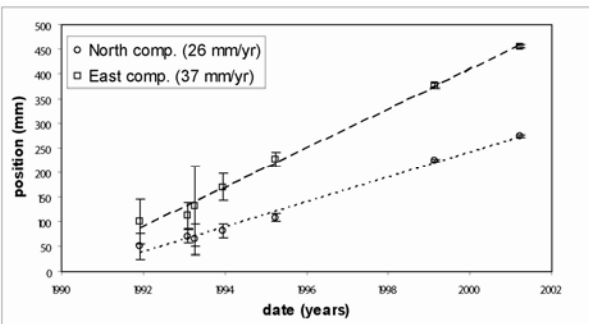


**Figure 1.** SANA time series in ITRF2000. North component (circles, short dashed line), East component (squares, long dashed line). Error bars show the  $3\sigma$  uncertainties.

series is in error, but that its uncertainty is not correct. When using continuous measurements and daily time series, robust mathematical models of different kinds of noise (white noise, random-walk noise, flicker noise) can be tested and applied to the data (for a complete discussion see e.g. [Williams *et al.*, 2004]). Unfortunately, for campaign like measurements it is an impossible task to infer the noise model from the data themselves and we have to use a-priori assumption on the noise nature. One way of estimating realistic uncertainties is to simply rescale them (i.e. multiply them with an “ad hoc” factor). This factor can be determined as the ratio between the long term noise (the difference between actual epoch positions and positions predicted using the linear fit) and the epoch formal uncertainty. A better way, more robust and better suited to GPS monuments behaviour, is to consider that a time dependent noise (i.e. random walk noise) is present in the determination of the stations position. In our processing, this is done by adding a moderate Markov noise ( $2 \text{ mm}/\text{sqrt(yr)}$ ) to the coordinates of stations when combining the daily solutions, following the procedures described in [Herring *et al.*, 1990] and [Herring *et al.*, 1999]. Applying this strategy does not affect the velocity determination by more than 1 to 2 mm/yr but leads to the estimation of more realistic velocity uncertainties (1-2 mm/yr instead of the formal a-priori value of 0.1 mm/yr). However, adding this noise to all stations would considerably alter the reference frame determination. Therefore we choose not to apply this noise model to the 22 global “reference” stations described earlier. Hence, these stations still exhibit sub-millimetre uncertainties. When used to determine a pole rotation for a given plate, we multiply these velocity uncertainties by a factor of 10, to make them comparable to the average uncertainty of regional stations (1.3 mm/yr).

As an example, figure 1 depicts the time series (station position as a function of time) of our station in Sana'a, Yemen. This station was occupied 7 times between 1991 and 2001, and although the older

measurements suffer from higher uncertainties and are affected by a less accurate realization of the reference frame, the velocity of this station is determined with a very small uncertainty (0.7 mm/yr on both horizontal components).

Inversion of velocity data to obtain an angular velocity vector and associated uncertainties was performed by minimization of the weighted, L1-norm sum of misfits. The choice of the L1 rather than L2 norm (or standard least squares) is justified by our wish to avoid too much emphasis on stations with large misfits (or “outliers”). Once an angular velocity is computed, we followed the procedure described by Fernandes *et al.* [2003] and checked that the obtained solution is stable with respect to the data set. First, we recompute the angular velocity vector with an unweighted scheme in order to check that the solution is not forced by the stations with the smaller uncertainties. Next, we checked that removing one or two of the stations does not change significantly the angular velocity vector.

## Results

Velocities in the ITRF2000 and relative to different plates are given in Table 2. Figure 2 depicts large scale velocities in a Eurasian reference frame. Given the limited number (16) of Eurasian stations used in this study (most of which actually being in Europe) we choose not to estimate our own Eurasian reference frame but to use an external and well determined Eurasia [Calais *et al.*, 2003]. Stations located in stable Eurasia exhibit very small residual velocities ( $< 1 \text{ mm/yr}$ ) in this reference frame, indicating that our solution is consistent with Calais *et al.* [2003]. However, stations in the most southern part of central Eurasia (ZECK, KIT3, POL2) show small but significant velocities relative to the rigid plate model. These velocities may be due to a slightly different rigid rotation pole, or may be representative of widespread deformation near these boundaries of the Eurasian plate [Nocquet *et al.*, 2001; Wang *et al.*, 2001; Banerjee and Bürgmann, 2002; Sella *et al.*, 2002].

### Motion of individual plates

The Africa (Nubia), Somalia and Arabia plate motions are difficult to assess precisely given the small number of sites on these plates. Nevertheless, it is very clear that sites on the eastern side of the East African Rift and supposedly on the Somalia plate (MALI, SEY1, REUN) show a different block motion than sites on the western side of the East African Rift (MAS1, RABT, LAMP, NKLG, GOUG) and supposedly on stable Africa. Some sites located closer to the East African Rift have needed closer inspection to determine whether they belong to Africa or Somalia, but the result was generally unambiguous: for instance, although HART and SUTH are located close to the plate boundary, their motion is

**Table 2.** station positions, velocities in ITRF2000 and relative to Eurasia, Africa, Somalia and Arabia plates, and uncertainties (1-□). Bold numbers highlight stations velocity residuals with respect to the plate they belong to. Station names in bold indicate stations used for the mapping in ITRF2000.

Plate Or country	ITRF2000												sigmas		Corr.	
	site	Long.	Lat.	Ve	Vn	Ve	Vn	Ve	Vn	Ve	Vn	dVe	dVn			
Eurasia	<b>BRUS</b>	4,36	50,80	18,0	13,8	<b>-0,4</b>	<b>-1,7</b>	4,5	-4,9	-3,2	-10,1	14,9	3,1	0,05	0,03	0,022
	<b>GRAZ</b>	15,49	47,07	21,8	14,2	<b>0,6</b>	<b>0,1</b>	4,6	-4,4	-3,8	-8,3	13,6	-2,0	0,06	0,04	-0,030
	MADR	-4,25	40,43	18,9	15,6	<b>0,1</b>	<b>-0,7</b>	4,1	-2,7	-2,8	-8,8	7,7	9,4	0,63	0,61	-0,001
	<b>MATE</b>	16,70	40,65	24,8	17,9	<b>2,4</b>	<b>4,0</b>	5,7	-0,7	-2,4	-4,4	11,0	1,2	0,05	0,03	0,005
	<b>METS</b>	24,40	60,22	20,5	11,5	<b>0,2</b>	<b>-1,0</b>	4,6	-6,5	-4,3	-9,2	20,9	-8,6	0,05	0,04	-0,038
	NOTO	14,99	36,88	21,5	18,1	<b>-1,0</b>	<b>4,0</b>	2,0	-0,5	-5,9	-4,4	5,0	2,2	0,91	0,90	0,000
	<b>ONSA</b>	11,93	57,40	17,2	13,5	<b>-1,2</b>	<b>-1,1</b>	3,9	-5,2	-4,4	-9,5	18,5	-1,0	0,04	0,03	-0,045
	SOFI	23,40	42,56	24,7	11,6	<b>1,5</b>	<b>-1,1</b>	4,6	-6,5	-3,9	-9,4	11,0	-8,1	0,86	0,85	0,000
	<b>WSRT</b>	6,61	52,92	18,3	15,3	<b>0,0</b>	<b>0,0</b>	5,0	-3,5	-2,9	-8,4	16,7	3,4	0,06	0,04	-0,019
	WTZR	12,88	49,14	20,9	14,4	<b>0,5</b>	<b>-0,1</b>	4,8	-4,3	-3,5	-8,5	14,9	-0,5	0,05	0,03	-0,003
	<b>ARTU</b>	58,56	56,43	23,8	4,0	<b>-1,5</b>	<b>-0,2</b>	-0,8	-8,0	-9,9	-5,9	8,3	-26,0	0,38	0,27	-0,023
	GLSV	30,50	50,36	20,9	12,2	<b>-2,3</b>	<b>1,0</b>	0,9	-5,1	-8,1	-7,0	11,6	-10,3	1,00	0,98	0,001
	<b>JOZE</b>	21,03	52,10	22,0	12,9	<b>0,6</b>	<b>-0,2</b>	4,7	-5,4	-4,0	-8,5	16,7	-5,7	0,06	0,04	0,016
	<b>KIT3</b>	66,89	39,14	30,9	3,2	<b>3,8</b>	<b>1,4</b>	3,2	-6,5	-5,1	-3,3	1,9	-27,7	0,07	0,04	-0,012
	<b>POL2</b>	74,69	42,68	26,2	3,0	<b>-0,9</b>	<b>3,4</b>	-2,2	-4,5	-10,2	-0,3	-3,9	-28,2	0,08	0,04	-0,044
	USUD	138,36	36,13	-4,2	-9,2	-25,7	6,0	-31,0	3,0	-34,2	11,1	-53,6	-22,8	0,71	0,67	-0,015
	ZECK	41,57	43,79	25,9	10,5	<b>0,5</b>	<b>1,8</b>	2,3	-5,1	-6,6	-5,4	8,1	-15,7	0,87	0,85	0,000
Africa	ADD1	38,77	9,04	25,3	16,5	1,8	7,1	<b>1,3</b>	<b>0,4</b>	-4,4	-0,3	-12,1	-8,9	0,70	0,65	0,002
	<b>GOUG</b>	<b>-9,88</b>	-40,35	22,7	18,4	7,6	1,8	<b>1,7</b>	<b>0,5</b>	1,4	-6,0	-28,4	15,2	0,16	0,09	-0,219
	<b>HARK</b>	27,71	-25,89	17,2	18,0	2,9	6,1	<b>-0,5</b>	<b>0,3</b>	-1,1	-1,9	-29,3	-3,5	0,09	0,05	0,077
	LAMP	12,61	35,50	19,9	18,3	-2,4	3,8	<b>0,5</b>	<b>-0,4</b>	-7,2	-4,6	2,7	3,5	1,11	1,07	-0,002
	<b>MAS1</b>	-15,63	27,76	16,6	17,2	-2,7	0,5	<b>0,0</b>	<b>0,0</b>	-6,0	-7,0	-4,9	17,1	0,06	0,03	0,045
	NKLG	9,67	0,35	17,1	23,6	-4,5	8,7	<b>-5,6</b>	<b>4,8</b>	-10,2	0,3	-23,5	10,2	1,30	1,23	-0,004
	MSKU	13,55	-1,63	34,6	28,8	13,3	14,4	<b>12,0</b>	<b>10,1</b>	7,7	6,0	-6,8	13,5	6,43	3,66	0,050
	RABT	-6,85	34,00	14,4	16,1	-5,1	-0,3	<b>-1,8</b>	<b>-2,1</b>	-8,4	-8,4	-2,2	11,3	1,35	1,28	-0,005
	<b>SUTH</b>	20,81	-32,38	15,7	18,7	3,0	5,5	<b>-1,3</b>	<b>0,4</b>	-1,1	-2,8	-32,1	0,1	0,10	0,06	0,003
	CBL0	43,07	11,46	29,4	16,1	5,5	7,8	5,0	0,7	<b>-1,0</b>	<b>0,6</b>	-7,3	-10,6	0,69	0,63	0,001
Somalia	GOR0	42,22	11,31	31,1	16,1	7,1	7,6	6,7	0,6	<b>0,7</b>	<b>0,4</b>	-5,6	-10,3	0,88	0,67	0,002
	LLL0	42,58	11,26	30,3	15,6	6,4	7,1	6,0	0,1	<b>0,0</b>	<b>0,0</b>	-6,4	-10,9	0,68	0,63	-0,002
	<b>MALI</b>	40,19	-3,00	26,5	14,2	5,7	5,1	4,3	-1,7	<b>0,3</b>	<b>-2,2</b>	-15,1	-11,6	0,14	0,05	-0,018
	REUN	55,57	-21,21	17,6	10,6	3,2	5,6	1,4	-2,1	<b>0,1</b>	<b>-0,4</b>	-24,0	-18,9	1,31	1,13	0,009
	SEY1	55,48	-4,67	21,2	9,1	1,0	4,1	-0,4	-3,6	<b>-4,2</b>	<b>-1,9</b>	-20,3	-20,4	1,36	1,05	0,028
	AMMN	35,88	32,03	20,8	17,5	-4,5	7,5	-3,1	0,9	-11,2	-0,2	<b>-3,4</b>	<b>-6,9</b>	1,34	1,30	0,000
Arabia	<b>BAHR</b>	50,61	26,21	31,6	28,6	5,4	22,3	5,6	14,8	-2,1	15,8	<b>0,6</b>	<b>0,1</b>	0,07	0,03	0,023
	DHAM	44,39	14,58	35,6	28,0	11,1	20,0	10,8	12,9	4,4	13,0	<b>0,1</b>	<b>1,0</b>	0,83	0,73	-0,016
	HODD	42,97	14,79	35,3	26,8	10,8	18,5	10,6	11,5	4,2	11,4	<b>0,1</b>	<b>0,2</b>	1,03	0,76	-0,053
	JNAR	43,44	13,32	37,2	26,7	12,9	18,5	12,6	11,5	6,3	11,4	<b>1,2</b>	<b>0,0</b>	1,29	0,83	-0,067
	KHAS	56,23	26,21	30,3	29,1	3,9	24,2	3,7	16,6	-3,8	18,3	<b>-2,0</b>	<b>-0,6</b>	1,50	1,40	-0,001
	KHOS	48,41	30,25	27,2	24,5	0,9	17,6	1,4	10,2	-6,6	10,9	<b>-1,2</b>	<b>-3,5</b>	1,60	1,45	-0,002
	MUSC	58,57	23,56	33,9	29,9	7,7	25,7	7,3	18,0	0,0	20,1	<b>-0,1</b>	<b>-0,1</b>	1,44	1,40	-0,002

	REIH	51,08	28,92	27,2	29,5	0,8	23,2	1,1	15,8	-6,8	16,8	<b>-2,6</b>	<b>0,8</b>	1,02	1,00	-0,001
	SANA	44,19	15,35	37,0	26,5	12,3	18,5	12,1	11,4	5,6	11,4	<b>1,8</b>	<b>-0,5</b>	0,77	0,72	-0,013
	DRAG	35,39	31,59	24,4	19,3	-0,9	9,2	0,5	2,7	-7,6	1,5	<b>0,0</b>	<b>-4,9</b>	1,14	1,09	0,004
	<b>RAMO</b>	34,76	30,60	17,7	15,8	-7,5	5,5	-6,2	-1,0	-14,2	-2,2	<b>-7,3</b>	<b>-8,3</b>	0,10	0,04	0,022
	RSB0	43,36	11,98	36,7	24,6	12,6	16,4	12,2	9,3	6,1	9,3	<b>0,2</b>	<b>-2,1</b>	1,21	1,01	-0,010
India	<b>DGAR</b>	72,37	-7,27	46,4	31,2	27,1	31,0	26,0	23,1	22,4	27,0	5,9	0,1	0,18	0,07	0,128
	<b>IISC</b>	77,57	13,02	37,4	32,9	12,7	34,2	11,3	26,4	5,4	30,9	-2,7	1,8	0,10	0,04	-0,036
	MALD	73,53	4,19	36,4	42,5	13,7	42,6	12,5	34,7	7,5	38,8	-4,2	11,3	1,10	1,06	0,001
Anatolia	<b>ANKR</b>	32,76	39,89	-2,2	13,1	-26,9	2,4	-24,7	-3,9	-33,3	-5,4	-20,3	-10,2	0,07	0,03	0,038
	NICO	33,40	35,14	19,2	14,6	-5,8	4,0	-4,0	-2,3	-12,3	-3,8	-2,4	-8,9	0,86	0,85	0,001
	NSSP	44,50	40,23	28,8	15,2	2,9	7,2	4,3	0,1	-4,4	0,2	7,7	-11,9	0,97	0,96	0,001
	TRAB	39,78	41,00	24,8	11,1	-0,6	2,0	1,2	-4,8	-7,5	-5,4	5,7	-14,6	1,30	1,26	0,003
Iran	AHVA	48,68	31,34	27,3	23,4	1,0	16,5	1,5	9,2	-6,6	9,9	-0,5	-4,7	2,19	2,04	0,005
	LADA	55,90	28,29	29,1	24,9	2,5	20,0	2,5	12,4	-5,3	14,1	-2,1	-4,6	1,20	1,16	-0,003
	MASH	59,47	36,31	24,9	6,3	-2,1	2,4	-2,1	-5,4	-10,4	-3,2	-3,2	-23,8	1,51	1,45	-0,003
	MIAN	46,16	36,91	25,9	21,1	-0,3	13,6	0,8	6,3	-7,8	6,7	2,1	-6,4	1,50	1,41	0,000
	MARI	51,81	35,73	27,8	17,2	1,2	11,2	1,8	3,7	-6,6	4,9	1,7	-11,5	1,46	1,40	-0,004
	NILO	48,34	32,42	20,2	25,6	-6,2	18,6	-5,5	11,3	-13,7	11,9	-6,9	-2,5	1,46	1,40	-0,002
	ROSE	53,82	32,31	23,6	19,8	-3,0	14,3	-2,8	6,7	-10,9	8,2	-5,0	-9,4	1,02	1,00	0,000
	SHIR	57,31	37,81	26,0	9,8	-0,9	5,3	-0,7	-2,5	-9,1	-0,5	-0,6	-20,0	1,48	1,40	0,000
	TEHN	51,33	35,70	32,4	16,5	5,8	10,4	6,4	2,9	-2,0	4,0	6,4	-12,1	2,16	2,03	0,001
	YAS1	58,46	35,29	31,2	12,3	4,3	8,1	4,3	0,4	-4,0	2,5	2,8	-17,7	1,03	1,00	-0,001
	ZABO	61,52	31,05	29,7	6,7	2,8	3,4	2,4	-4,5	-5,5	-2,0	14,9	3,1	1,52	1,45	-0,003

better fit with Africa than with Somalia (although the difference is small), in agreement with their location to the west of the East African Rift.

## Africa

*Sella et al.* [2002] used five sites on the African plate (GOUG, HART, HRAO, MASP and SUTH), two of them being very close (HRAO and HART) making their solution actually constrained by only four sites. *Fernandes et al.* [2003] used a larger data set of ten stations, including five IGS stations (MAS1, HRAO, SUTH, GOUG and NKLG). In addition to MAS1, SUTH, GOUG and NKLG (we did not use HRAO because no data was available during the campaigns), we used five additional sites in our analysis: HARK (that replaced HART), RABT, LAMP and NOTO in North Africa and Sicily, and ADD1, the site in Addis Ababa that belongs to our regional network. In spite of the small number (9) of sites, the African plate is spatially reasonably well covered. We computed an angular velocity vector ( $50.48^{\circ}\text{N}$ ,  $82.01^{\circ}\text{W}$ ,  $0.265^{\circ}/\text{Myr}$ ) with respect to ITRF2000 (Table 3), not significantly different from that of *Fernandes et al.* [2003] at the  $1-\square$  level. It differs from that of *Sella et al.*'s [2002] but the reference frame (ITRF97) is also different. Note that since *Calais et al.* [2003] do not

give the parameters of rotation for Africa with respect to ITRF2000, we computed them from their Africa-Eurasia solution and from the Eurasia motion in ITRF2000 with an angular velocity vector ( $52.3^{\circ}\text{N}$ ,  $107.0^{\circ}\text{W}$ ,  $0.245^{\circ}/\text{Myr}$ ) [*Calais*, pers. comm., 2004]. Figure 4 shows the individual misfits at the 9 sites we used. The RMS residual is 0.9 mm/yr and the misfit at all stations is less than 2 mm/yr except for RABT and NKLG. These two stations however may not be reliable. The north component of the velocity at RABT indeed shows oscillations and the time series is noisy, and the velocities at NKLG provided by various processing centres are surprisingly very different, suggesting some technical problems. However, we kept these two stations, because removing them does not change significantly the solution ( $50.43^{\circ}\text{N}$ ,  $-82.96^{\circ}\text{E}$ ,  $0.266^{\circ}/\text{Myr}$ ). We also recomputed the angular velocity vector with an unweighted procedure and found a very small difference ( $0.2^{\circ}$  in latitude,  $0.3^{\circ}$  in longitude, same rate). Finally, we concur with *McClusky et al.* [2003] and *Fernandes et al.* [2003] that the geodetic African motion, in spite of the relatively small number of stations and the use of stations close to plate boundary which velocity could be affected by deformation is now reasonably well constrained.

## Afar 91 - 03 - sol28m2 (ITRF 2000)

relative to GPS Eurasia (52.3,-107.0,0.245)

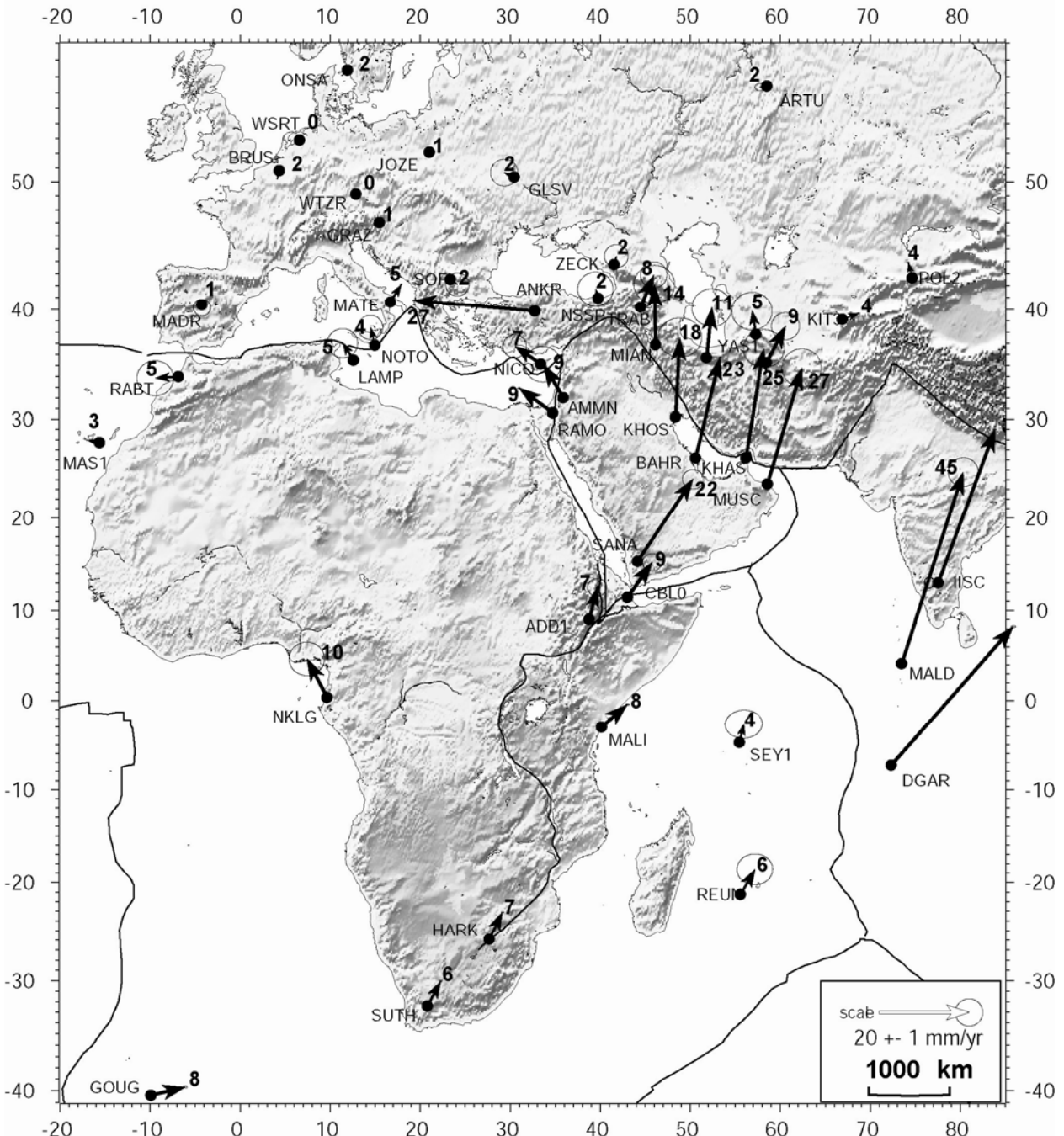


**Figure 2.** Large scale velocities in the ITRF2000 reference frame, relative to Eurasia as defined by Calais et al. (2003). Ellipses show the 99% confidence level of the a-priori formal uncertainties given in table 2. Numbers next to arrow heads indicate the station velocity in mm/yr.

### Somalia

The motion of Somalia is constrained by even less data than Africa: only two sites (MALI and SEY1) were used by Sella et al. [2002], making the

determination of the pole unambiguous, but not well constrained. Fernandes et al. [2003] used four sites (MALI, SEY1, REUN and RBAY). We did not use RBAY in our computations because no data was available during the various campaigns, but we added three sites of the Djibouti regional network which are

## Afar 91 - 03 - sol28m2 (ITRF 2000)

relative to GPS Arabia (52.6,-15.7,0.461)

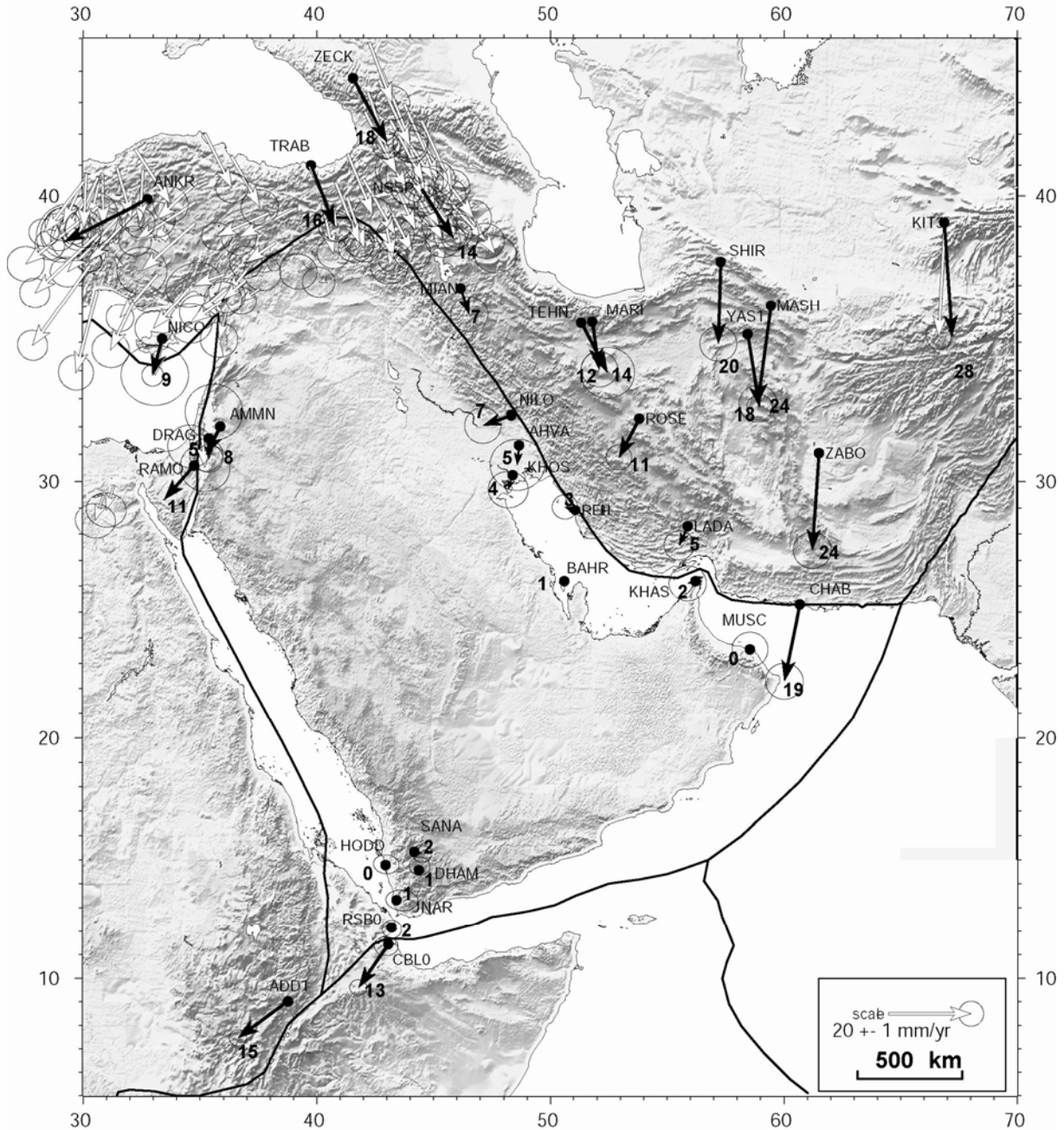


**Figure 3.** Arabian sites velocities in the ITRF2000 reference frame, relative to Arabia defined in this work. Black arrows depict our solution, white arrows are for McClusky *et al.* [2000]. For our solution, ellipses show the 99% confidence level of the velocity uncertainties given in table 2. Numbers next to arrow heads indicate the station velocity in mm/yr.

clearly outside the deforming zone: CBL0, LLL0 and GOR0 [Vigny *et al.*, submitted, 2004]. Inversion of the velocities at these 6 sites leads to an angular velocity vector ( $47.69^{\circ}\text{N}$ ,  $98.32^{\circ}\text{W}$ ,  $0.330^{\circ}/\text{Myr}$ ). In spite of a poor fit at SEY1 (4 mm/yr), the RMS residual on the 6 velocities is 0.8 mm/yr (Figure 5). We checked the stability of our solution in the same way as for Africa. The unweighted inversion leads to nearly the same

angular velocity vector (only the latitude differs by  $0.04^{\circ}$ ) but removing SEY1, for which the time series shows numerous gaps, slightly changes the solution ( $48.12^{\circ}\text{N}$ ,  $97.75^{\circ}\text{W}$ ,  $0.329^{\circ}/\text{Myr}$ ) (Table 3). Our solution for Somalia thus significantly differs from previous ones because it uses constraints in the northern part of the plate (sites CBL0, LLL0 and GOR0). Sella *et al.*'s [2002] and Fernandes *et al.*'s [2003] models show

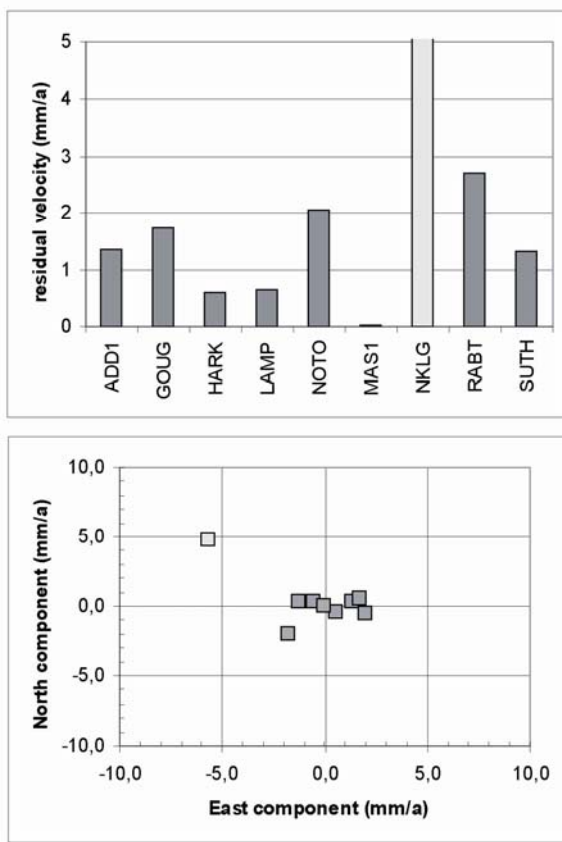


**Figure 4.** African plate stations residual velocities with respect to our determination of the African plate motion. Velocity magnitudes (top) and velocity components (bottom) in mm/yr. Light grey shaded symbols depict stations with high velocity uncertainties or lying in deformation zones (usually not used in the pole determination).

discrepancies of 2 to 4 mm/yr at these northern sites. At other sites (MALI, REUN, SEY1), the difference is small. Although the angular velocity vector is not as well constrained as the Africa one, we are thus fairly confident that our determination of the Somalia motion provides a better estimate than previously done, a point that will be critical when dealing with relative motion around the Africa-Arabia-Somalia triple junction. Because it uses data in the northern part of the Somalia plate, our Somalian angular velocity vector provides a better estimate of the motion of Arabia with respect to the nearby part of Somalia, which was not the case with previous models.

### Arabia

In this work, the Arabia plate motion is constrained by a total of eleven sites: four stations in Yemen (DHAM, HODD, JNAR and SANA), two in Oman (MUSC, KHAS), one in Bahrein (BAHR) and two in Iran (KHOS, REIH), one in northern Djibouti, on the stable Danakil block (RSB0) and one in Jordan (AMMN) (Figure 3). We did not use DRAG in our kinematic inversion because it shows elastic coupling with the Levant Fault. In terms of the number of sites and, even more important, spatial coverage, this is a significant improvement over previous models that used from only two [Sella et al., 2002], four [McClusky et al., 2003] and six [Vernant et al., 2004]. Velocities of those 11 stations fit a rigid rotation about an angular velocity vector ( $52.26^{\circ}\text{N}$ ,  $12.27^{\circ}\text{W}$ ,  $0.470^{\circ}/\text{Myr}$ ). The RMS residual is 1.2 mm/yr, although one station (AMMN) shows a very large misfit (9 mm/yr). Although no technical problem has been reported, the time series available show that the north component of the velocity does not fit a straight line. Discarding this station gives an angular velocity vector ( $52.59^{\circ}\text{N}$ ,  $15.74^{\circ}\text{W}$ ,  $0.461^{\circ}/\text{Myr}$ ) (Table 3), thus more to the West at nearly the same latitude and accordingly with a smaller rate. As for Africa and Somalia, we checked that our solution is stable with respect to the inversion scheme.

**Table 3.** Rotation parameters of Africa (AFR), Somalia (SOM), Arabia (ARA), and India (IND) with respect to ITRF2000 (ITRF-97 for Sella et al.). Uncertainty on the pole location is given by the semi-major ( $\square$  maj) and semi-minor ( $\square$  min) axes of the  $1-\square$  error ellipse (azim. is the azimuth of the semi-major axis)

Plate	Lat. $^{\circ}\text{N}$	Long. $^{\circ}\text{E}$	Rate $^{\circ}/\text{Myr}$	Rate $\sigma$ $^{\circ}/\text{Myr}$	$\sigma_{\text{maj}}$ ( $^{\circ}$ )	$\sigma_{\text{min}}$ ( $^{\circ}$ )	azim. ( $^{\circ}$ )	Reference
AFR	50.48	-82.01	0.265	0.003	1.26	0.74	276	this work
	46.64	-86.32	0.251					Calais et al. [2003]
	50.86	-81.47	0.261	0.002	1.03	0.60	95	Fernandes et al. [2003]
	52.25	-80.18	0.253	0.004	1.6	0.9	277	Sella et al. [2002]
SOM	48.12	-97.75	0.329	0.008	4.36	0.70	316	this work
	54.63	-93.61	0.315	0.007	2.30	0.73	54	Fernandes et al. [2003]
	53.51	-101.55	0.310	0.002	0.9	0.1	42	Sella et al. [2002]
ARA	52.59	-15.74	0.461	0.011	2.98	0.42	81	this work
	51.47	2.89	0.521	0.024	3.1	0.7	290	Sella et al. [2002]
IND	50.90	-12.13	0.487	0.010	5.11	0.61	288	Socquet et al. [2004]

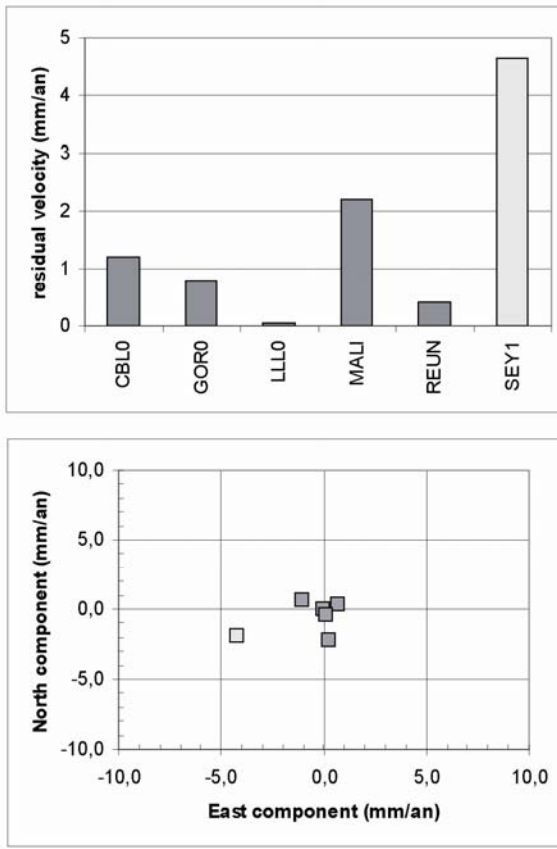


**Figure 5.** Somalian plate stations residual velocities with respect to our determination of the Somalian plate motion. Velocity magnitudes (top) and velocity components (bottom) in mm/yr. Light grey shaded symbols depict stations with high velocity uncertainties or lying in deformation zones (usually not used in the pole determination).

Removing the two stations with misfits larger than 2 mm/yr (KHOS and REIH) slightly displace the pole of rotation toward the West (by about  $2^\circ$ ) and reduces accordingly the angular rate, but, in the same way as for the two poorly fit African stations (RABT and NKLG), we decided to keep these two stations in our solution.

Two other stations may pose problem: KHAS in Oman is extremely close to the boundary in the straits of Hormuz and RSB0 in Djibouti on the Danakil block is within the Afar triple junction. Their velocity could be affected by elastic effects due to coupling with plate boundaries (KHAS) or distributed strain in a complex RRR triple junction (RSB0). However, rejecting them (which was done in a first estimation) does not change the determination of the plate angular velocity. Thus, it is an a-posteriori conclusion that, despite their proximity with plate boundaries, these stations velocities are in fact not affected by deformation. Or, if they are, it is small enough and affecting a sufficiently small number of points (2 out of 11) so that it does not affect the determination of the plate motion. The rotation

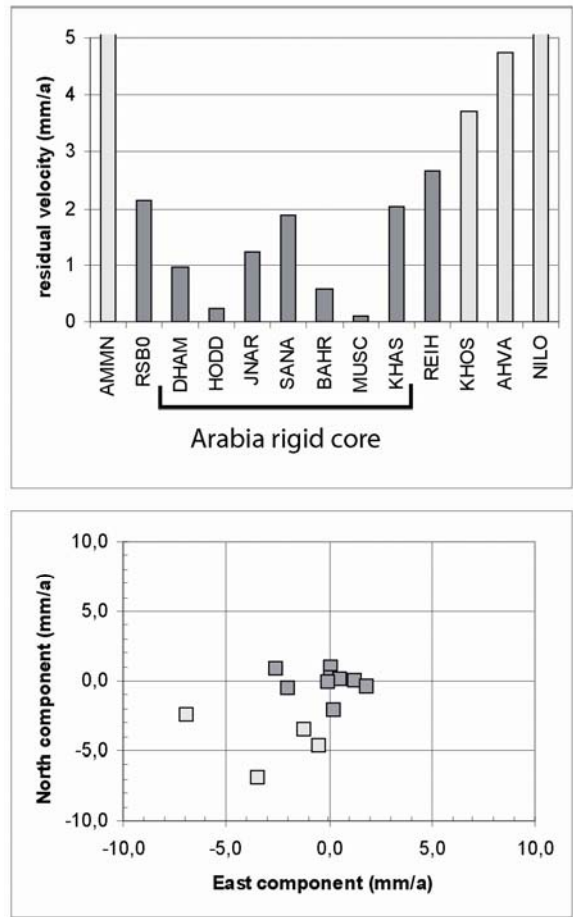


**Figure 6.** Arabian plate stations residual velocities with respect to our determination of the Arabian plate motion. Velocity magnitudes (top) and velocity components (bottom) in mm/yr. Light grey shaded symbols depict stations with high velocity uncertainties or lying in deformation zones (usually not used in the pole determination).

parameters we computed significantly differ from those determined by *Sella et al.* [2002]. Unfortunately, *McClusky et al.* [2003] and *Vernant et al.*, [2004] do not provide their velocities and rotation parameters in ITRF, so that we cannot make a direct comparison with our solution. When compared with our measurements in Yemen, the predictions of *Sella et al.*'s [2002] model show significant, 3 to 4 mm/yr discrepancies. Consequently, as in the case of the Somalia plate, adding new sites where data were not previously available does change the rotation parameters, even if the predicted motion on previously existing sites is not significantly modified. In other words, we find a different rotation pole than previous studies because of new vectors in Yemen, but this different pole still predicts the same velocities than those previous studies at common stations (in particular in Oman). Therefore, these previous studies are not erroneous (decimating our data we obtain the same results), but simply lack data in the South-Western "corner" of the plate. With the

exception of AMMN and, to a less extend of KHOS and REIH, the residual velocities are small at all sites ( $< 2 \text{ mm/yr}$ ) and show no systematic trend (Figure 6). Even at KHOS and REIH, the misfit does not exceed the  $2\sigma$  uncertainty. We thus consider that these residual velocities represent the noise of our solution and therefore demonstrate the rigidity of the Arabian plate at this level of around  $2 \text{ mm/yr}$ , or less than  $10^{-9}$  strains/yr.

### Relative plate motions

A first test of our results and their implications is to compare the predictions in terms of relative motion with observations. The relative rate shown by our data between ADD1 in Ethiopia (west of East African Rift) and AR00, CBL0, LLL0 and GOR0 in Djibouti (east of the East African Rift) is about  $5 \text{ mm/yr}$ , east-west trending, consistent with other estimates of the East African Rift separation rate. *Bilham et al.* [1999] used a combination of SLR and GPS data to derive a rate of  $4.5+1 \text{ mm/yr}$  at  $N108^\circ+10^\circ E$  across the northern Ethiopian rift at the latitude of Addis Ababa, in good agreement with previous "geological" estimates of *Jestin et al.* [1994] ( $5 \text{ mm/yr}$  at  $N102^\circ E$ ) and *Chu and Gordon* [1999] ( $6 \text{ mm/yr}$  at  $N95^\circ E$ ). Combining our African and Somalian angular velocities gives a Somalia/Africa vector of relative motion at ( $28.95^\circ S$ ,  $43.70^\circ E$ ,  $0.084^\circ/\text{Myr}$ ) which is only slightly east of *Chu and Gordon's* [1999] "geological" solution but very different from that of *Fernandes et al.*'s [2003]. However, due to the close locations of the two African and Somalia vectors, their sum is very sensitive to small variations (either in pole location or in angular rate) and the result is quite erratic in the absence of further constraints (see a discussion of this effect in combining two nearby poles in *Jestin et al.*, 1994). This is well illustrated by the large uncertainties obtained in combining the two covariance matrixes (semi-axes of the  $1\sigma$  error ellipse are  $11^\circ$  and  $4^\circ$ ). Thus the only way to determine with confidence a Somalia-Africa pole would be to compare it with measurements, which unfortunately are still lacking in the central and southern parts of the East African Rift.

### Arabia-Africa: the Red Sea and the Levant fault

Combining our African and Arabian rotations leads to an angular velocity vector ( $31.64^\circ N$ ,  $20.29^\circ E$ ,  $0.308^\circ/\text{Myr}$ ) (Table 4). The RMS misfit on observed velocities is less than  $1.2 \text{ mm/yr}$ . Our pole is close in latitude and longitude (within 1 sigma, i.e. around  $3^\circ$ ) to those of *Jestin et al.* [1994] and *Chu and Gordon* [1998], established from oceanic magnetic anomalies in the Red Sea. It differs more in longitude from both *McClusky et al.* [2003] and *Sella et al.* [2003] ( $5^\circ$  and  $9^\circ$  respectively, i.e. more than 2 sigmas). However, it is our rate which differs more: we confirm that the geodetic angular rate of rotation is significantly smaller than the "geological" one ( $0.308^\circ/\text{Myr} \pm 0.05$  at 3 sigmas vs.  $0.400$  to  $0.418^\circ/\text{Myr}$ , with a pole longitude

however slightly more to East). *McClusky et al.* [2003] already suggested some reduction of this rate (with  $0.37^\circ/\text{Myr}$ ) but did not consider this reduction to be significant because of their larger uncertainty of  $0.04^\circ/\text{Myr}$ . Compared to *Chu and Gordon's* [1998] estimates based on magnetic anomalies, the Red Sea spreading is reduced from  $9 \text{ mm/yr}$  in the northern part, and  $18 \text{ mm/yr}$  in the southern one, to  $8$  and  $15 \text{ mm/yr}$ , respectively, thus by about 15%. The difference is clearly hardly significant, but corroborates an actual decrease in the Red Sea spreading rate since 3 Ma (or less), as argued by *Calais et al.* [2003] for the Africa-Eurasia-North America relative motions. Meanwhile, our predicted azimuths (023 and 044 in northern and southern Red Sea, respectively) are slightly more northerly than those predicted by *Chu and Gordon* [1998] (026 and 047). Again, those very small differences of  $3^\circ$  in direction are not really significant. Anyhow, since there is no clear transform directions in the Red Sea, we cannot test those predictions. In conclusion, if inferred on Red Sea data only, one could still argue against the decrease in rates of plate motion. Taking their uncertainties into account, GPS and Nuvel-1A rates are almost indistinguishable there.

Along the Levant (Dead Sea) Fault system, our predicted rate of  $7 \text{ mm/yr}$  is very close to both the  $8 \text{ mm/yr}$  predicted by *Chu and Gordon* [1998], and the  $6 \text{ mm/yr}$  given by *McClusky et al.* [2003] but twice the  $4 \text{ mm/yr}$  predicted by *Sella et al.* [2002]. All these estimates fit well with the  $4+2 \text{ mm/yr}$  geological estimate of *Klinger et al.* [2000]. Based on three GPS stations and a locked fault model (because two GPS stations – KATZ and ELAT – are close to the fault), *Pe'eri et al.* [2002] infer a  $2.6+1.1 \text{ mm/yr}$  north-south component of motion, which is therefore a minimum estimate. Based on a larger network of 11 stations, *Wdowinski et al.* [2004] obtained a current slip rate of  $3.3+0.4 \text{ mm/yr}$  along the Levant fault system. This however might not be directly comparable to our  $7 \text{ mm/yr}$  estimate since GPS data show a significant motion of the Sinai sub-plate with respect to Africa. *Wdowinski et al.* [2004] predict a  $2.4 \text{ mm/yr}$  velocity along azimuth  $20^\circ$  across the Suez rift, between Sinai and Africa. This azimuth is nearly the trend of the Levant fault, which implies a total relative motion of  $5.7 \text{ mm/yr}$  between Arabia and Africa, in very good agreement with *McClusky et al.* ( $6 \text{ mm/yr}$ ) and our estimate ( $7 \text{ mm/yr}$ ).

### Arabia-Somalia: the Gulf of Aden

A further test of a possible slowing down of the Arabia motion is to look at the Gulf of Aden. Combining our Somalia and Arabia motions relative to ITRF2000 gives an angular velocity vector ( $20.07^\circ N$ ,  $25.49^\circ E$ ,  $0.356^\circ/\text{Myr}$ ) (Table 4). This is significantly different compared with all previously proposed solutions. When the Arabian sites velocities are rotated

**Table 4.** Relative motion parameters of Arabia (ARA), Africa (AFR), Arabia (ARA), India (IND) and Eurasia (EUR) based on GPS and conventional kinematic data<sup>a</sup>.

Plate pair	Lat. °N	Long. °E	Rate °/Myr	$\sigma$ rate °/Myr	$\sigma$ maj $\Delta$ Lat	$\sigma$ min $\Delta$ Lon	Azim. (°)	Reference
ARA-AFR	31.64	20.29	0.308	0.018	2.5	1.1	290	this work
	30.50	25.70	0.370	0.04	1.0	2.3	-	<i>McClusky et al. [2003]</i>
	31.26	29.55	0.400	0.030	1.8	1.3	275	<i>Sella et al. [2002]</i>
	31.50	23.00	0.400	0.05	1.2	2.7	-	<i>Chu and Gordon [1998]</i>
	32.59	23.70	0.418	-	-	-	-	<i>Jestin et al. [1994]</i>
ARA-SOM	20.07	25.49	0.356	0.026	2.3	1.2	286	this work
	21.06	28.62	0.441	0.029	1.8	1.0	55	<i>Sella et al. [2002]</i>
	25.24	23.39	0.423	-	-	-	-	<i>Jestin et al. [1994]</i>
	24.10	24.00	0.40	0.05	4.9	1.3	295	<i>DeMets et al. [1994]</i>
ARA-EUR	28.27	12.12	0.364	0.017	2.5	0.66	276	this work+ <i>Calais (pers. com. 2004)</i>
	27.90	19.50	0.410	0.1	0.5	1.4	-	<i>Vernant et al. [2004]</i>
	26.20	20.40	0.437	0.023	3.7	0.9	77	<i>Kreemer et al. [2003]</i>
	27.40	18.40	0.400	0.04	1.0	2.5	-	<i>McClusky et al. [2003]</i>
	26.22	22.87	0.427	0.029	2.1	1.1	76	<i>Sella et al. [2002]</i>
	24.60	13.70	0.52	0.05	5.2	1.7	288	<i>DeMets et al. [1994]</i>
ARA-IND	19.73	20.42	-0.035	0.025	65.2	11.5	285	this work + <i>Socquet et al. [2004]</i>
	10.5	61.83	0.099	0.073	17.2	10.4	88	<i>Sella et al. [2002]</i>
	3.0	91.5	-0.03	0.04	26.1	2.4	302	<i>DeMets et al. [1994]</i>

<sup>a</sup> Uncertainty on the pole location is given either by the semi-major ( $\sigma$  maj) and semi-minor ( $\sigma$  min) axes of the 1- $\sigma$  error ellipse (azim. is the azimuth of the semi-major axis) or by the uncertainty in latitude ( $\Delta$ Lat) and longitude ( $\Delta$ Lon). Note that the NUVEL1 (*DeMets et al.*, 1994) solution for ARA-AFR is actually ARA-SOM (Africa being treated as a single plate and data coming from the Gulf of Aden alone).

with respect to (our) Somalia, our solution gives a RMS misfit of 1.5 mm/yr. With *Sella et al.*'s [2002] solution, the misfit is 3 mm/yr on average, but everywhere larger than 2 mm/yr.

Geologically-based models [*DeMets et al.*, 1994; *Jestin et al.*, 1994] do not fit the GPS data, showing much larger predicted rates as well as azimuths rotated clockwise. In Oman, predicted velocities are 22-23 mm/yr instead of 19-20 mm/yr measured. In Yemen, predicted and observed values are 16 and 13 mm/yr, respectively. Along the Gulf of Aden, observed spreading rates range from 16 to 22 mm/yr from west to east, while our geodetic model predicts 13 to 18 mm/yr, about 20% less. This 3 mm/yr difference between velocities derived from GPS and from magnetic anomalies is larger, although only slightly, than the uncertainties. Our measurements thus indicate a present-day spreading rate in the Gulf of Aden reduced by about 15 to 20% with respect to the rate averaged over the last 3 Ma. In terms of directions, we have compared the predicted values on three well-defined transform faults (Maita-Al Khalib, Alula-Fartak and Socotra) with their actual trends and found a 6 to 7° clockwise rotation. A similar, although larger (18°), clockwise rotation of the spreading direction has been suggested by *Tamsett and Searle* [1988] on the basis of small-scale morphology. However, the change has been dated approximately at 3.5 Ma. If this is correct, it

should also have been recorded in the magnetic anomalies, which does not seem to be the case. More work is thus needed to try to date the time of this kinematic change – a 20% decrease in velocity and a small clockwise rotation.

#### Arabia-India: the Owen fracture zone and Murray ridge

The Owen fracture zone is a slowly slipping transform fault that accommodates right-lateral motion between the Indian and Arabian plates. Further North and before it reaches the Pakistan triple junction the plate boundary in the vicinity of the Murray ridge is made of transform segments that strike parallel to the Owen fracture zone. Using slip vector azimuth data from *Quittmeyer and Kafka* [1984], NNR-Nuvel-1A constrained the relative motion between the two plates to a small 2 mm/yr right-lateral strike slip motion with an azimuth ranging from N20°E in the South to N40°E in the North. Because it comes from present day seismicity, this motion should match instantaneous rates inferred from geodesy on the last decade. In other words, any revision of the Arabia plate motion should be accompanied by a similar revision of the India plate motion, in order to preserve their close to zero relative motion. Recent geodetic determinations confirm a slower Indian rotation rate compatible with the slowing down of Arabia [eg *Paul et al.*, 2001; *Sella et al.*, 2002; *Socquet et al.*, 2004]. However, when *Paul et al.* [2001]

is still too fast by 10%, *Sella et al.* [2002] relative pole predicts East-West compression on the plate boundary, in disagreement with observed strike slip seismicity and transform fault azimuths. Using the angular velocity vector determined by *Socquet et al.* [2004] for India in the ITRF2000 ( $50.9^{\circ}\text{N}$ ,  $12.13^{\circ}\text{W}$ ,  $0.487^{\circ}/\text{Myr}$ ) (Table 2) we find an Arabia-India angular velocity ( $19.73^{\circ}\text{N}$ ,  $20.42^{\circ}\text{E}$ ,  $-0.035^{\circ}/\text{Myr}$ ) (Table 3). This predicts 2 mm/yr of strike slip motion with an azimuth ranging from N-S in the North to N $15^{\circ}\text{E}$  in the South of the Owen Fracture Zone, in fair agreement with the direction of slip vectors in the area but with a reverse sense of motion: sinistral instead of dextral. In other words, the present day geodetic determination of Indian and Arabian plates finds India is still relatively faster than Arabia, when tectonic evidence from earthquakes fault plane solutions point the opposite. Mostly because they are small plates, finding a pole describing accurately the relative motion of India and Arabia with geodetic tools is a difficult task. In our solution, the residual motion of Bangalore (IISC) with respect to Arabia is very small : 0.9 mm/yr. This indicates we roughly respect the close to zero relative motion between Arabia and India condition but cannot refine further.

#### Arabia-Eurasia: the Zagros collision zone

A last test of our solution is the Arabia-Eurasia collision in Iran, where GPS data were made recently available [*Nilforoushan et al.*, 2003; *Vernant et al.*, 2004]. We derived the Arabia-Eurasia rotation parameters ( $28.27^{\circ}\text{N}$ ,  $12.12^{\circ}\text{E}$ ,  $0.364^{\circ}/\text{Myr}$ ) from our solution for Arabia and from *Calais et al.*'s [2003] solution for Eurasia. Our pole is located far to the west of poles previously proposed on the basis of GPS data (Table 4). It is close to NUVEL1A [*DeMets et al.*, 1994] pole, but the angular rate is reduced to  $0.364^{\circ}/\text{Myr}$ , much less than NUVEL1A  $0.520^{\circ}/\text{Myr}$ . These parameters give a rate of convergence reduced to 21 to 27 mm/yr in the Zagros – Makran areas (instead of 32 to 38 mm/yr predicted by NUVEL1A – a 30% reduction), consistent with the previous findings of *McClusky et al.* [2000], *Sella et al.* [2002], *Nilforoushan et al.* [2003], *McClusky et al.* [2003] and *Vernant et al.* [2004]. So again, we find a different rotation pole than previous studies because of new vectors in Yemen, but this different pole still predicts the same velocities than those previous studies at stations in Bahrein and Oman.

*McClusky et al.* [2000] used their own determination of Eurasia to define their reference frame. Because they don't give velocities in ITRF, direct comparison with our solution might be difficult. However, because the Eurasian determination of *Calais et al.* [2003] uses many common stations with *McClusky et al.* [2000], and in particular in Europe, the

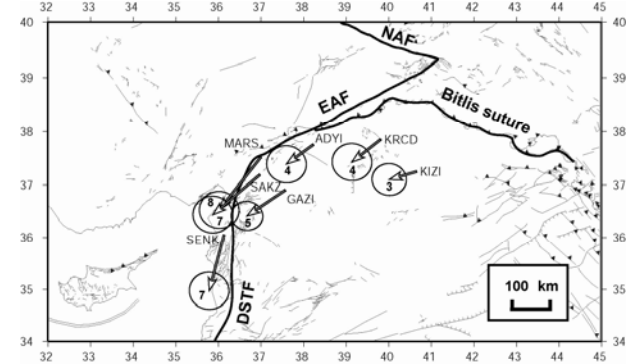


**Figure 7.** North Arabia sites velocities from *McClusky et al.* [2000] rotated in our Arabian reference frame. Numbers next to arrow heads indicate the station velocity in mm/yr. Ellipses depict the  $1-\sigma$  uncertainties. Thick lines roughly depict faults in the area : East Anatolian Fault (EAF), North Anatolian Fault (NAF), Dead Sea Transform Fault (DSTF) and Bitlis suture zone.

different frames should not generate discrepancies larger than 1-2 mm/yr, at least over our area of interest. In fact we find exactly the same velocities (within less than 1 mm/yr) for stations NICO, NSSP, TRAB, and ZECK (figure 3). Therefore, we feel confident that we can “import” *McClusky et al.* [2000] velocities in our reference frame without introducing significant distortion. Station KIZI although it is around 150 km away from the East Anatolian Fault, has a residual velocity of  $3 \text{ mm/yr} \pm 1.5$  (figure 7). Stations KRCD and GAZI are closer to the East Anatolian Fault (within 70 km) and have slightly higher residual velocities of 4 and 5 mm/yr respectively. Finally, stations lying very close to the fault (MARS, SAKZ, SENK) show even higher residuals at 7 to 8 mm/yr (with the exception of ADYI 4 mm/yr). Those residual velocities are not erratic, but rather follow nicely the azimuth of the East Anatolian Fault (figure 5). Also, although the numbers are small and one should be cautious because of GPS uncertainties, the decrease of residual velocity with the distance from the fault looks very much like the arctangent profile expected across a strike slip fault locked at depth. Therefore, we conclude that stations within 100 km from the East Anatolian Fault are affected by elastic deformation and should not be used to infer the rigid rotation parameters of the Arabian plate. On the opposite, they can be used to characterize the interseismic behaviour of the fault and assess its locking depth. Given the far reach of the deformation (at least 100km) and the slow rate on the fault ( $< 10 \text{ mm/yr}$ ), this would imply a very large locking depth of at least 50 km, which seems unrealistic. Therefore we conclude that either our import of *McClusky et al.* data in our reference frame is not 100% correct and is affected by unconstrained reference frame rotations, or there is widespread strain in addition to the elastic coupling. A fully comprehensive and more robust

combination of the two data sets at the level of daily GPS observations is needed to investigate further this question.

## Conclusion

*Yang and Liu [2002]* have addressed the problem of the discrepancy between GPS data and NUVEL-1A at three convergent plate boundaries: the Andes, the Himalayas and Taiwan. They concluded that the misfit can be explained by intraplate deformation. In the case of the Arabia-Eurasia convergence, such an explanation can be ruled out because we showed that the GPS rates of separation between Arabia and both Africa (in the Red Sea) and Somalia (in the Gulf of Aden) are reduced by 15 to 20% with respect to rates of spreading based on magnetic anomalies (and averaged over the last 3 Ma). We acknowledge the fact that differences in both rates and directions in the Red Sea are hardly significant and that this finding is better supported by Gulf of Aden data. Meanwhile, *Calais et al. [2003]* have shown that the Africa-Eurasia convergence rate has decreased since 3 Ma, and rotated counter-clockwise. We find, in agreement with former studies, that the rate of Arabia-Eurasia convergence has also decreased by about 30% and showed that this is not only due to the decrease in the Africa-Eurasia convergence, but also to a significant decrease in the separation rate between Arabia and Africa in the Red Sea (-15%) and Arabia and Somalia in the Gulf of Aden (-20%). We suggest that slowing down the Arabia-Eurasia convergence, is due to decreasing of the slab pull force, resulting in reduced extension between Arabia and Africa-Somalia. Further east, in the India-Eurasia convergence zone, GPS data also suggest a decrease in the convergence rate [*Paul et al., 2001; Wang et al., 2001, Socquet et al., 2004*]. With our definition of Eurasia, that follows that of *Calais et al. [2003]*, and the rotation of India from *Socquet et al. [2004]* we also find a lower India-Eurasia collision rate than NUVEL-1A. This discrepancy is due to either an overestimation of the rate in Nuvel-1A or to an actual slowing down of the Indian plate. If the second possibility is confirmed, then it would appear that the whole collision zone between Africa, Arabia, India and Eurasia has slowed down in the last 3 Ma.

## Acknowledgments

We thank the many people – too numerous to be all cited - involved in the acquisition of the GPS data from 1991 to 2001: especially the IT-Iran group (represented by D. Hatzfeld) for their recent measurements in Oman and Iran, P. Briole for sharing his data on La Réunion, the Yemen Survey Authority and the University of Sana'a for their support in Yemen, and A. Abdallah (ISERST) and all people at “Observatoire d’Arta” in the Republic of Djibouti for their continuous efforts. Financial support for both the field work and the data analysis was provided by the french INSU/CNRS (programmes AFAR, Tectoscope-positionnement,

PNTS, IT-Iran, IT-Panaches) and the French Embassy in the Republic of Yemen.

## References

- Altamimi, Z., Sillard, P., Boucher, C, ITRF2000: A new release of the International Terrestrial Reference frame for earth science applications, *J Geophys Res.-SA* 107 (B10): art. no. 2214, 2002.
- Argus, D.F., and R.G. Gordon, No-net-rotation model of current plate velocities incorporating plate motion model NUVEL-1, *Geophys. Res. Lett.*, 18, 2039-2042, 1991.
- Banerjee, P., and R. Bürgmann, Convergence across the northwest Himalaya from GPS measurements, *Geophys. Res. Letters.*, 29 (13), 10.1029, 2002.
- Beutler, G., J. Kouba, and T. Springer, Combining the orbits of the IGS processing centers, in *proceedings of IGS analysis center workshop*, edited by J. Kuba, 20-56, 1993.
- Bilham, R., R. Bendick, K. Larson, P. Mohr, J. Braun, S. Tesfaye, and L. Asfaw, Secular and tidal strain across the Main Ethiopian Rift, *Geophysical Research Letters*, 26 (18), 2789-2792, 1999.
- Calais, E., C. DeMets, and J.-M. Nocquet, Evidence for a post-3.16-Ma change in Nubia-Eurasia-North America plate motions?, *Earth Planet. Sc. Lett.*, 216, 81-92, 2003.
- Chu, D., and R.G. Gordon, Current plate motions across the Red Sea, *Geophys. J. Int.*, 135, 313-328, 1998.
- Chu, D., and R.G. Gordon, Evidence for motion between Nubia and Somalia along the southwest Indian Ridge, *Nature*, 398, 64-67, 1999.
- DeMets, C., R. G. Gordon, D. Argus, and S. Stein, Effect of recent revisions to the geomagnetic reversal time scale on estimates of current plate motions, *Geophys. Res. Letters.*, 21, 2191-2194, 1994.
- Dewey, J.F., M.L. Helman, E. Turco, D.H.W. Hutton, and S.D. Knott, Kinematics of the western Mediterranean, in *Alpine Tectonics*, edited by M.P. Coward, D. Dietrich, R.G. Park, Geological Society, London, Special Publication, 45, 265-283, 1989.
- Fernandes, R.M.S., B.A.C. Ambrosius, R. Noomen, L. Bastos, M. Wortel, W. Spakman, and R. Govers, The relative motion between Africa and Eurasia as derived from ITRF2000 and GPS data, *Geophys. Res. Lett.*, 30(16), 1828, 2003, doi:10.1029/2003GL017089.
- Gordon, R.G., D.F. Argus, and M.B. Heflin, Revised estimate of the angular velocity of India relative to Eurasia, *EOS Trans. AGU*, 80 (46 (Fall meeting suppl.)), F273, 1999.
- Herring, T. A., Davis, and Shapiro, Geodesy by radio Interferometry : the application of Kalman filtering to the analysis of very long baseline interferometry data, *J. Geophys. Res.*, 95, 12561-12581, 1990.
- Herring, T. A., Documentation for the GLOBK software version 5.01, *Mass. Inst. of Technol., Cambridge*, 1999.

- Jestin, F., P. Huchon and J.M. Gaulier, The Somalia plate and the East African Rift system: present day kinematics, *Geophys. J. Int.*, 116, 637-654, 1994.
- King, R. W., and Y. Bock, Documentation for the GAMIT GPS software analysis version 9.9, *Mass. Inst. of Technol., Cambridge*, 1999. (ou 2000?)
- Klinger, Y., J.P. Avouac, N. Abou Karaki, L. Dorbath, D. Bourles and J.L. Reyss, Slip rate on the Dead Sea transform fault in northern Arabia valley (Jordan), *Geophys. J. Int.*, 142, 755-768, 2000.
- Kreemer, C., W.E. Holt, and J. Haines, An integrated global model of present-day plate motions and plate boundary deformation, *Geophys. J. Int.*, 154, 1-27, 2003.
- Larson, K. M., J. T. Freymueller, and S. Philipsen, Global plate velocities from the Global Positioning System, *J. Geophys. Res.*, 102, 9961-9981, 1997.
- Larson, K. M., R. Burgmann, R. Bilham, and J. T. Freymueller, Kinematics of the India-Eurasia collision zone from GPS measurements, *J. Geophys. Res.*, 104, 1077-1093, 1999.
- McClusky et al., Global Positioning System constraints on plate kinematics and dynamics in the eastern Mediterranean and Caucasus. *J. Geophys. Res.*, 115, 5695-5719, 2000.
- McClusky, S., R. Reilinger, S. Mahmoud, D. Ben Sari, and A. Tealeb, GPS constraints on Africa (Nubia) and Arabia plate motions, *Geophys. J. Int.*, 155, 126-138, 2003.
- Neilan, R., The evolution of the IGS global network, current status, and future aspects, in Zumberge JF et al. (eds), *Pasadena JPL, CA, USA, IGS annual report*, JPL publ 95-18, pp 25-34, 1995.
- Nilforoushan, F., P. Vernant, F. Masson, C. Vigny, J. Martinod, M. Abbassi, H. Nankali, D. Hatzfeld, R. Bayer, F. Tavakoli, A. Ashtiani, E. Doerflinger, M. Daignières, P. Collard, and J. Chéry, GPS network monitors the Arabia-Eurasia collision deformation in Iran, *Journal of Geodesy*, 77, 422-441, 2003.
- Nocquet, J.M., E. Calais, Z. Altamimi, P. Sillard and C. Boucher, Intraplate deformation in western Europe deduced from an analysis of the ITRF97 velocity field, *J. Geophys. Res.*, 106, 11239-11258, 2001.
- Patriat, P., and J. Achache, India Eurasia collision chronology has implications for crustal shortening and driving mechanism of plates, *Nature*, 311, 615-621, 1984.
- Paul, J., R. Burgmann, V.K. Gaur, E. Bilham, K.M. Larson, M.B. Ananda, S. Jade, M. Mukal, T.S. Anapuma, G. Satyal, and D. Kumar, The motion and active deformation of India, *Geophys. Res. Letters*, 28, 647-650, 2001.
- Pe'eri, S., S. Wdowinski, A. Stibelman, N. Bechor, Y. Bock, and M. van Domselaar, Current deformation across the Dead Sea Fault, as observed from three years of continuous GPS monitoring, *Geophys. Res. Lett.*, 29 (14), 10.1029, 2002.
- Prawirodirdjo, L. and Y. Bock, Instantaneous Global Plate Motion Model from 12 Years of Continuous GPS Observations, *J. Geophys. Res.*, 109, doi: 10.1029/2003JB002944, 2004.
- Reilinger, R., S.C. McClusky, M.G. Oral, R.W. King, M.N. Tosoz, A.A. Barka, I. Kinkik, O. Lenk, and I. Sani, Global Positioning System measurements of present-day crustal movements in the Arabia-africa-Eurasia plate collision zone, *Journal of Geophysical Research*, 102, 9983-9999, 1997.
- Rosenbaum, G., G.S. Lister, and C. Duboz, Relative motions of Africa, Iberia and Europe during alpine orogeny, *Tectonophysics*, 359, 117-129, 2002.
- Ruegg, J.C., P. Briole, K. Feigl, C. Vigny, M. Anis Abdallah, O. Bellier, P. Huchon, S. Al Khirbush, A. Laike, N. d'Oreye, and M. Prevot, First Epoch Geodetic GPS Measurements Across the Afar Plate Boundary Zone. *Geophys. Res. Lett.*, 20, 1899-1902, 1993.
- Sella, G.F., T. H. Dixon, and A. Mao, REVEL: a model for recent plate velocities from space geodesy, *J. Geophys. Res.*, 107 (B4), 10.1029, 2002.
- Socquet, A., C. Vigny, W. Simons, N. Chamot-Rooke, C. Rangin, and B. Ambrosius, GPS determination of the relative motion between India and Sunda and its accommodation in Myanmar, *J. Geophys. Res.*, in press, 2004.
- Tamsett, D., and R. Searle, Structure and development of the midocean ridge plate boundary in the Gulf of Aden: evidence from GLORIA side scan sonar, *Journ. Geophys. Res.*, 93 (B4), 3157-3178, 1988.
- Vernant, P., F. Nilforoushan, D. Hatsfeld, M. Abassi, C. Vigny, F. Masson, H. Nankali, J. Martinod, A. Ashtiani, F. Tavakoli, and J. Chéry, Contemporary crustal deformation and plate kinematics in Middle East constrained by GPS measurements in Iran and northern Oman, *Geophys. J. Int.*, 157, 381-398, doi:10.1111/j.1365-246x.2004.02222.x, 2004.
- Vigny, C., J.B. DeChabalier, J.C. Ruegg, P. Huchon, K. Feigl, L. Asfaw, and K. Kanbari, 12 years of geodetic measurements in the Asal Rift, Djibouti, *submitted to J. Geophys. Res.*, 2004b.
- Walpersdorf A., C. Vigny, J.-C. Ruegg, P. Huchon, L. M. Asfaw, and S. Al Kirbush, 5 Years of GPS Observations in the Afar Triple Junction Area. *Journal of Geodynamics*, 28 (2-3), 225-236, 1999.
- Wang, Q., P-Z. Zhang, J. T. Freymueller, R. Bilham, K.M. Larson, X. Lai, X. You, Z. Niu, J. Wu, Y. Li, J. Liu, Z. Yang, and Q. Chen, Present-day crustal deformation in China constrained by Global Positioning System measurements, *Science*, 294, 574-577, 2001.
- Wdowinski, S., Y. Bock, G. Baer, L. Prawirodirdjo, N. Bechor, S. Naaman, R. Knafo, Y. Forrai, and Y. Melzer, GPS measurements of current crustal movements along the Dead Sea Fault, *J. Geophys. Res.*, 109, B05403, doi:10.1029/2003JB002640, 2004.
- Williams, S. D. P., Y. Bock, P. Fang, P. Jamason, R. M. Nikolaidis, L. Prawirodirdjo, M. Miller and D. J. Johnson, Error analysis of continuous GPS position Time Series, *J. Geophys. Res.*, 109, B03412,

doi:10.1029/2003JB0022741, 2004.

Yang, Y., and M. Liu, Deformation of convergent plates: evidence from discrepancies between GPS

velocities and rigid-plate motions, *Geophys. Res. Lett.*, 29 (10), 10.1029, 2002.

# 25 years of geodetic measurements along the Tadjoura-Asal rift system, Djibouti, East Africa.

Christophe Vigny<sup>1</sup>, Jean-Bernard de Chabalier<sup>2</sup>, Jean-Claude Ruegg<sup>2</sup>, Philippe Huchon<sup>3</sup>, Kurt L. Feigl<sup>4</sup>, Rodolphe Cattin<sup>1</sup>, Laike Asfaw<sup>5</sup>, Khaled Kanbari<sup>6</sup>.

**Abstract.** Since most of Tadjoura-Asal rift system sits on dry land in the Afar depression near the triple junction between the Arabia, Somalia and Nubia plates, it is an ideal natural laboratory for studying rifting processes. We analyze these processes in light of a time series of geodetic measurements from 1978 through 2003. The surveys used triangulation (1973), trilateration (1973, 1979 and 1981 to 1986), leveling (1973, 1979, 1984-1985, and 2000), and the Global Positioning System (GPS, in 1991, 1993, 1995, 1997, 1999, 2001 and 2003). A network of about 30 GPS sites covers the Republic of Djibouti. Additional points were also measured in Yemen and Ethiopia. Stations lying in the Danakil block have almost the same velocity than Arabian plate indicating that the opening of the Red Sea at its southern tip is almost totally accommodated in the Afar depression. Inside Djibouti, the Asal-Ghoubbet rift system accommodates  $16 \pm 1$  mm/yr of opening perpendicular to the rift axis, and exhibits a pronounced asymmetry with essentially null deformation on its southwestern side and significant deformation on its northeastern side. This rate, slightly higher than the large-scale Arabia-Somalia motion ( $13 \pm 1$  mm/yr), suggests transient variations associated to the relaxing processes after the Asal-Ghoubbet seismo-volcanic sequence of 1978. Inside the rift, the deformation pattern exhibits clear 2-D pattern. Along the rift axis, the rate is decreasing to the northwest, suggesting propagation of the system in the same direction. Perpendicular to the rift axis, the localization of the opening is clearly shifted to the northeast, relatively to the topographic rift axis, in the “Petit Rift”, a rift-in-rift structure, where is concentrated most of the active faults and the present seismicity. Vertical motions (comparisons of leveling profiles) also confirm this asymmetry, with a current bulge of the northeastern shoulder. Finally, all sites inside the rift system show varying vertical motions from 0 to 10 mm/yr, but always positive, indicating that although the internal floor is subsiding relative to the rift shoulders, the whole system is moving upward.

## Introduction

The Afar depression, at the triple junction between Arabia, Somalia, and Nubia, is actively deforming by continental stretching, rifting and volcanism. Here the three extensional structures of the Sheba Ridge, the Red Sea Ridge and the East African Rift join in a complicated geometry. Both the Red Sea Ridge and Sheba Ridge have been propagating for the last 30 Myr, toward the south and west, respectively. Yet they penetrate into the Afar depression, rather than connecting directly through the Straits of Bab el Mandeb. Consequently, the recent tectonic action there focuses around a set of disconnected, but

overlapping, propagating rift segments, that have created a complex network of normal faults (e.g., *Huchon et al.* [1991]; *Manighetti et al.* [1997]). To better understand the kinematics and the processes taking place in this area, we use geodetic measurements which characterize the deformation at three scales defined by different geophysical objects: the plates (distances  $\sim 1000$  km), tectonic regions (between  $\sim 1000$  km and  $\sim 10$  km), and rift segments ( $\sim 10$  km).

At the scale of the plates, the existing long-term kinematic models disagree markedly. The conventional NUVEL-1A model considers Africa as a single plate to predict divergence between Africa and Arabia at a rate of about 16 mm/yr and N28°E in azimuth at the southern tip of the Red-Sea [*Demets et al.*, 1994]. Separating Africa into two plates, Somalia and Nubia, *Jestin et al.* [1994] propose a similar relative velocity: 17 mm/yr at azimuth N30°E. Yet the rate of Arabia-Somalia motion varies along the Sheba Ridge from 22 mm/yr at the horn of Africa to 17 mm/yr at the entrance of the Gulf of Tadjoura [*DeMets et al.*, 1994]. For the East African Rift (EAR), that splits Africa into Somalia and Nubia, estimates of the divergence rate also vary considerably: 1 mm/yr [*Asfaw et al.*, 1992], 5 mm/yr [*Jestin et al.*, 1994], or 6 mm/yr [*Chu and Gordon*, 1999].

In contrast, recent GPS measurements in this area clearly differ from plate kinematic predictions. Different

<sup>1</sup>Laboratoire de Géologie, Ecole Normale Supérieure (ENS), CNRS, Paris, France

<sup>2</sup>Institut de Physique du Globe (IPGP), Paris, France

<sup>3</sup>Laboratoire de Tectonique, Université Pierre et Marie Curie-Paris6 & Institut Océanographique, Paris, France

<sup>4</sup>Centre National de Recherche Scientifique (CNRS) Toulouse, France

<sup>5</sup>Addis Observatory, Department of Geophysics, Addis Ababa University, Addis Ababa, Ethiopia

<sup>6</sup>Department of Geosciences, University of Sana'a, Sana'a, Yemen

geodetic studies show that the plate rates consistent with the GPS observations are about 30% slower than the NUVEL-1A estimates for Arabia-Eurasia [McClusky et al., 2000, 2003; Sella et al., 2002; Vernant et al., 2004; Vigny et al., 2006] and Arabia-Somalia [Fernandes et al., 2003; Vigny et al., 2006]. These results suggest that spreading in the Red Sea and the Gulf of Aden, and thus the convergence rate between Arabia and Eurasia, have slowed during the last 3 Ma [Vigny et al., 2006].

At the smaller, regional scale of the Afar Depression, the complexity of the active fault and rift systems leads to various interpretations. Tectonic observations and paleomagnetic declinations suggest that the Danakil and Ali Sabieh blocks are both rotating [Sichler et al., 1980; Courtillot et al., 1980; Souriot and Brun, 1992; Manighetti et al., 1998]. The rotations can be understood as a consequence of rift propagation, either as “oceanic micro-plates” [Acton and Stein, 1991] or “continental bookshelf faulting” [Tapponnier et al., 1990; Sigmundsson et al., 1992; Manighetti et al., 1998; 2001a and b]. Implicit in all these models is the idea that the deformation transfers from one rift to another and therefore evolves in space and in time. This complication makes evaluating these models by comparing their predictions to quantitative geodetic measurements quite challenging. Confronting long-term, plate-scale models with short-term regional geodetic surveys, requires accounting for the dynamics of the underlying processes.

In this paper, we focus on the boundary between the Arabia plate and the Somalia where Sheba Ridge enters into the Afar depression. This narrow, WNW trending zone of active volcanism and tectonics includes Maskali transform fault, the Tadjoura rift and the Asal-Ghoubbet rift. To the NW, it links to the Mak'arassou fault system and the Manda Inakir rift (figures 1 and 2). The Asal-Ghoubbet rift is special because we can observe it on dry land to better understand slow-spreading ridges in oceanic lithosphere. Reconstructing the edifice of Fieale volcano indicates an average spreading rate of 17 to 29 mm/yr over the last 87,000 to 150,000 years at an azimuth of  $N40^{\circ}E \pm 5$  that is consistent with plate kinematic estimates [de Chabalier and Avouac, 1994]. The spreading rate is not constant, however, as evidenced by a rifting event in 1978. Then, a swarm of earthquakes (two events had magnitudes near 5) reactivated several normal faults, producing a total of 2 m of extension, during a week of volcanic activity at a new eruptive center (e.g., Abdallah et al. [1979]). The geodetic measurements performed during the years following this sequence corroborate the very high strain rates localized in the Asal rift [Ruegg et al., 1979; Ruegg and Kasser, 1987]. All these observations indicate that the Asal-Ghoubbet rift accommodates most of the present-day motion between Arabia and Somalia. Outside the rift, no direct measurements have yet been published to

determine which other structure might accommodate any remaining motion.

In this paper we present 12 years of GPS campaign measurements in Djibouti, Yemen, and Ethiopia. At the regional scale, we discuss the strain concentrated in the active rifts spanned by the GPS network. At the local scale, we use over 25 years of geodetic data to argue that transient rifting episodes like the one in 1978 at Asal are the dominant process in accommodating the motion across this plate boundary. Finally, we corroborate this interpretation by considering the vertical displacements measured by GPS and leveling.

### GPS data analysis

In November 1991, the first GPS observations were performed in Djibouti and the neighboring parts of Yemen and Ethiopia [Ruegg et al., 1993]. A small subset of this network was surveyed again in 1993 (3 times), 1995, and 1997. More complete surveys of the rift network were performed in 1999, 2001, and 2003 (Auxiliary Table 1). The points in Yemen were measured for the second time in 2001, ten years after the first survey. All sites were measured using a mix of Ashtech and Trimble dual frequency receivers equipped with different kind of antennas (see Auxiliary table 1 for details) During all campaigns, three points (Arta in Djibouti, Sana'a in Yemen, and Addis Abbeba in Ethiopia) were measured continuously in 24-hour sessions. Other sites in Djibouti were measured for 6 to 24 hours a day over 1 to 6 days (Auxiliary Table 1).

We reduce these data in 24-hour sessions to daily estimates of station positions using the GAMIT software [King and Bock, 2000] choosing the ionosphere-free combination and fixing the ambiguities to integer values. We use precise orbits from the International GPS Service for Geodynamics (IGS) [Beutler et al., 1993]. We also use IGS tables to describe the phase centers of the antennae. We estimate one tropospheric delay parameter per station every 3 hours. The horizontal components of the calculated relative position vectors are precise to within a few millimeters for pairs of stations less than 150 km apart, as measured by the root mean square (RMS) scatter about the mean.

In the second step, we combine the daily solutions using the GLOBK software [Herring et al., 1990] in a “regional stabilization” approach [McClusky et al., 2000]. To define a consistent reference frame for all epochs, we include tracking data from the permanent IGS stations around our study area available at the time of our campaigns (4 stations in 1991, 42 in 2003) [Neilan, 1995]. These fiducial stations are also included in the daily global GAMIT solutions from the IGS data center at Scripps, including more than 200 stations spread all over the globe. We combine all these daily solutions using Helmert-like transformations to estimate translation, rotation, scale and Earth orientation parameters (polar motion and rotation). The “stabilization” procedure defines a reference frame by

**Table 1:** Site positions and velocities in ITRF2000 and relative to Somalia plate. Latitude and longitude are in decimal degrees, all velocities and velocity uncertainties are in mm/yr.

SITE	Position		Horizontal Velocities				Vertical		Velocity uncertainties (1□)			
	Long.	Lat.	/ ITRF2000	/ Somalia	East	North	East	North	East	North	Up	Correl.
ARO0	42,85	11,53	33,1	16,2	2,7	0,7	-4,8		0,7	0,7	0,8	-0,004
AS00	42,46	11,64	35,5	14,1	5,0	-1,5	11,7		1,1	1,0	1,4	0,000
BY00	42,54	11,59	49,5	25,0	13,0	9,4	2,7		1,3	1,0	1,9	0,012
CBL0	43,07	11,46	29,4	16,1	-1,0	0,6	-1,7		0,7	0,6	0,9	0,001
CCC0	42,43	11,54	31,4	15,8	0,9	0,2	6,1		0,8	0,7	1,2	-0,047
CF00	42,49	11,62	35,1	23,7	4,7	8,1	4,4		0,9	0,7	1,2	0,012
DF00	42,52	11,60	39,4	24,9	9,0	9,3	7,1		0,9	0,8	1,1	0,043
EP00	42,50	11,57	35,6	16,2	5,2	0,6	1,4		1,0	0,8	1,4	0,026
FFF0	42,52	11,65	40,8	28,0	10,3	12,4	10,6		1,1	1,0	1,7	0,007
FG00	42,47	11,58	30,4	16,6	-0,1	1,0	16,5		4,0	1,4	5,6	0,267
GK00	42,47	11,60	38,5	16,7	8,0	1,0	-11,1		3,0	1,1	3,5	-0,086
GM00	42,56	11,62	41,8	25,4	11,3	9,9	5,4		0,9	0,7	1,2	0,020
GOR0	42,22	11,31	31,1	16,1	0,7	0,4	-8,0		0,9	0,7	1,7	0,002
HD00	42,50	11,61	32,9	18,7	2,5	3,1	1,5		1,7	1,5	3,4	0,007
HM00	42,50	11,55	36,9	16,5	6,5	0,8	19,0		4,6	2,2	8,4	0,168
HX00	42,43	11,59	36,3	19,6	5,9	3,9	5,0		1,3	1,0	2,3	0,021
III0	42,56	11,47	40,1	17,6	9,7	2,0	6,8		1,3	1,0	2,1	0,003
LLL0	42,58	11,26	30,3	15,6	-0,4	-0,2	-2,0		0,7	0,6	0,9	-0,002
LS00	42,52	11,57	36,7	15,6	6,3	0,0	-2,1		0,9	0,7	1,5	0,020
MMM0	42,58	11,62	42,1	26,3	10,7	10,7	6,9		1,1	0,8	2,2	0,009
PPP2	42,64	11,75	41,3	25,6	10,8	10,1	1,3		2,2	1,3	5,4	0,098
QQQ0	42,63	11,44	33,7	16,7	3,2	1,2	1,9		0,8	0,7	1,4	0,008
RRR0	42,67	11,58	43,9	26,6	13,5	11,1	3,3		1,4	1,0	2,8	-0,308
RSB0	43,36	11,98	36,7	24,6	6,1	9,3	0,8		0,8	0,7	1,8	-0,010
SAD0	42,69	11,61	39,1	19,8	8,6	4,3	9,5		2,2	1,5	4,4	0,021
SN00	42,52	11,59	39,1	16,4	8,7	0,8	4,0		1,5	1,1	3,2	0,079
TDJ0	42,91	11,79	36,9	24,2	6,4	8,7	-2,1		0,9	0,8	1,4	-0,024
ADD1	38,77	9,04	25,3	16,5	-4,4	-0,3	-0,5		0,7	0,7	0,8	0,002
DHAM	44,39	14,58	35,6	28,0	4,4	13,0	-1,9		0,8	0,7	1,3	-0,016
HODD	42,97	14,79	35,3	26,8	4,2	11,3	-4,5		1,0	0,8	1,9	-0,053
JNAR	43,44	13,32	37,2	26,7	6,3	11,4	-5,7		1,3	0,8	2,9	-0,067
SANA	44,19	15,35	37,0	26,5	5,6	11,4	-1,1		0,8	0,7	0,9	-0,013

minimizing, in the least-square sense, the departure from a priori values based on the International Terrestrial Reference Frame (ITRF) 2000 [Altamimi *et al.*, 2002], of the positions and velocities for a set of 22 well-determined stations in and around our study area. The misfit to these “stabilized” stations is 2.8 mm in positions and 1.6 mm/yr in velocity. More details about this solution and velocity residuals can be found in Vigny *et al.* [2006].

### Horizontal velocities

This procedure leads to the horizontal velocities listed in table 1 with respect to the ITRF2000. We compute velocities relative to the Somalian plate by using the angular velocity of this plate (48.12°N, -

97.75°W, 0.329°/Myr) given by [Vigny *et al.*, 2006]. In this reference frame three sites in southern Djibouti (CBL0, LLL0, GOR0) located far from the rift axis and supposedly on the Somalian plate, show velocities smaller than 1 mm/yr (Figure 1, 2, Table 1). Three more stations immediately south of the Asal-Tadjoura rifts (ARO0, QQQ0, and CCC0) also exhibit little motion, whereas site III0 is a notable exception. (Figure 2, Table 2). Therefore we chose to show all velocities in this reference frame (relative to Somalia plate). This choice has the advantage of highlighting the deformation in and around the Asal rift because the velocities of sites on the stable area south of it appear as short, insignificant arrows.

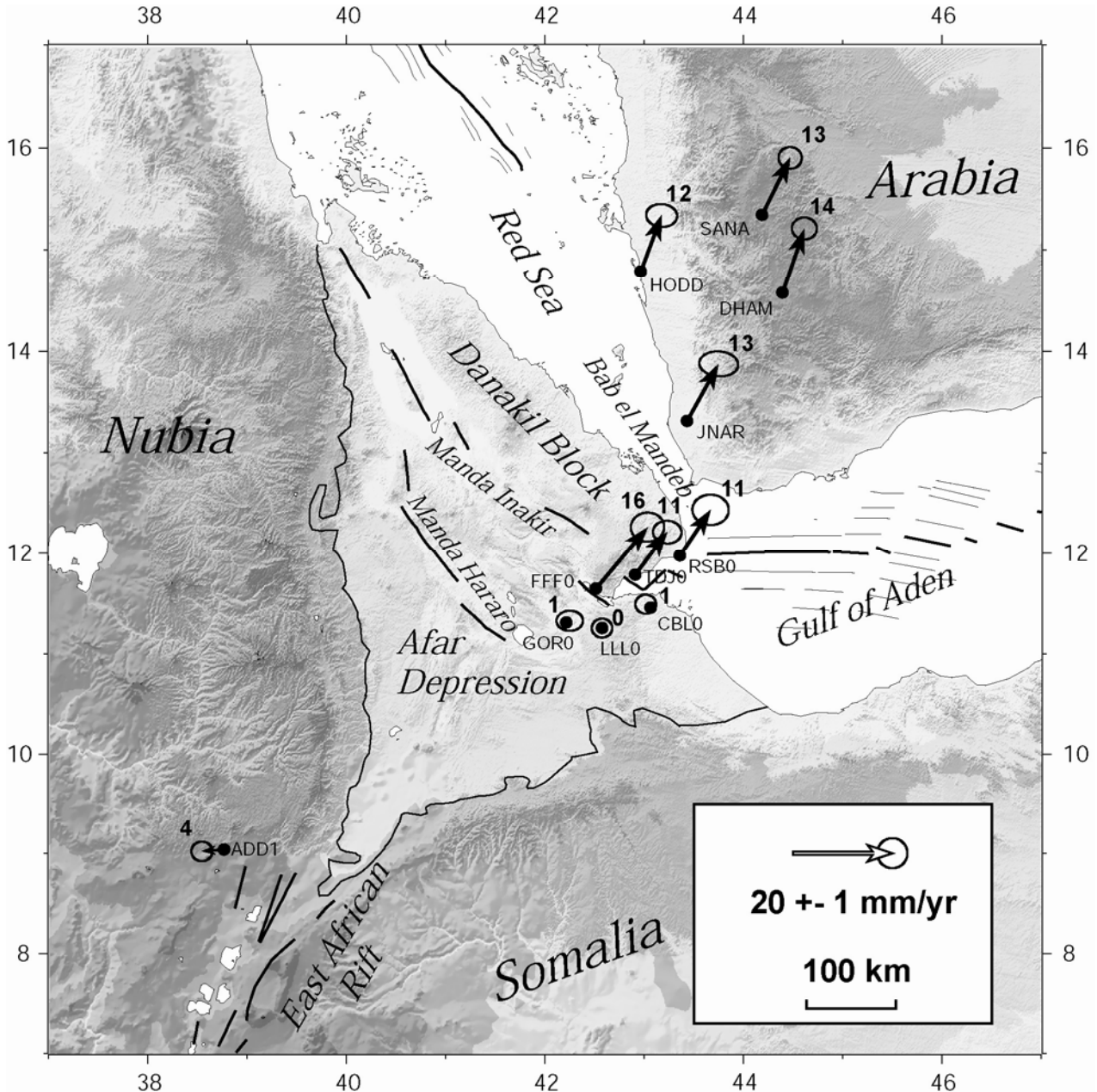


**Figure 1.** Triple junction and Afar depression (circle by solid line). Dots show locations of GPS stations. Arrows depict their horizontal velocities with respect to a reference frame fixed on the Somalia Plate. Bold numbers aside the arrows indicate the velocity in mm/yr. Ellipses depict the region of 99% confidence using the uncertainties in Table 1.

### Far-field velocities

In this Somalia-fixed reference frame, the residual velocity in Addis Ababa (ADD1), west of the East African Rift (EAR), is 4 mm/yr ( $\pm 1$  mm/yr at 1-sigma), oriented roughly West (figure 1, table 1). The amplitude of this residual vector depends on the angular velocity estimated for the Somalia plate. Different solutions give velocities between 3 and 6 mm/yr (coherent at 2-sigmas) and azimuths between West and North-West, roughly perpendicular to the

EAR trace at this latitude. Therefore, we conclude that our value of 4 mm/yr  $\pm 2$  is an upper bound for the EAR opening rate just south of the Afar depression.

The stations in Yemen (DHAM, HODD, JNAR, SANA) move together as a coherent block that represents a part of the Arabia plate with very little internal deformation (figure 1). The azimuth of their average velocity ( $N25^\circ \pm 5$ ) is compatible with the orientations of Gulf of Aden transform faults used in the NUVEL-1 model [Demets et al., 1990]. On the contrary, their mean opening speed ( $13 \pm 2$  mm/yr) is 30% slower

than the Nuvel-1A rate [Vigny *et al.*, 2006]. This definition of the Arabia plate implies that two stations located at the southern tip of the Danakil block (TDJ0 and RSB0) are close to having “Arabian” velocities (figure 1). Their residual motion with respect to the four stations in Yemen is less than 2 mm/yr. This confirms that the opening rate of the Red Sea at this latitude is negligible, which is not surprising given the absence of magnetic anomalies on the sea floor there. Therefore, we conclude that most (possibly all) of the present day opening is accommodated west of the “Danakil block” represented by RSB0 and TDJ0 (figure 1).

With respect to the African plate defined in [Vigny *et al.*, 2006] ( $50.48^{\circ}\text{N}$ ,  $-82.01^{\circ}\text{W}$ ,  $0.265^{\circ}/\text{Myr}$ ) the motion of these 2 points (RSB0 and TDJ0) is  $15 \pm 2$  mm/yr oriented  $\text{N}54 \pm 6^{\circ}$ . Assuming that the Danakil block rotates about a pole near its northern end (at  $16^{\circ}\text{N}$ ,  $40^{\circ}\text{E}$ ), we find an angular velocity of  $1.6 \pm 0.1^{\circ}/\text{Myr}$  for the Danakil block. This rate compares very well with paleomagnetic rotations in the area ( $10.7^{\circ} \pm 4^{\circ}$  over 7 Ma), which give an average spin rate of  $1.5 \pm 0.6^{\circ}/\text{Myr}$  or  $26 \pm 10$  mrad/yr [Manighetti *et al.*, 2001a; Besse and Courtillot, 1991]. Therefore, we conclude that the fact that the opening of Arabia-Africa at this latitude is absorbed west of the “Danakil block”, (i.e. along the deformation zones of the Afar depression) can be extended to the last 7 Ma at least.

#### Djibouti and the gulf of Tadjoura

Deformation along the northern side of the Gulf of Tadjoura (Figure 2) exhibits a clear gradient from 16 mm/yr on the north-eastern Asal-Ghoubbet rift shoulder to 11 mm/yr in the Danakil block (RSB0, TDJ0). Stations FFF0, MMM0, and RRR0, lying at the same distance of the Asal-Ghoubbet rift axis, display a particularly coherent velocity ( $16 \pm 1$  mm/yr and  $\text{N}45^{\circ} \pm 8^{\circ}$  on average). We are particularly confident in the velocity of point FFF0 since it has been measured four times during the last 12 years, with a remarkably stable time series. Point PPP0, located at intermediate distance between the “Danakil-Arabian” area and the rift shoulder, has a transitional velocity of  $15 \pm 3$  mm/yr with the same azimuth.

On the southwestern side of the Asal-Ghoubbet rift, we observe no significant velocity gradient between the southern rift shoulder (CCC0 or QQQ0) and the Somalia plate as we have defined it. Yet this interpretation is subject to two caveats: First, there are no sites between GOR0 in the far-field and the southern rift shoulder. Second, the motions of QQQ0 and III0 differ markedly: the former has a small insignificant residual velocity while the latter has an unexpected and probably erroneous high velocity of 10 mm/yr. Despite these caveats, we infer an asymmetry in the extensional deformation pattern between the northern part and the southern part of the Asal-Ghoubbet rift. This asymmetry is also apparent in the vertical deformation recorded by the

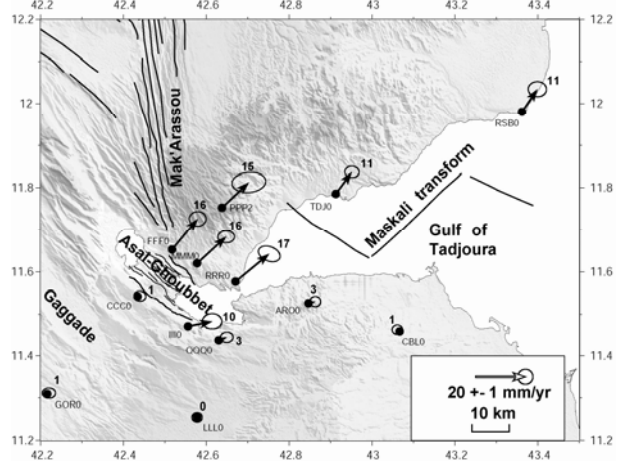


**Figure 2.** Djibouti and Gulf of Tadjoura. Dots show locations of GPS stations. Arrows depict their horizontal velocities with respect to a reference frame fixed on the Somalia plate. Bold numbers aside the arrows indicate the velocity in mm/yr. Ellipses depict the region of 99% confidence using the uncertainties in Table 1. Thick black lines show the principal directions of active rifting (Mak'Arassou, Asal-Ghoubbet, Gulf of Tadjoura) and the Maskali transform fault. Thin grey lines depict faults in the Asal-Ghoubbet rift.

topography, the faults activated during the 1978 sequence, and individual faults shifting their activity to the northeast [Ruegg *et al.*, 1990; Stein *et al.*, 1991; Ruegg and Kasser, 1987].

All these results confirm that most of, and in fact more than, the present motion of Arabia-Somalia is absorbed in the Asal-Ghoubbet rift during the 12-year observation period. In particular, no deformation can be detected in the Tadjoura rift or attributed to the faults located between the Tadjoura rift and the Asal rift, despite the sparse GPS network along the Gulf of Tadjoura. Nor do we see any evidence for slip or creep on the dense Gaggade-Hanle active fault system, southwest of Asal rift. Accordingly, we infer that the faults there are locked during this period.

Why, then, is the extension rate of 16 mm/yr across the Asal rift some 50% faster than the Arabia-Somalia plate motion? The most probable explanation involves the transient processes that took place in the rift following the 1978 seismo-volcanic sequence, when up to 1.9 m of extension were measured across the rift [Ruegg *et al.*, 1979]. During the following decade, extension at a rate of 60 mm/yr has been measured across the inner rift fault system that has been activated during the 1978 sequence [Ruegg and Kasser, 1987]. After 1987 this rate decreased to about 1 cm/yr, smaller than the far field rate imposed by large-scale plate tectonics (Figure 3). That the rate of opening changed drastically in the 6 years following the 1978 rifting event suggests two possible interpretations.

In the first interpretation, the opening continued at a constant rate of 53 mm/yr from 1980 through 1986

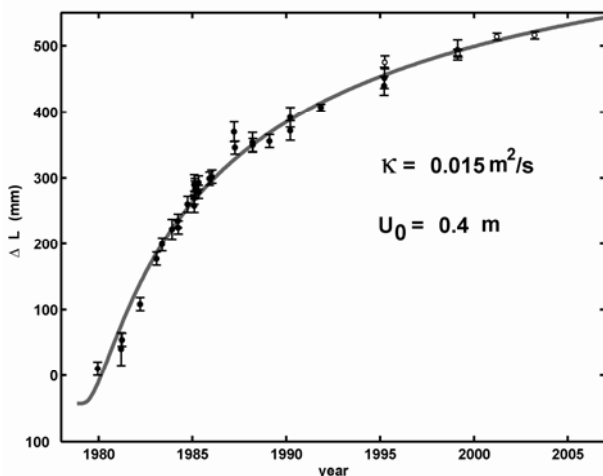


**Figure 3.** Time dependent opening of the rift following the 1978 rifting event. The dots show the distance between stations EP00 and DF00 on opposite sides of the rift (see figure 4 for location). Black symbols depict range measurements, open symbols are for GPS measurements (since 1995). The vertical bars show one standard deviation for each measurement. The dark curve shows the erf<sub>c</sub> visco-elastic model that best fits the data.

[Ruegg and Kasser, 1987]. Then the rate of opening slowed abruptly to 13 mm/yr, close to the geologic plate rate, suggesting that driving processes ceased abruptly. Although this model, with three parameters (two slopes and an intercept), is the simplest possible description of the time series shown in Figure 3, it does not appear to be compatible with other geophysical observations. In particular, there is no suggestion of a similar change in the seismicity around 1986. Nor did field observations suggest that the seismo-volcanic activity that "boiled over" in the 1978 crisis continued to simmer for the next 8 years. Fresh lava, for example, was observed only in 1978.

The second interpretation involves post-seismic relaxation in the years following the 1978 rifting event. The simplest possible model for this is a 1-dimensional Elsasser model of an elastic layer over a viscous half-space, as suggested for a similar rifting event in 1974 at Krafla, Iceland [Foulger et al., 1992]. Accordingly, the 1.9 meters of opening in 1978 constitutes the initial condition in a diffusion problem. Subsequently, a strain pulse diffuses away from the rift. This process produces variations in both time and space. In time, the cumulative displacement varies as

$$u(x,t) = U_0 \operatorname{erfc} \frac{x}{2\sqrt{\kappa t}} \quad (1)$$

where  $x$  is the distance from the rift, and  $\operatorname{erfc}$  is the complementary error function [Foulger et al., 1992]. Fitting the geodetically observed values in Figure 3,

we find a diffusivity of 0.015 m<sup>2</sup>/s, and an initial half-opening of  $U_0 = 0.4$  m.

Having established that velocities in the area change with time, one might worry that velocities inferred from campaign GPS measurements represent only an average on the time interval between two epoch measurements. In this case, comparing measurements made at different epochs at different locations might cause aliasing. However, time series of the EP00-to-DF00 baseline across the rift axis shows that a constant rate is a reasonable first-order approximation for the interval between 1987 and 2003 (figure 3). In other words, the transient has decayed sufficiently so that it can be fit reasonably well by a constant linear rate for the time span of our GPS campaigns (1991-2003). The data misfit is less than 2 mm/yr, consistent with the uncertainties in the GPS velocity estimates.

### The Asal Rift

Figure 4 shows the details of the deformation field inside the Asal rift, as measured by the relative velocities of about 20 points throughout the rift valley (figure 4). As at the larger scale, the rate of opening observed on the NE shoulder of the Asal rift is very coherent, with a constant rate of 16 mm/yr ± 1 at azimuth N45° ± 8° for the line through stations FFF0, GM00, MMM0, and RRR0. These stations move together as a unit that we call a "panel" that can be defined by the geomorphic expression of the active faults bounding it.

Nearer the rift axis, on the next panel to the southwest, we observe a marked variation along the strike of the panel: 16 mm/yr at BY00, 13 mm/yr at DF00, 10 mm/yr at CF00 and 6 mm/yr at AS00. This last line of points is located at the northern border of the "Petit Rift", a rift-in-rift structure with a dense network of faults, open fissures and cracks that appears to be the most active part of the Asal rift. This line of points also marks the northern boundary of the set of faults that slipped during the 1978 seismo-volcanic sequence. The GPS stations' velocities decrease from SE to NW, following the shape of the "Petit Rift" that terminates just southeast of station CF00 [deChabalier and Avouac, 1994]. This rate variation indicates propagation from the SE to the NW, as suggested from geomorphologic observations [Manighetti et al., 1998]. This propagation appears to be shallow, probably less than 3-4 km deep, because its effects do not reach the previous panel: FFF0, GM00, MMM0 and RRR0 move with the same velocity.

On the southwestern side of the rift, the velocity field is not so clear, mainly because many points were measured less frequently and display large error ellipses (HM00, FG00, GK00, and HX00). Nonetheless, we can define a shoulder panel including the stations HX00, FG00, and HM00 with 1 to 7 mm/yr, and another panel including stations GK00, EP00, and LS00 with a velocity of about 5 to 8 mm/yr. Points HD00 and SN00, located close to the rift axis, show rates of 4 and 9 mm/yr with respect to the Somalian plate, respectively.

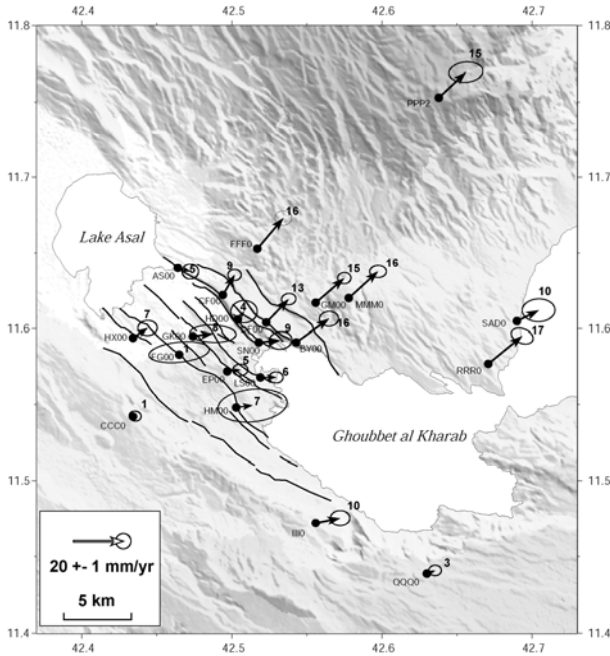


**Figure 4:** Asal rift. Dots show locations of GPS stations. Arrows depict their horizontal velocities with respect to a reference frame fixed on the Somalia plate. Bold numbers aside the arrows indicate the velocity in mm/yr. Ellipses depict the region of 99% confidence using the uncertainties in Table 1. Black lines show the Asal rift main active faults.

The general pattern on the southwest side of the rift indicates a small, gradual increase in velocity from the southwestern shoulder to the axis.

To visualize the high strain rates concentrated in the Asal rift, we project the velocities onto 4 profiles striking 45E°, perpendicular to the rift axis (Figure 5). The average strain rate is 1 mm/yr/km (or  $3 \times 10^{-14} \text{ s}^{-1}$ ). Most of the points on the NE side of the rift axis move faster than this average strain rate, while those in the SW part move more slowly. If we neglect stations HX00 and AS00 (profile 4), which are located close to Lake Asal, and therefore are perturbed by the along-strike variation due to the northwestward propagation, this signature becomes clearer. Indeed, it is expected from the diffusive model. The curve in Figure 5 shows the velocity calculated using the 1-dimensional Elsasser model (equation 4 in Foulger *et al.* [1992]) with the diffusivity and initial opening  $U_0$  estimated above, an elapsed time of 19 years between the crisis in 1978 and the mean date of our GPS campaigns (i.e. 1997), and centered 1 km northeast of the main rift axis. The deformation concentrates to the NE of the geomorphologic long-term rift axis such that the highest velocity gradient is in the "Petit Rift" between stations SN00 and DF00-BY00 (Figure 5). This area coincides with the maximum of fault breaks observed during the 1978 sequence [LeDain *et al.*, 1979; Ruegg *et al.*, 1979] and

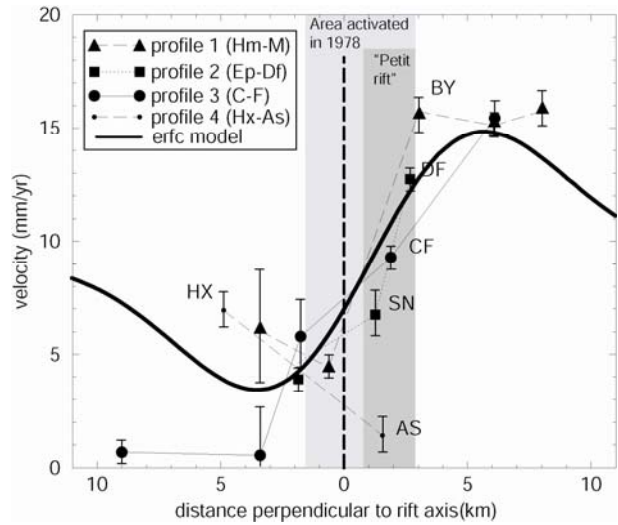


**Figure 5:** Asal rift horizontal velocity components plotted along profiles perpendicular to the rift axis. The thick dashed line show the rift axis. Rectangular shaded areas indicate the extents of the 1978 rifting event (light) and the "Petit Rift" (dark). The thick black curve depicts the Erfc visco-elastic model computed with the parameters inferred from model curve in figure 3 and  $t=19$  years since 1978 and centered at +1 km. Triangles and dashed line depict the first profile near Ghoubbet (HM00 – LS00 – BY00 – GM00 – MMM0), squares and dotted line depict the second profile (EP00 – SN00 – DF00), circles and full line depict the third profile near lake Asal (CCC0 – FG00 – GK00 – CF00 – FFF0), dots and long dashed line depict the last 2 points at lake Asal (HX00 – AS00). Error bars represent the 1-sigma uncertainties of table 1.

with the present-day seismicity, which is mostly located in the northern part [Dubre *et al.*, 2006]. Furthermore, the fastest points, showing the location of the post-seismic diffusive pulse in 1997, fall 3 to 5 km away northeast from the "Petit Rift" axis. However, the major limitation of this simple model lies in its symmetry with respect to the rift axis, which results in the large misfit at station CCC0 on the southwestern side. Therefore, we conclude that this model is only a first order approximation and that creep on dipping faults in particular must be taken into account.

### Rates of vertical motion

Conditions in Asal rift are good for measuring the vertical component of the tectonic deformation field because we expect the ratio of tectonic signal to geodetic noise to be larger than unity. The floor of the innermost valley in the rift could be subsiding as fast as 10 mm/yr with respect to the shoulders. Some points of our network have been measured many times over a 12 year period. Measurement campaigns were usually conducted at the same time of the year, during winter. Relative distances between points are small. Finally, almost all points are located on good, solid outcrops, clearly attached to the bedrock.

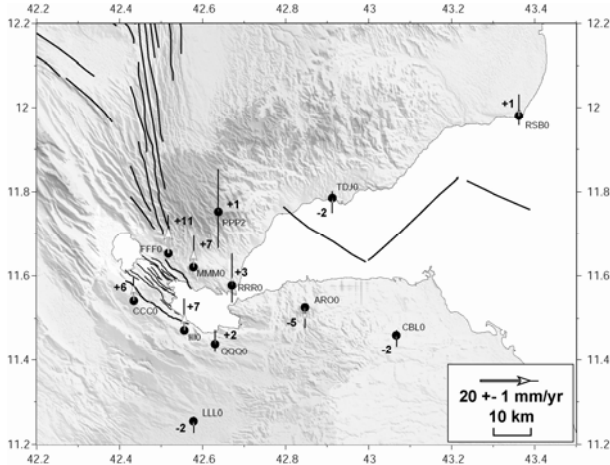


**Figure 6.** Vertical velocities in Djibouti. Dots show locations of GPS stations measured at least 3 times. Arrows depict the GPS vertical velocities at those locations: arrows pointing North (resp. South) indicate upward (resp. downward) velocities. Vertical thin lines at the arrow heads give the 99% confidence level using table 1 vertical velocity uncertainty. Numbers aside the arrow head indicate the velocity in mm/yr.

### Intermediate-scale GPS

Selecting stations measured at least four times, we define a subset of points around the rift with vertical velocities determined to within  $\pm 5$  mm/yr (figure 6). Stations located far from the rift: RSB0 and TDJ0 on the north side, and CBL0 and LLL0 on the south side, show no motion to within  $\pm 2$ - $3$  mm/yr. They represent a stable reference frame for analyzing vertical motions in the rift. Near the eastern tip of the rift, stations RRR0 and QQ0 also show small, but marginally significant, velocities of +2 to +3 mm/yr upward with respect to the far-field reference. Points located further west on the shoulders of the rift show a fairly symmetric and significant uplift between 6 and 11 mm/yr. From these values, we can estimate an average uplift value of  $8 \pm 3$  mm/yr, and locate the maximum uplift in the central part of the rift, midway between Lake Asal and Ghoubbet Al Kharab.

### Small scale: leveling and GPS inside the rift

Small-scale vertical displacements are usually better determined with classical leveling profiles than with GPS. It is not unusual to keep the drift of leveling tools below  $10^{-6}$  (i.e. 1 mm per km) and therefore detect millimeter-sized vertical displacements between two leveling surveys made on the same line at different epochs. A precise leveling line with about 200 marks was established in 1973 along 100 km of the track crossing the rift. The central part of this line was measured for the second time in 1979, after the

Ardoukoba seismo-volcanic crisis [Abdallah *et al.*, 1979; Ruegg *et al.*, 1979] and again in the winter of

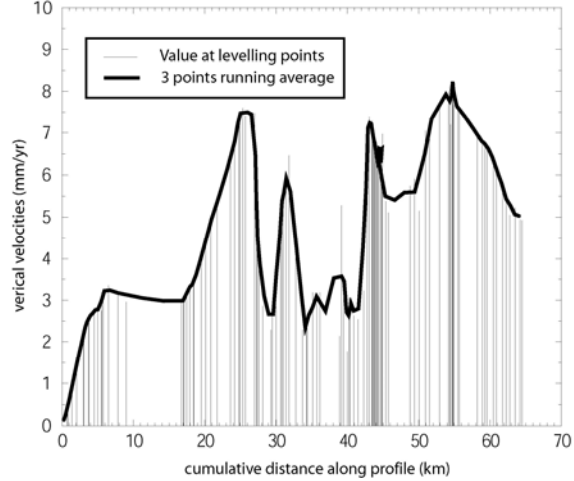


**Figure 7:** Leveling profile velocities (2000 – 1985) projected on an axis perpendicular to the rift (strait grey line on figure 8). The vertical thin lines indicate the difference between 2000 and 1985 measurement at each benchmark of the profile. The thick curve is a 3-point running average of these measurements.

1984–1985 [Ruegg and Kasser, 1987]. Over this 6-year period, uplift rates as fast as 10 to 15 mm/yr were detected. The uplift was similar on both shoulders of the rift, with the inner floor subsiding with respect to them but still rising with respect to the far-field points. This line was measured for the fourth time in 2000.

The 1985–2000 comparison gives vertical rates over a 15-year period (figure 7). The inferred pattern of deformation shows both similarities and differences with the one of 20 years ago. Both intervals show the same pattern of uplift of the rift shoulders and relative subsidence of the inner floor. Yet the rates for the 1985–2000 interval are 50% slower than those for 1978–1985, indicating that the post-seismic transient after the 1978 crisis is still decaying. The peak around Km 32 in the inner rift floor appears to represent the same two-dimensional effect as seen in the horizontal velocities. Since this portion of the leveling line runs parallel to the rift axis, the uplift varies as a function of position along strike, probably reflecting the same propagation process. The points on the NE side (after km 45) differ from previous measurements. They suggest that the uplifting area was wider after 1985 than before, consistent with the diffusive Elsasser model.

This finding is coherent with recent INSAR results obtained on the 1997–2003 period which also show the same trend [Dubre *et al.*, 2005]. Yet this finding should be taken with some caution. Precise leveling can be affected by systematic errors that could produce such a pattern. The difference in height at the end of the line is only 75 mm with respect to the starting point 65 km away. The overall trend is only slightly more than 1 mm/km, close to the limit of accuracy. Unfortunately, the line was measured in forward run, which keeps us

from using the overall mis-closure to estimate, a-posteriori, an overall drift proportional to the distance covered. Also, the measurements stopped short of the end point of the 1973 line in the far field. Consequently, we must rely on the analysis of internal errors and biases to evaluate the level of precision in this leveling profile. The lines of sight were kept short: 15 m on average and very seldom longer than 30 m (Aux. Figure 1a). Forward and backward lines of sight were symmetric within 10 to 20% to cancel out any asymmetric behavior of the leveling instrument (Aux. Figure 1b). We avoided as much as possible hitting the surveyor's pole at low heights, too close to ground level where atmospheric distortions are largest (Aux. Figure 1c). Finally, the ten small loops of length shorter than 1 km all closed with 1 mm, without any systematic trend (Aux. Figure 1d). Considering all these reasons together, we can exclude systematic errors as the cause of the uplift observed on the NE side of the rift.

However, a change of height does not necessarily imply a change of topographic elevation. It could be that the local geoid changed over the 15 years time span between the two leveling profiles. Indeed, some indication that this may have occurred comes from gravity measurements conducted in the area in 1999 [Ballu et al., 2003]. These measurements suggest that the gravitational acceleration decreased in this area which between 1985 and 1999. Such a change can be interpreted in terms of some combination of uplifting the benchmarks or decreasing the density of the rocks below them.

We can glean a little more information from a two-dimensional comparison with the vertical velocities for the GPS stations inside the rift. Again selecting stations measured at least four times, we see some coherent signal (Figure 8). The results are similar if we select three occupations over a minimum of 8 years. First of all, this map view highlights the two-dimensional distribution of the vertical motions. Far from being a straight line across the rift, the leveling line meanders around faults and cliffs and samples the uplift at different locations along the rift axis. Thus the signal on the rift inner floor varies along its strike: less than 1 mm/yr near the Ghoubbet shore but close to 5 mm/yr some 5 km inland. Second, there is a general good agreement between the GPS and leveling estimates on the NE side of the rift. Both techniques see the shoulder uplifting at 5 to 7 mm/yr (GM00 and DF00). The next panel, represented by station CF00, is rising by only 4 mm/yr with respect to the valley floor, but subsiding with respect to the shoulder. The inner rift floor is clearly subsiding, with 2 to 4 mm/yr in the "Petit Rift" (stations HD00 and SN00). Points on the other side of the rift axis, but close to the Ghoubbet have very small velocities (+2 mm/yr at EP00, -2 mm/yr at LS00). All these values are consistent with the leveling values, except GK00 and FG00 which have large uncertainties. They indicate the sum of two signals: a subsidence of the inner floor with respect to

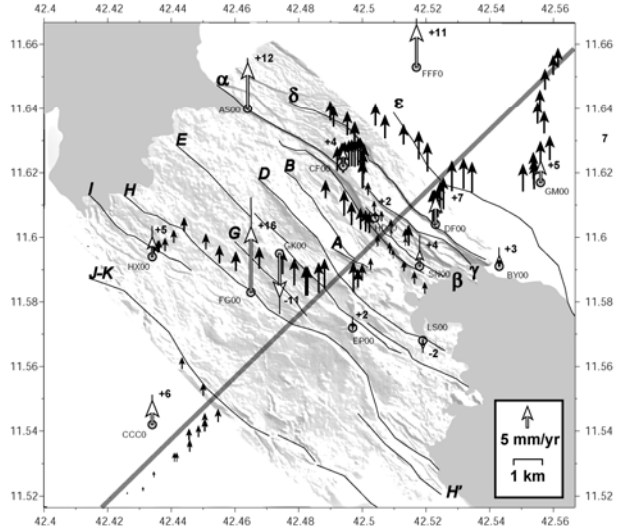


**Figure 8:** Vertical velocities inside the Asal rift. Dots show locations of GPS stations. Open arrows depict the GPS vertical velocities, dark arrows depict the velocities obtained from leveling profiles. Arrows pointing North (resp. South) indicate upward (resp. downward) velocities. Vertical thin lines at the arrow heads give the 99% confidence level using table 1 vertical velocity uncertainty (no uncertainties for the leveling velocities). Bold numbers aside the arrow head indicate the velocity in mm/yr. Grey line shows the direction along which the 1D profile of figure 7 is plotted. The background topography is from the 10 m-resolution digital elevation model made from aerial photography [de Chabalier and Avouac, 1994]. Fault labels (A-K,  $\square$ ) are from [Stein et al., 1991].

the shoulders and an inflation signal located in the middle of the rift. The SW side of the rift is different: GPS vectors indicate an uplift of the rift shoulder where the leveling returns to zero (HX00, CCC0).

## Conclusions

Vigny et al. [2006] have shown that the far-field plate rates estimated from GPS data acquired over the 12-years interval are 30% slower than predicted by plate-motion models based on the last several million years. Our estimate for the rate of opening across the Asal rift between Somalia and the Danakil block is  $11 \pm 1$  mm/yr based on ten GPS stations observed between 1991 and 2003. Clearly, the deformation pattern across this complex plate boundary is more complicated than supposed by classical plate tectonics, which assumes that the angular velocity is constant in space for all points on the same plate.

The rifting event in 1978 created a significant transient in the deformation pattern. Over 25 years later, the inner rift is still opening at a rate faster than the far-field value. This observation can be explained to first order by a simple one-dimensional Elsasser visco-elastic model. For the 1978 Asal crisis in Djibouti, however, the estimated diffusivity is two orders of magnitude

smaller than estimated for the 1974 Krafla crisis in Iceland [Foulger et al., 1992]. The diffusivity measures the ratio of the length scale to the square root of the time scale. The time scale is the time between the rifting episode and the second geodetic survey, i.e. 19 years at Asal and 11 years at Krafla. The length scale is the distance from the rift axis to the fastest-moving point, 3 km at Asal, considerably shorter than the 25 km at Krafla. The diffusivity ratio for Asal with respect to Krafla is  $\sim 1/70$ , implying that the top elastic layer (crust ?) is at least an order of magnitude thinner beneath Asal and/or that the viscosity of the underlying half-space (mantle ?) is at least an order of magnitude higher at Asal than at Krafla. Although these differences are qualitatively consistent with the tectonic settings of Djibouti and Iceland, their stark quantitative contrast suggests that the 1-dimensional analysis oversimplifies the problem somewhat.

In a subsequent paper [Cattin et al., 2005], we argue that the geometric considerations (multiple dipping, non-planar faults) and thermal effects (post-rifting cooling increases viscosity) require a complete 3-dimensional approach, using numerical modeling. Such a model is required to explain the details of the inner rift deformation. For example, the geodetic data suggest that the northern part of the rift zone accommodates more (some 70%) of the extension than the southern part.

Considering the amount of extension absorbed in the Asal rift during the 1978 sequence, the high post-seismic velocity, and the present-day velocity, we infer that the opening rate across the Asal rift will have to decrease significantly before the next such seismo-volcanic crisis can occur. The deformation recorded by the topography as well as the deformation recorded by the lake Asal Holocene markers, suggest that the recurrence time of such a crisis is about 120 to 300 yr [Ruegg et al., 1990; Stein et al., 1991; Manighetti et al., 1998]. However, the ongoing high rate and the fact that the whole system is being uplifted is an indication that magma injection still prevails over extension as the active process driving the rifting today.

## Acknowledgments

We are grateful to many people who occasionally participated in measurement campaigns: in particular people from the “Observatoire d’Arta”, and especially to J.-C. Delmont who was director during the 1991 campaign and participated in 1995 and 1999. The leveling line was surveyed by A. Coulomb from IGN. Very special thanks to Moumin in Djibouti. The Afar geodetic program was sponsored by CNRS/INSU programs (Tectoscope-Positionnement, IDHYL, IT). We also appreciate the guidance of Peter Molnar, whose NSF grant (OCE8916680) boosted the 1991 campaign.

## References

- Abdallah, A. V. Courtillot, M. Kasser, A.Y. Le Dain, J.C. Lepine, B. Robineau, J.C. Ruegg, P. Tappognier and A. Tarantola, Relevance of Afar seismicity and volcanism to the mechanics of accreting plate boundaries, *Nature*, 282, 17-23, 1979.
- Acton, G.D., and Stein S., Block rotation and continental extension in Afar: a comparison to oceanic microplate systems. *Tectonics*, 10, 501-526, 1991.
- Altamimi, Z., P. Sillardand C. Boucher, ITRF2000: A new release of the International Terrestrial Reference frame for earth science applications, *J. Geophys. Res.-SA* 107 (B10): art. no. 2214, 2002.
- Asfaw, L. R., R. Bilham, M. Jackson and P. Mohr, Recent inactivity in African rift, *Nature*, 357, 447, 1992.
- Ballu, V., M. Diament, P. Briole and J.C. Ruegg, 1985-1999 gravity field variations across the Asal rift: insights on vertical movements and mass transfer, *Earth Planet. Sci. Lett.*, 208, 41-49, 2003.
- Besse, J., and V. Courtillot, Revised and synthetic apparent polar wander paths of the African, Eurasian, North American and Indian plates, and true polar wander since 200 Ma, *J. Geophys. Res.*, 96, 4029-4050, 1991.
- Beutler, G., J. Kouba, and T. Springer, Combining the orbits of the IGS processing centers, in proceedings of IGS annalysis center workshop, *edited by J. Kuba*, 20-56, 1993.
- Cattin, R., C. Doubre, J.B. de Chabalier, G. King, C. Vigny, J.P. Avouac and J.C. Ruegg, Numerical modelling of quaternary deformation and post-rifting displacement in the Asal-Ghoubbet rift (Djibouti, Africa), *Earth Planet. Sc. Lett.*, 239, 352-367, 2005.
- Courtillot, V., A. Galdeano and J.L. LeMouel, Propagation of an accreting plate boundary: a discussion of new aeromagnetic data in the gulf of Tadjourah and southern Afar. *Earth Planet. Sci. Lett.*, 47, 144-160, 1980.
- Chu, D., and R.G. Gordon, Evidence for motion between Nubia and Somalia along the southwest Indian Ridge, *Nature*, 398, 64-67, 1999.
- Courtillot et al., 1980.
- De Chabalier, J.B. and J.P. Avouac, Kinematics of the Asal rift (Djibouti) determined from the deformation of Fieale volcano, *Science*, 265, 1677-1681, 1994.
- DeMets, C., et al., Current plate motions, *Geophys. J. Int.*, 101, 425-478., 1990
- DeMets, C., R. G. Gordon, D. Argus, and S. Stein, Effect of recent revisions to the geomagnetic reversal time scale on estimates of current plate motions, *Geophys. Res. Letters.*, 21, 2191-2194, 1994.
- Doubre, C., G. Peltzer, I. Manighetti and E. Jacques, Eight years of surface deformation in the Asal-Ghoubbet rift (Afar depression) observed with SAR data, AGU fall meeting, G42A04, 2005.
- Doubre, C. et al. Crustal structure and magmato-tectonic processes in an active rift (Asal-Ghoubbet, Afar, East-Africa). Part 2: Insights From the 23-Year

- Recording of Seismicity Since the Last Rifting Event. *J. Geophys. Res.*, Submitted (2006).
- Doubre, C. et al. Crustal structure and magmatic-tectonic processes in an active rift (Asal-Ghoubbet, Afar, East-Africa). Part 1: Insights from a five-month seismological experiment. *J. Geophys. Res.*, In review (2006).
- Fernandes, R.M.S., B.A.C. Ambrosius, R. Noomen, L. Bastos, M. Wortel, W. Spakman, and R. Govers, The relative motion between Africa and Eurasia as derived from ITRF2000 and GPS data, *Geophys. Res. Lett.*, 30(16), 1828, 2003, doi:10.1029/2003GL017089.
- Foulger, G. R., C.-H. Jahn, G. Seeber, P. Einarsson, B. R. Julian and K. Heki, Post-rifting stress relaxation at the divergent plate boundary in Northeast Iceland, *Nature*, 358, 1992.
- Herring, T. A., Davis, and Shapiro, Geodesy by radio Interferometry : the application of Kalman filtering to the analysis of very long baseline interferometry data, *J. Geophys. Res.*, 95, 12561-12581, 1990.
- Huchon, P., F. Jestin, J.M. Cantagrel, J.M. Gaulier, S. Al Khirbash and A. Gafaneh, Extensional deformations in Yemen since Oligocene and the Afar triple junction, *Annales Tectonicae* 5 (2), 141-163, 1991.
- Huchon, P., I. Manighetti, M. Al-Aawah, S. Al-Khirbash, L. Audin, O. Coulon, O. Dauteuil, H. Hebert, E. Jacques, K. Khanbari, S. Levasseur, A. Omar, T. Souriot, and P. Tapponnier, Propagation of the Arabia-Somalia plate boundary in the western Gulf of Aden: new results of the 1995 TADJOURADEN cruise, in Rift sedimentation and tectonics in the Red Sea – Gulf of Aden region,(abstr.) Sana'a, Yemen, 1995.
- Jestin, F., P. Huchon and J.M. Gaulier, The Somalia plate and the East African Rift system: present day kinematics, *Geophys. J. Int.*, 116, 637-654, 1994.
- King, R. W., and Y. Bock, Documentation for the GAMIT GPS software analysis version 9.9, *Mass. Inst. of Technol.*, Cambridge, 2000.
- Le Dain, A.Y., B. Robineau and P. Tapponnier. «Les effets tectoniques de l'événement sismique et magmatique de novembre 1978 dans le rift d'Asal-Ghoubbet. *Bull. Soc. Géol. France* 7(6) :817-822, 1979
- Manighetti, I., Dynamique des systèmes extensifs en Afar, *Paris6 University Thesis*, 242p, 1993.
- Manighetti, I., P. Tapponnier, V. Courtillot, S. Gruszow and P.Y. Gillot, Propagation of rifting along the Arabia-Somalia plate boundary: the gulfs of Aden and Tadjoura, *J. Geophys. Res.*, 102 (B2), 2681-2710, 1997.
- Manighetti, I., P. Tapponnier, P.Y. Gillot, E. Jacques, V. Courtillot, R. Armijo, J.C. Ruegg, and G. King, Propagation of rifting along the Arabia-Somalia plate Boundary: into Afar, *J. Geophys. Res.* 103 (B3), 4947-4974, 1998.
- Manighetti, I., P. Tapponnier, V. Courtillot, Y. Gallet, E. Jacques, and P.Y. Gillot, Strain transfer between disconnected, propagating rifts in Afar, *J. Geophys. Res.*, 106 (B7), 13613-13665, 2001a.
- Manighetti, I., G.C. King, Y. Gaudemer, C.H. Scholz, and C. Doubre, Slip accumulation and lateral propagation of active normal faults in Afar, *J. Geophys. Res.*, 106 (B7), 13667-13696, 2001b.
- McClusky, S., et al. (2000), Global Positioning System constraints on plate kinematics and dynamics in the eastern Mediterranean and Caucasus, *J. Geophys. Res.*, 105, 5695-5720.
- McClusky, S., R. Reilinger, S. Mahmoud, D. Ben Sari, and A. Tealeb, GPS constraints on Africa (Nubia) and Arabia plate motions, *Geophys. J. Int.*, 155, 126-138, 2003.
- Neilan, R., The evolution of the IGS global network, current status and future aspects, in IGS annual report, edited by J.F. Zumberge et al., *JPL Publ.*, 95-18, 25-34, 1995.
- Ruegg, J.C., J.C. Lépine, A. Tarantola, and M. Kasser, Geodetic measurements of rifting associated with a seismovolcanic crisis in Afar, *Geophys. Res. Lett.*, 6, 817-820, 1979.
- Ruegg, J.C., and M. Kasser, Deformation across the Asal-Ghoubbet Rift, Djibouti, uplift and crustal extension 1979-1986, *Geophys. Res. Lett.*, 14, 745-748, 1987.
- Ruegg, J.C., F. Gasse and P. Briole, Mouvements du sol holocènes dans le rift d'Asal à Djibouti, *C.R. Acad. Sci. Paris*, 310, 1687-1694, 1990.
- Ruegg, J.C., P. Briole, K. Feigl, C. Vigny, M. Anis Abdallah, O. Bellier, P. Huchon, S. Al Khirbash, A. Laike, N. d'Oreye, and M. Prevot, First Epoch Geodetic GPS Measurements Across the Afar Plate Boundary Zone. *Geophys. Res. Lett.*, 20, 1899-1902, 1993.
- Sella, G.F., T. H. Dixon, and A. Mao, REVEL: a model for recent plate velocities from space geodesy, *J. Geophys. Res.*, 107 (B4), 10.1029, 2002.
- Sichler, B., La bielette danakile : un modèle pour l'évolution géodynamique de l'Afar, *Bull. Soc. Géol. Fr.*, 6, 925-933, 1980.
- Sigmundsson, F., P. Einarsson, R. Bilham, Magma chamber deflation recorded by the Global Positioning System, the Hekla 1991 eruption, *Geophys. Res. Lett.*, 19(14) 1483-1486, 1992.
- Souriot, T., and J.P. Brun, Faulting and block rotation in the Afar triangle East Africa: the Danakil crank arm model. *Geology*, 20, 911-914, 1992.
- Stein, R.S., Briole, P., Ruegg, J.C., Tapponnier, P. and F. Gasse. Contemporary, Holocene and Quaternary deformation of the Asal rift, Djibouti – implications for the mechanics of slow spreading ridges. *J. Geophys. Res.*, 96, 21789-21806, 1991.
- Tapponnier, P., R. Armijo, I. Manighetti, and V. Courtillot, Bookshelf faulting and horizontal block rotations between overlapping rifts in southern Afar, *Geophys. Res. Lett.*, 17, 1-4, 1990.
- Vernant, P., F. Nilforoushan, D. Hatsfeld, M. Abassi, C. Vigny, F. Masson, H. Nankali, J. Martinod, A. Ashtiani, F. Tavakoli, and J. Chéry, Contemporary

crustal deformation and plate kinematics in Middle East constrained by GPS measurements in Iran and northern Oman, *Geophys. J. Int.*, 157, 381-398, doi:10.1111/j.1365-246x.2004.02222.x 2004.

Vigny, C., P. Huchon, J.C. Ruegg, K. Khanbari, and L. Asfaw, Confirmation of Arabia plate slow motion by new GPS data in Yemen. *J. Geophys*

*Res.*, 111, B02402, doi:10.1029/2004JB003229, 2006.

Walpersdorf A., C. Vigny., J.-C. Ruegg, P. Huchon, L. M. Asfaw and S. Al Kirbashi., 5 Years of GPS Observations in the Afar Triple Junction Area. *Journal of Geodynamics*, 28, 2-3, 225-236, 1999.

## Electronic supplement to :

### 25 years of geodetic measurements along the Tadjoura-Asal rift system, Djibouti, East Africa.

**Table S1:** Site occupation. Bold numbers indicate the number of sessions at each site, the following codes indicate the type of equipment used. Receivers are Trimble 4000 SLD (TSLD) or SST (TSST); or Ashtech codeless L2 (AL12), P-code L2 (AP12), Z-tracking (AZ12), micro-Z (AZX). Antennas are Trimble SLD (L1/L2 4000 model 12562 - square ground plane) or SST (L1/L2 4000 model 14532 – round ground plane); or Ashtech L12 (geodetic L1/L2 type 1 - closed holes on ground plane – IGS#: ASH700228A), P12 (geodetic L1/L2 type 2 - open holes on ground plane – IGS#: ASH700228D), GD3 (geodetic L1/L2 type 3 - large ground plane “whopper” – IGS#: ASH700718A), MRA (dual frequency marine – IGS#: 700700.A), DMG (Dorne-margolin “choke ring” – IGS#: ASH700936A) or GD4 (geodetic type 4 - small antenna without ground plane –IGS#: ASH701975.01A).

SITE	1991	1993	1995	1997	1999	2001	2003
ARO0	<b>45</b> AL12-L12	<b>25</b> TSST-SST	<b>13</b> AZ12-GD3	<b>11</b> AZ12-GD3	<b>14</b> AZ12-DMG	<b>14</b> AZ12-DMG	<b>13</b> AZ12-GD3
			AP12-P12				
AS00					<b>2</b> AZX-DMG	<b>5</b> AZX-DMG	<b>10</b> AZX-GD4
BY00			<b>1</b> AZ12-P12		<b>2</b> AZ12-DMG		<b>3</b> AZX-GD4
CBL0	<b>8</b> AL12-L12		<b>1</b> AZ12-P12		<b>2</b> AZ12-DMG	<b>2</b> AZX-DMG	<b>2</b> AZX-GD4
CCC0	<b>3</b> AL12-L12				<b>3</b> AZX-DMG	<b>2</b> AZ12-DMG	<b>6</b> AZX-GD4
CF00			<b>1</b> AZ12-P12		<b>5</b> AZX-DMG	<b>5</b> AZ12-DMG	<b>4</b> AZX-GD4
DF00			<b>3</b> AZ12-P12		<b>10</b> AZX-DMG	<b>9</b> AZX-DMG	<b>12</b> AZX-DMG
EP00			<b>3</b> AZ12-L12		<b>5</b> AZ12-DMG	<b>6</b> AZX-DMG	<b>4</b> AZX-GD4
FFF0	<b>2</b> TSST-SST				<b>2</b> AZX-DMG	<b>1</b> AZX-MRA	<b>3</b> AZX-GD4
FG00			<b>1</b> AZ12-P12		<b>1</b> AZX-DMG		<b>2</b> AZX-GD4
GK00			<b>1</b> AZ12-P12		<b>1</b> AZX-DMG	<b>1</b> AZ12-DMG	
GM00			<b>2</b> AZ12-P12		<b>4</b> AZ12-DMG	<b>2</b> AZX-DMG	<b>4</b> AZX-GD4
GOR0	<b>3</b> AL12-L12						<b>1</b> AZX-GD4
	TSST-SST						
HD00						<b>2</b> AZX-DMG	<b>2</b> AZX-GD4
HM00						<b>1</b> AZ12-DMG	<b>2</b> AZX-GD4
HX00			<b>1</b> AZ12-P12		<b>2</b> AZX-DMG	<b>1</b> AZ12-DMG	<b>2</b> AZX-GD4
III0	<b>1</b> TSST-SST				<b>2</b> AZX-DMG	<b>2</b> AZ12-DMG	<b>2</b> AZX-GD4
LLL0	<b>16</b> TSST-SST	<b>3</b> AP12-P12	<b>2</b> AZ12-P12	<b>1</b> AZ12-GD3	<b>2</b> AZ12-DMG	<b>2</b> AZ12-MRA	<b>3</b> AZX-GD4
	AL12-L12						
LS00			<b>1</b> AZ12-P12		<b>1</b> AZ12-DMG	<b>3</b> AZ12-DMG	<b>3</b> AZX-GD4
MMMO	<b>2</b> TSST-SST				<b>2</b> AZX-DMG	<b>2</b> AZ12-DMG	<b>2</b> AZX-GD4
	AL12-L12						
PPP2	<b>1</b> AL12-L12						<b>1</b> AZX-GD4
QQQ0	<b>6</b> AL12-L12		<b>1</b> AZ12-P12		<b>2</b> AZX-DMG	<b>2</b> AZ12-DMG	<b>2</b> AZX-GD4
RRR0	<b>2</b> AL12-L12					<b>2</b> AZ12-MRA	
RSB0	<b>9</b> TSLD-SLD				<b>2</b> AZ12-DMG	<b>2</b> AZ12-DMG	<b>4</b> AZX-GD4
SAD0						<b>2</b> AZX-DMG	<b>2</b> AZX-GD4
SN00					<b>1</b> AZX-DMG	<b>1</b> AZ12-DMG	<b>4</b> AZX-GD4
TDJ0			<b>1</b> AZ12-P12		<b>2</b> AZX-DMG	<b>2</b> AZ12-DMG	<b>3</b> AZX-GD4
ADD1	<b>20</b> AL12-L12		<b>9</b> TSSE-SST	<b>7</b> TSSE-SST	<b>13</b> TSSE-SST	<b>13</b> TSSE-SST	<b>14</b> TSSE-SST
DHAM	<b>4</b> AL12-L12					<b>3</b> AZ12-P12	
HODD	<b>3</b> AL12-L12					<b>3</b> AZ12-P12	
JNAR	<b>2</b> AL12-L12					<b>2</b> AZ12-P12	
SANA	<b>15</b> AL12-L12	<b>26</b> AP12-P12	<b>9</b> AP12-P12		<b>12</b> AZ12-P12	<b>9</b> AZ12-P12	

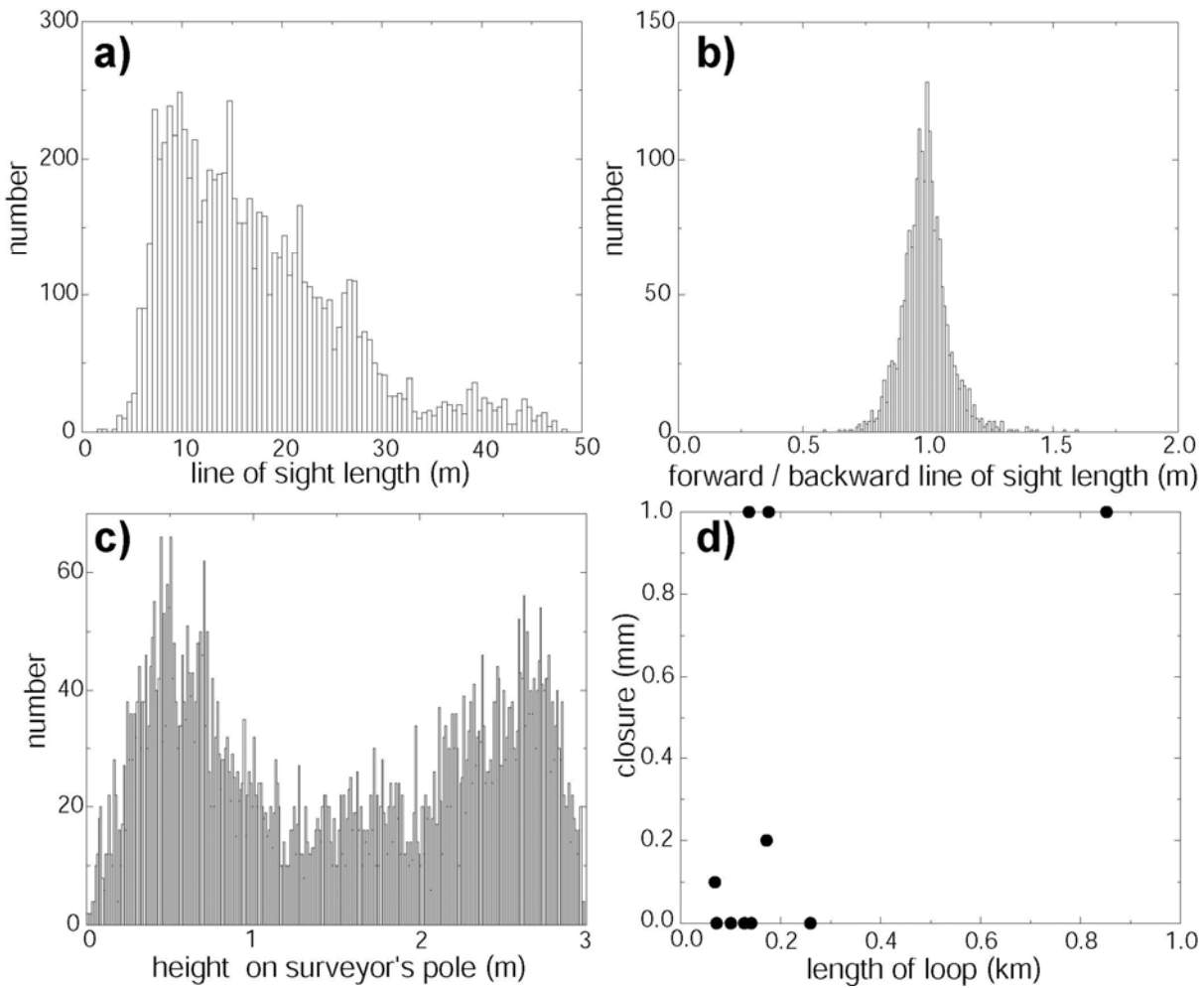


**Figure S1:** Leveling profile technical characteristic and quality assessment. Histograms of: (a) length of line of sights, (b) ratio of forward and backward line of sight lengths, (c) heights hit on the surveyor's pole; and (d) misclosure of small loops.